

AD 768 730

LIBRARY
TECHNICAL REPORT SECTION
NAVAL POSTGRADUATE SCHOOL
MONTEREY, CALIFORNIA 93940

NUC-TP- 353



CALIFORNIA UNDERSEA AQUEDUCT RECONNAISSANCE: THE OCEANOGRAPHY (CUARO)

by

Robert H. Riffenburgh

Undersea Surveillance and Ocean Sciences Department

August 1973



**BEST
SCAN
AVAILABLE**

Approved for public release; distribution unlimited.



NAVAL UNDERSEA CENTER, SAN DIEGO, CA. 92132

AN ACTIVITY OF THE NAVAL MATERIAL COMMAND

ROBERT H. GAUTIER, CAPT, USN

Commander

Wm. B. McLEAN, Ph.D.

Technical Director

ADMINISTRATIVE INFORMATION

The work in this report was performed from January 1972 to February 1973 by members of the Marine Environment Division, Undersea Surveillance and Ocean Sciences Department. The report was prepared for the U. S. Bureau of Reclamation, Denver, Colorado, and Sacramento, California.

Released by
M. A. BEAL, Head
Marine Environment Division

Under authority of
G. B. ANDERSON, Head
Undersea Surveillance and Ocean
Sciences Department

UNCLASSIFIED

Security Classification

DOCUMENT CONTROL DATA - R & D

(Security classification of title, body of abstract and indexing annotation must be entered when the overall report is classified)

1. ORIGINATING ACTIVITY (Corporate author) Naval Undersea Center San Diego, California 92132		2a. REPORT SECURITY CLASSIFICATION UNCLASSIFIED	
		2b. GROUP	
3. REPORT TITLE CALIFORNIA UNDERSEA AQUEDUCT RECONNAISSANCE: THE OCEANOGRAPHY (CUARO)			
4. DESCRIPTIVE NOTES (Type of report and inclusive dates) Research and Development January 1972 to February 1973			
5. AUTHOR(S) (First name, middle initial, last name) Robert H. Riffenburgh			
6. REPORT DATE August 1973		7a. TOTAL NO. OF PAGES 158	7b. NO. OF REFS 36
8a. CONTRACT OR GRANT NO.		9a. ORIGINATOR'S REPORT NUMBER(S) NUC TP 353	
b. PROJECT NO.			
c.		9b. OTHER REPORT NO(S) (Any other numbers that may be assigned this report)	
d.			
10. DISTRIBUTION STATEMENT Approved for public release; distribution unlimited.			
11. SUPPLEMENTARY NOTES		12. SPONSORING MILITARY ACTIVITY U. S. Bureau of Reclamation Denver, Colorado, and Sacramento, California	
13. ABSTRACT <p>This report discusses the possibility of conveying fresh water from northern to southern California via a subsurface offshore aqueduct (the California Undersea Aqueduct). The specific region investigated was between Crescent City and San Diego from the 20- to 200-m depth contour.</p> <p>All available data on relevant variables were analyzed to provide information for aqueduct planning decisions. The variables and analyses most influential in planning the California Undersea Aqueduct were divided into two categories: variables influencing the 100-year survival of the aqueduct (century risks) and variables influencing the construction and maintenance of the aqueduct.</p> <p>Waves, surges, tsunamis, density, and light do not appear on the basis of reconnaissance data to pose insurmountable problems. Surface, water column, and bottom currents, including upwelling and internal wave phenomena, may or may not be prohibitive; data are inadequate, and additional information must be obtained from <i>in situ</i> observations. Canyons are not an insurmountable threat, but will pose innovative engineering challenges and probably be quite expensive. Additional data will also be required on these processes.</p>			

UNCLASSIFIED

Security Classification

14 KEY WORDS	LINK A		LINK B		LINK C	
	ROLE	WT	ROLE	WT	ROLE	WT
California Undersea Aqueduct Fresh water Aqueducts						

ACKNOWLEDGMENTS

CUARO TEAM

The CUARO team, initiated in January 1972 under the direction of Mr. William F. Potter (NUC), was assisted part-time by Dr. Robert H. Riffenburgh of NUC and Mr. John B. Dahl and Ms. Susan Chandler, students at California State University, San Diego (CSUSD). Mr. Potter had early responsibility for initial planning and archive searching. In April 1972, Mr. Potter left NUC, and Dr. Riffenburgh assumed command. Mr. Dahl and Ms. Chandler continued, joined by Mr. Robert Butler, a CSUSD student. The students worked full-time during the summer, joined by Messrs. Richard Downie and Vernon Turner, also CSUSD students. After September, Messrs. Dahl and Butler and Ms. Chandler continued part-time to the end of the project. Mr. Dahl had early responsibility for some of the archive search and later considerable responsibility for tsunami and surface-current development; he also assisted in charting and overlay shading. Ms. Chandler was in charge of charting, overlay shading, and light transmittance. Considerable responsibility for wave and bottom surge development was given to Mr. Downie, and the responsibility for bottom current data handling, before it was abandoned for EPRF modelling, belonged to Mr. Turner. Mr. Butler had the primary responsibility for computer programming and for interfacing data management with other team members; he also assumed the responsibility for wave and surge data after Mr. Downie left. Dr. Riffenburgh had early responsibility for part of the archive search and later overall responsibility; he was completely responsible for the data analysis methodology and the report's preparation.

ASSISTANCE

Following Mr. Potter's departure, Mr. Edward Tunstall of NUC, on leave for doctoral studies at SIO, served as a consultant in physical oceanography; however, errors remaining in this work must be considered the responsibility of Dr. Riffenburgh. Outstanding assistance was given by Mr. Jerry Giefer, Water Resources Center Archives Librarian, UCB, and Ms. Margaret Robinson, SIO. Professor Robert Wiegel, UCB, provided several telephone consultations. The Department of Oceanography and the library, NPGS, gave many hours of dedicated assistance. EPRF, Monterey, donated considerable manpower to provide a bottom-current model when CUARO funds were inadequate to cover the entire cost of the project. Dr. William G. Van Dorn inspired our approach to tsunamis, and Mr. James L. Cairns, SIO, on leave from NUC, suggested many improvements to the manuscript.

*"The fecundity of the unexpected far
exceeds the statesman's prudence."*

— *Pierre Joseph Proudhon*

SUMMARY

PROBLEM

Prepare a reconnaissance report on the subsurface offshore conveyance of fresh water from northern to southern California by studying the physical properties of the oceanic water column, especially near the seafloor, along the California coast. Specifically, investigate the region between Crescent City and San Diego from the 20- to the 200-m depth contour.

RESULTS

All available data on relevant variables were analyzed to provide information for aqueduct planning decisions. The variables and analyses most influential in planning the California Undersea Aqueduct were divided into two categories: variables influencing the 100-year survival of the aqueduct (century risks) and variables influencing the construction and maintenance of the aqueduct.

Waves, surges, tsunamis, density, and light do not appear on the basis of reconnaissance data to pose insurmountable problems. Surface, water column, and bottom currents, including upwelling and internal wave phenomena, may or may not be prohibitive; data are inadequate, and additional information must be obtained from *in situ* observations. Canyons are not an insurmountable threat, but will pose innovative engineering challenges and probably be quite expensive. Additional data will also be required on these processes.

CONTENTS

GLOSSARY	viii
INTRODUCTION	1
DATA AVAILABILITY AND SOURCES	4
Organizations and Individuals Contacted	4
Density: Data Availability and Sources	5
Waves: Data Availability and Sources	5
Currents: Data Availability and Sources	6
Tsunamis: Data Availability and Sources	6
Light Transmission: Data Availability and Sources	6
DEVELOPMENT OF METHODOLOGY FOR 100-YEAR EXTREMES	7
DATA ANALYSIS OF CENTURY RISKS: THEORY, ASSUMPTIONS, AND CALCULATIONS	11
Density on the Bottom	11
Bottom Surge	12
Bottom Currents	14
Tsunami Surge on the Bottom	16
RESULTS AND DISCUSSION OF CENTURY RISKS	89
Density on the Bottom	89
Bottom Surge	97
Bottom Currents	97
Tsunami Surge on the Bottom	97
CONSTRUCTION VARIABLES	111
General Approach to Construction Variables	111
Density	112
Waves and Bottom Surge	112
Surface Currents	118
Bottom Currents	118
Light Transmittance	134

PROBABILITIES OF CONFLUENCES OF SURVIVAL THREATS TO THE CUA	136
CONCLUSIONS AND RECOMMENDATIONS	141
REFERENCES	142
APPENDIXES:	
A. Institutional Sources of Archived Data	145
B. Individuals as Sources of Data	147

GLOSSARY

AMBAG	Association of Monterey Bay Area Governments
CalCOFI	California Cooperative Oceanic Fisheries Investigations
CSUSD	California State University, San Diego
CUA	California Undersea Aqueduct
CUARO	California Undersea Aqueduct Reconnaissance: Oceanography
EPRF	Environmental Prediction Research Facility
GRD	Geological Research Division
IGPP	Institute of Geophysics and Planetary Physics
MLRG	Marine Life Research Group
MPL	Marine Physical Laboratory
MTC	Marine Technology Center
NCEL	Naval Civil Engineering Laboratory
NMFS	National Marine Fisheries Service
NOAA	National Oceanic and Atmospheric Administration
NPGS	Naval Postgraduate School
NUC	Naval Undersea Center
ORD	Oceanic Research Division
SCCWRP	Southern California Coastal Water Resources Project
SIO	Scripps Institution of Oceanography
UCB	University of California, Berkeley
UCSD	University of California, San Diego
USC	University of Southern California
USCGS	United States Coast and Geodetic Survey
USGS	United States Geological Survey

INTRODUCTION

With the excessive growth of population resulting in increased demands for the movement of personnel and goods and with diminished space and inflated construction and maintenance costs, serious consideration is frequently being focused on novel systems of transport. Among these is a transport structure on the seafloor in coastal waters. One coast with a very large amount of transport, and which is experiencing a rapidly increasing need for even more transport, is the California coast.

While many transport needs are of interest and should be considered, one which has the potential for erupting into demands involving economic, political, and international aspects is the transport of water. Southern California uses a considerable portion of water from the Colorado River and California's Central Valley. It is possible that the Colorado River Basin, Mexico, and the Central Valley regions will demand large proportions of their water, possibly with limited notice, forcing southern California to find water elsewhere. One potential source is the considerable runoff into the sea from the Klamath and Eel Rivers in northern California. Such a situation would immediately call to mind the possibility of an undersea aqueduct from northern to southern California. The U. S. Bureau of Reclamation was requested by the 90th Congress to prepare a reconnaissance report on the subsurface offshore conveyance of water for such a route. The Bureau of Reclamation formed the California Undersea Aqueduct (CUA) study team. The Naval Undersea Center assisted the CUA study team in the oceanographic aspects of the reconnaissance. This report represents the California Undersea Aqueduct Reconnaissance: Oceanography (CUARO).

The objective was to study the physical properties of the oceanic water column, especially near the seafloor, along the California coast. The region of interest to CUA planners was between Crescent City and San Diego, from the 20-m depth contour to the 200-m depth contour (this region will be called the CUA strip in this report). The study consisted of searching out and acquiring all available data on relevant variables and analyzing these data to provide information on which to base aqueduct planning decisions. The variables and the analyses believed to be most influential in planning the CUA can be divided into two almost disjoint categories: variables influencing the 100-year survival of the aqueduct ("century risks") and variables influencing the construction and maintenance of the aqueduct. The variables within each category are listed in table 1.

To enable the reader to visualize coastal locations and their characteristics, a chart of the coastline is included in a pocket in the back of this report. This figure, the California Undersea Aqueduct Region Location Chart, presents the California coastline in a 5-ft long strip (scale: approximately 1:866,000). The shaded portion represents the area of greatest interest to CUA planning, *i.e.*, that between the 100- and 200-m depth contour.

Table 1. Variables, parameters, and physical causes for factors affecting the proposed California Undersea Aqueduct.

Century Risks		
Variable	Parameter	Influence and Source of Variable
Density: high Density: low (given as σ_t , where $\sigma = 1000(\rho - 1)$, where ρ is in g/ml)	The most extreme value to be expected in 100 years in terms of confidence bounds from probability distributions. Distributions generalized from existing data to entire coastline between the 20- and 200-m depth contours.	Controls the buoyancy of pipeline, which influences vertical stress or movement (sinking and floating), affecting mooring. σ_t depends upon temperature and salinity.
Bottom surge (given in cm/sec of water speed)		Horizontal cyclic water advection over the seafloor influences horizontal stress or movement and lift. Surge depends on bottom depth and on surface wave height and length, which result from storm winds.
Bottom current (given in cm/sec of water speed)		Horizontal and continuous water advection over the seafloor influences horizontal stress or movement and lift. Current depends on permanent current component, tides, and wind of long fetch and duration.
Tsunami surge (given in cm/sec of water speed)	Single surge values calculated for 20, 50, 75, 100, 150, and 200 m over the entire coastline from worst tsunami in over 100 years.	Horizontal "occasional shock" water advection over the seafloor influences horizontal stress or movement and lift. The "one shot" tsunami surge depends on the height of a seismic sea wave and the depth and slope of the seafloor.

Table 1. Continued.

Construction Variables		
Variable	Parameter	Influence and Source of Variable
Density: surface (given as σ_t , where $\sigma = 1000 (\rho - 1)$, where ρ is in g/ml) Density: 50 m (given as σ_t , where $\sigma = 1000 (\rho - 1)$, where ρ is in g/ml) Density: 200 m (given as σ_t , where $\sigma = 1000 (\rho - 1)$, where ρ is in g/ml)	Averages and standard deviations in the aqueduct region for winter and summer for locations at which data were found.	Controls buoyancy affecting sinking, manipulation, installation, and repairing of pipe sections.
Waves, surface (given in m of wave height)	Averages and standard deviations at surface above 20-, 50-, 100-, and 200-m depth for winter and summer for locations at which data were found.	Influences station-keeping and stability of platforms used in construction and maintenance operations; wind determined.
Surge, bottom (given in cm/sec of water speed)	Averages and standard deviations at 20-, 50-, 100-, and 200-m depth for winter and summer for locations at which data were found.	Buffeting effect influencing manipulation, installation, and repairing of pipe sections, <i>i.e.</i> , drag and lift. Surge depends on surface wave height and length, resulting from storm winds, and on bottom depth.
Currents, surface (given in cm/sec of water speed)	Averages and standard deviations in aqueduct region for summer and winter for locations at which data were found.	Continuous surface-water advection influences station-keeping and sinking control of pipe sections. Current depends on permanent current component, tides, and wind of long fetch and duration.

Table 1. Continued.

Construction Variables		
Variable	Parameter	Influence and Source of Variable
Currents, bottom (given in cm/sec of water speed)	Averages and standard deviations at 20-, 50-, 100-, and 200-m depth irrespective of season. (Winter and summer bottom currents are similar except for a small summer decrease in the far south.) Only locations completely modelled are used; no data were found.	Continuous bottom-water advection influences manipulation, installation, and repairing of pipe sections by creating lift and drag.
Light transmittance (given in %/m)	Averages and standard deviations for 20- to 60-, 60- to 130-, and 130- to 200-m depth intervals for winter and summer for locations at which data were found.	Incident daylight has dropped below the human threshold by 50 m. Transmittance shows the capability of the water to be artificially illuminated. At 50 m and below, night work will be as efficient as day work.

To enable the reader to visualize coastal locations and their characteristics, a chart of the coastline is included in a pocket in the back of this report. This figure, the California Undersea Aqueduct Region Location Chart, presents the California coastline in a 5-ft long strip (scale approximately 1:866,000). The shaded portion represents the area of greatest interest to CUA planning, *i.e.*, that between the 100- and 200-m depth contour.

DATA AVAILABILITY AND SOURCES

ORGANIZATIONS AND INDIVIDUALS CONTACTED

The archives of institutions where relevant data were likely to be found were studied, and the persons responsible for data management and archiving were contacted for assistance. (See appendix A.) A number of individuals working in areas related to CUA interests and who might either have data or be able to recommend sources were also contacted. (See appendix B.)

Generally, the data were sparse and of poor quality for several reasons. The physics of the open sea are much simpler than for coastal areas, and open-sea results can be generalized

to much larger areas. Thus, it appears that researchers have felt that deep-sea research gives a larger return on the research dollar than near-shore work and have neglected the latter. Also, when data were present for coastal areas, they had often been subjected to inappropriate analysis techniques that were directly carried over from deep-sea work. For example, data were often averaged from nonrandomly positioned stations over a 1-deg square or even a Marsden square (10-deg square). In CUA analysis, information is often useless if amalgamated over more than 1-min squared, and even greater resolution is usually required for near-shore work.

For the majority of the California coast, especially in northern California, there were no usable data. When data were present, they were usually grossly amalgamated, rendering the information useless, and if the original data were present, they were neither representative nor random in either time or location (for a given time and location, each possible value given the same opportunity to occur). Furthermore, most stations did not have data taken near the bottom, the region of greatest interest to the CUA study. For the rare phenomena of greatest threat to an aqueduct, such as tsunamis, surges from severe storms, and locations of extreme bottom currents, no investigator has been successful in (or perhaps attempted) sampling velocity and stress variables. The CUARO team asked experienced oceanographers, divers, and others who had spent decades in interface with the sea for expert opinions to supplement the data. In the less obvious questions, experienced persons differed in their predictions of phenomena, judgment of what factors were the most influential under varying conditions, and time scales of likely events. This disparity apparently arose because the experienced personnel were experienced in only one or a few of the interacting variables, rather than having a system view of the problem.

DENSITY: DATA AVAILABILITY AND SOURCES

Oceanographic stations taken at sea are numerous; most provide temperature readings of some sort, and many also include salinity measurements. From these, theoretical densities can be calculated. However, because the gear was not lowered near the bottom in most experiments, the plethora of near-surface data curtails rapidly with depth, and data are very sparse in regions of prime interest to the CUA.

What data are available in a form sensitive to CUA needs have been collected mostly by the California Cooperative Oceanic Fisheries Investigations (CalCOFI) at standard stations over several years. The CUARO team obtained data types from CalCOFI for near-shore stations along the entire California coast and calculated temperature- and salinity-dependent densities, *i.e.*, σ_t (see Sverdrup, [1942]).

WAVES: DATA AVAILABILITY AND SOURCES

Wave data in the form of sea state observed by sailors are plentiful. Dependable measurements under storm conditions exist, but are rare, and measurement of bottom surge past the surfline is almost nonexistent.

After considerable examination of available data sources, the following were selected: Bixby [1962], Humble [1970, 1971], Marine Advisors [1961], National Marine Consultants [1960, 1960], Oceanographic Services [1969], Pierson [1955], Sverdrup [1942], and Wiegel [1964].

CURRENTS: DATA AVAILABILITY AND SOURCES

Surface current information is available as time averages over gross areas, but little exists as accurate data suitable for input into CUA planning. It was necessary to calculate current from tides, winds, and geostrophic flow. Calculations were simple vector addition of velocities given in the following references: CalCOFI Atlas No. 4 [1966], Naval Weather Service [1971], NOAA [1971 and 1972], and USCGS [1972].

Some time-dependent current measurements spaced throughout the water column, all located just off Santa Barbara, are given in Paquette [1972]. While the current values are not very useful in this context, the form of the probability distribution with time and the measures of spread should be applicable.

Strict bottom current information is almost nonexistent. Most experimenters do not lower their gear to the bottom because of the risk of loss and lack of interest. Dr. Douglas Inman, SIO, has placed current meters on the rim of La Jolla Canyon, but they have been lost by strong advective flow. Several investigators have also used bottom drifters, but an analysis of the data shows them to be useless for CUA purposes; samples are biased, no information on current speed or variability can be obtained, and only net distance and direction are available as opposed to the actual path taken. For bottom currents, the CUARO team was forced to depend entirely on computer simulation, which is discussed in the section, Data Analysis of Century Risks.

TSUNAMIS: DATA AVAILABILITY AND SOURCES

An extensive search produced no data on tsunami-generated bottom surge from actual measurements, and from all inquiries we are led to believe there are none. There do exist run-up and tide-gauge data from several tsunamis. However, because shore influences initiated hydrodynamic distortions which could not be filtered out in returning to the incoming wave location at sea, these data proved of no use in the back-extrapolation of beach data to the 20- to 200-m contour areas of CUA interest. There were two remaining possible sources of information: deterministic predictions from a model developed by Tetra-Tech, Inc., outlined in their brochure *'Deterministic Prediction of Tsunami Effects'* [1972], or use of Tetra-Tech data on dynamical topography of the sea surface to bring tsunami waves to shallow water by solitary wave theory, ignoring the subtleties of diffraction and other local influences. Tetra-Tech quoted the cost of their model for CUA purposes as \$600,000; the wave theory approach was chosen.

Tsunamis are rare, and there is no reason to believe that the present warning system will not be continued. Therefore, tsunamis are considered in this report only in the century risk section as affecting aqueduct survival.

LIGHT TRANSMISSION: DATA AVAILABILITY AND SOURCES

Two classes of available light transmission data are secchi disk measurements and alphameter measurements. Secchi disk measurements were dropped from consideration because they are only vertical, only surface, not susceptible to rigorous scientific calibration, and confounded with sunlight penetration. Six reports gave alphameter measurements, five

of which fell in the area between Monterey and San Francisco and the sixth between Santa Barbara and La Jolla. These reports were Baker [1970], Drake [1970], Labyak [1969], Shepard [1970], Soluri [1971], and Yeske and Waer [1968].

Most alphameter measurements have been taken at shallow depths, as evidenced by several authorities in addition to the archives search. The 100- and 200-m depths are virtually unexplored with respect to light transmission.

Light transmission is considered only as a construction and maintenance variable since it is believed that century extremes of light penetration into the water will pose no survival risk to the aqueduct.

DEVELOPMENT OF METHODOLOGY FOR 100-YEAR EXTREMES

Suppose there exists a probability density $f_X(x)$ on a variate X . Let us use X = wave height (vertical component of trough-to-crest distance) in meters as an example throughout this section; other variates follow the same theory and methodology, but have different forms of $f_X(x)$. We are concerned with extreme values. In our example, we wish to predict the greatest wave height which will occur in the next hundred years. The first impulse is to find b such that

$$P[X \leq b] = \int_{-\infty}^b f(X) dX = 1 - \alpha, \quad (1)$$

and then to say, "We are $100(1 - \alpha)$ percent confident that the greatest value on X which will ever be observed is b ." However, several objections occur in this approach. (1) Gumbel [1958] has shown that extreme values, or records, over a time period increase monotonically with the length of the time period, so that no "greatest . . . ever be observed" is possible to predict. (2) The physical circumstances which generate common values on X may be sufficiently different from those which generate record values so that influences found to be negligible in one may be important in the other and *vice versa*. Thus, the probability distribution for common occurrences may be different from that for extremes. (3) The difference between the true and assumed probability densities may become large in the tails. Consider figure 1. In this figure, f_X represents the assumed probability density, the one we can manipulate and calculate, and g_X represents the true density, which we can never know. If f_X should deviate very far from g_X , empirical frequency distributions of samples from g_X would so indicate in the region of the bulk of observations; herein lies the problem. The bulk of observations are in the central part of the curve. The reasonable agreement lies in the central region, not in the extremes. Traditional statistical methods study central parameters and variability about central parameters; the area under a tail is used only for measuring the separation between values of central location or central variability parameters. For example, in figure 1, the difference between the two curves, *i.e.*, the percent error in density in assuming f_X when g_X is true, is about 6 percent in the vicinity of the mean, but it is about 400 percent in the vicinity of point a .

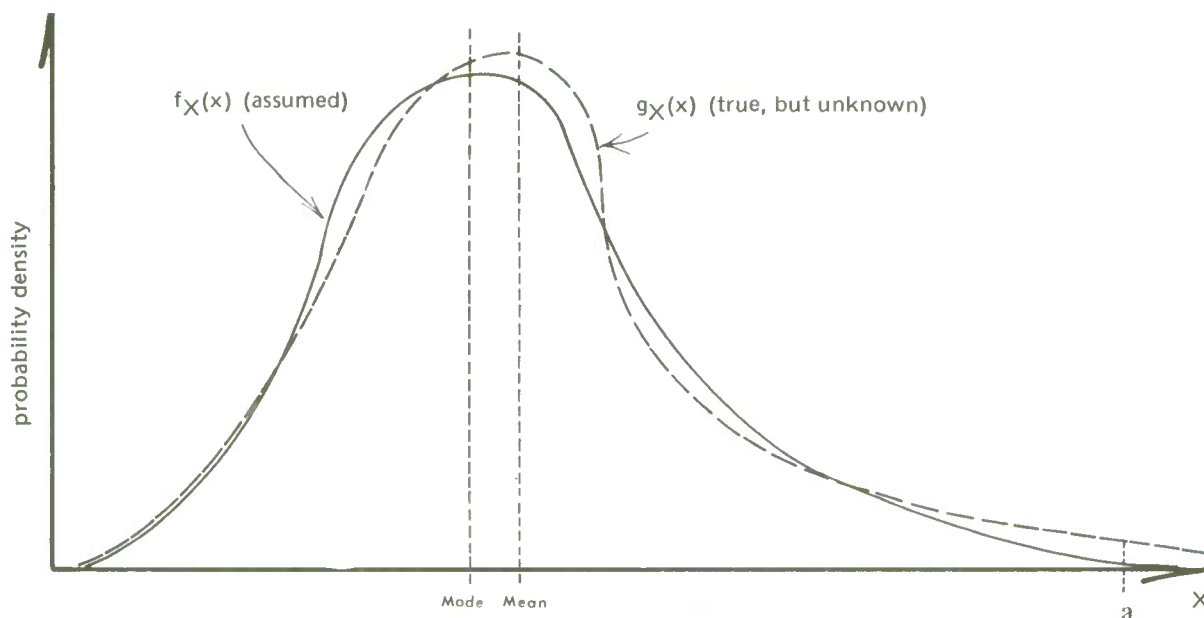


Figure 1. Examples of true and assumed probability distributions.

What we require is the probability distribution of extreme values. Gumbel [1958] and Borgman [1961] have derived probability distributions for the number of times an existing record will be exceeded during an ensuing time interval of given length, but they say nothing of the values of the exceedence. Thompson [1969] proved that the distribution function of the values of the extremes follows the form

$$H_X(x) = e^{-e^{-(x-\beta)/\gamma}} \quad (2)$$

for the parameters

$$\beta = \text{mode}(x) \text{ and } \gamma = (\sqrt{6}/\pi) \times (\text{standard deviation of } x). \quad (3)$$

$h_X(x)$, the density associated with the distribution $H_X(x)$, is illustrated in figure 2 in its relation to g_X . Although Thompson has given the form of h_X , observations from h_X are not available to estimate the parameters of h_X , and we have been able to find no general development in the literature which allows observations from g_X to estimate h parameters. The analytic derivation of an approximation to h_X has appeared in the literature for only certain of the g_X forms we use, and even for those forms sample sizes and time interval relations prevent the approximation from being adequate in many cases. (For a review of such work, see Barlow and Singpurwalla [1972].) Since any analytic method developed must depend on the form of g_X , necessitating a new development for each form of g_X , we developed a simulation algorithm to be utilized on a computer so that the same program could be used for any g_X . Steps in the simulated algorithm are listed on page 10.

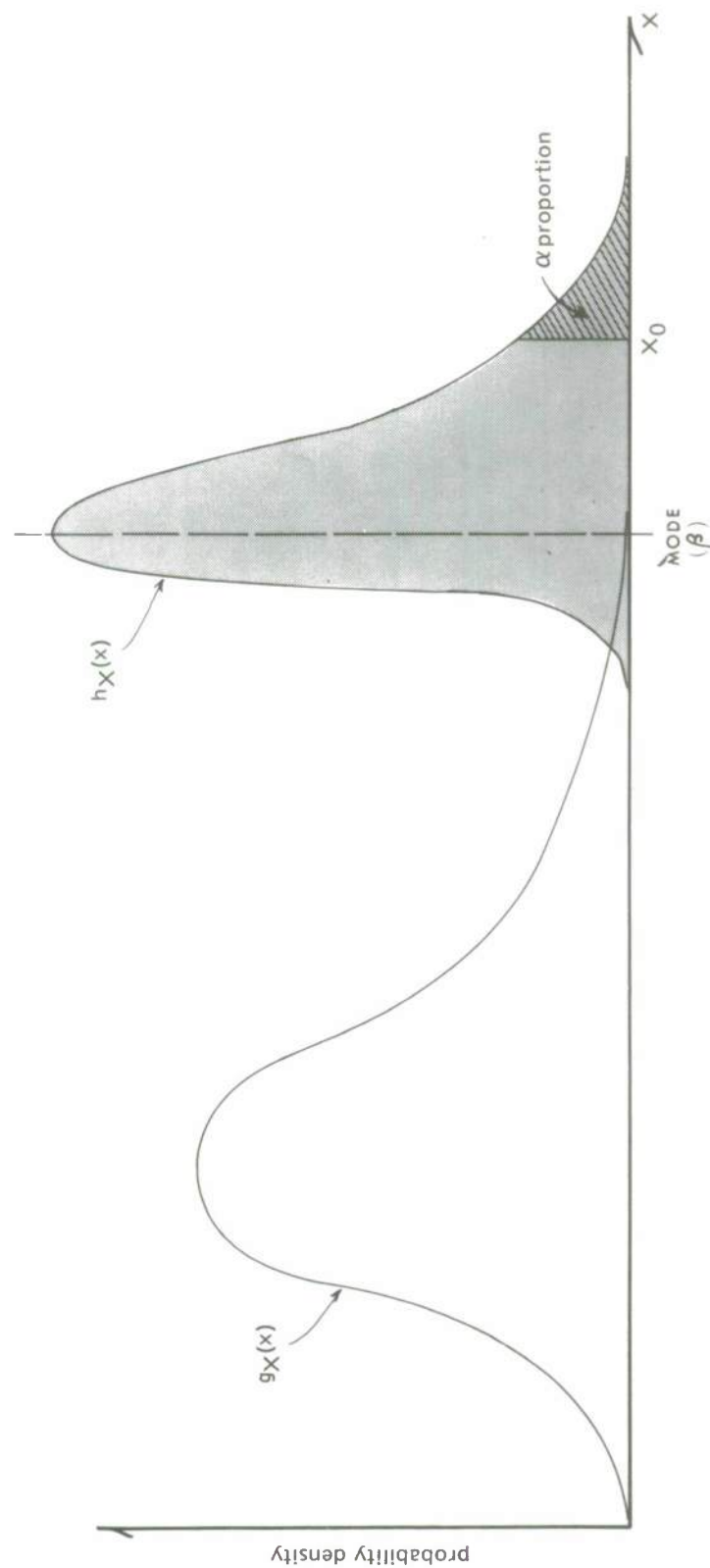


Figure 2. The Thompson extreme distribution h_X on the tail of g_X .

1. Obtain observations (x) on X . Desirably, x can appear only at discrete time intervals of, say, t_0 in length. For example, if X is the wave height during a storm and there are about three storms per year, then t_0 is about 4 months. Alternatively, X may be continuous, in which case x_t (x at time t) may be correlated with $x_{t+\epsilon}$ (ϵ small and positive) because of continuity constraints of the physical process. Worse, a simulation sampling can yield an arbitrarily large extreme because any size sample may be taken from any nonzero time interval. As an *ad hoc* solution for CUA purposes, an arbitrary time period, say t_0 , was taken in continuous cases, and the midinterval or largest x in this interval was used as a datum. t_0 was chosen large enough to damp out the autocorrelation. An example of such a variable is the density of seawater, which exists and is measurable at any moment at any place in the sea.

2. Predict by f_X the functional form of g_X , and verify by goodness-of-fit tests on the empirical frequency function, which is illustrated in figure 3. Estimate parameters of f_X from data.

3. Using a computer, take a randomly chosen sample of n values drawn from the fitted f_X ; record the largest of the n values. Suppose we wish to predict the most extreme values on X to appear in the time interval t_1 ($> t_0$); for CUARO, $t_1 = 100$ years. Then $n = t_1/t_0$. This procedure provides one observation on X drawn from h_X , and satisfies objection 1. Steps 1 and 3 together satisfy objection 2.

4. Repeat step 3 m times ($m = 500$ for the CUA study), and use these m data from h_X to estimate the parameters β and γ of h_X . This step satisfies objection 3.

5. Find an x_0 so that $H_X(x) = 1 - \alpha$ by

$$x_0 = -\gamma \ell \eta [-\ell \eta (1 - \alpha)] + \beta \quad (4)$$

to compute a $100(1 - \alpha)$ percent confidence bound on the greatest value of X to be observed in time period t_1 . This bound, x_0 , is shown in figure 2.

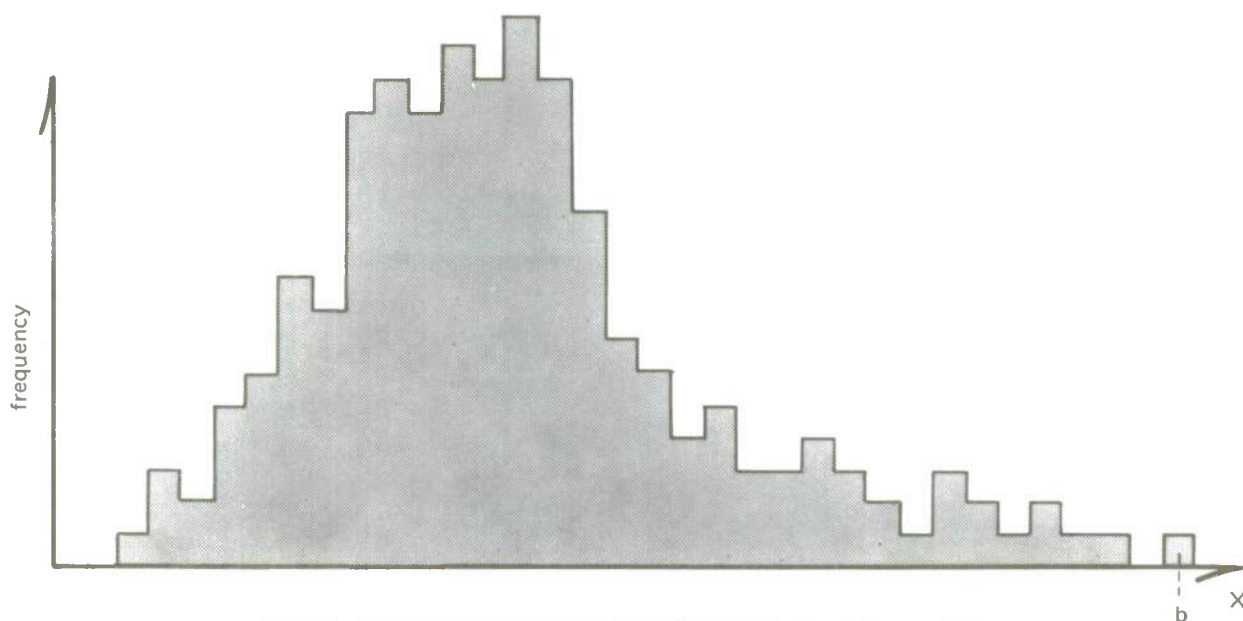


Figure 3. A possible random sample of 200 observations drawn from $g_X(x)$.

DATA ANALYSIS OF CENTURY RISKS: THEORY, ASSUMPTIONS, AND CALCULATIONS

DENSITY ON THE BOTTOM

Our major concern with density is its effect on aqueduct buoyancy. Phillips [1966] defines buoyancy as

$$b = -g \left(\frac{\rho - \rho_0}{\rho_0} \right),$$

where g is the gravitational constant, ρ is the buoyancy of the object or water body in question, and ρ_0 is the average density of the world's oceans. For CUARO purposes, ρ_0 will represent the average density at a potential aqueduct location rather than a world average. When extremes are calculated, b will be obtained for coastal water bodies with the highest and lowest values of σ_t , using a " ρ_t " defined as $1 + \sigma_t \times 10^{-3}$. When the CUA planning team considers potential materials for aqueduct construction, they may calculate b for each material for each location as needed; however, they must use ρ and not ρ_t .

It was desired to estimate 100-year extreme values of σ_t . In accordance with the theory of the section, *Development of Methodology for 100-Year Extremes*, a t_0 of 2 months was found adequate to eliminate time-adjacent autocorrelation. The first σ_t in a 2-month interval was chosen, and the remainder dropped from consideration. σ_t was calculated from temperature and salinity measurements in cases for which it had not been previously calculated. Most density measurements did not fall in the 20- to 200-m CUA contour strip. To obtain enough data for analysis, and with the concurrence of the CUA Denver team, it was assumed that density for a depth z in the water column at any offshore station approximated the density where z was the actual sounding. For example, it was assumed that the density at the bottom in 100 m of water was the same as the density at 100 m in water of greater depth. Means, standard deviations, and empirical frequency distributions were obtained for the retained densities at CUARO standard depths (20, 50, 100, and 200 m) from amalgamations of observed densities at each location for which densities could be found. The amalgamations were performed ignoring upwelling. Because upwelling is a rather slow process relative to other variables, its influence should not be large, and because it is very local in both space and time, its influence in the century context is decreased. Most authorities believe that most upwelling influences occur too far offshore to affect the CUA strip. Samples with less than five observations were dropped from consideration as being too small to yield statistically reliable results. Because of absent data at some locations and depths and inadequate sample sizes at others, results could be given for only certain depths at some locations. Several consultants at SIO, NUC, and NPGS independently stated that the probability distribution of seawater density at a fixed location is normal in form. The empirical frequency distributions agreed; normality was accepted as an assumption. The extremes simulation algorithm was followed to obtain the probability distributions of extremely high and extremely low density values (as h_X) by making one simulation for each tail of the basic density distribution (as f_X). Confidence bounds were computed for levels of confidence of 0.80, 0.85, 0.90, 0.95, 0.96, 0.97, 0.98, 0.99, 0.995, and 0.999 for each available locale. These appear in the next section.

The next task was to generalize the density pattern from locations at which data were present to the entire California coast to permit the results to be displayed as overlay shadings (see figures 4 through 38, part A). The 99 percent confidence values were extracted from the tables, transferred to coastal charts, and contoured on the charts in the same manner that bathymetry is contoured. The shading differences were chosen to be approximately 10 percent of the area contained in the 20- to 200-m contour strip. The most extreme densities are dark gray (5 percent low tail, 5 percent high tail); the 10 percent of the area representing the medium extreme densities are light gray (half each tail); and the remaining 80 percent are unshaded (white). The outlines of the shaded strips were contoured and then filled in with the appropriate shading. While the large mylar charts (35 areas for each of four variables) are not reproduced in this report, the reproductions of reduced size (figures 4 through 38) will increase the understanding of the reader.

BOTTOM SURGE

Water particles in surface waves follow an orbital motion. However, when moving toward the bottom, the motion approaches a horizontal back-and-forth alternation or surge. Direct observations of bottom surge are virtually nonexistent. The necessary approach was to generate surface-wave extremes and carry the energy to the bottom via Airy wave theory.

For the generation of an extreme surge, data from the worst storm in several years were used, which obviated the continuous variate problem and provided a t_0 of 1 year. Means, standard deviations, and empirical frequency distributions were computed for amplitudes and periods of surface waves at each location where storm data were available. Consultants independently stated that storm wave amplitude and period would both be distributed as log normal in form, and the empirical frequency distributions agreed.

A log normal distribution is given by the form

$$f_X(x) = \frac{1}{\sqrt{2\pi}} X^{-1} e^{-(\ell\eta X - a)^2/2b^2}, \quad X > 0, b > 0, \quad (5)$$

where a and b are parameter estimates obtained by

$$a = -\frac{1}{2} \ell\eta [s^2 e^{-4\ell\eta \bar{x}} + e^{-2\ell\eta \bar{x}}] \quad (6)$$

and

$$b = (2\ell\eta \bar{x} - 2a)^{1/2}, \quad (7)$$

where \bar{x} is the sample mean and s is the sample standard deviation. Using these parameter estimates and the log normal f_X assumption, the extremes simulation algorithm was followed to obtain the probability distributions h_X of extremely high waves and long periods.

From Wiegel [1964], surge velocities associated with the extreme waves of the century were computed. If z denotes water depth, L denotes wave length, H denotes wave height, and T denotes wave period, the bottom surge velocity V is given by

$$V = \frac{\pi H}{T} \times \frac{1}{\sinh(2\pi z/L)} \quad (8)$$

The functional relationship to find L in intermediate water ($\frac{L}{20} < Z < \frac{L}{2}$) from known variables such as T and/or H is not explicit. A computer convergence routine was used to approximate L from Wiegel's Eq. (2.39):

$$L = \frac{gT^2}{2\pi} \tanh \frac{2\pi z}{L} \quad (9)$$

To bring extreme waves into shore, fetch must be considered since the data stations are some miles out to sea. Any storm capable of generating the century's greatest wind wave must be large enough so that fetch will continue from a station into shore, unless hindered by a large physical impediment such as the Channel Islands. Thus, it was assumed that waves approaching the coast were wind driven throughout their path if north of Pt. Conception, but were carried into shore by wave propagation if in the lee of the Channel Islands. A graph in Pierson, Neuman, and James [1955] was used to obtain the effect of island protection on the wave parameters.

Bottom surge increases in a predictable form as depth diminishes until the wave breaks, after which the velocity probably remains the same or is perhaps slightly reduced (Le Méhauté [1955]). Breaking depth was obtained from another graphical relationship in Wiegel, and surge velocity was held constant at breaking velocity after breaking. Heights of breaking waves were calculated by a formula from Komar [1972].

Confidence bounds on the greatest wave height and length were computed from h_X for confidence levels of 0.80, 0.85, 0.90, 0.95, 0.96, 0.97, 0.98, 0.99, 0.995, and 0.999 for each available locale; the waves were brought in and down as previously discussed; and the respective extreme bottom surge velocities were calculated.

The next task was to generalize the bottom-surge velocity pattern from locations at which data were present to the entire California coast to permit the preparation of overlay shadings (figures 4 through 38, part B). The stations for which data were present were so patchy that the CUA strip could not be as dependably contoured as was density. The 99 percent confidence values were extracted from the tables and ordered. The upper quartile (which was found to be 134 to 290 cm/sec) was chosen for dark gray; the third quartile (68 to 127 cm/sec) was chosen for light gray; and the lower two quartiles (13 to 67 cm/sec) were unshaded. (The result is similar in shading ranges to the velocity breakdown for tsunamis, which had the two extreme deciles of the coastal area shaded like density.) The pattern became clear, and the simpler boundaries were contoured and filled in with the appropriate shading.

BOTTOM CURRENTS

In the absence of adequate data, the CUARO team sought guidance from scientists with personal knowledge of bottom currents, e.g., scuba divers* for depths of 20 to 50 m and submersible operators** for greater depths. The amalgamation of opinion was that bottom currents are directionally variable, their spatial average of time extremes will not exceed 75 cm/sec (a figure which agrees with results in Paquette [1972]), and in shallow water they are a much less severe problem than surge. Many consultants raised the question of canyon hydrodynamics, suggesting that it might be a serious problem in both aqueduct construction and survival. SIO has recently conducted studies, not yet published, into the theory of canyon flushing, which suggest severe velocity and turbulence problems. We entered into the computer simulations with these problems in mind.

Another complication is internal waves, which can reach the bottom as they come into the depths of CUA interest and thus act as currents. Little data were found, none satisfactory for CUA purposes. It is expected that no internal wave particle velocity will exceed 25 cm/sec and usually will be much less. With no data and no theory adequately advanced for modelling, the CUARO team found it necessary to neglect internal waves.

A search for modelling capability led to the Navy's Environmental Prediction Research Facility (EPRF), Monterey, which has further evolved the Hansen Hydrodynamical Model. (For a description, see Laevastu and Rabe [1972].) It is a numerical model which has proved successful in the North Sea, Mekong Delta, Barents Sea, San Diego Bay, Straits of Florida, and Strait of Gibraltar. It uses the sum of currents caused by geostrophic flow, tides, and winds to produce a new current velocity in the water column. Verification of the model's practical efficacy can be found in Hamilton and Laevastu [1972], Laevastu [1972], and Laevastu and Hamilton [1972a, 1972b]. The CUARO team contracted with EPRF to produce a modelling of areas with representative current-influencing parameters along the California coast. Funds limited the modelling to three areas: a flat-bottomed area (north of San Francisco), a steep rocky area (Big Sur area), and a canyon (Carmel Canyon). EPRF was requested to produce average and extremely high current outputs. The permanent current component is nearly the same in either case. Models with average and extreme tidal components were generated. The net wind component was set at 8-m/sec velocity for all modelling, but it was adjusted to 36 m/sec *a posteriori* by the CUARO team for extremes. The depth at which wind can be influential was computed by Ekman transport theory similar to that used by Hunkins [1966]. The depth of the frictional influence D has been given as

$$D = \pi \sqrt{a/\rho\Omega\sin\phi}, \quad (10)$$

where a denotes an eddy viscosity coefficient of approximately 100 g/cm sec^2 , Ω denotes an angular velocity of $0.729 \times 10^{-4} \text{ r/sec}$, and ϕ denotes latitude. D was calculated for latitudes from 42 deg (near Crescent City) in the north to 33 deg (near San Diego) in the south.

*Dr. Robert Dill of NOAA, Mr. Edward Tunstall of NUC and SIO, divers employed by Crescent City, Dr. Robert Riffenburgh of the CUARO team, etc.

**Dr. Dill, Mr. William Potter recently of the CUARO team, Mr. Neil Marshall of SIO, Dr. Eric Barham of NUC, etc.

D for Crescent City was about 44 m, and D for San Diego was about 49 m. With an exponential particle velocity diminution, frictional influence anywhere near the 44- to 49-m bound will be negligible. It may be concluded that wind influences are of concern only at the CUARO standard depth of 20 m.

Let us consider bounds on the wind components. Let us denote wind velocity by w (m/sec), depth by z (m), and particle velocity at depth z by V_z (cm/sec). The relationship of w to V_0 may be given by

$$V_0 = 3.8\sqrt{w} \quad (11)$$

where 3.8 is an empirical constant [Hubert and Laevastu, 1965]. Given surface flow V_0 , V_z may be related to z by

$$V_z = V_0 e^{-\pi z/D}, \quad (12)$$

when fetch and duration are large enough to reach equilibrium conditions, which is the case under extreme storm conditions. Some values of V_0 and V_{20} given by bounds of latitude for CUA are in table 2.

Table 2. Values for V_0 and V_{20} for CUA.

Location	Storm Wind Speed	
	Average ($w = 15.5$)	Extreme ($w = 36$)
V_0 at any latitude	15.0	22.8
V_{20} at 42 deg (Crescent City)	3.6	5.5
V_{20} at 33 deg (San Diego)	4.2	6.3

The output delivered by EPRF was remarkable in its detail. Very large changes, e.g., doubling of velocity, occur between two points perhaps 1 km apart. The variability in a grid of 15 or 20 km was so remarkable that a very sophisticated geodetic methodology appeared to be the only alternative to a complete modelling of the coastline, which was fiscally impossible. Attempts to develop such a geodetic methodology were not successful. However, in the process, the CUARO team became so familiar with the nature of current variability that they could predict EPRF's modelled output to a reasonable accuracy by examining the bathymetry. It was clear that current increased when entering an enshallowing region, roughly proportional to the gradient of the bottom, and decreased when entering a deepening region, roughly proportional to the reciprocal of the depth gradient. There are, of course, additional subtleties, such as how easily the water can escape from a rise. Also, the current increased when passing around a promontory, roughly proportional to the radius of curvature of its altered path, and decreased when expanding to fill a bay or passing into shelter from the primary current flow, roughly proportional to the reciprocal of the gradient of water volume

increase. These generalizations permitted contouring the coastline (figures 4 through 38, part C), although the process was more intuition than science. The CUARO team is confident that the figures will provide a very gross, but not incorrect, picture of bottom current behavior along the coast; however, no detailed planning should depend upon them.

The generation of extreme bottom current values for each locality was not possible because of local variability. However, an extreme for the coastline at large was reasonable and should prove of some value. The EPRF regions included areas of some of the coast's strongest local currents, including those in the Carmel Canyon vicinity. Under the assumption that the points showing the greatest currents in the modelled regions would not be very different in value from the points showing the greatest currents for other coastal regions, the greatest modelled currents could be considered representative of spatial extremes. The greatest velocities found are listed below.

	water column depth, m	20	50	100	200
and	greatest current velocity, cm/sec	169	150	214	224.

To use the extremes methodology, temporal (rather than spatial) distributions of current were necessary. The Hansen model yields deterministic results, which may be considered as expected or average. Thus, the spatial model output maximum was taken as the coastal mean for the maximum-generating location. Paquette [1972] shows the temporal distribution of currents at a location to be log normal in form and gives means and standard deviations over 45 sets of time-dependent data, varying from 277 to 170,127 observations per set. The standard deviation was plotted against the mean for these 45 pairs, which appear to be correlated where the standard deviation is a second-degree polynomial function of the mean. The standard deviation was extrapolated by this function to estimate its value for the coastal temporal mean of spatial maximum. These parameters, coupled with the log normal distribution assumption, were used in the extremes methodology to generate confidence bounds on the California coast's greatest bottom current at CUARO standard depths.

TSUNAMI SURGE ON THE BOTTOM

Tetra-Tech tsunami wave heights were inputs, and solitary wave theory was used to estimate the tsunami surge at the bottom. Wiegel [1964] gives formulae for converting an open-ocean tsunami wave height to a shallow water wave height and for converting shallow water wave height to horizontal bottom particle velocity. Let h denote open-ocean wave height, d_2 the depth at the outer edge of the shelf, d_1 the depth of the water where we seek bottom particle velocity, and g the gravitational constant. Then wave height H is given by

$$H = h[d_2/d_1]^{1/2} \quad (13)$$

and the horizontal bottom particle velocity V at d_1 is given by

$$V = H [g/d_1]^{1/2} \quad (14)$$

(Of course, they can be combined to

$$V = \frac{h}{d_1} \sqrt{gd_2} \text{ .) } \quad (15)$$

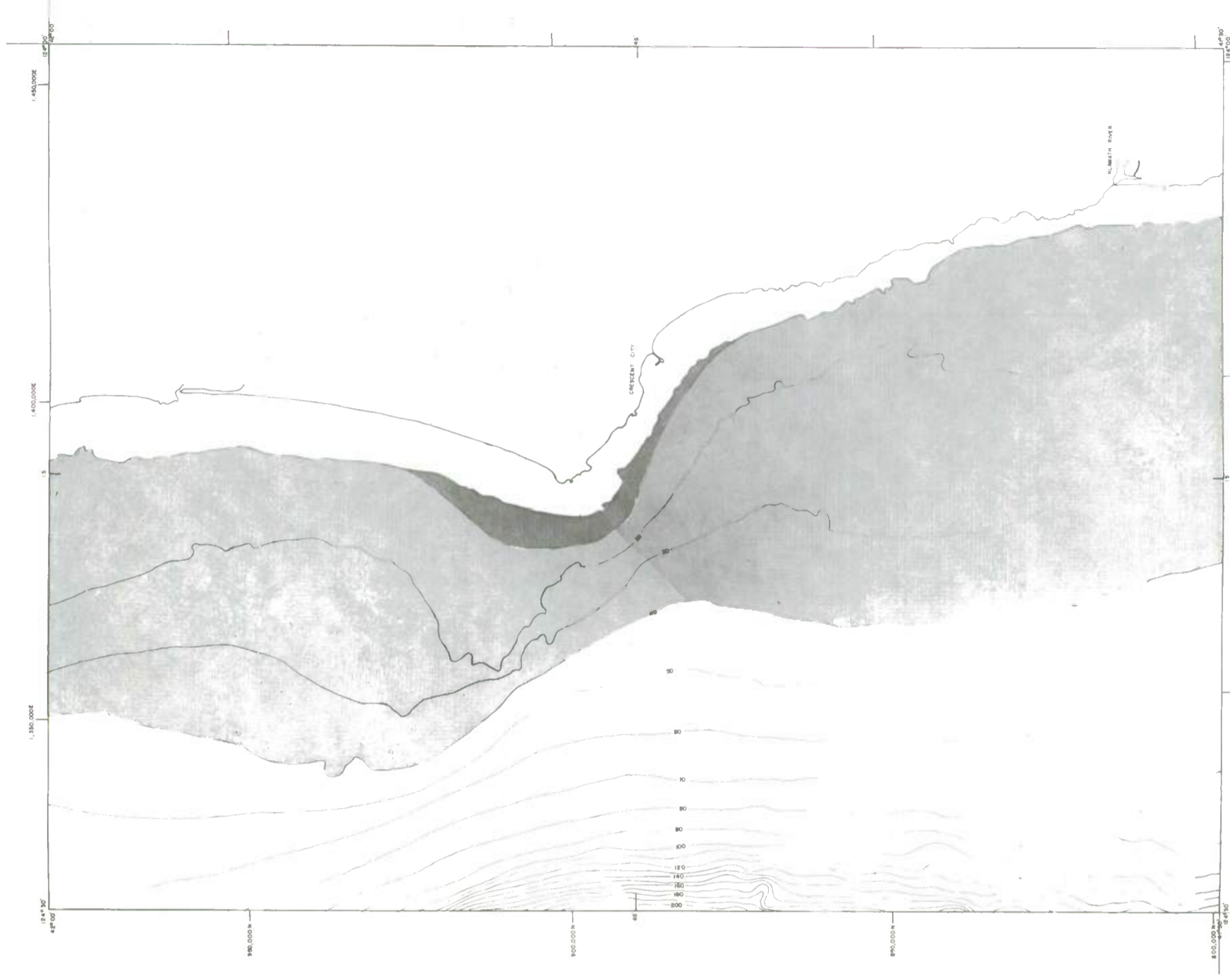
Data for a 100-year extreme were easy to obtain without using the extremes simulation algorithm. Data exist for open-ocean wave heights for the tsunami resulting from the 1964 Alaskan earthquake, which generated the worst tsunami forces on the California coast since a large but unmeasured tsunami in 1815. The availability of these data is fortunate since tsunami measurements are too sparse for adequate statistical sampling.

Tsunamis are waves of remarkable period — 10 minutes to 2 hours. The effects of local topography for a wave of such a long period are limited to features of approximately 130 km². Such waves virtually ignore coastal angles and even islands as large as the Channel Islands. It is possible that resultants of gross feature effects will be expressed in the form of trapped edge waves propagated along the coast in a highly localized manner and perhaps captured in basins and bights and converted to standing waves. A successful hydrodynamic treatment of such an event has not yet been made. However, it is the belief of at least one prominent tsunami expert (Dr. Van Dorn of SIO) that some damping will occur and that these effects are not likely to combine in a manner which would result in bottom particle velocities exceeding those predicted by the primary wave theory. It was accepted as a conservative (for CUA purposes) hypothesis that maximum bottom advection velocities were those predicted by solitary wave theory.

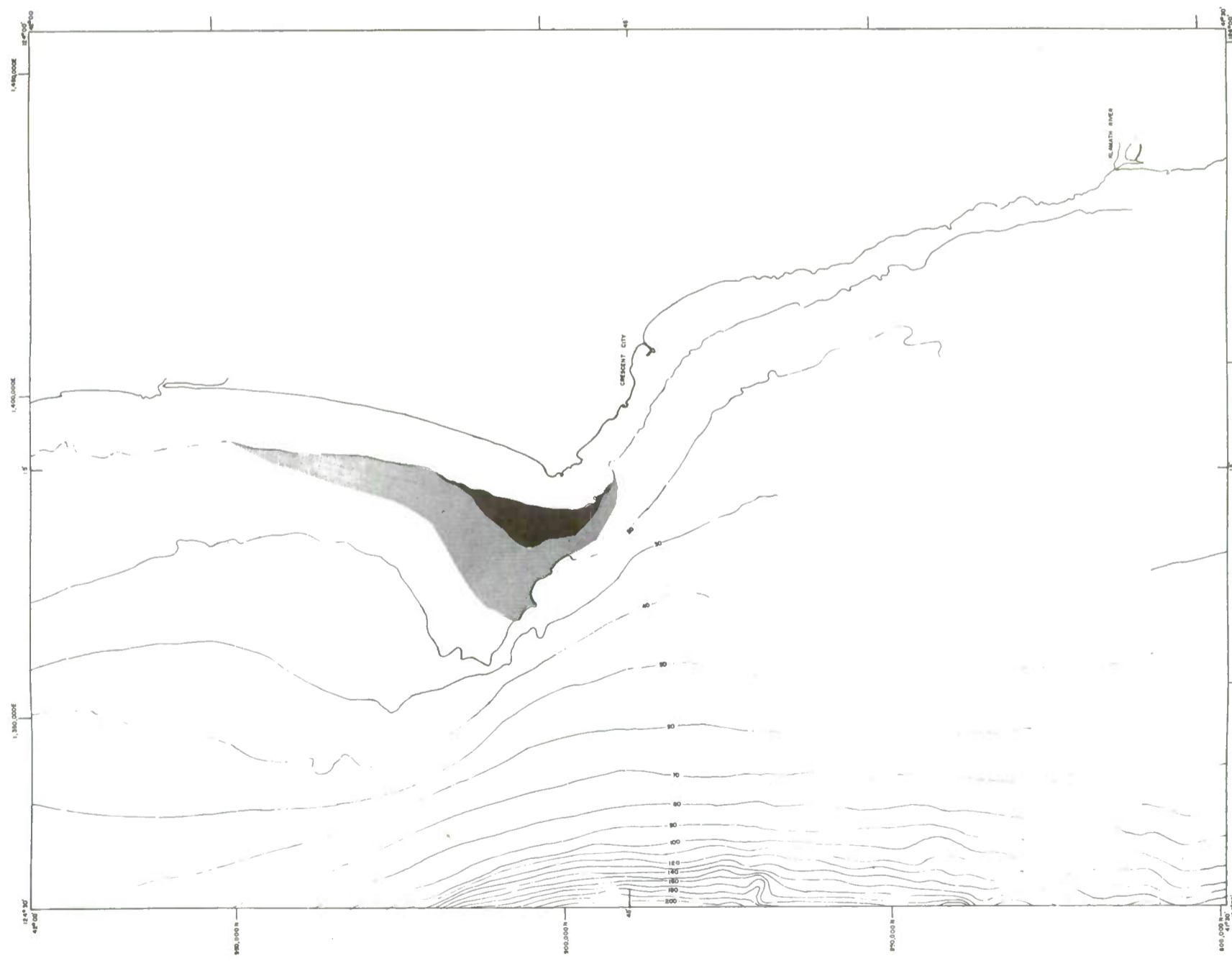
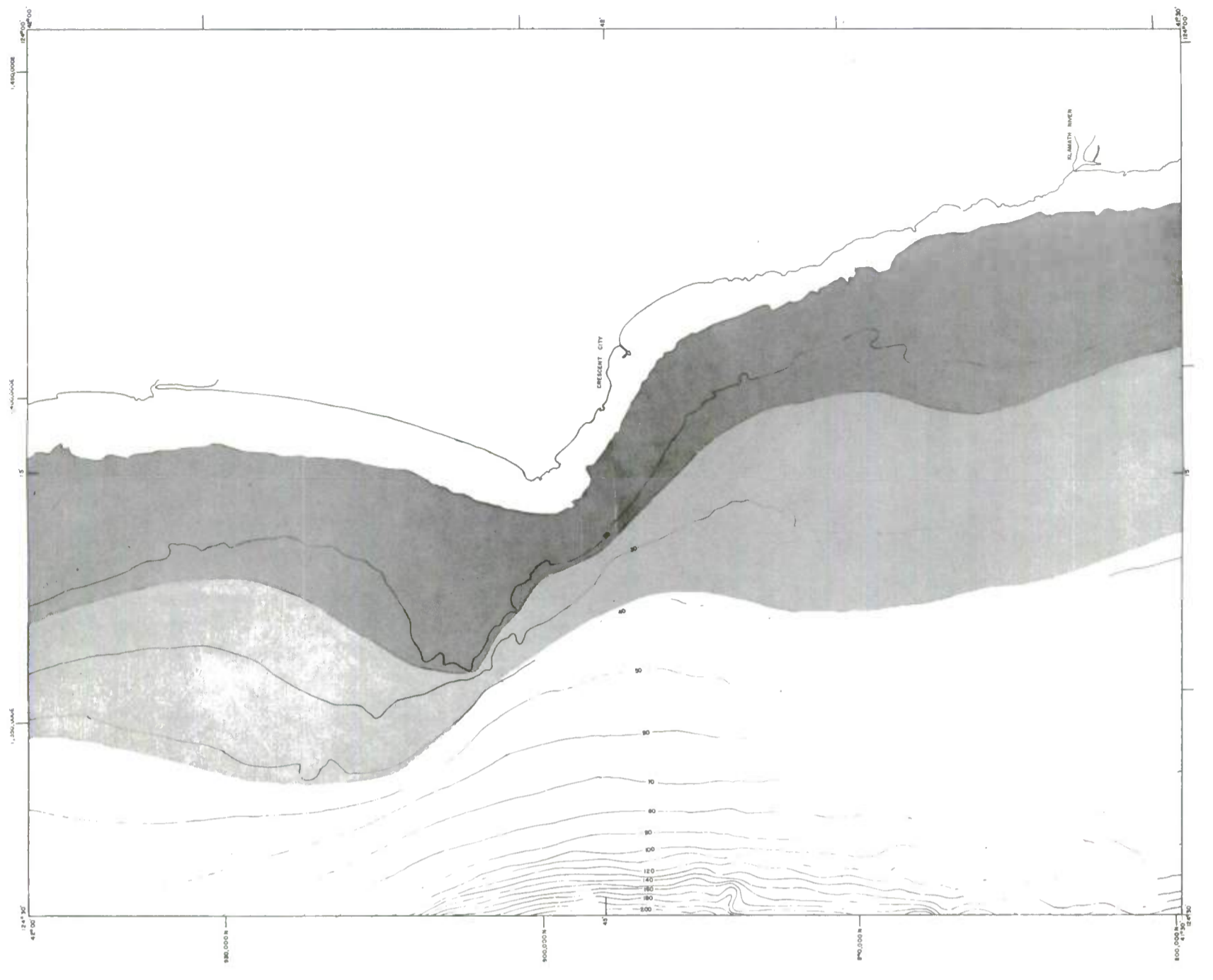
Bottom advection velocities for tsunami forces were predicted from the 1964 Alaskan earthquake data at equal intervals from Crescent City to San Diego at depths of 20, 50, 75, 100, 150, and 200 m. The resultant velocities were contoured. The upper decile area (area associated with the upper 10 percent of velocities) was taken as the region of dark gray shading, and the second upper decile area as the region of light gray shading. The shading limits were contoured, and the shading filled in (see figures 4 through 38, part D).

Figure 4. Predicted regions of century extremes for chart number 1.

Part A. Density.



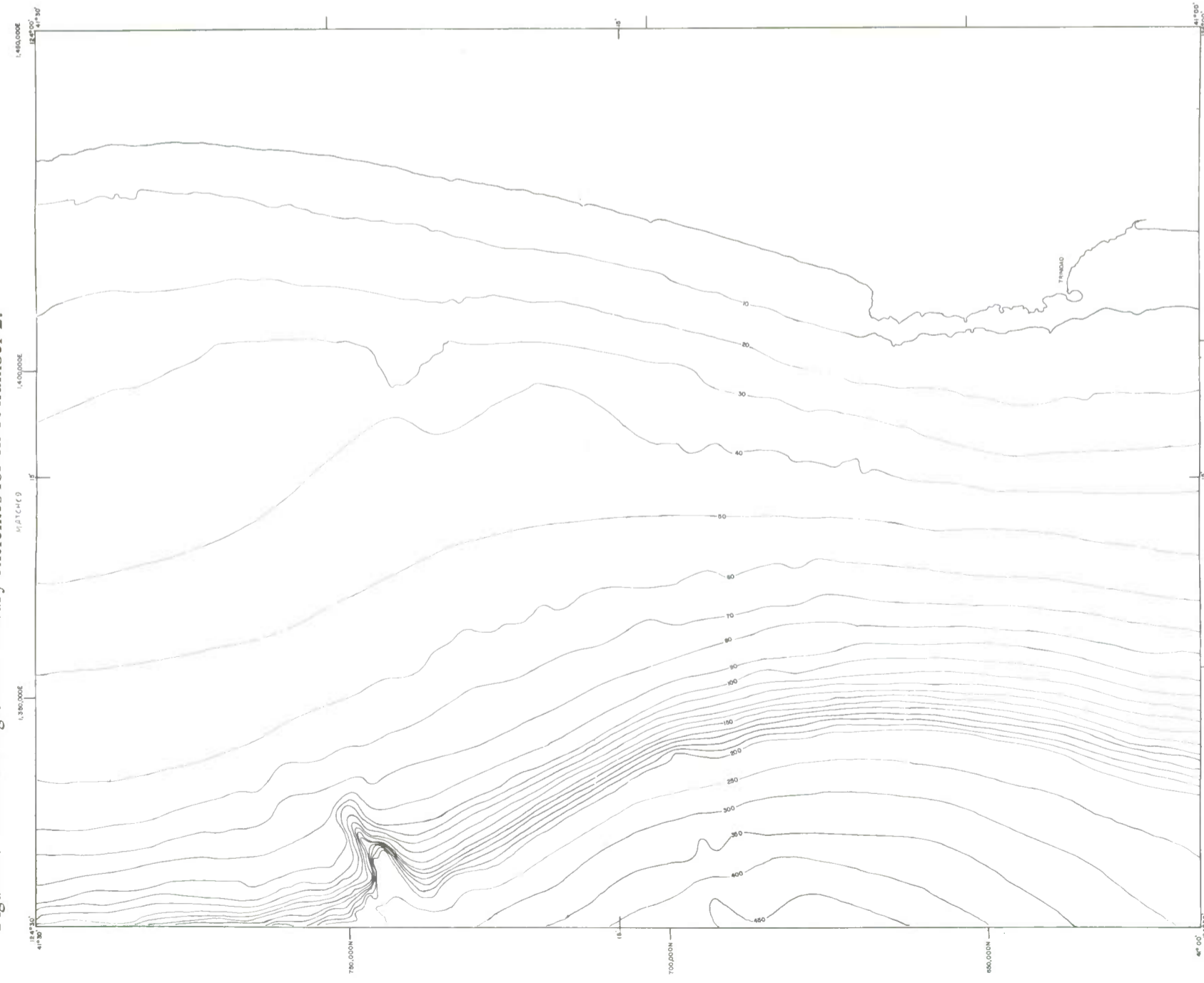
Part B. Bottom wave surge.



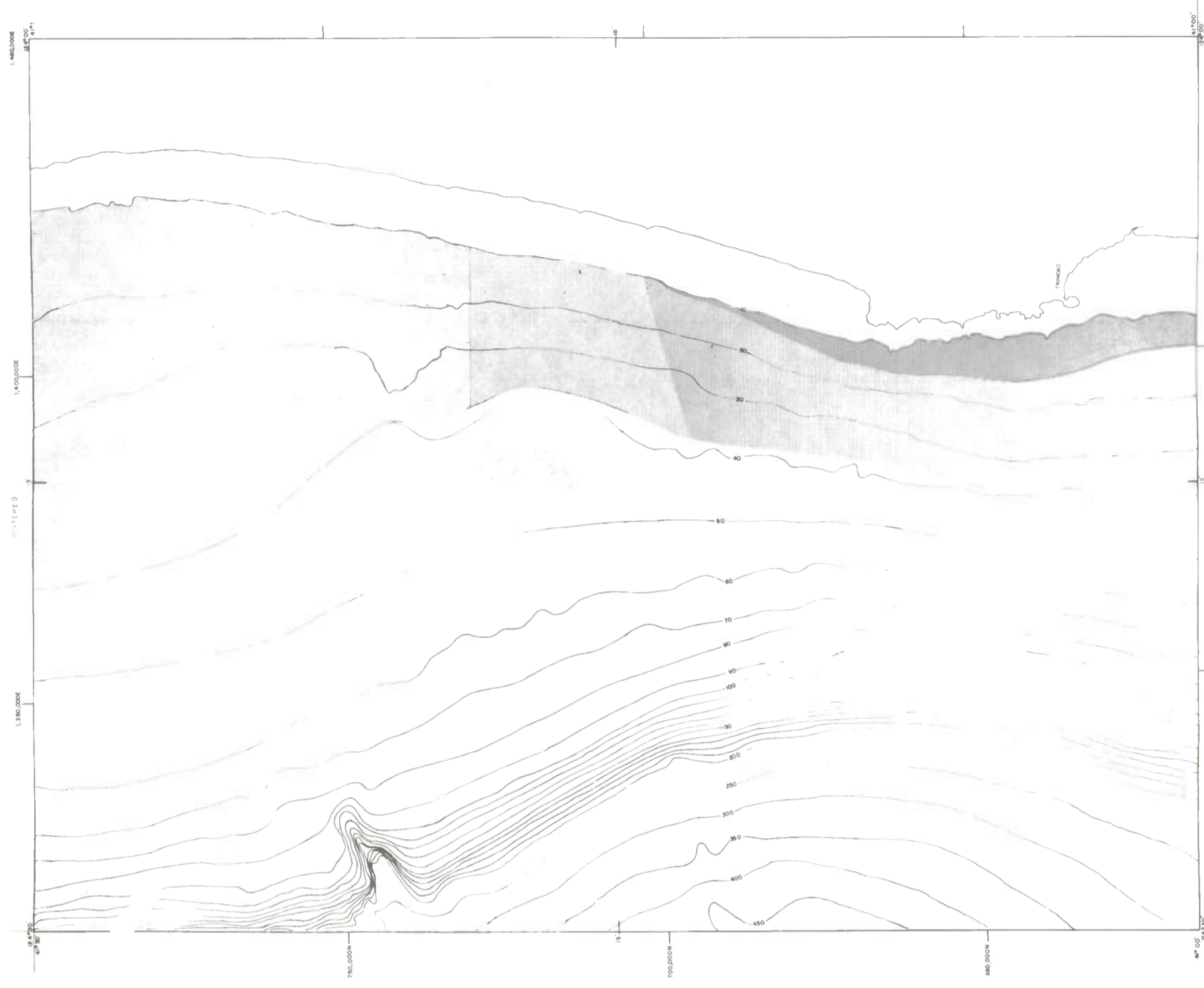
Part D. Bottom tsunami surge.

Part C. Bottom current velocity.

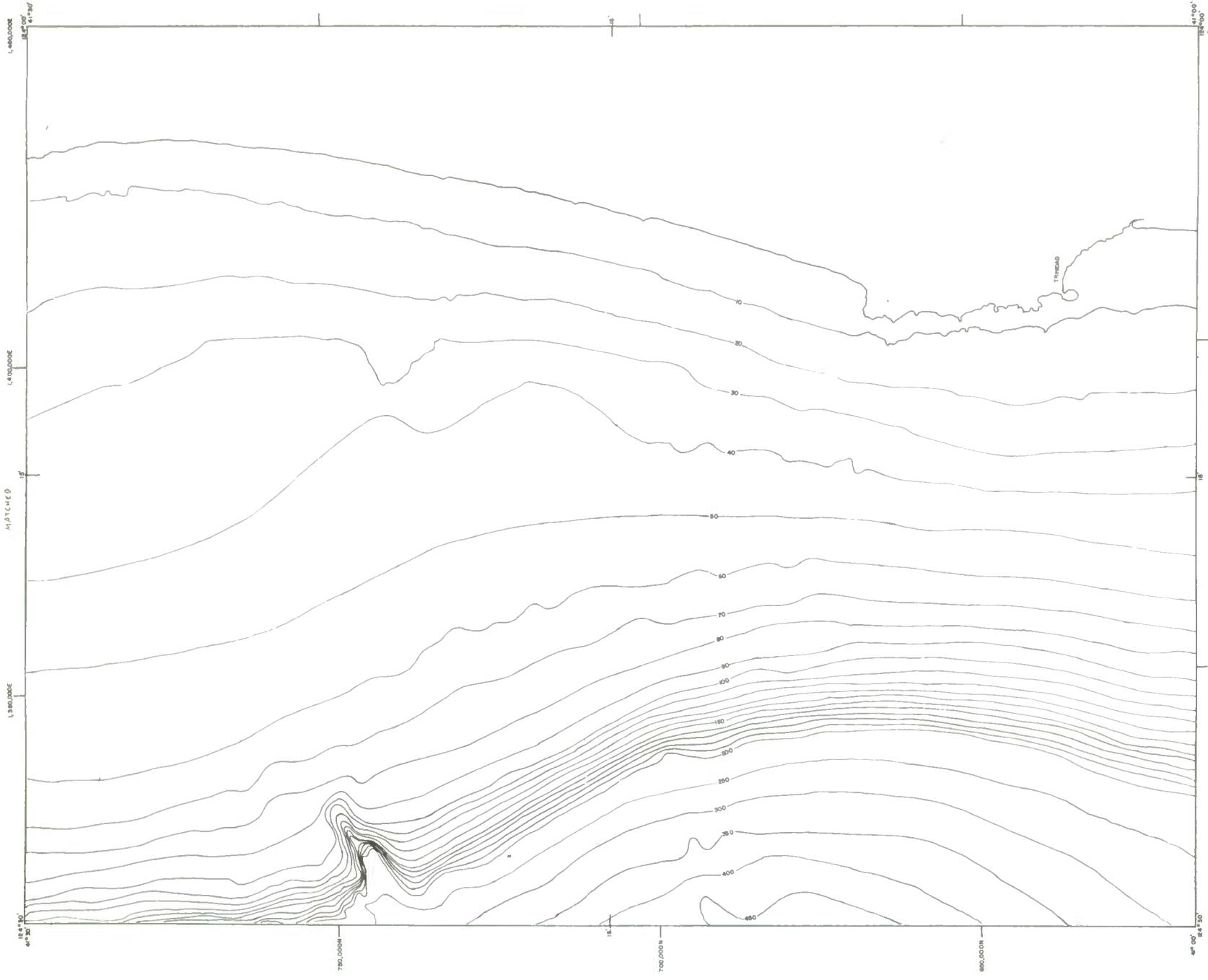
Figure 5. Predicted regions of century extremes for chart number 2.



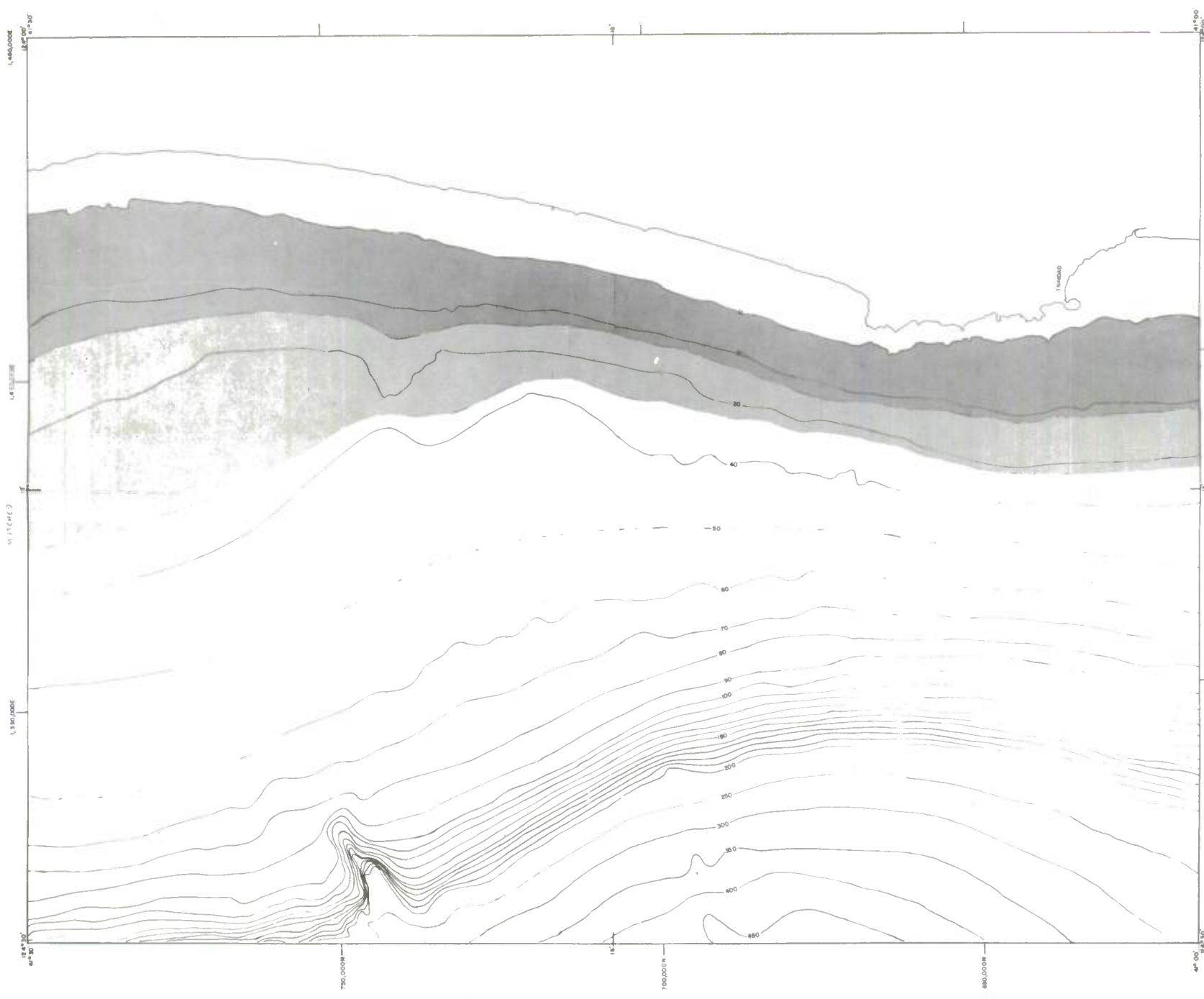
Part A. Density.



Part B. Bottom wave surge.



Part C. Bottom current velocity.



Part D. Tsunami surge.

Figure 6. Predicted regions of century extremes for chart number 3.

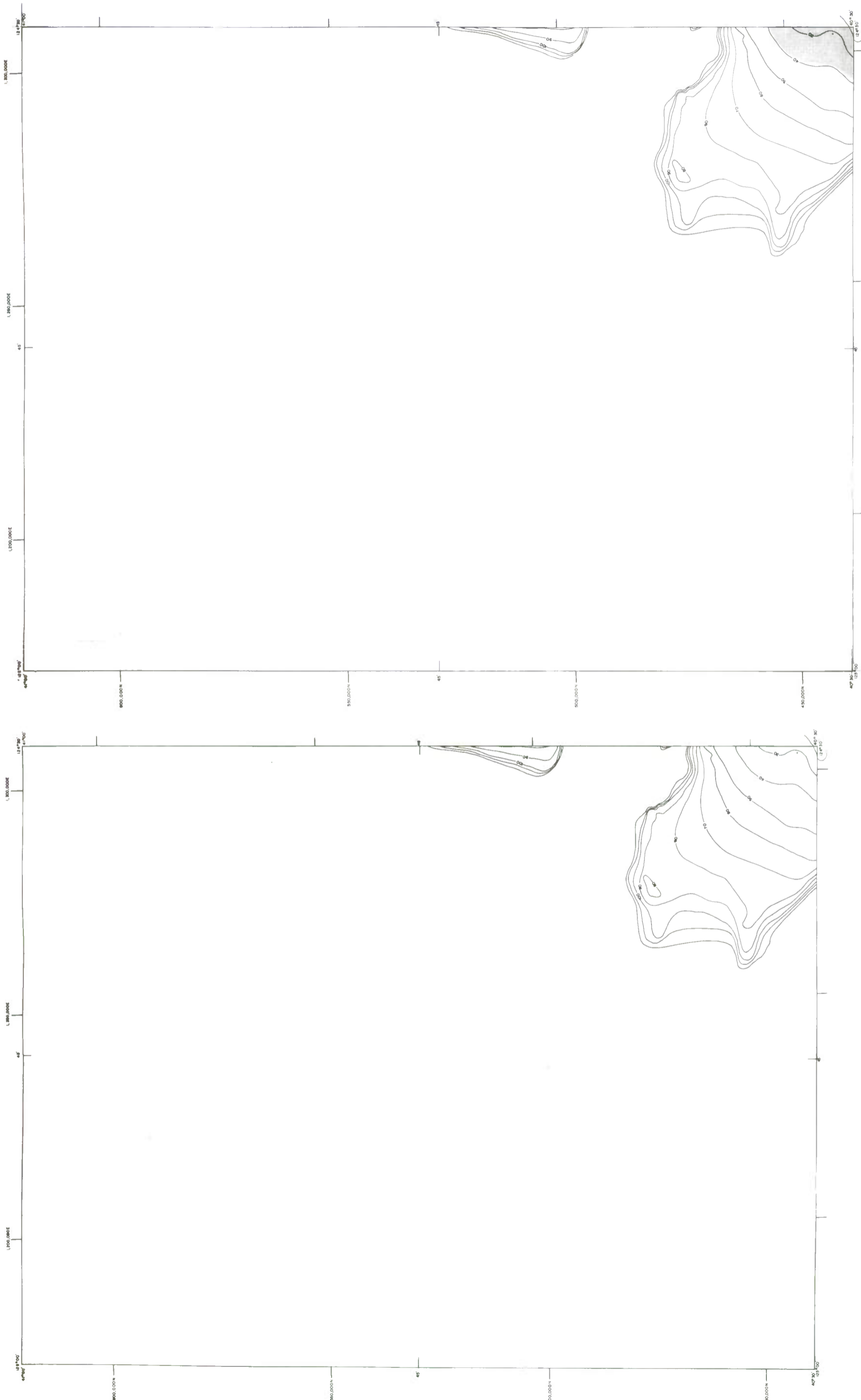
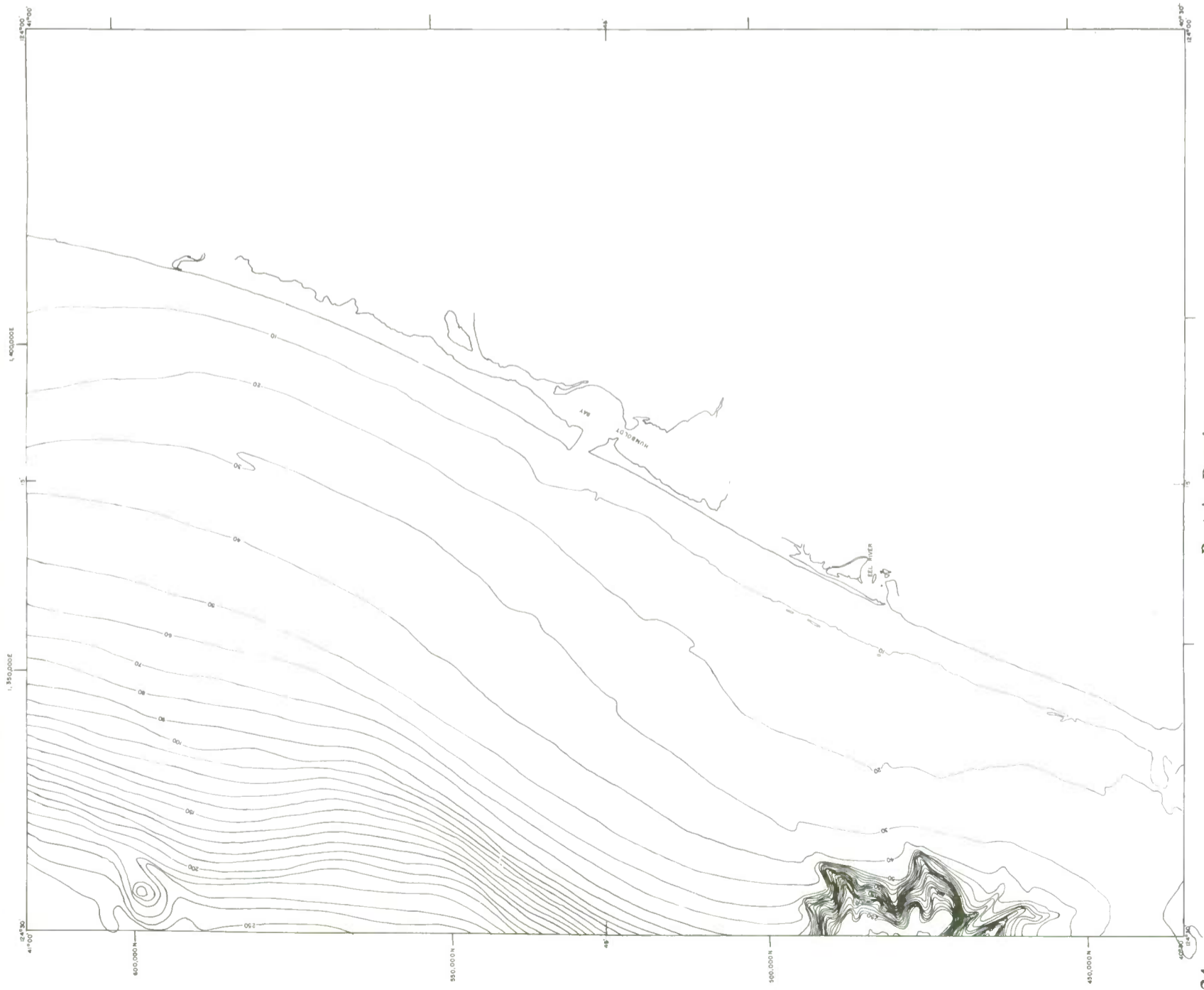
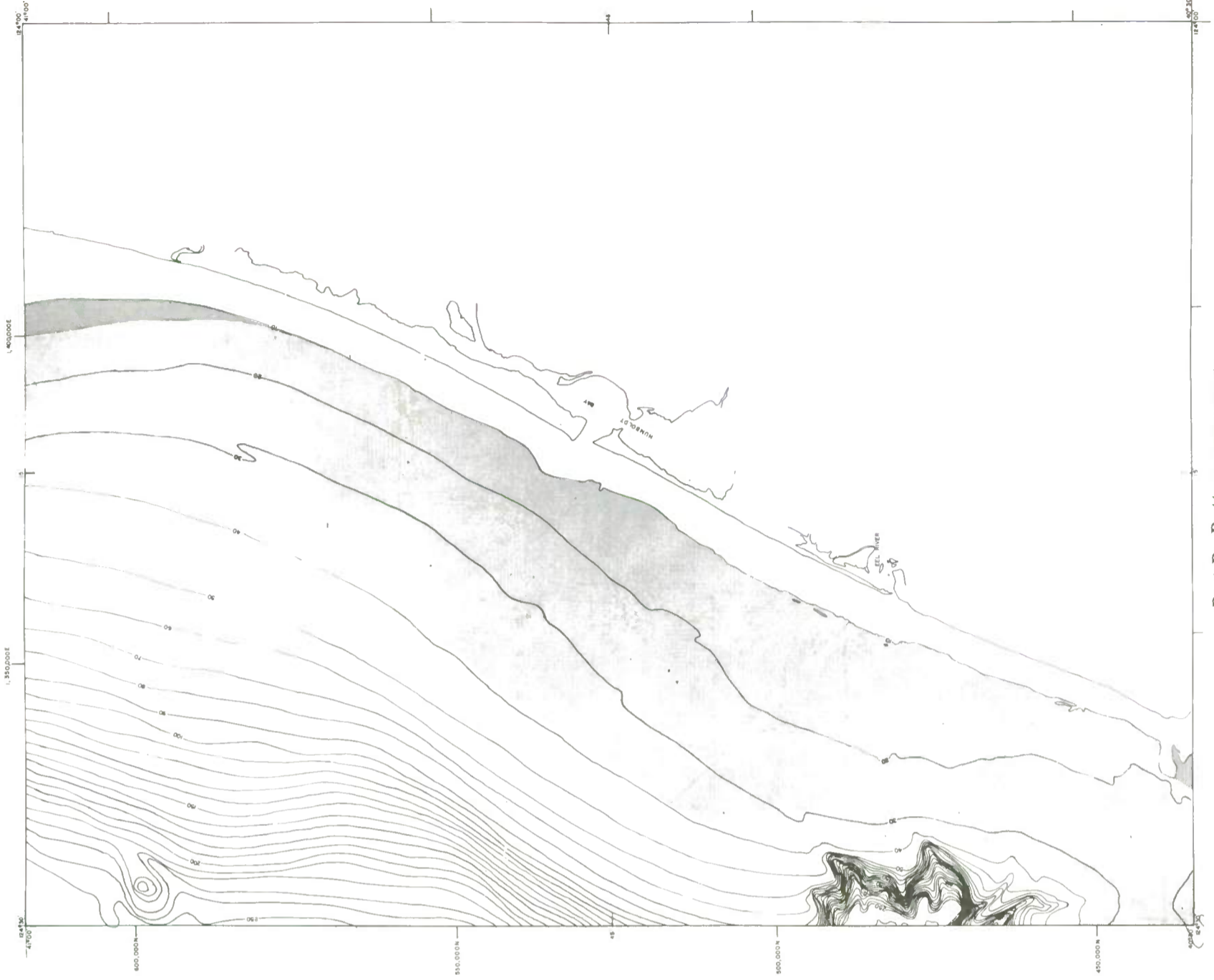


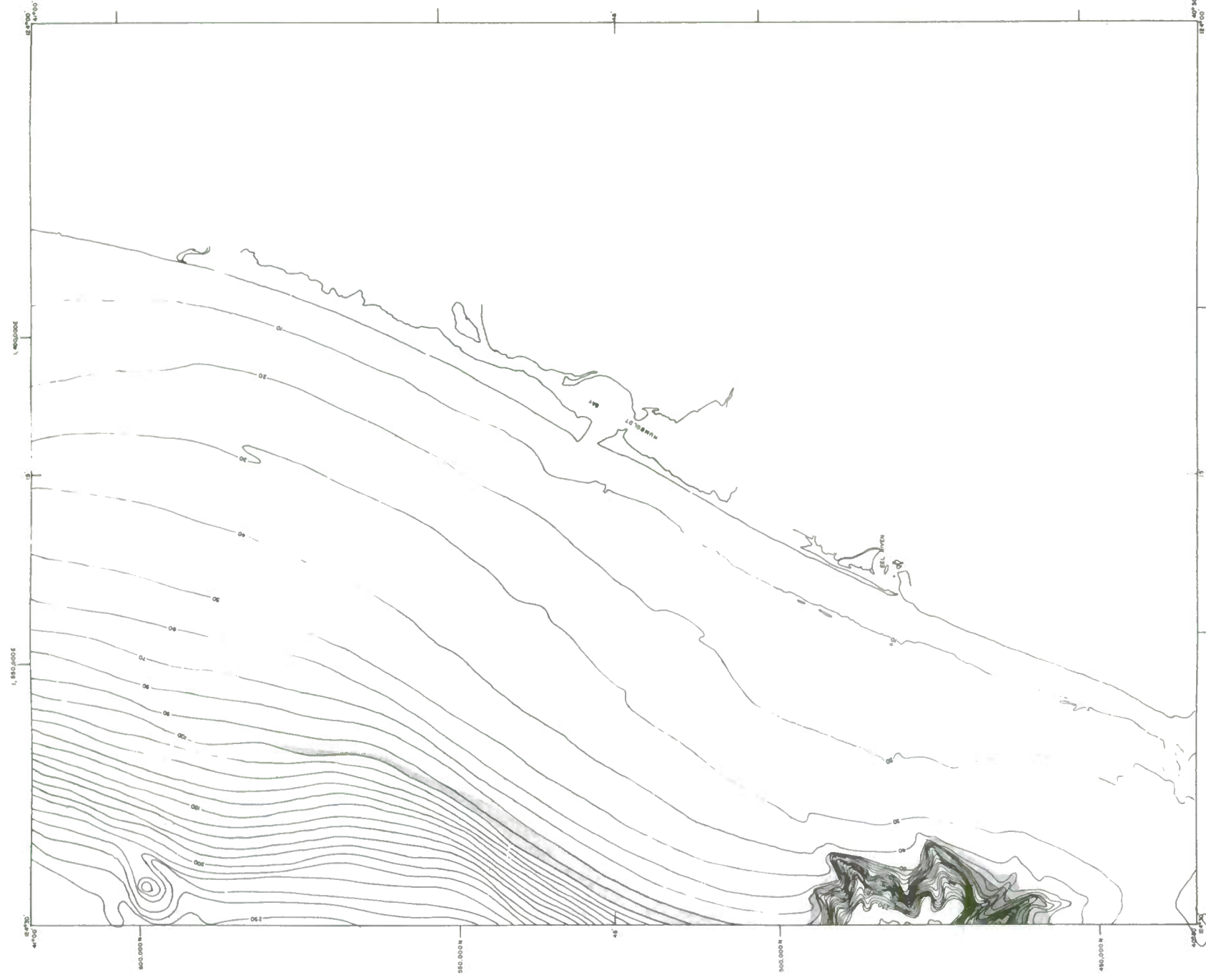
Figure 7. Predicted regions of century extremes for chart number 4.



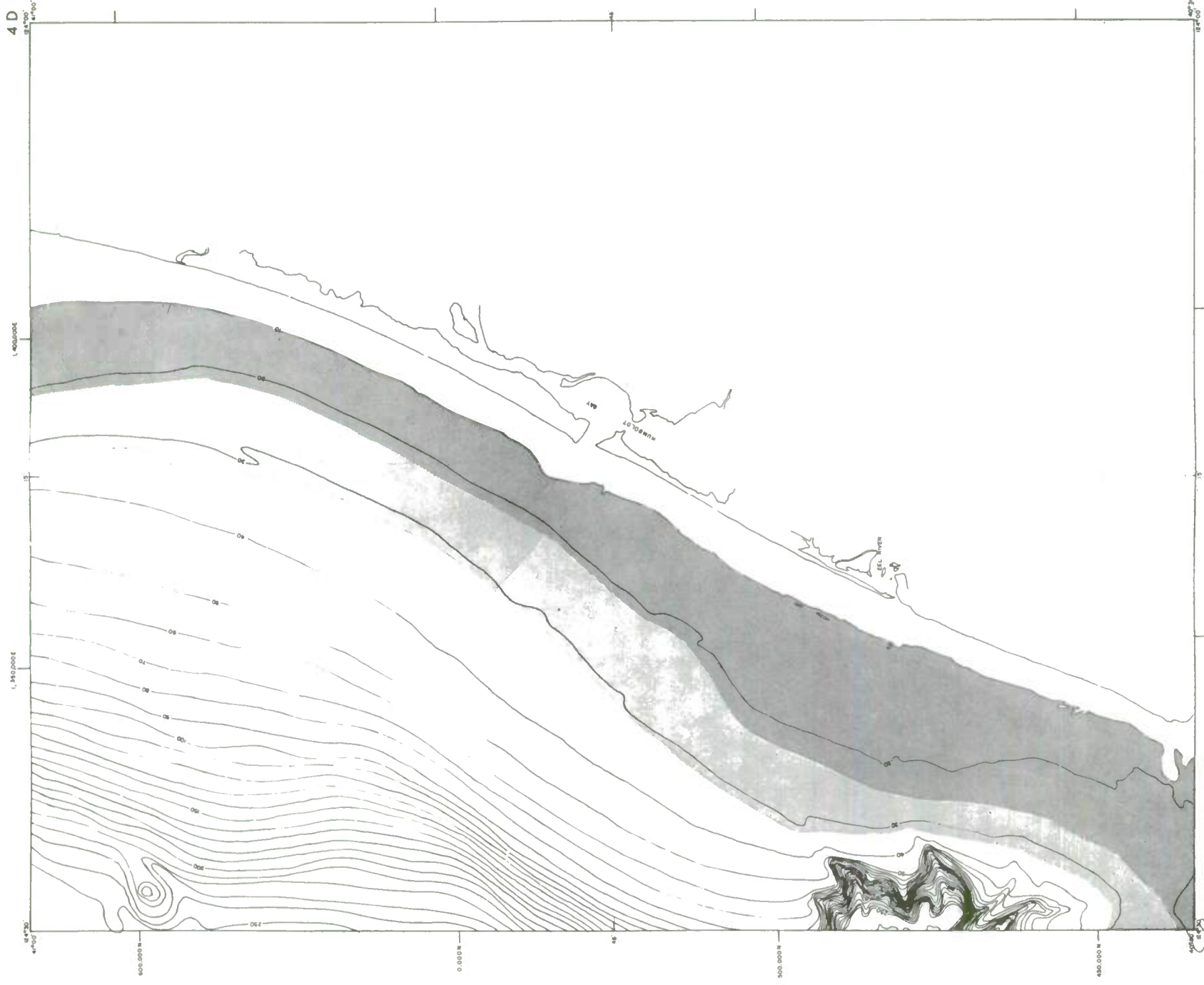
Part A. Density.



Part B. Bottom wave surge.

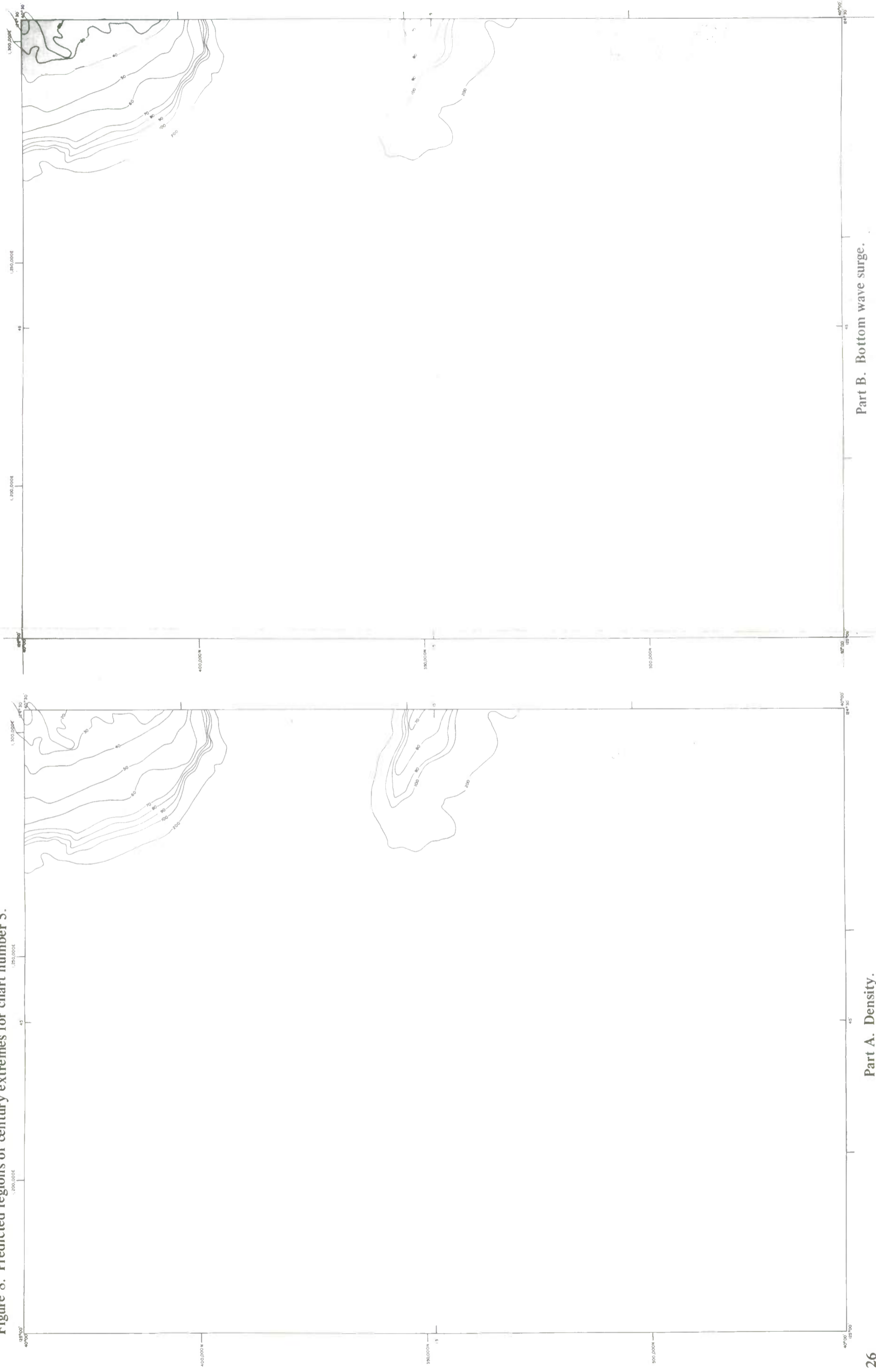


Part C. Bottom current velocity.



Part D. Tsunami surge.

Figure 8. Predicted regions of century extremes for chart number 5.



Part A. Density.

Part B. Bottom wave surge.

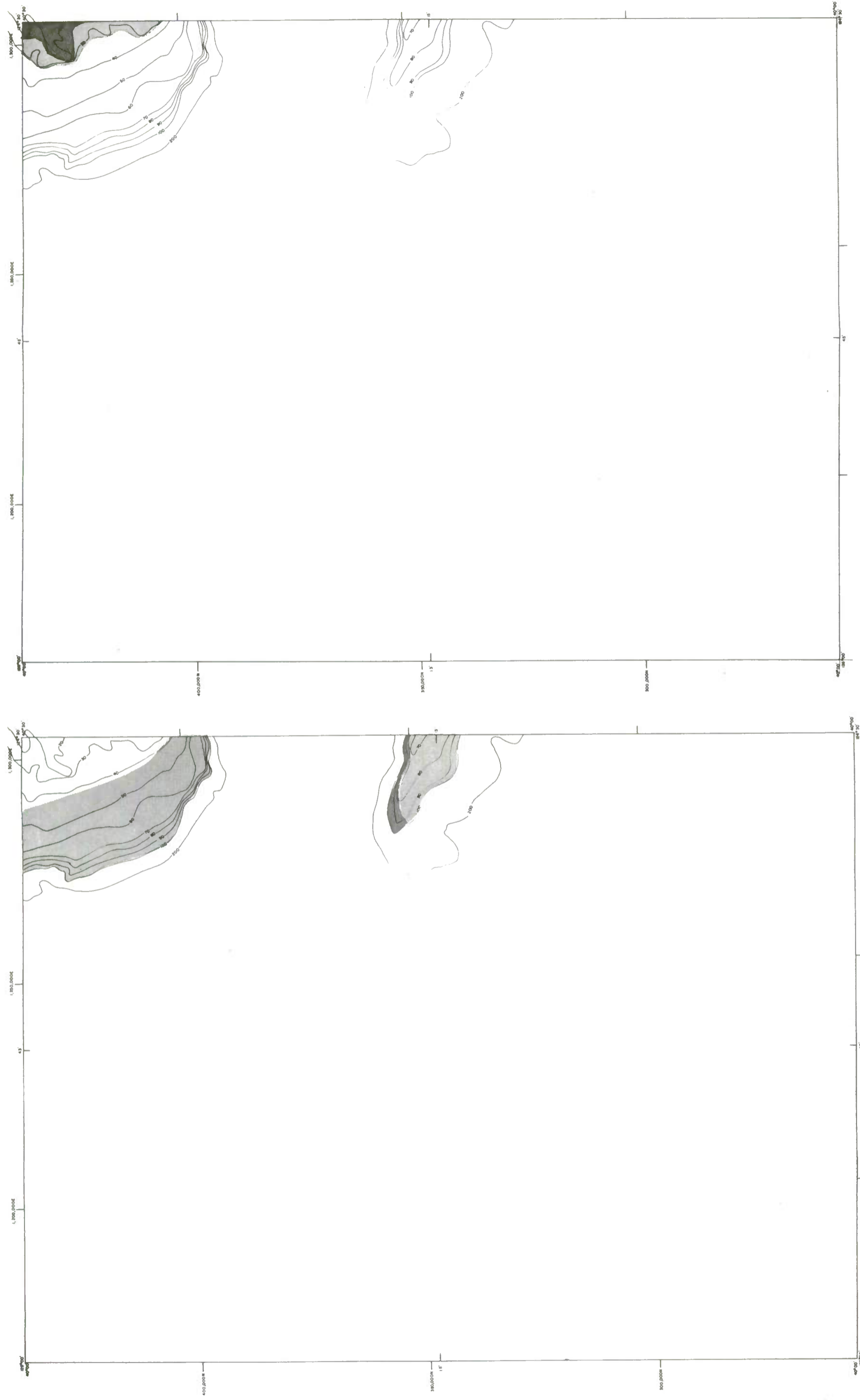
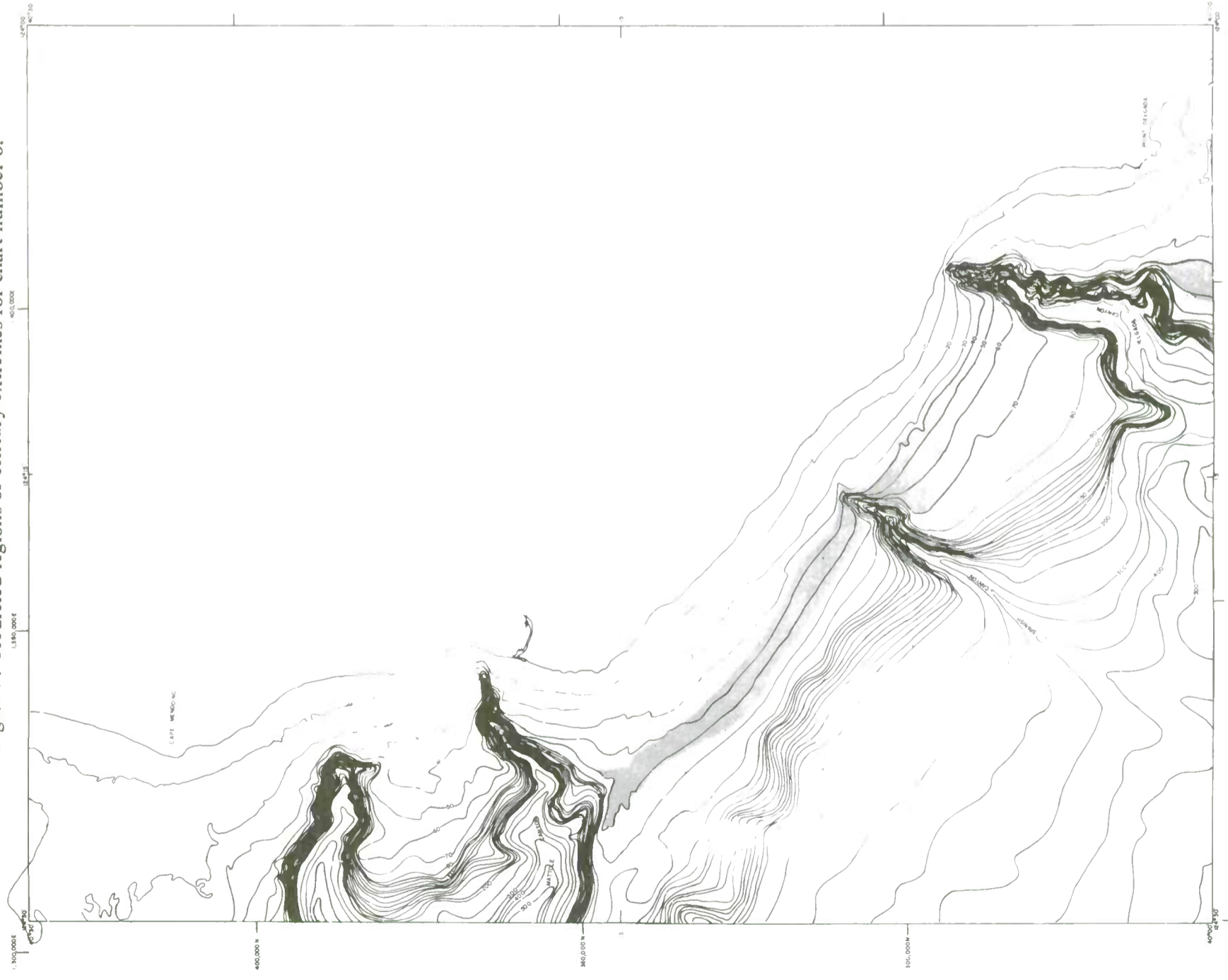
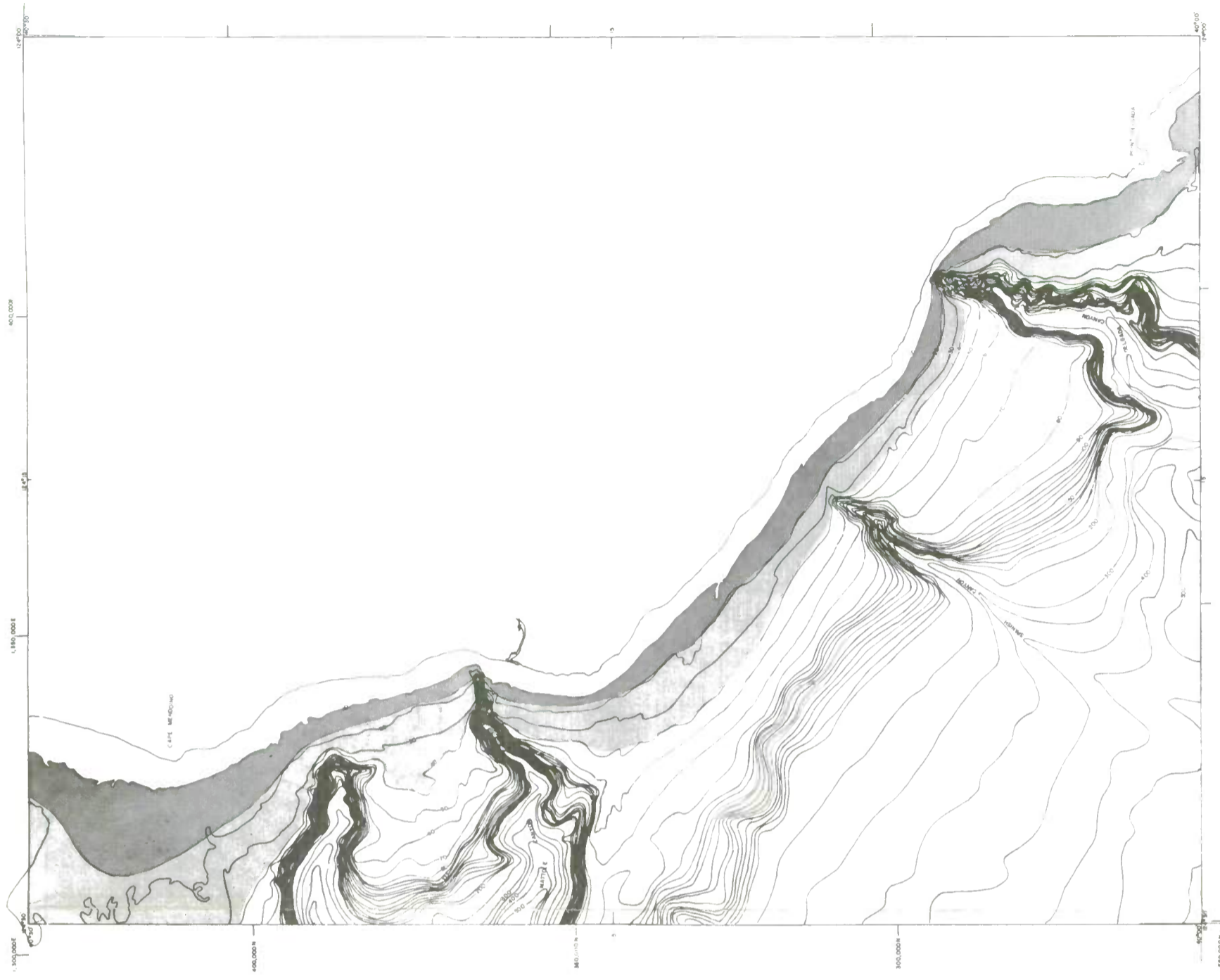


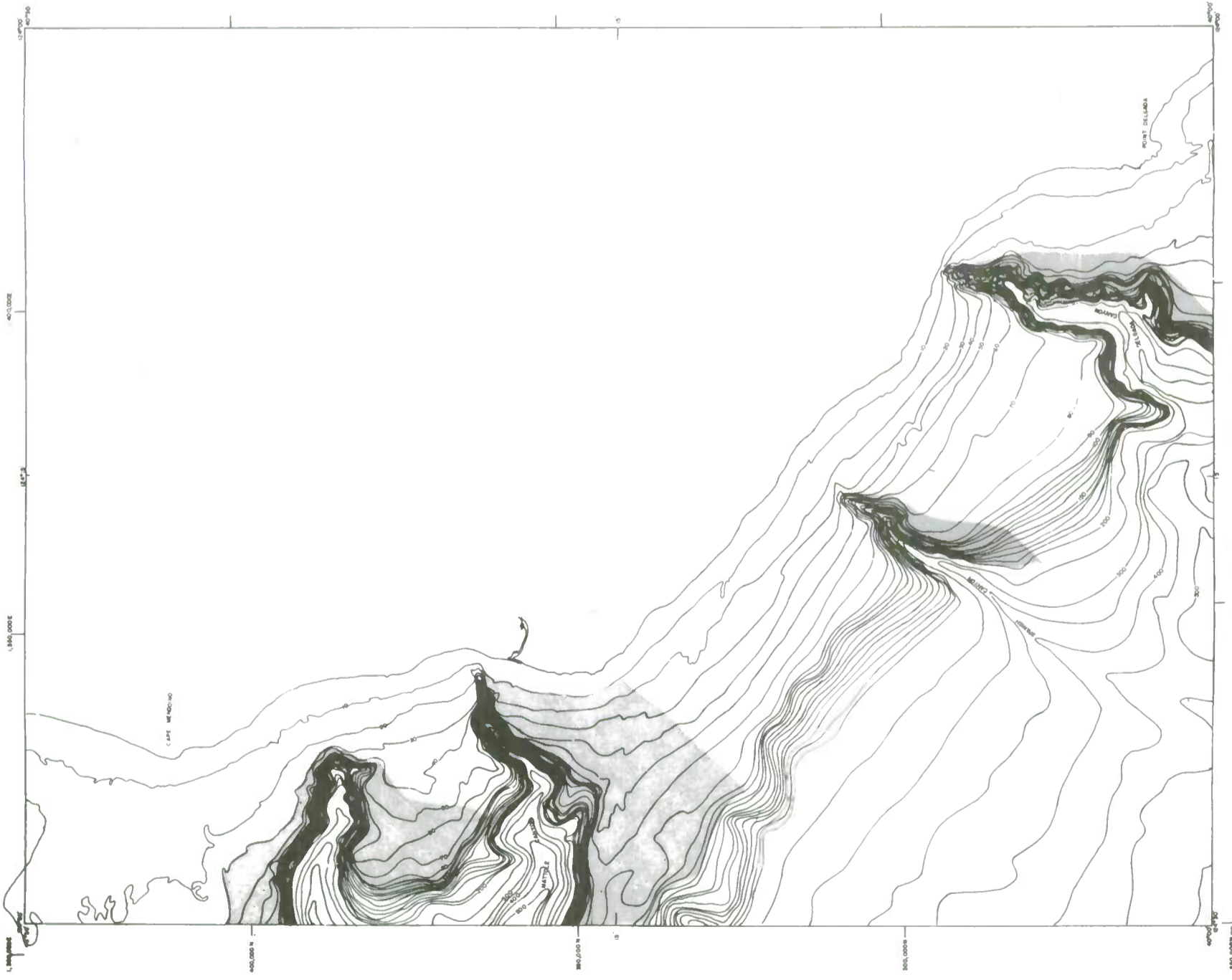
Figure 9. Predicted regions of century extremes for chart number 6.



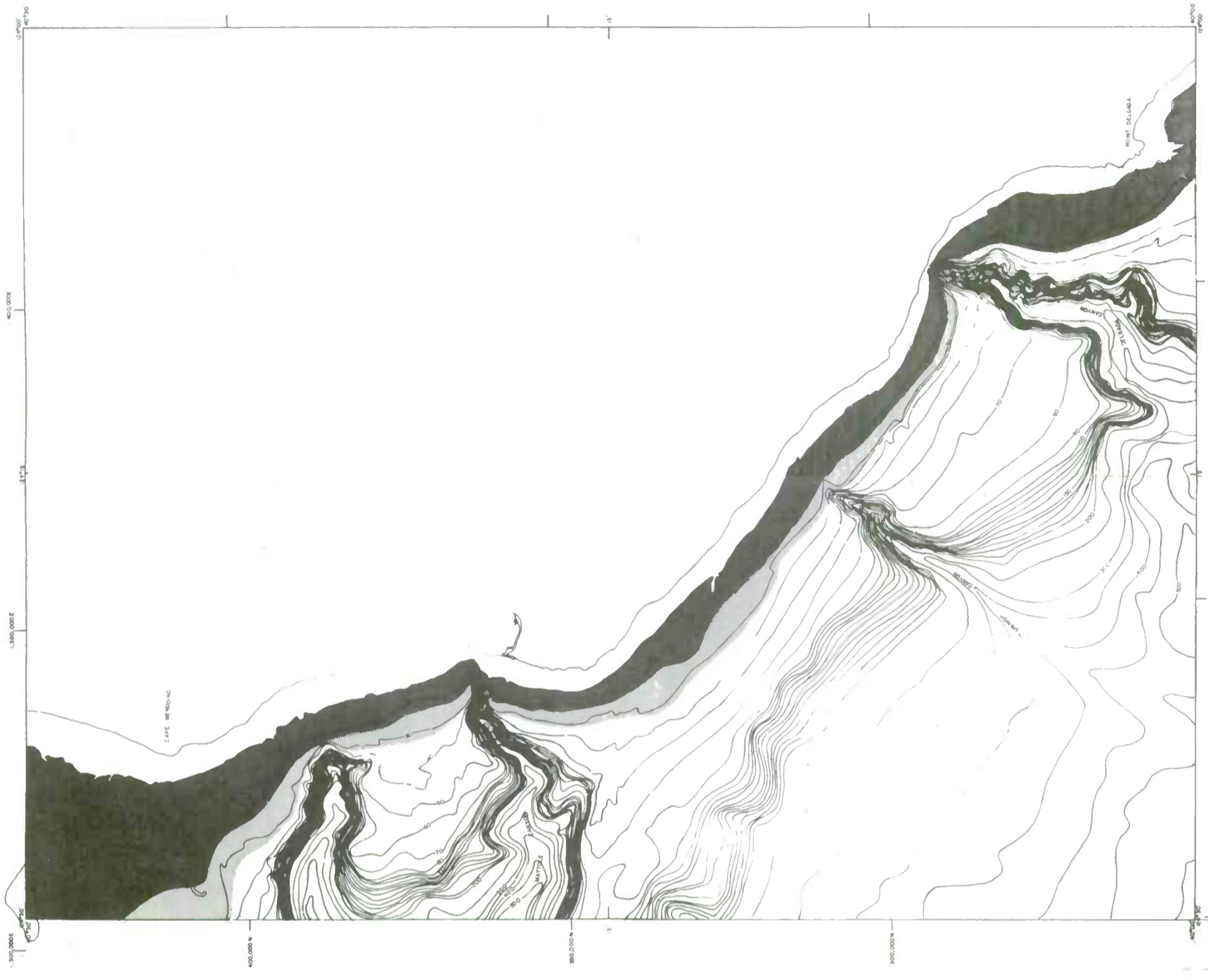
Part A. Density.



Part B. Bottom wave surge.

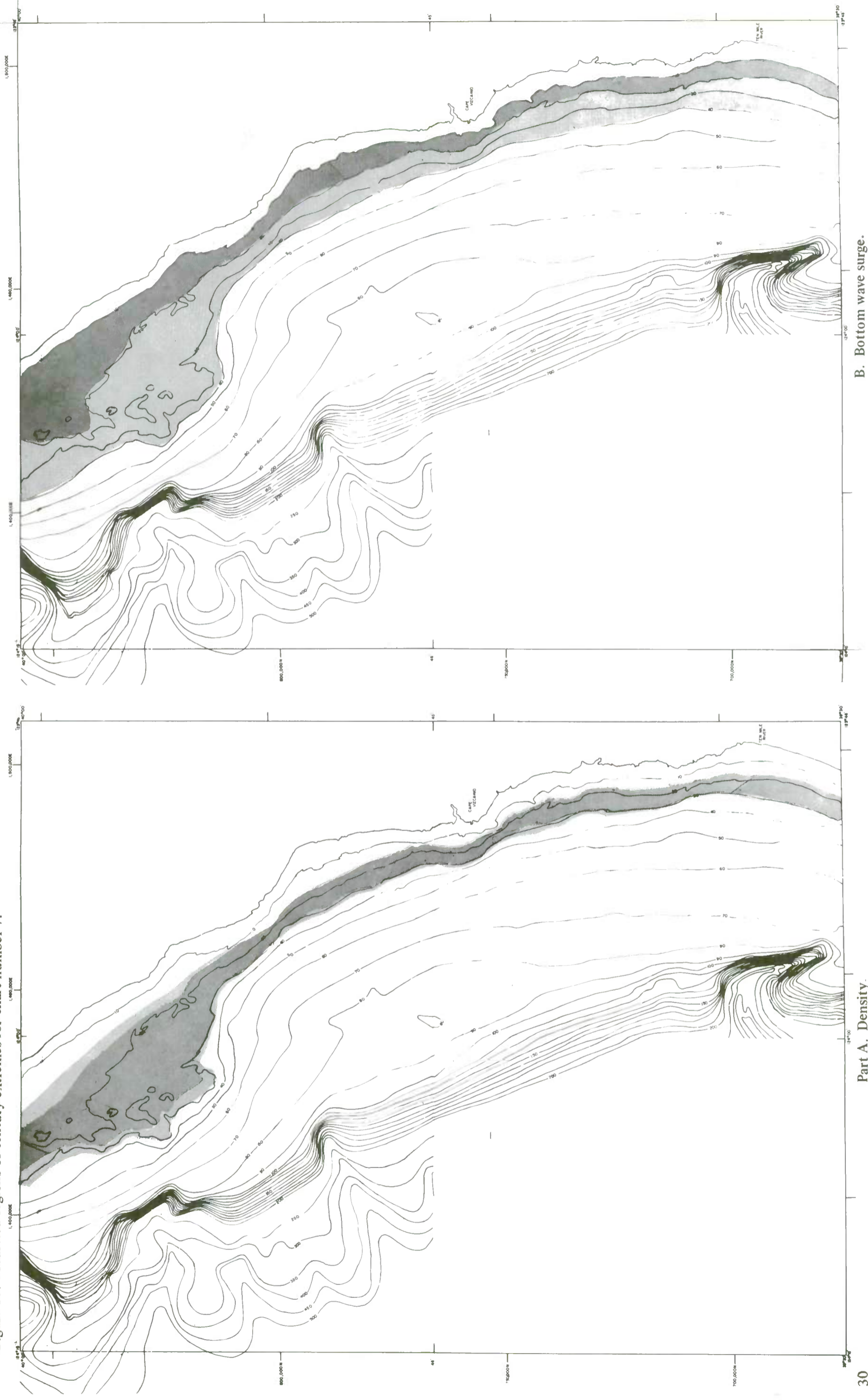


Part C. Bottom current velocity.



Part D. Tsunami surge.

Figure 10. Predicted regions of century extremes for chart number 7.



Part D. Tsunami surge.

Part C. Bottom current velocity.

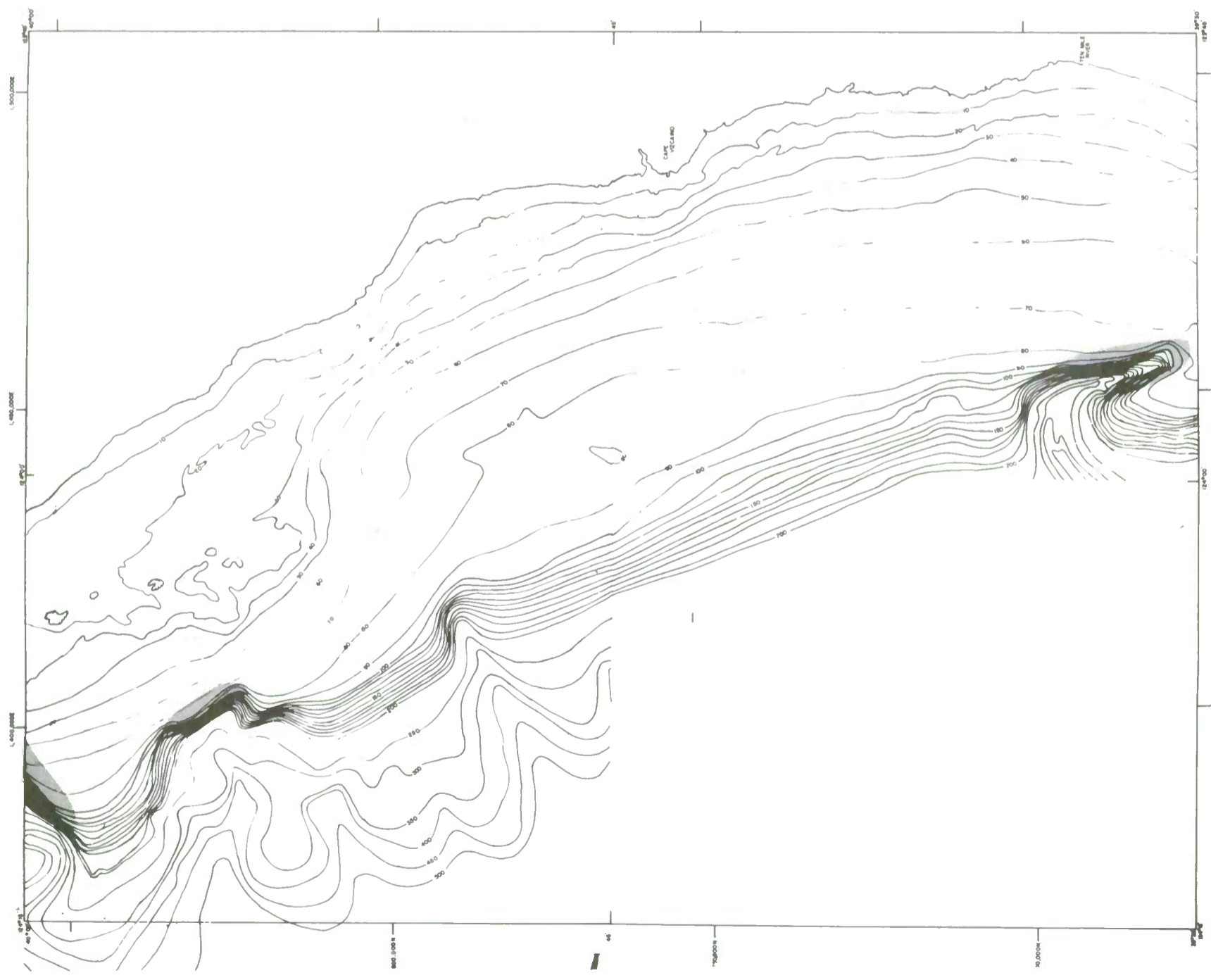
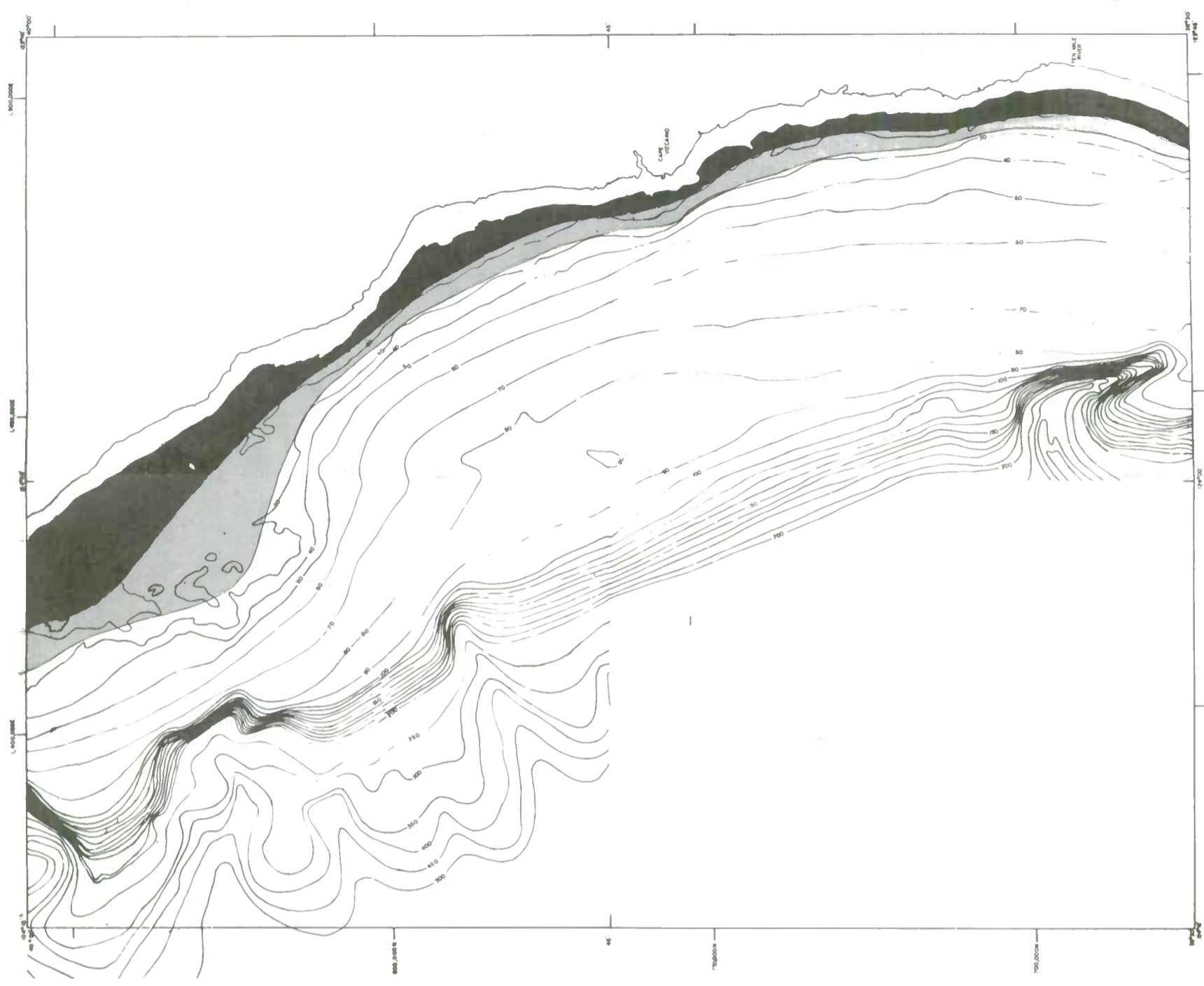
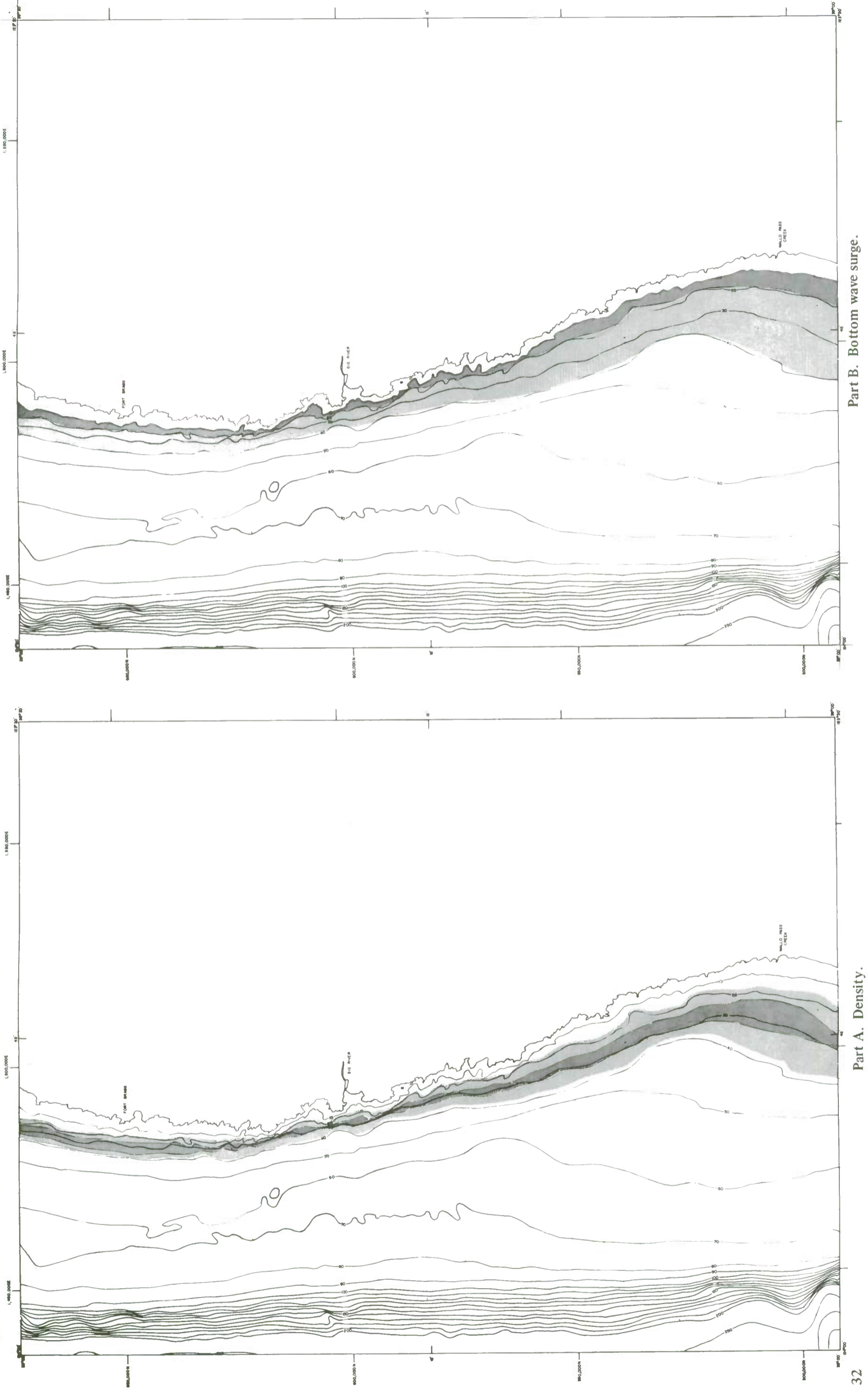
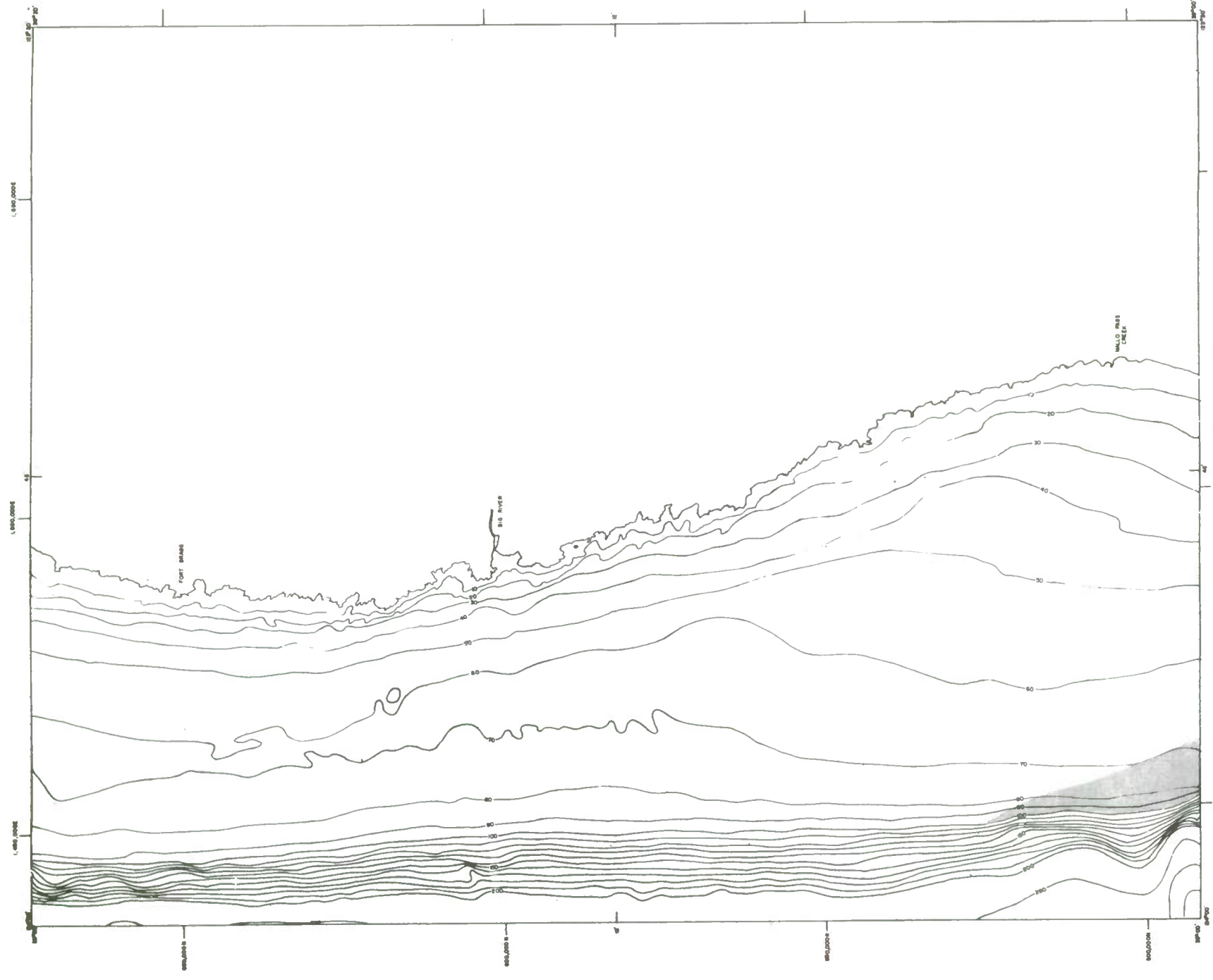
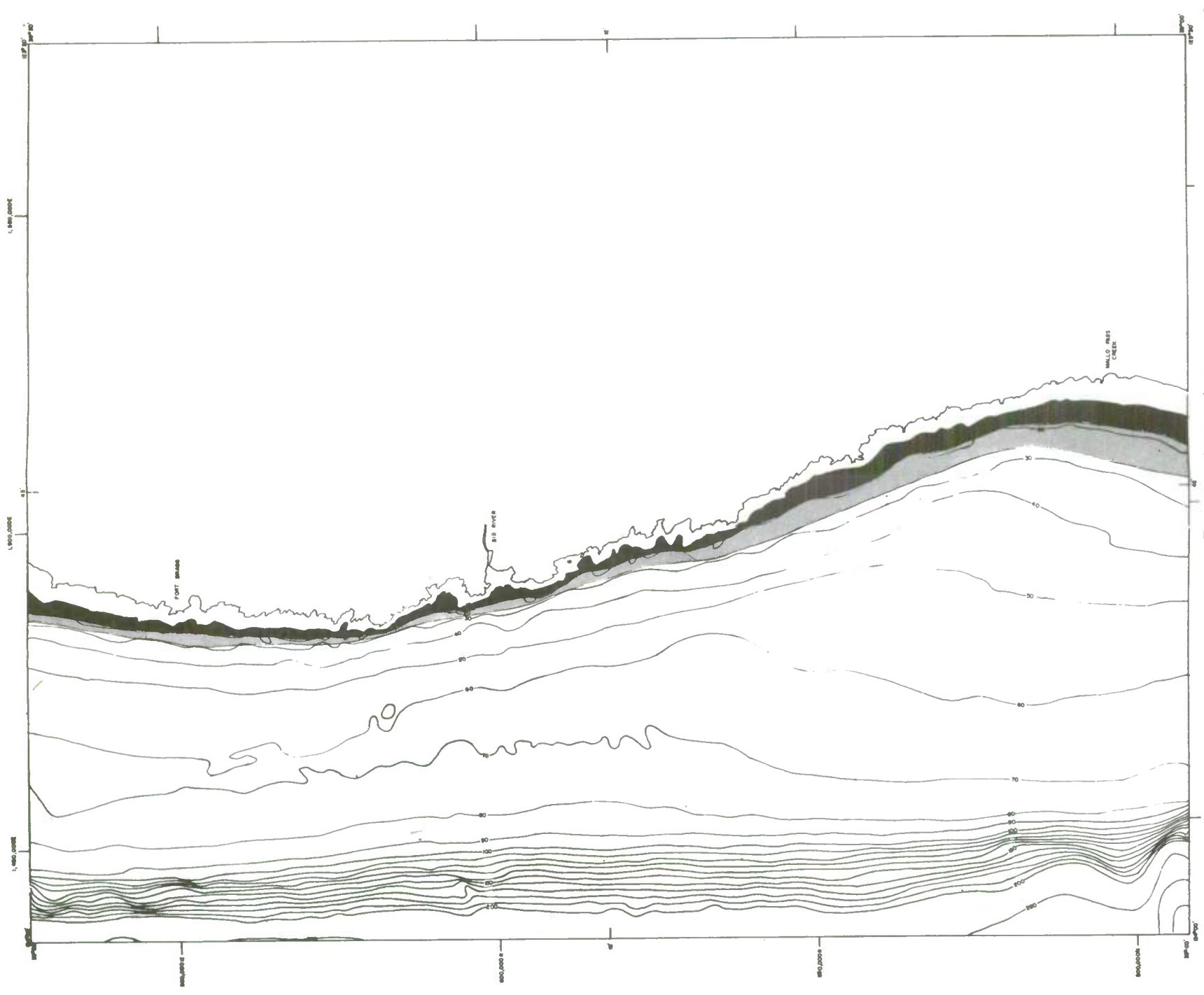


Figure 11. Predicted regions of century extremes for chart number 8.



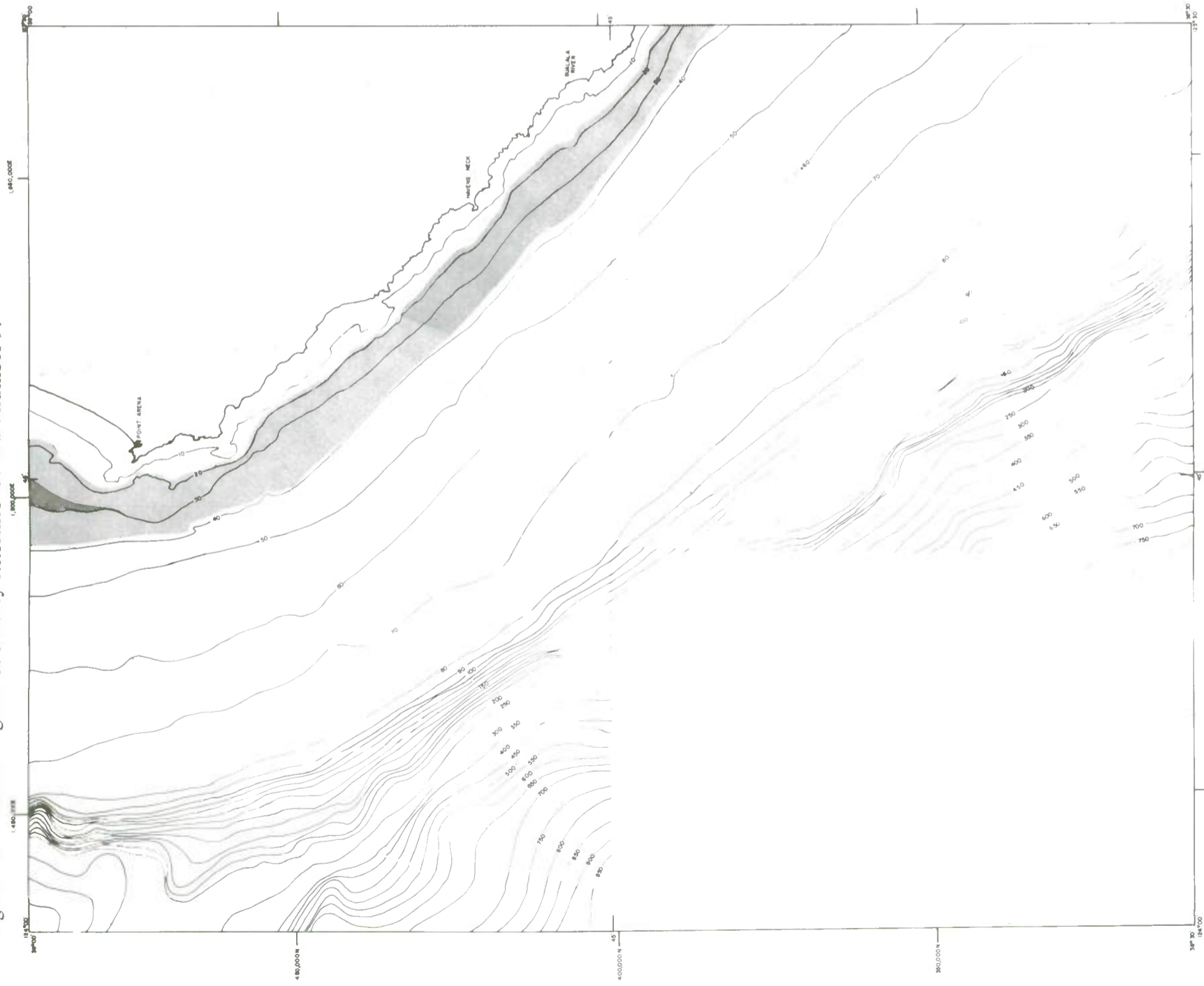


Part C. Bottom current velocity.

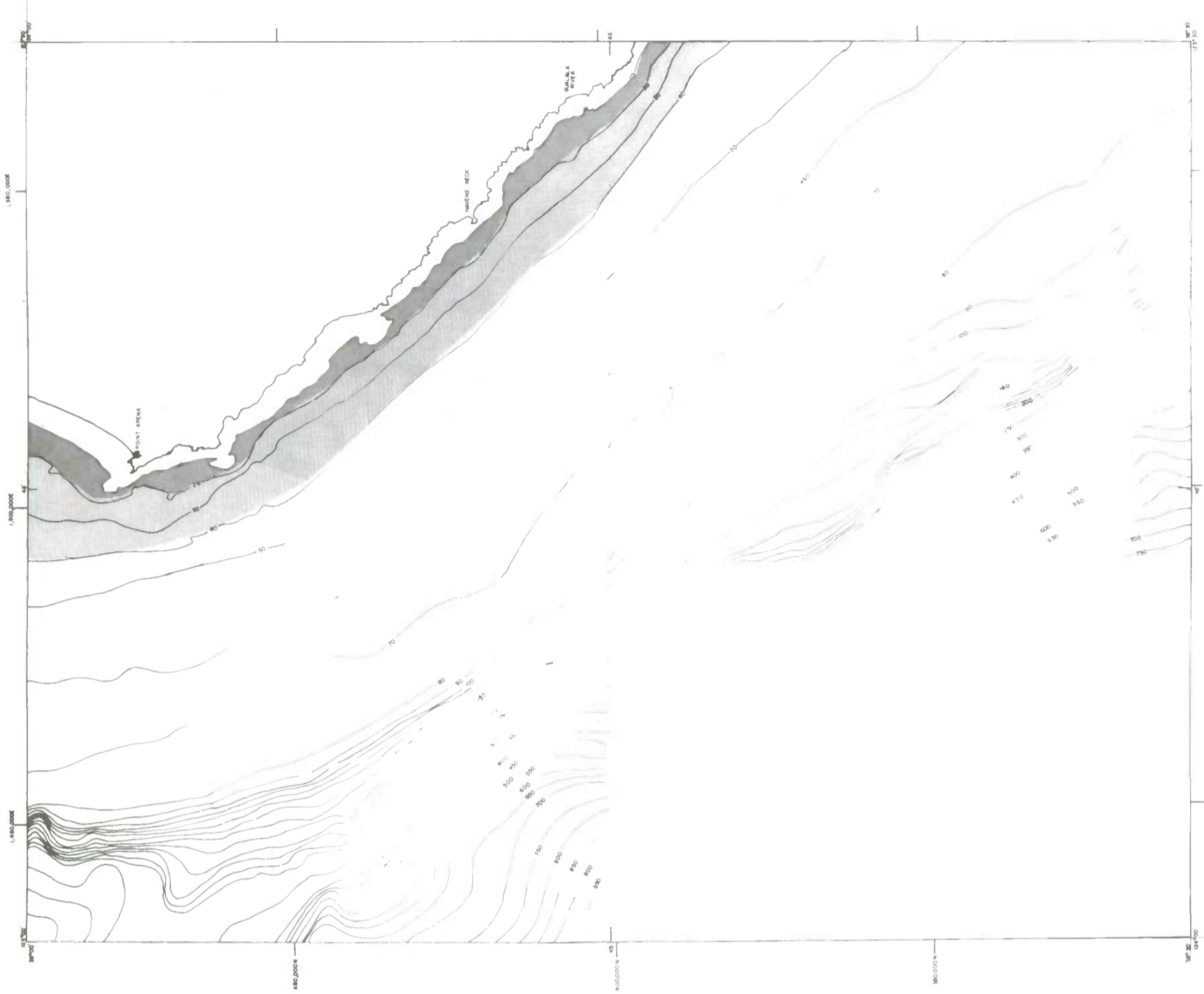


Part D. Tsunami surge.

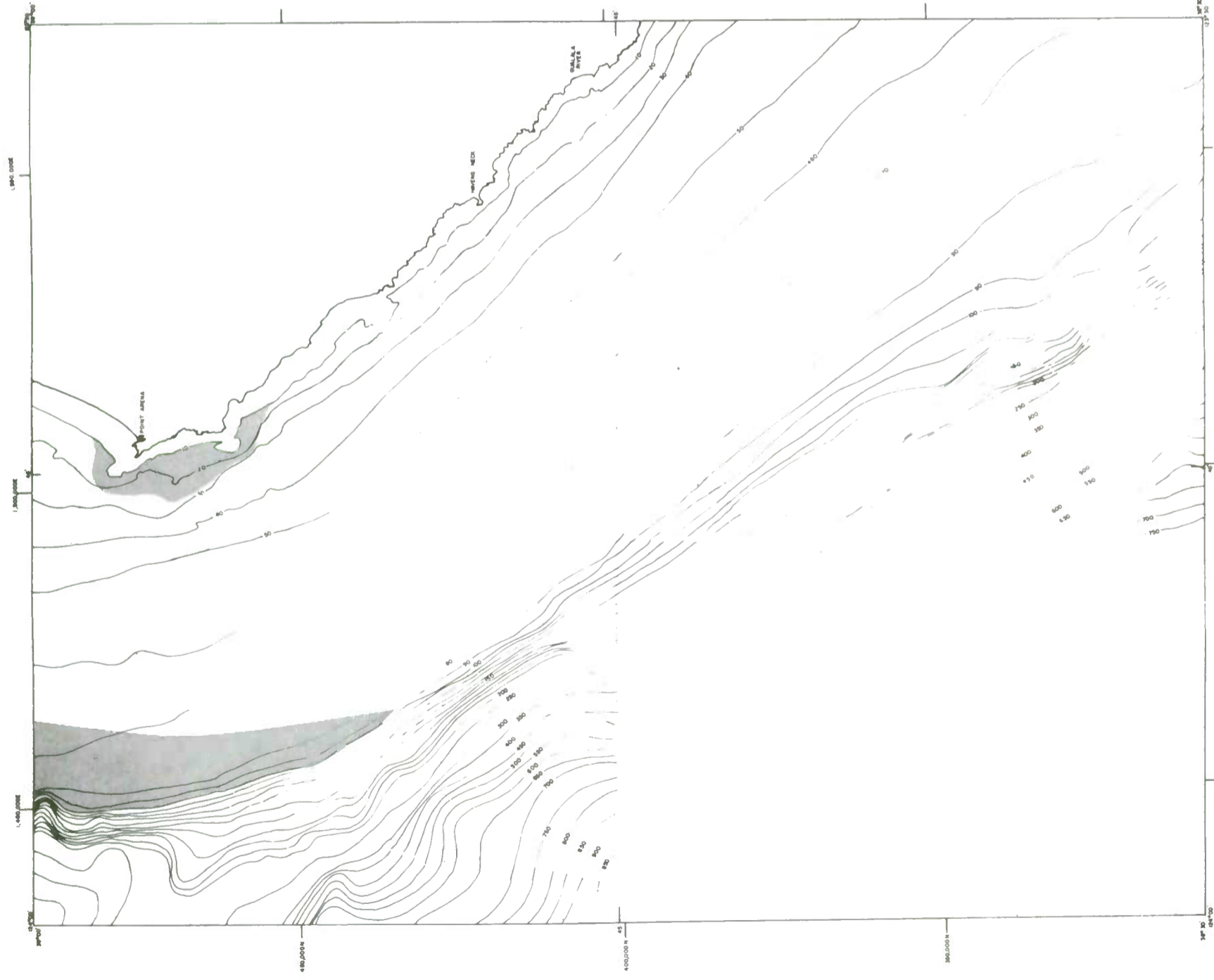
Figure 12. Predicted regions of century extremes for chart number 9.



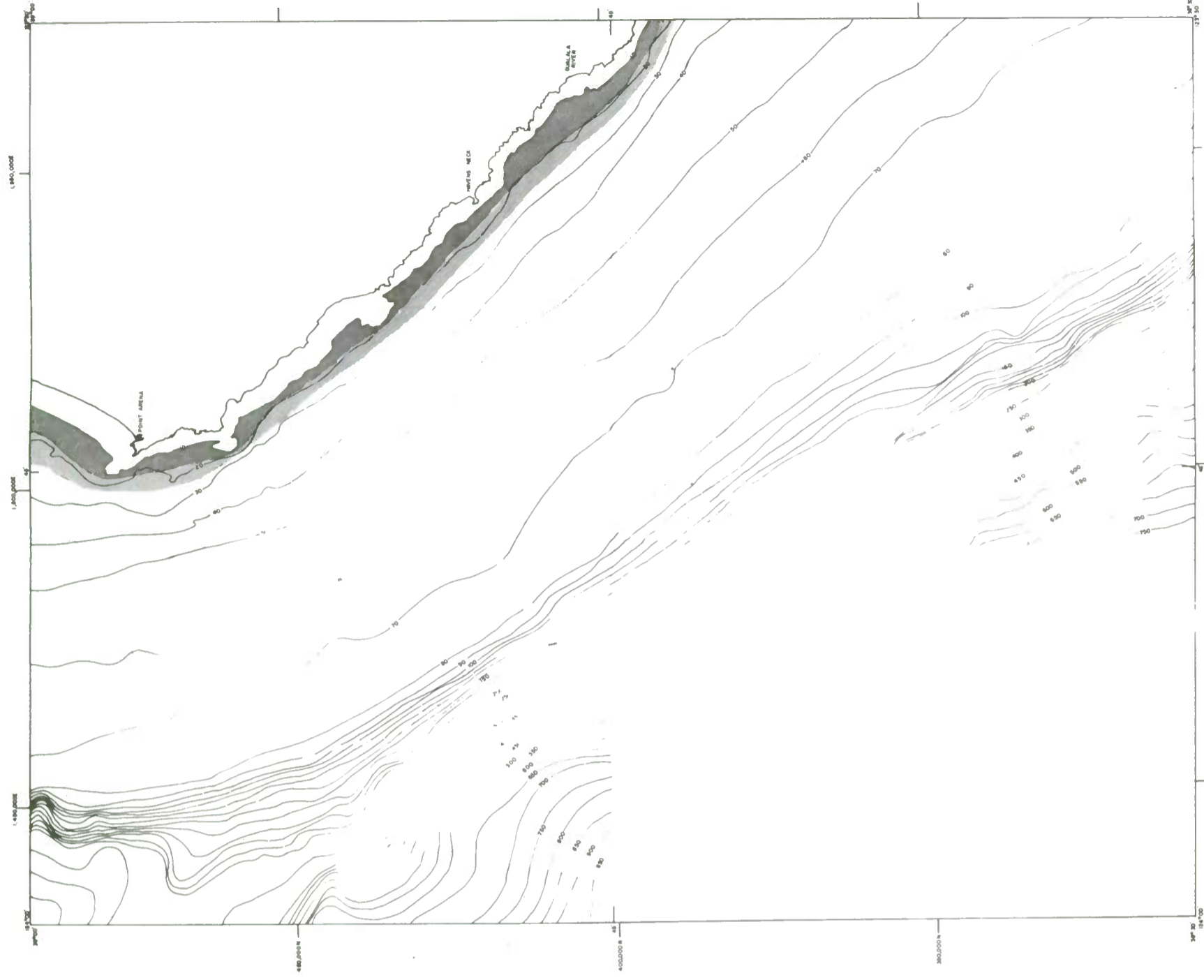
Part A. Density.



Part B. Bottom wave surge.

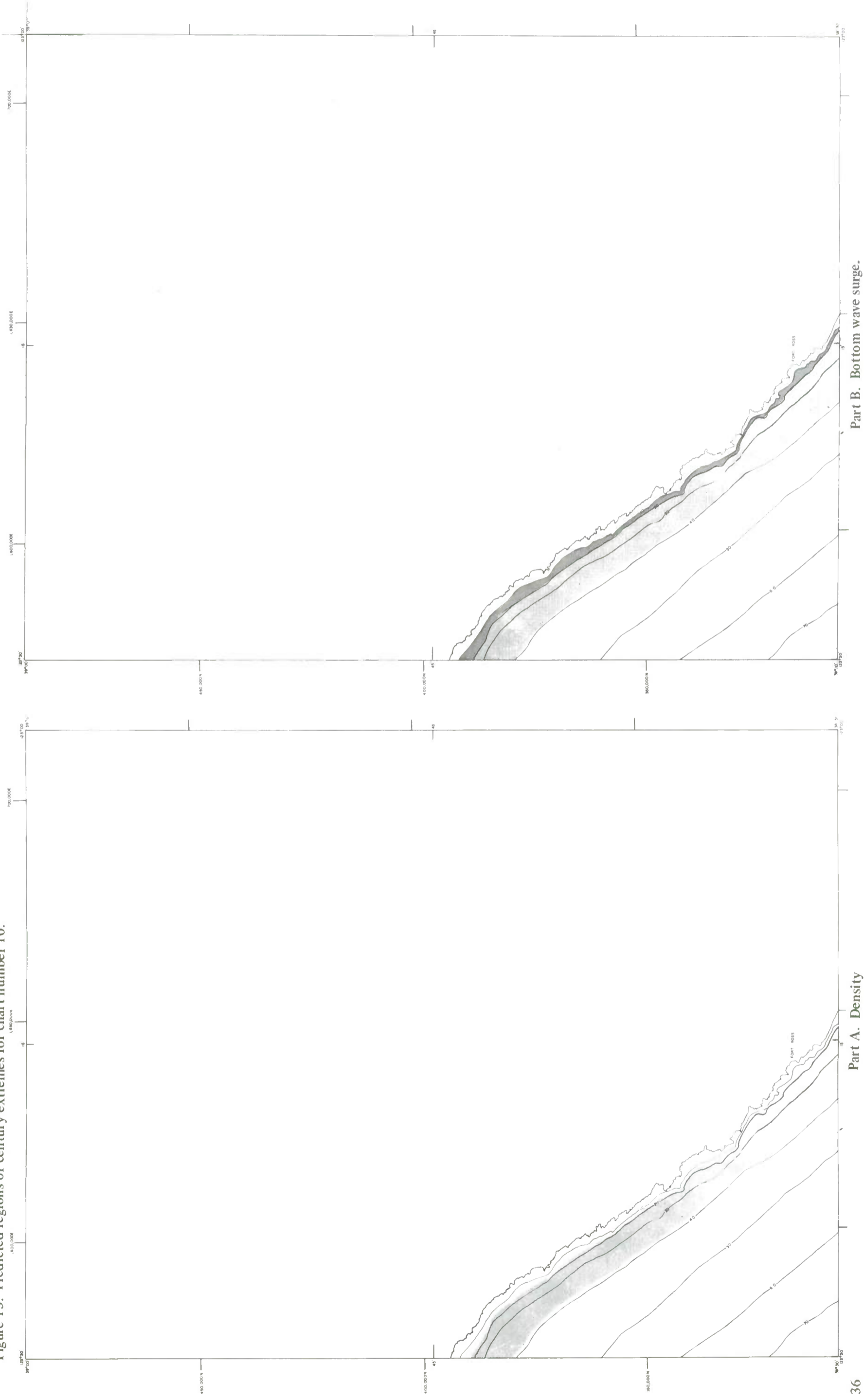


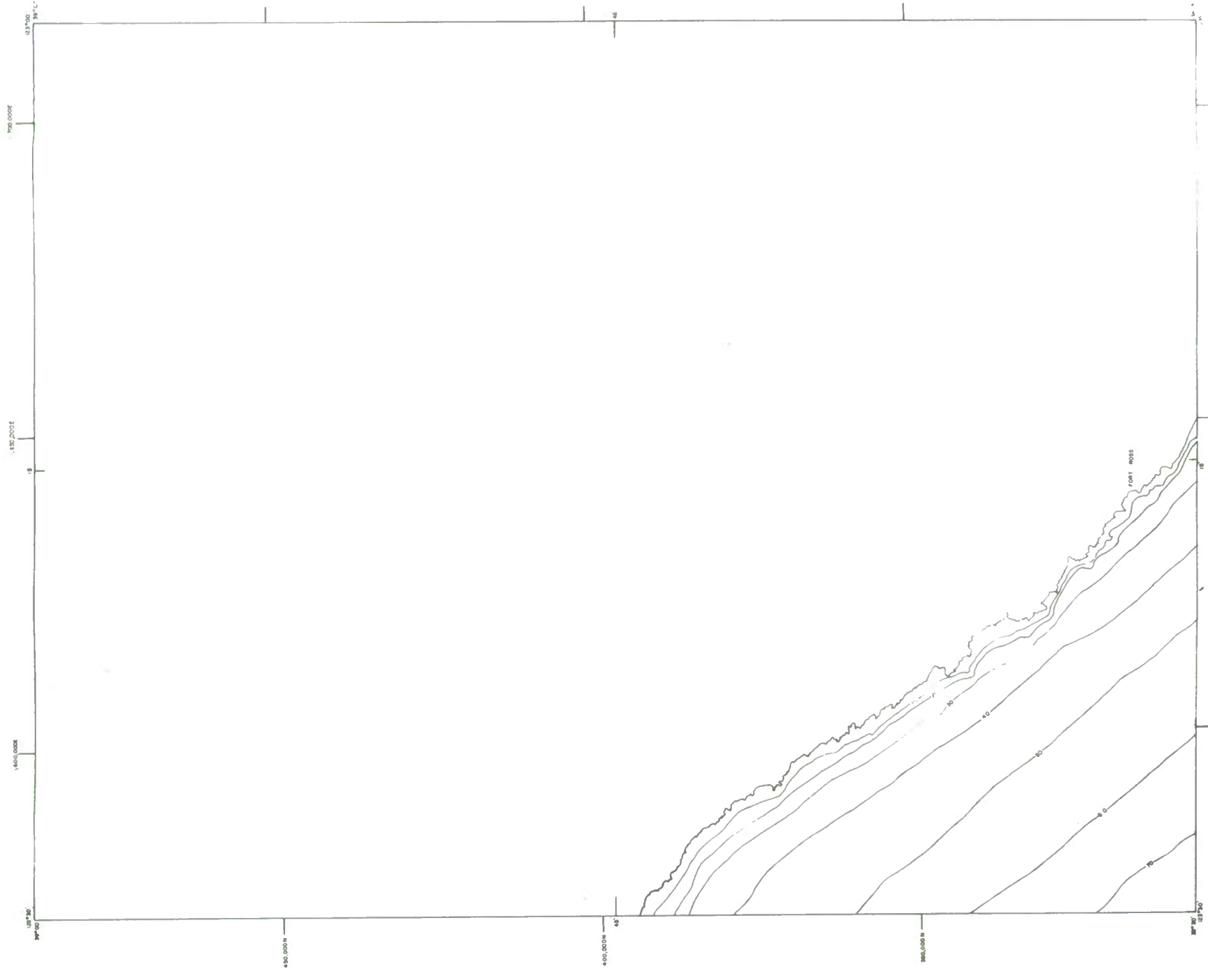
Part C. Bottom current velocity.



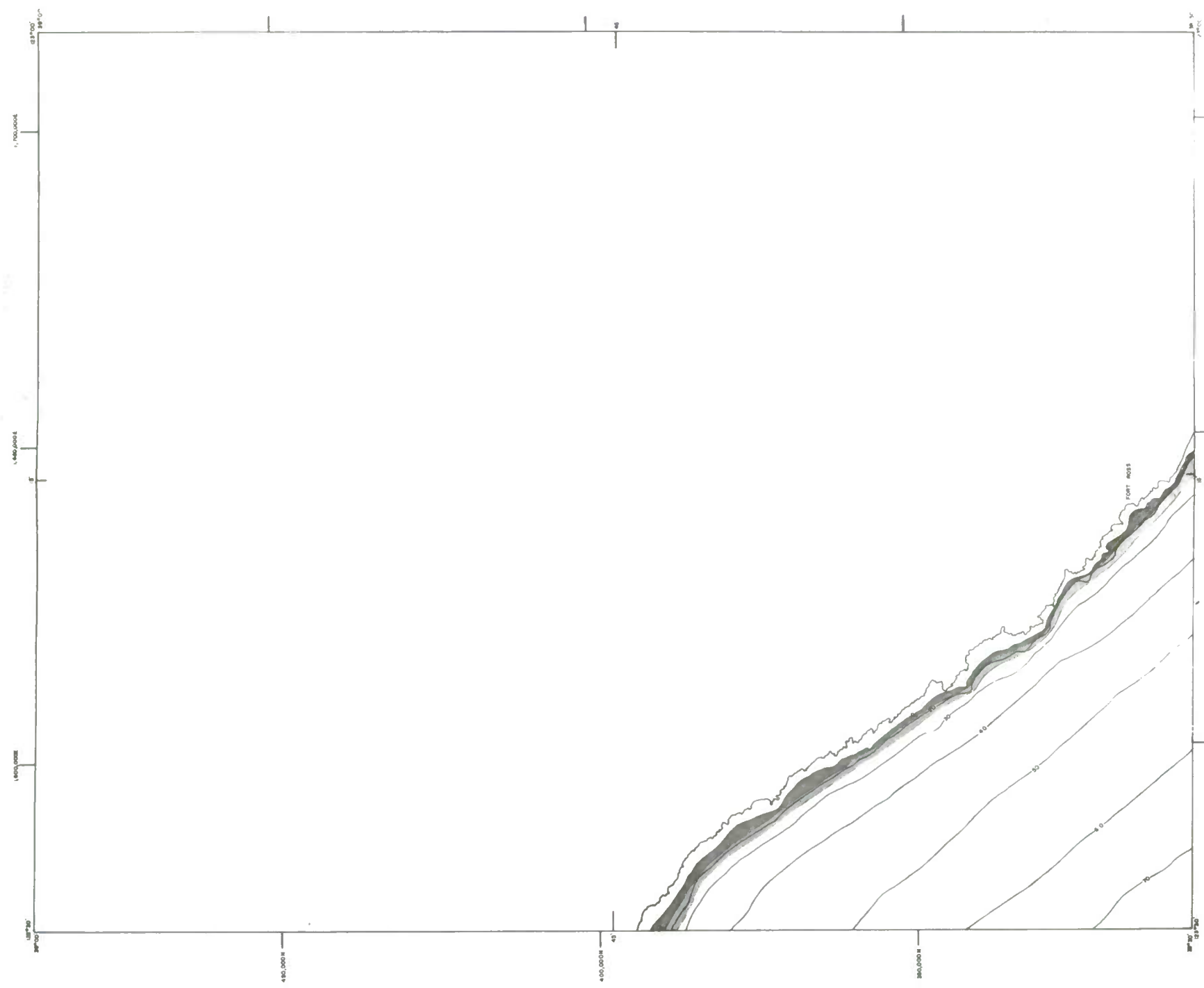
Part D. Tsunami surge.

Figure 13. Predicted regions of century extremes for chart number 10.



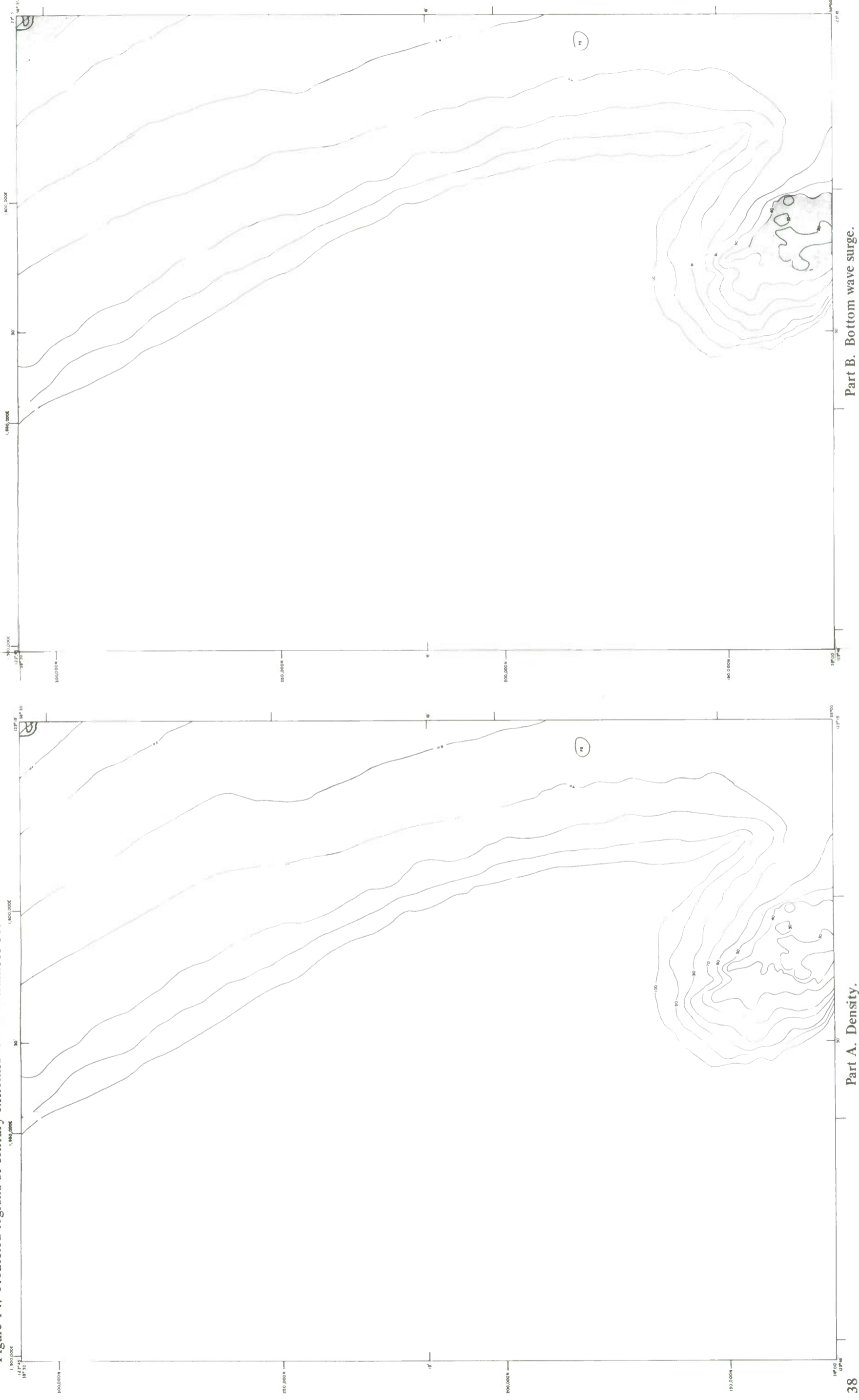


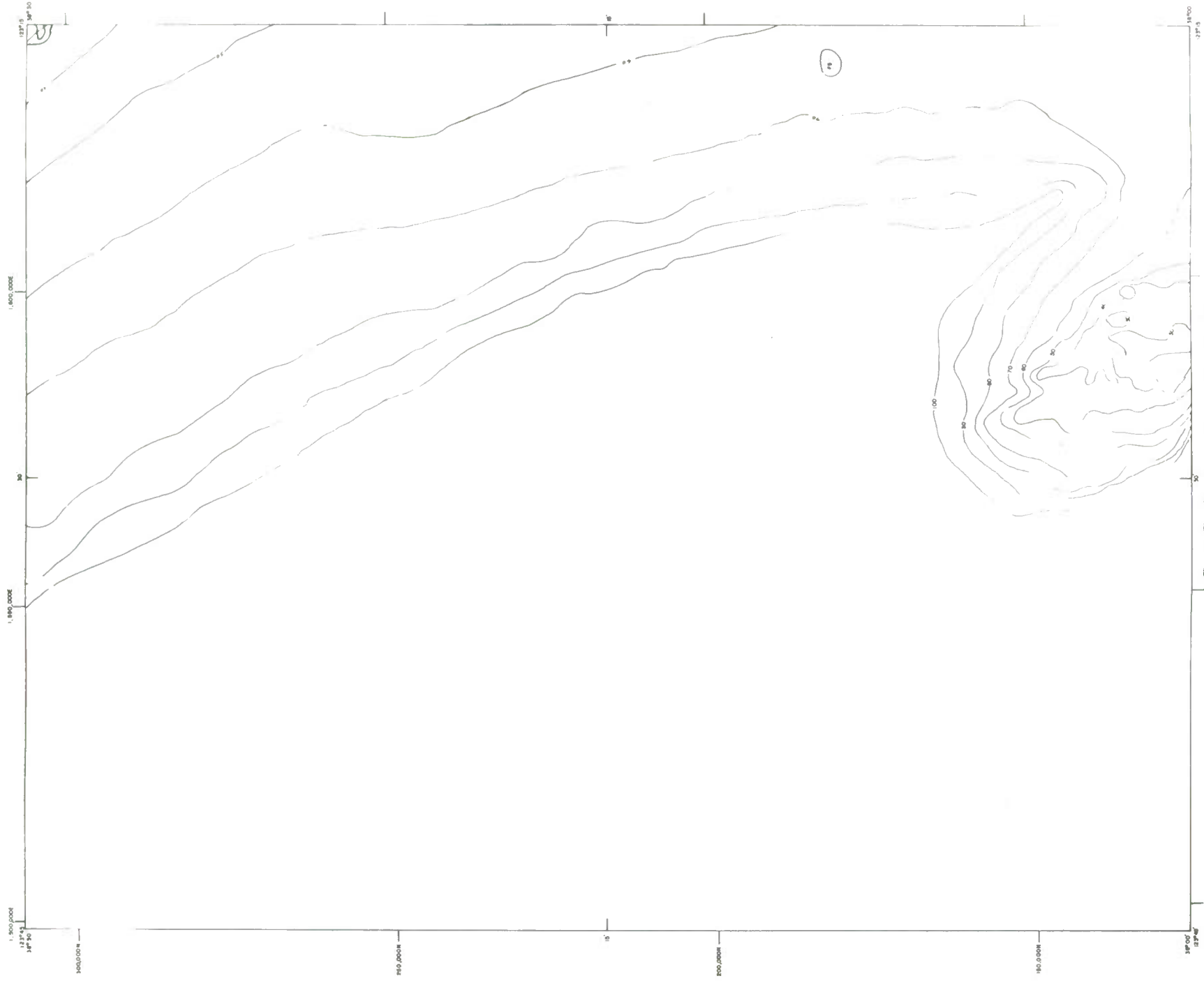
Part C. Bottom current velocity.



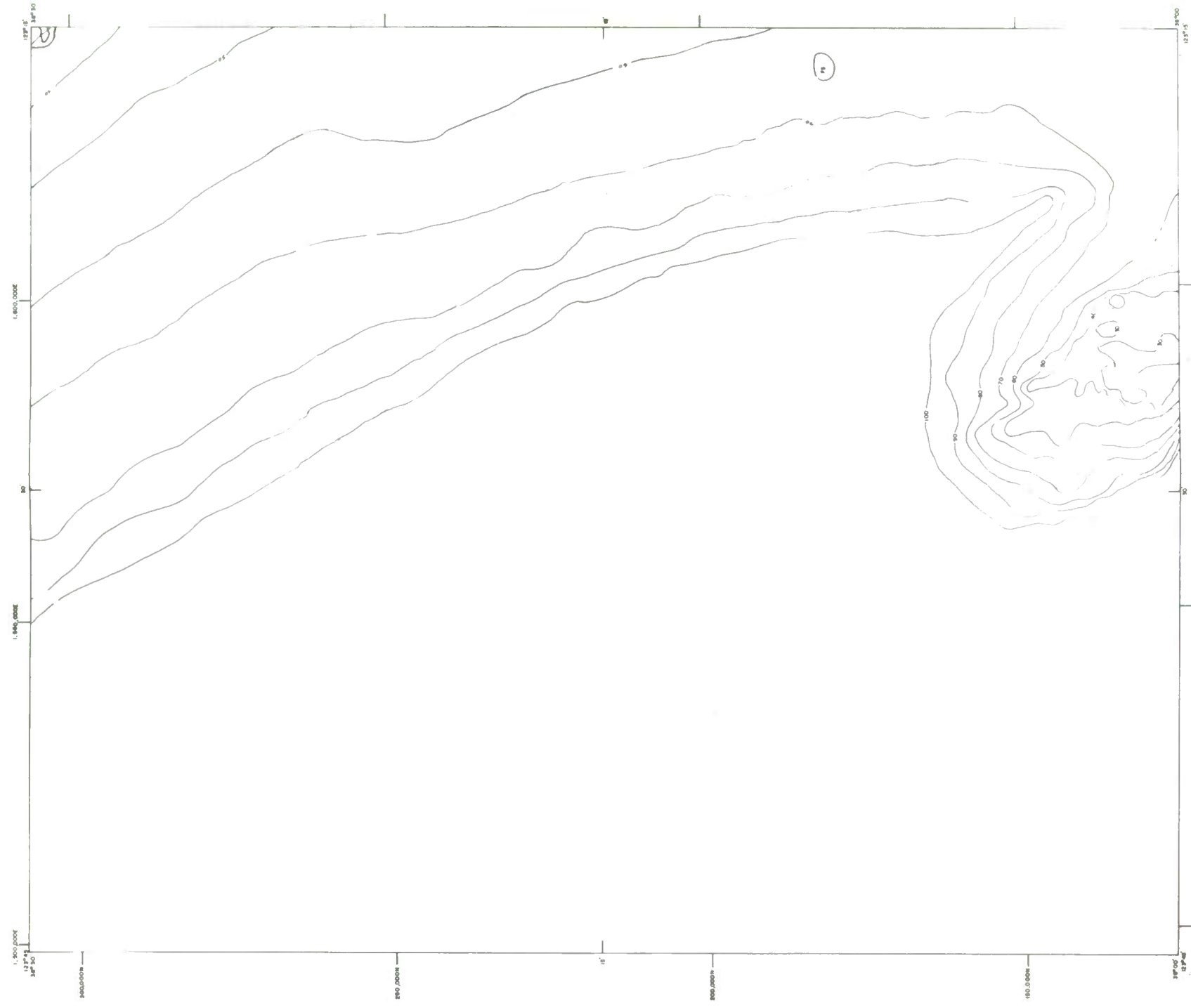
Part D. Tsunami surge.

Figure 14. Predicted regions of century extremes for chart number 11.



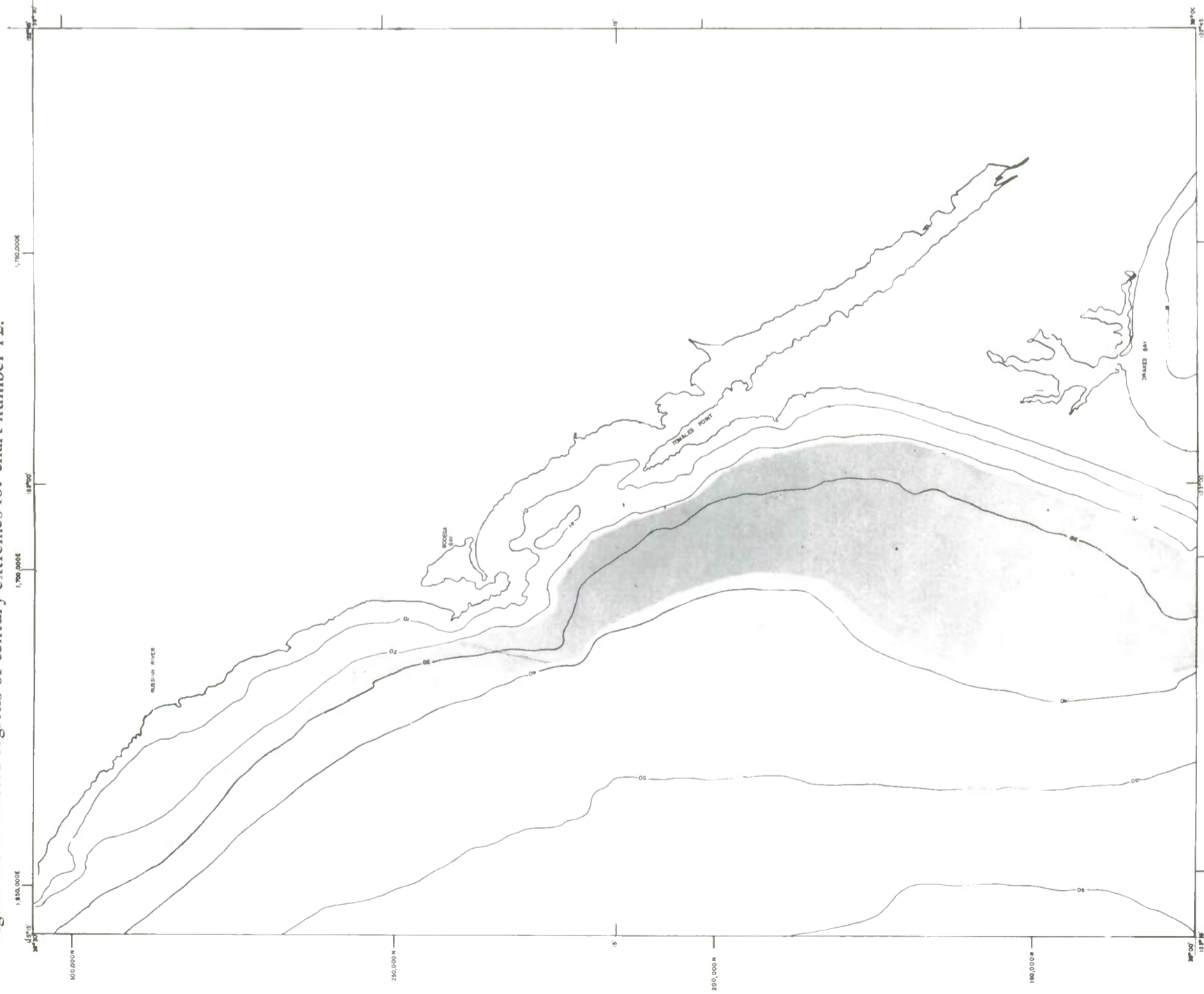


Part C. Bottom current velocity.

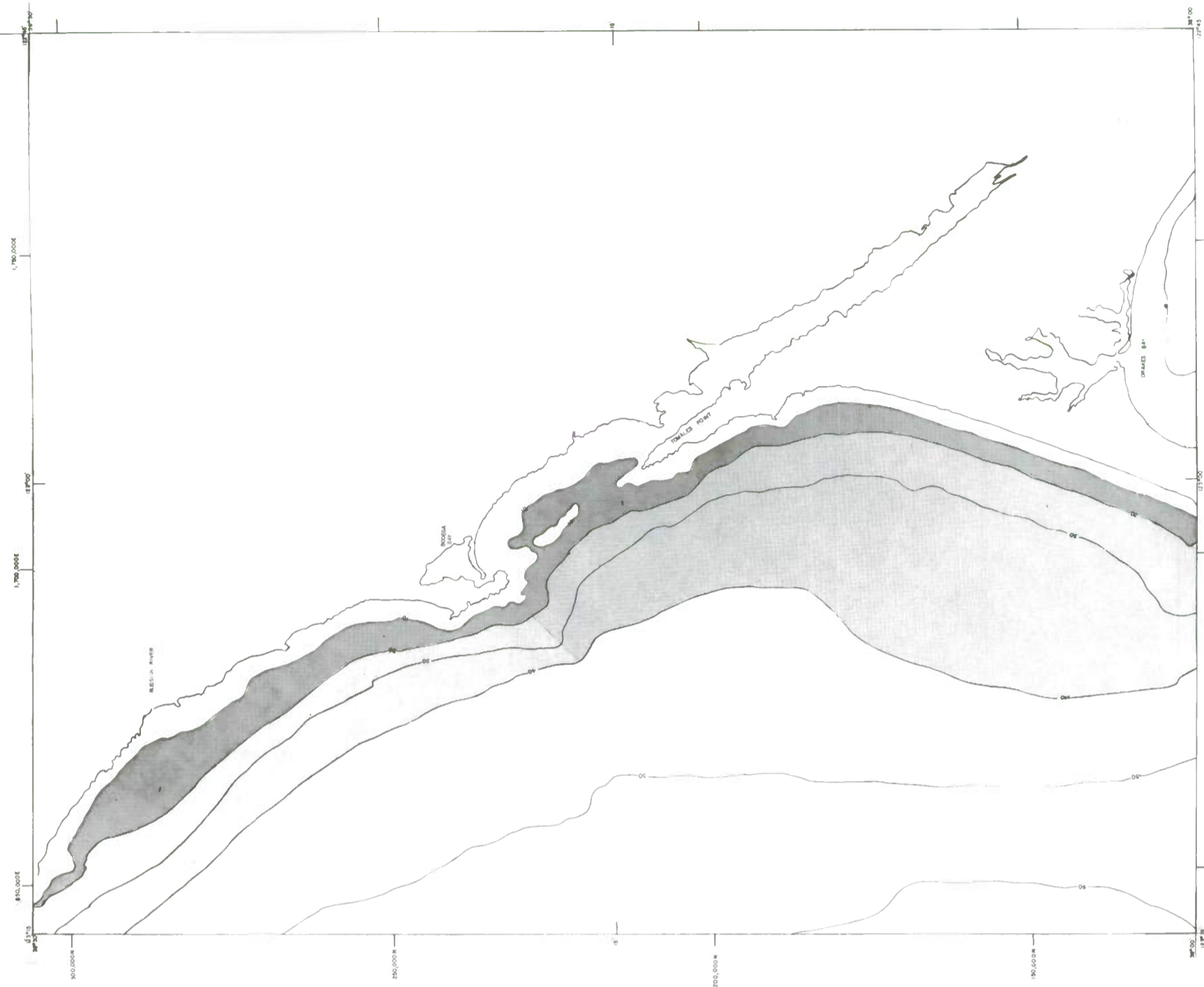


Part D. Tsunami surge.

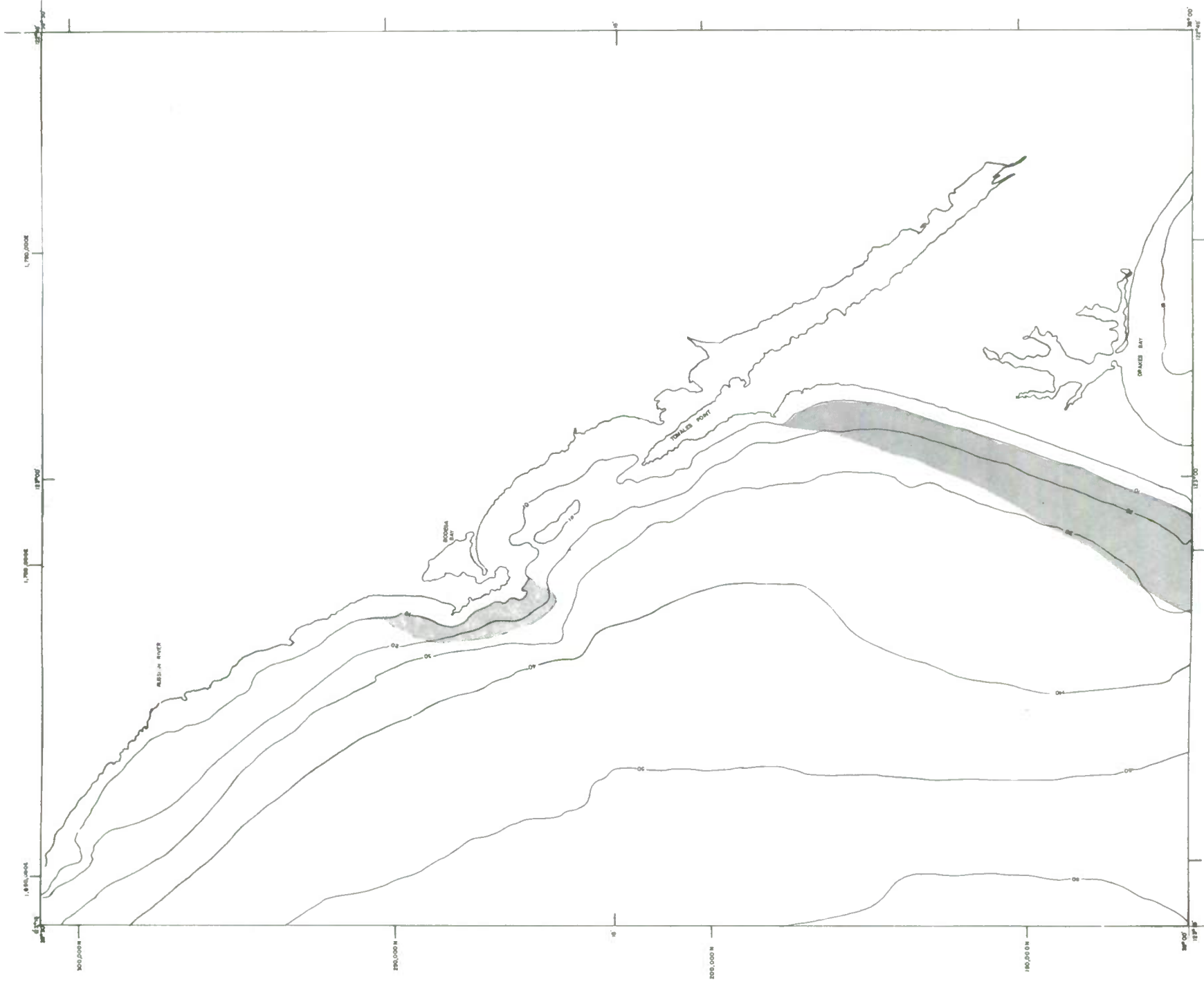
Figure 15. Predicted regions of century extremes for chart number 12.



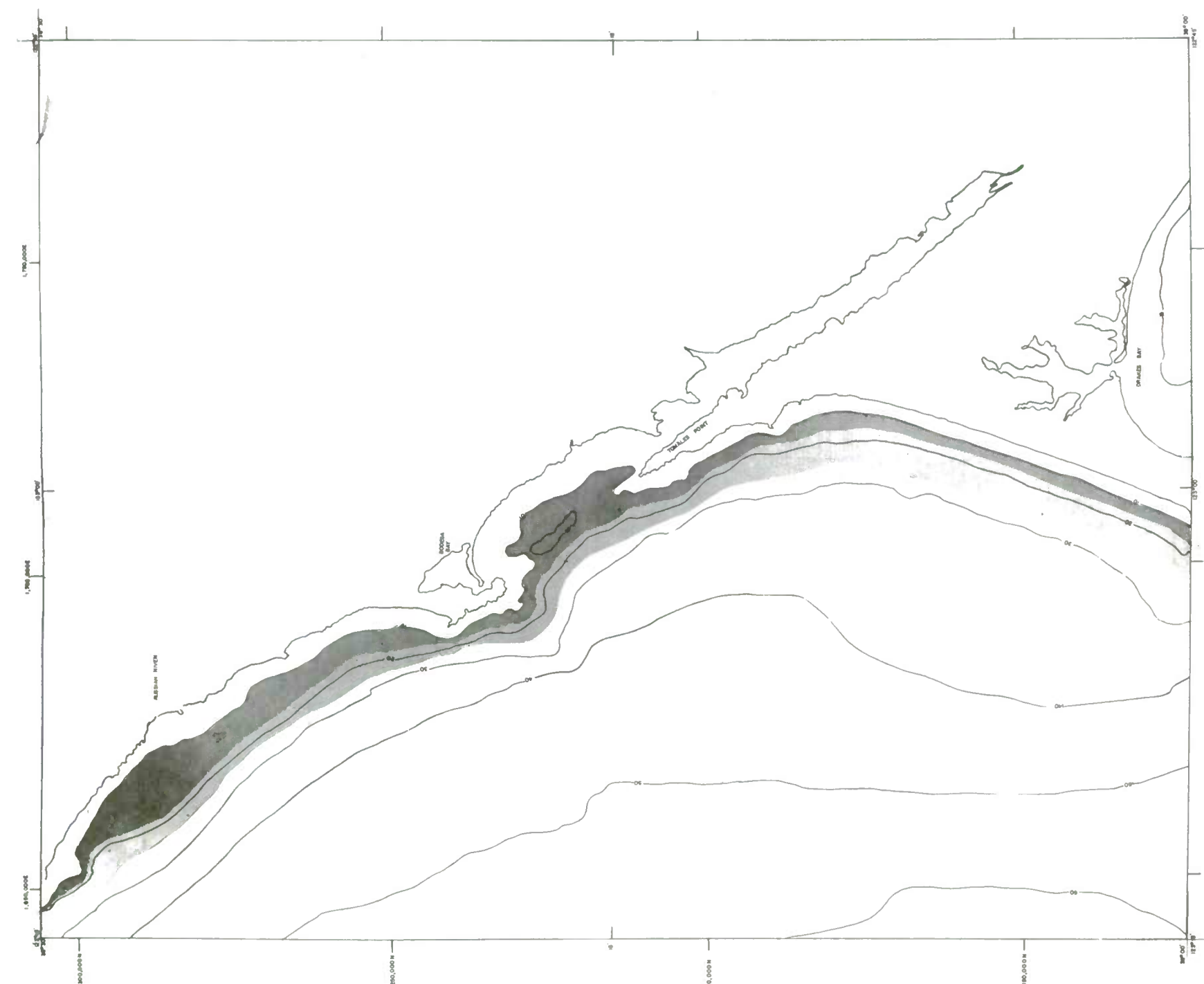
Part A. Density.



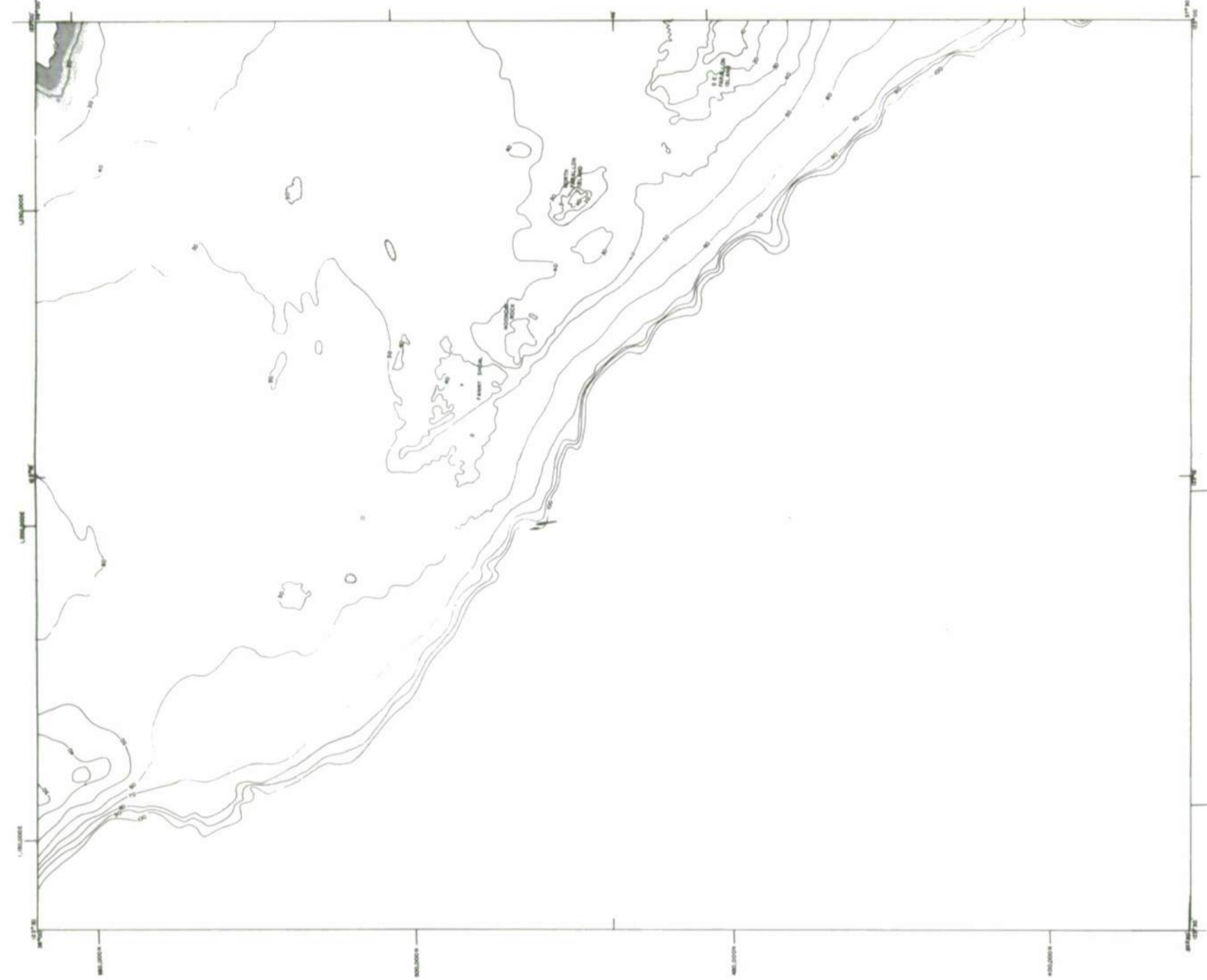
Part B. Bottom wave surge.



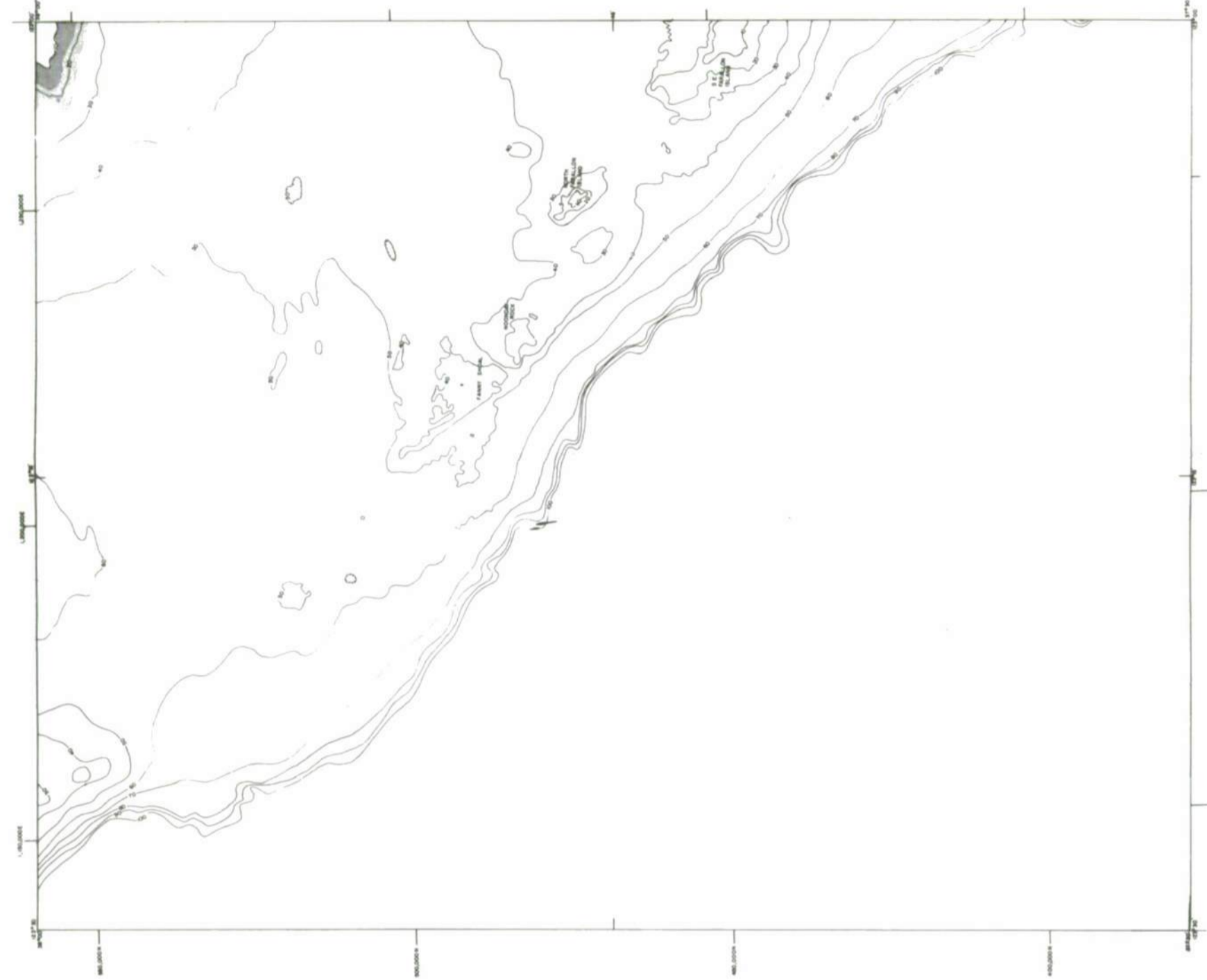
Part C. Bottom current velocity.



Part D. Tsunami surge.

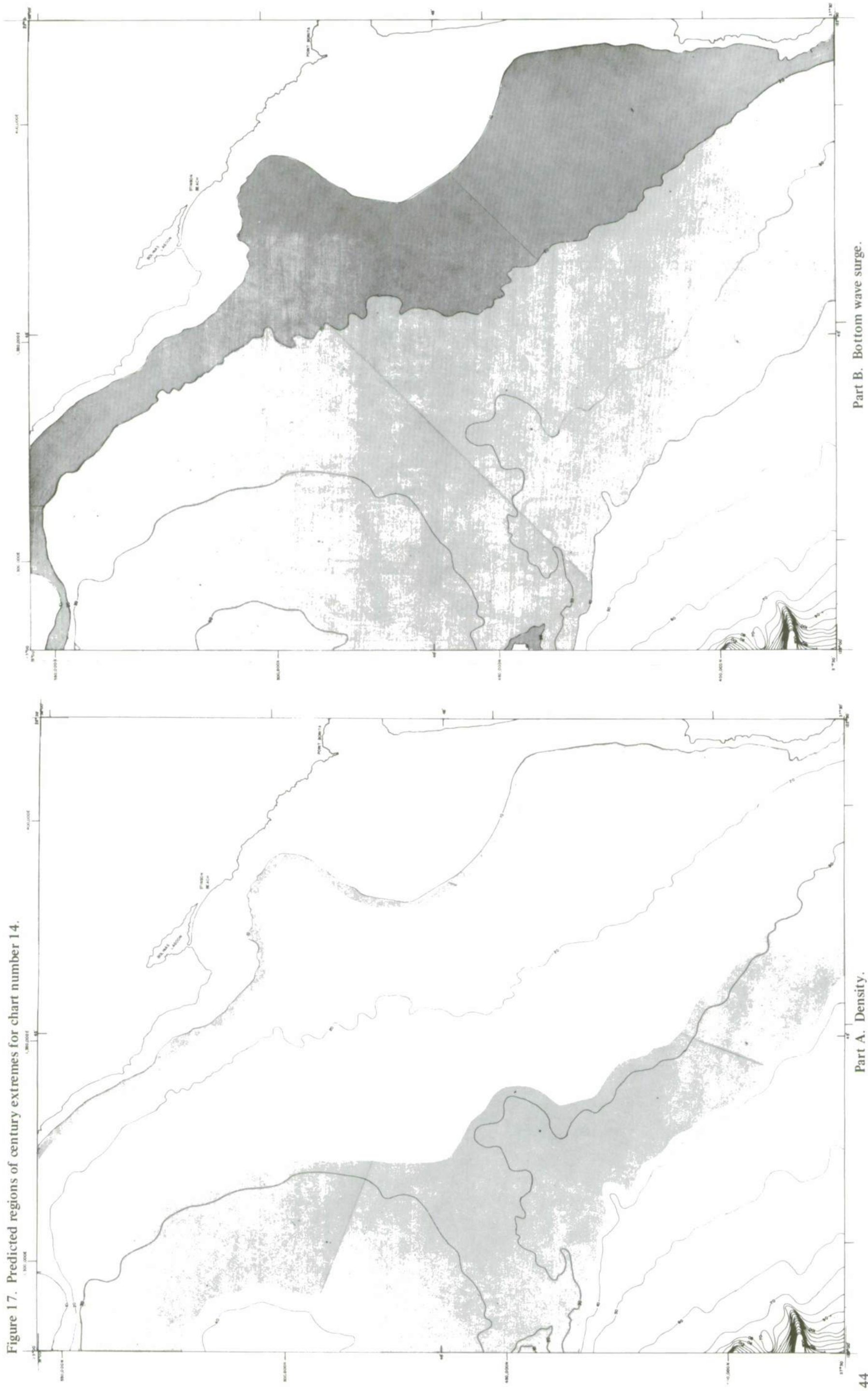


Part C. Bottom current velocity.



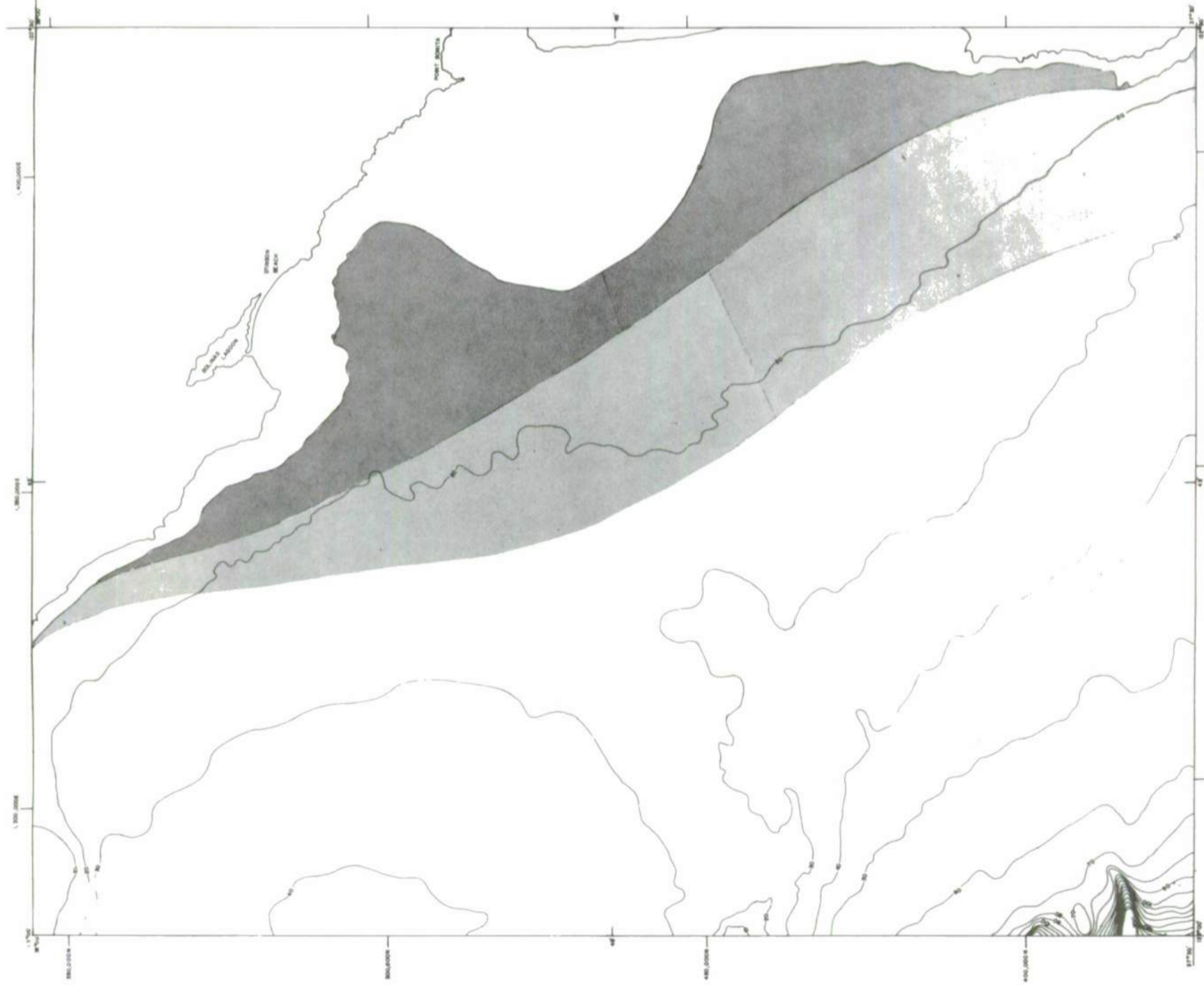
Part D. Tsunami surge.

Figure 17. Predicted regions of century extremes for chart number 14.

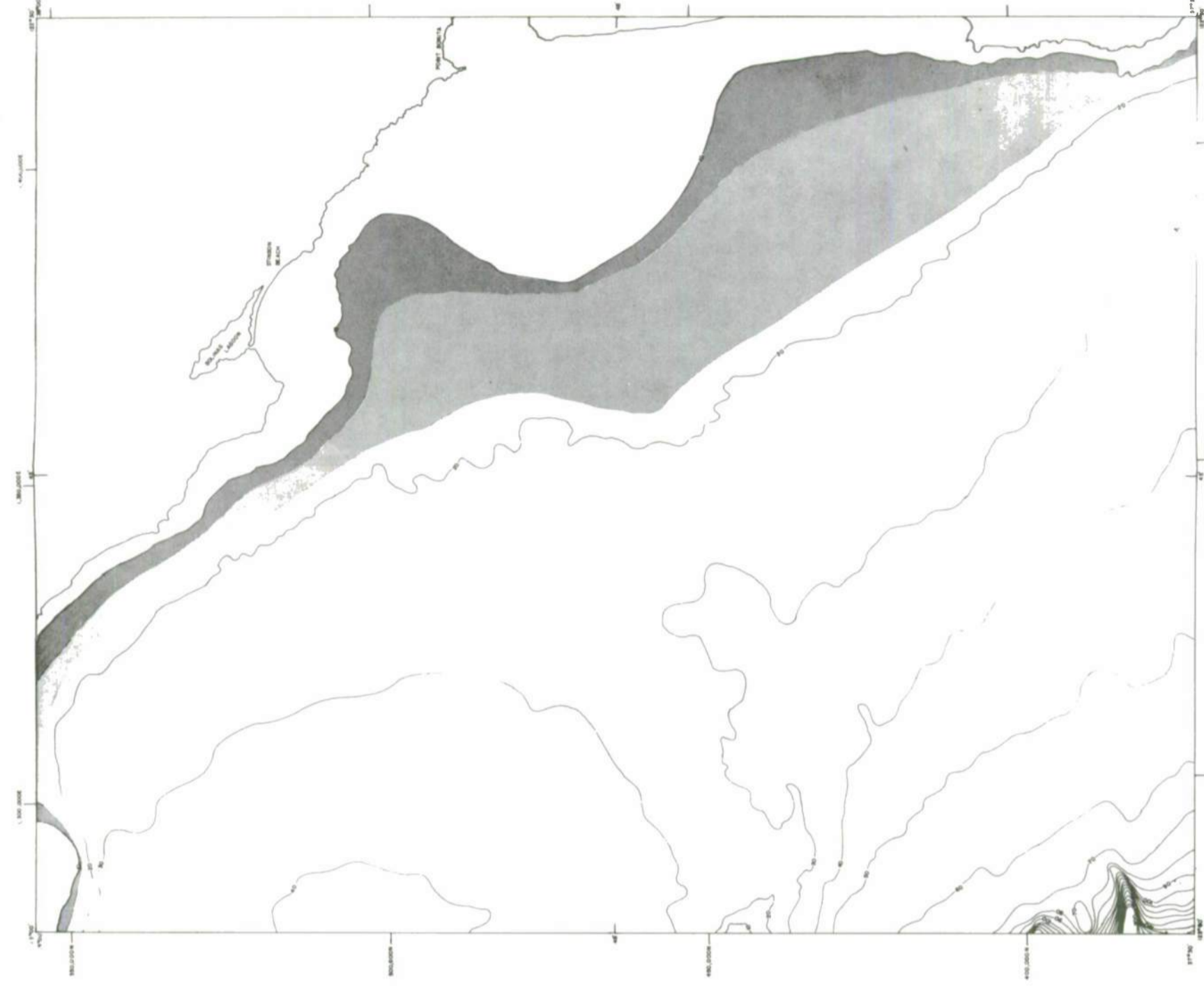


Part B. Bottom wave surge.

Part A. Density.

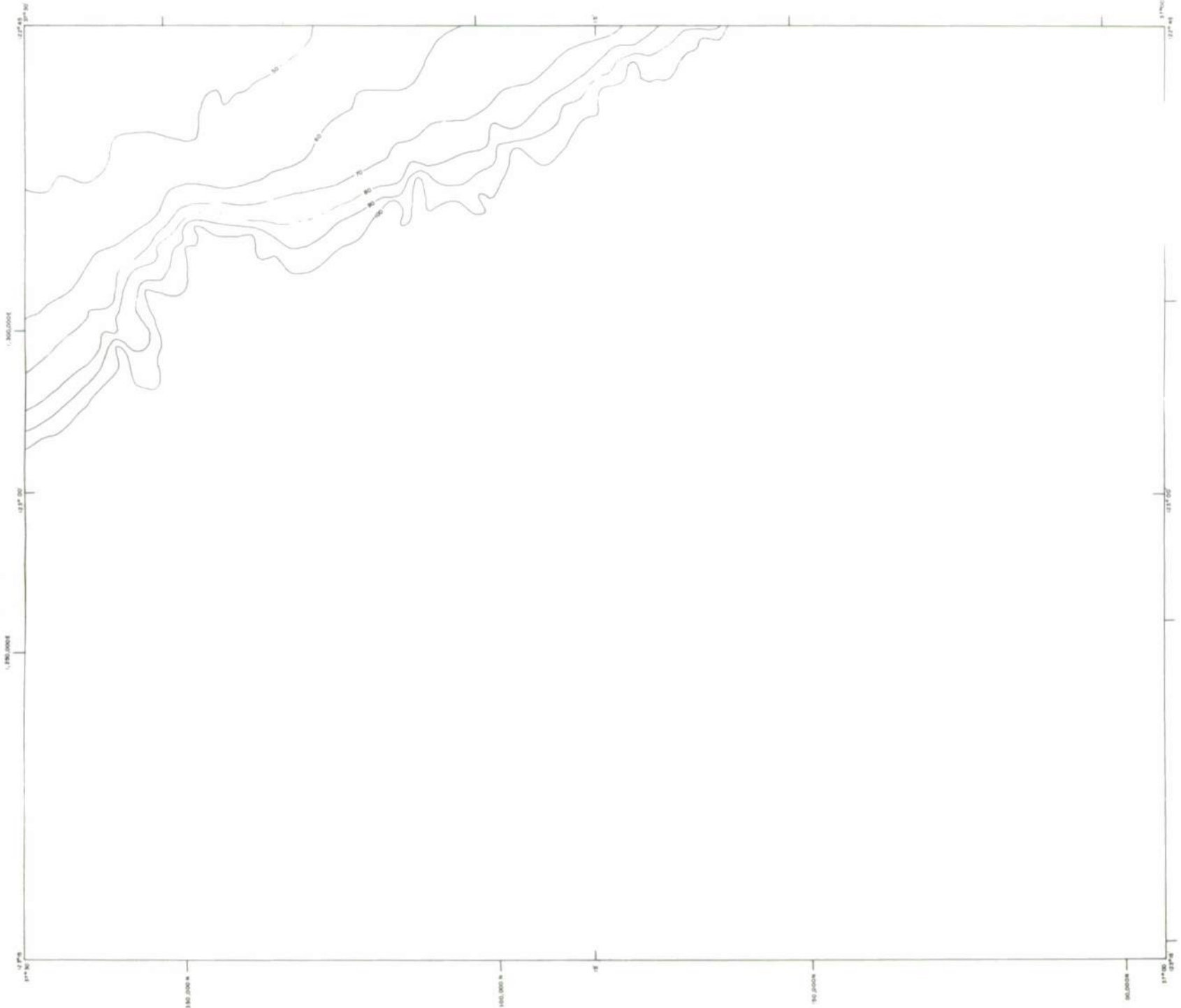


Part C. Bottom current velocity.

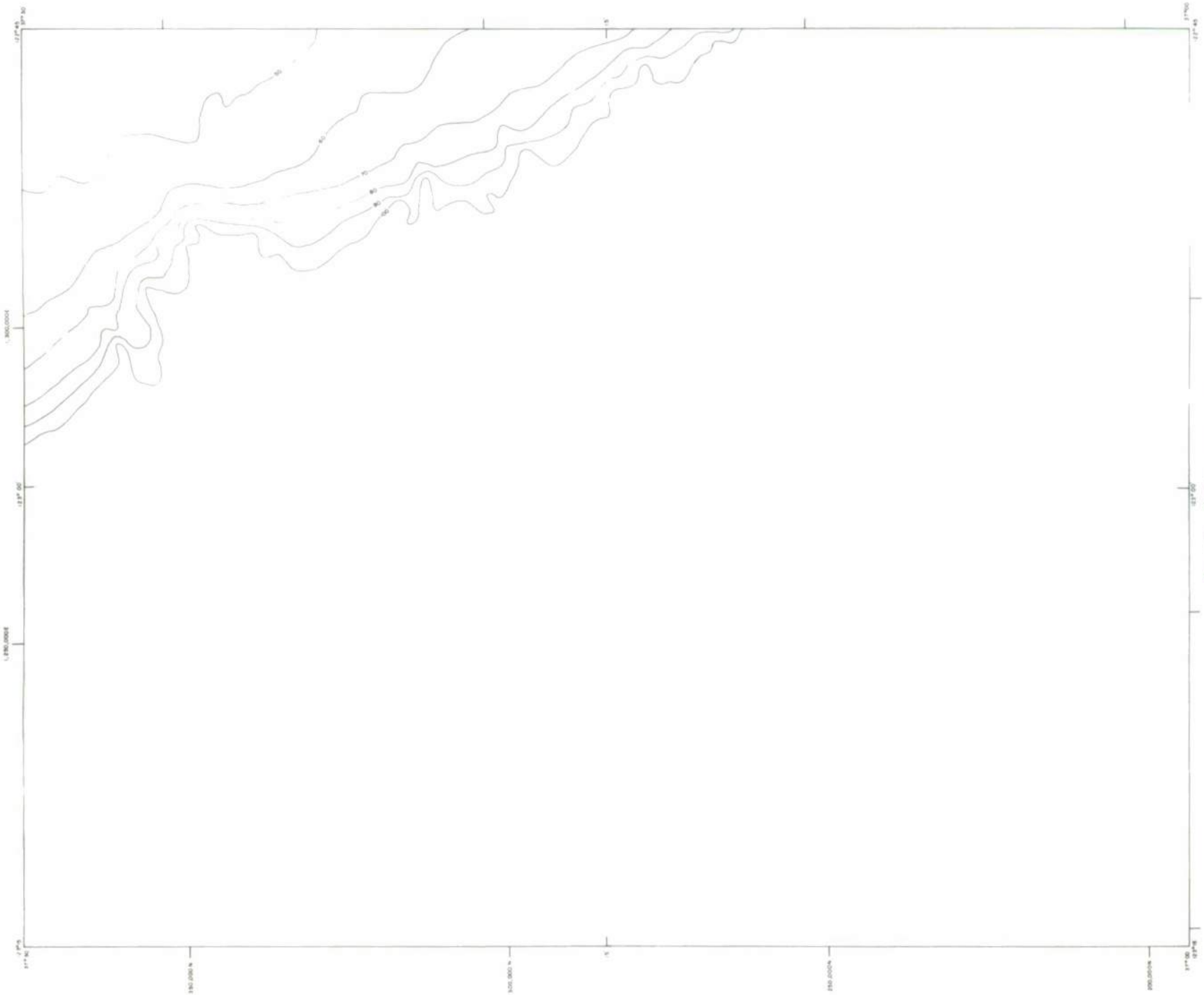


Part D. Tsunami surge.

Figure 18. Predicted regions of century extremes for chart number 15.

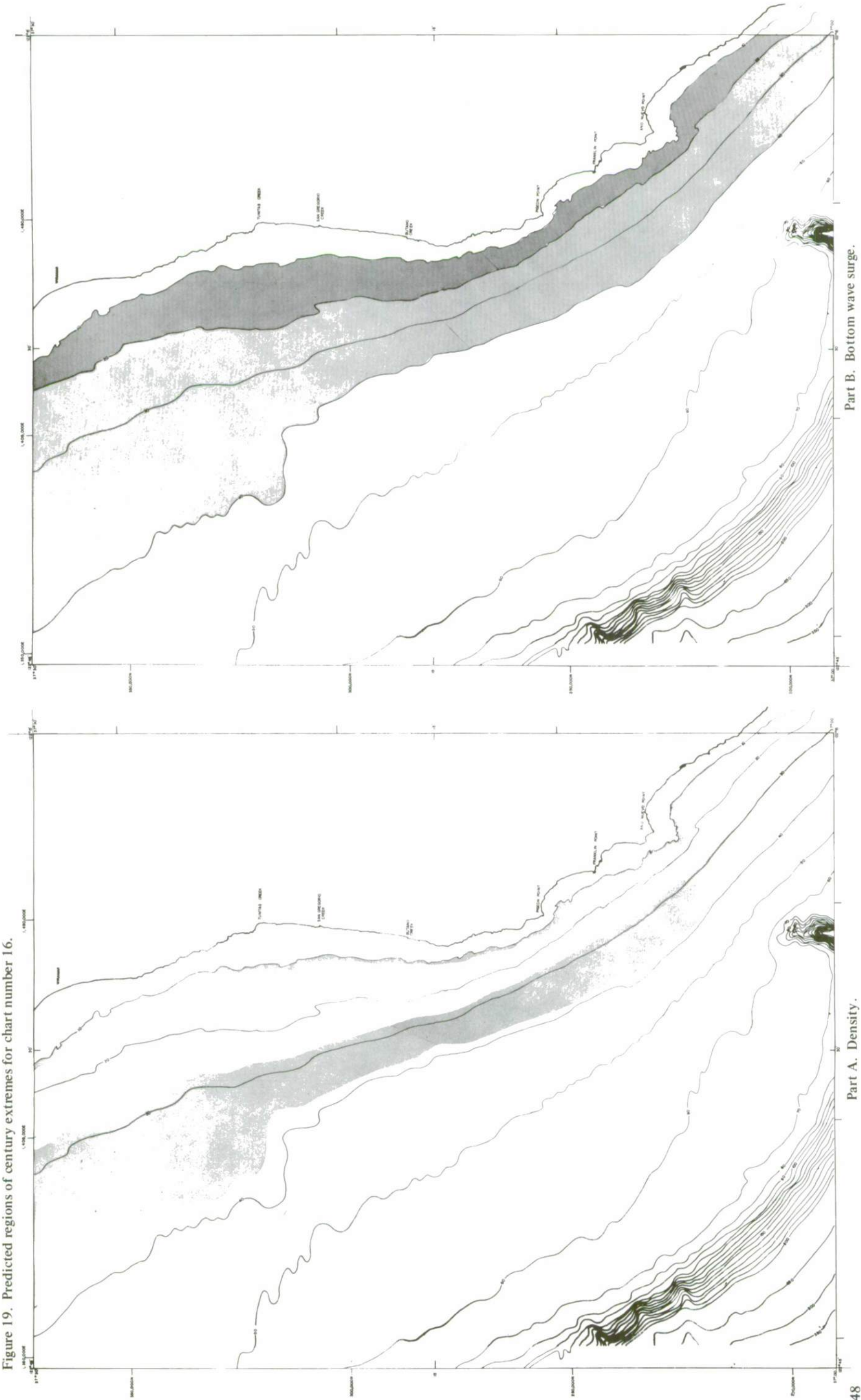


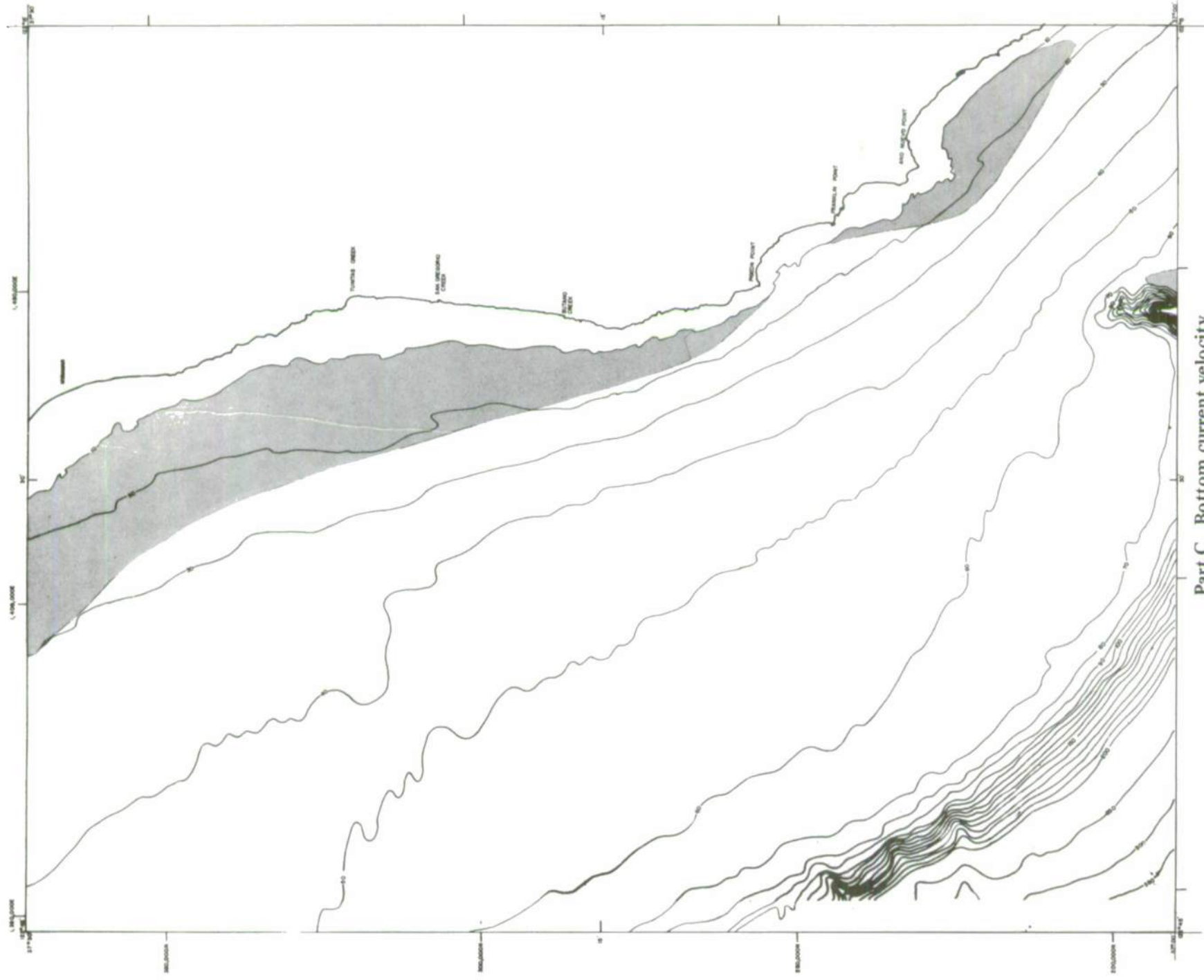
Part A. Density.



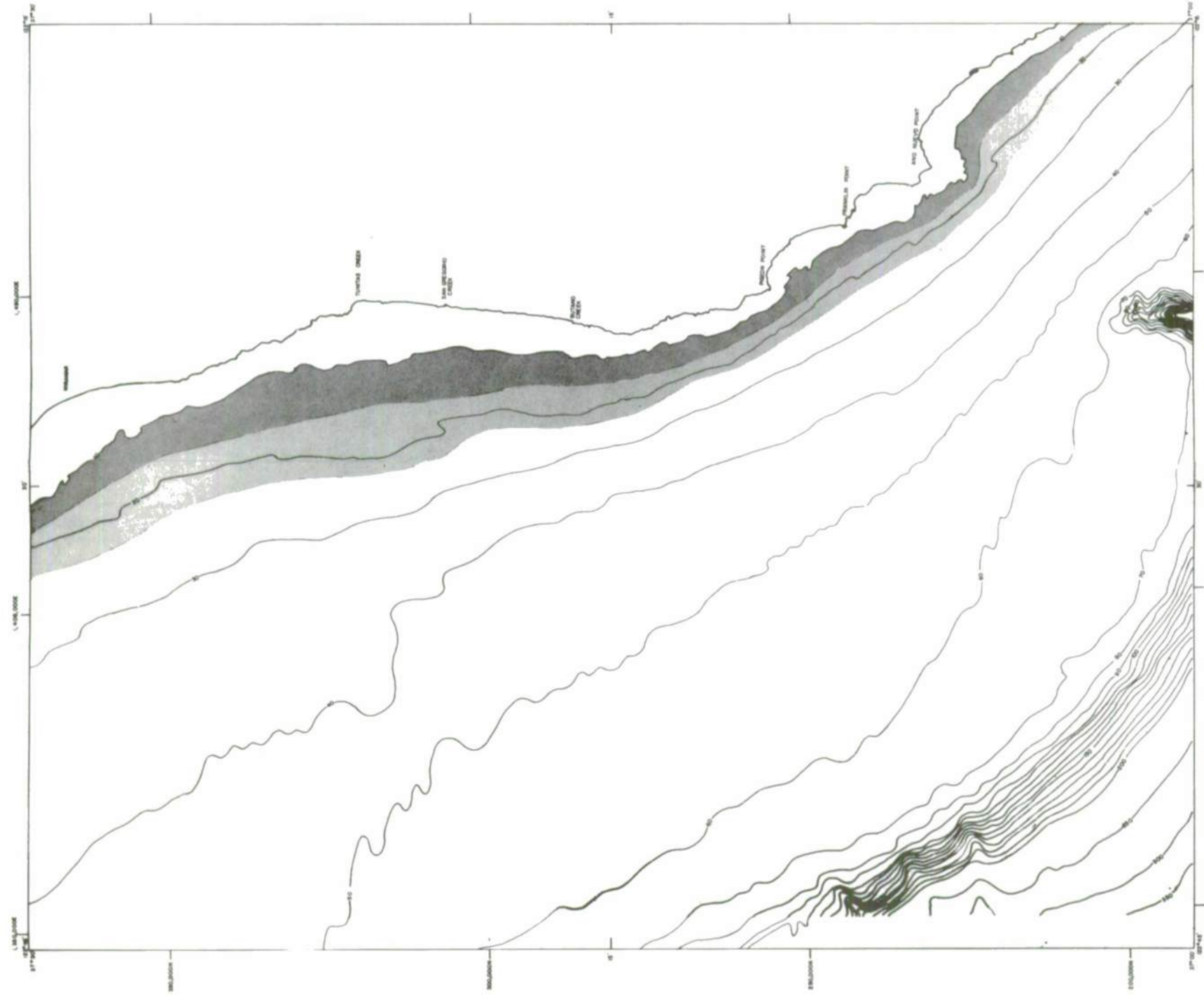
Part B. Bottom wave surge.

Figure 19. Predicted regions of century extremes for chart number 16.



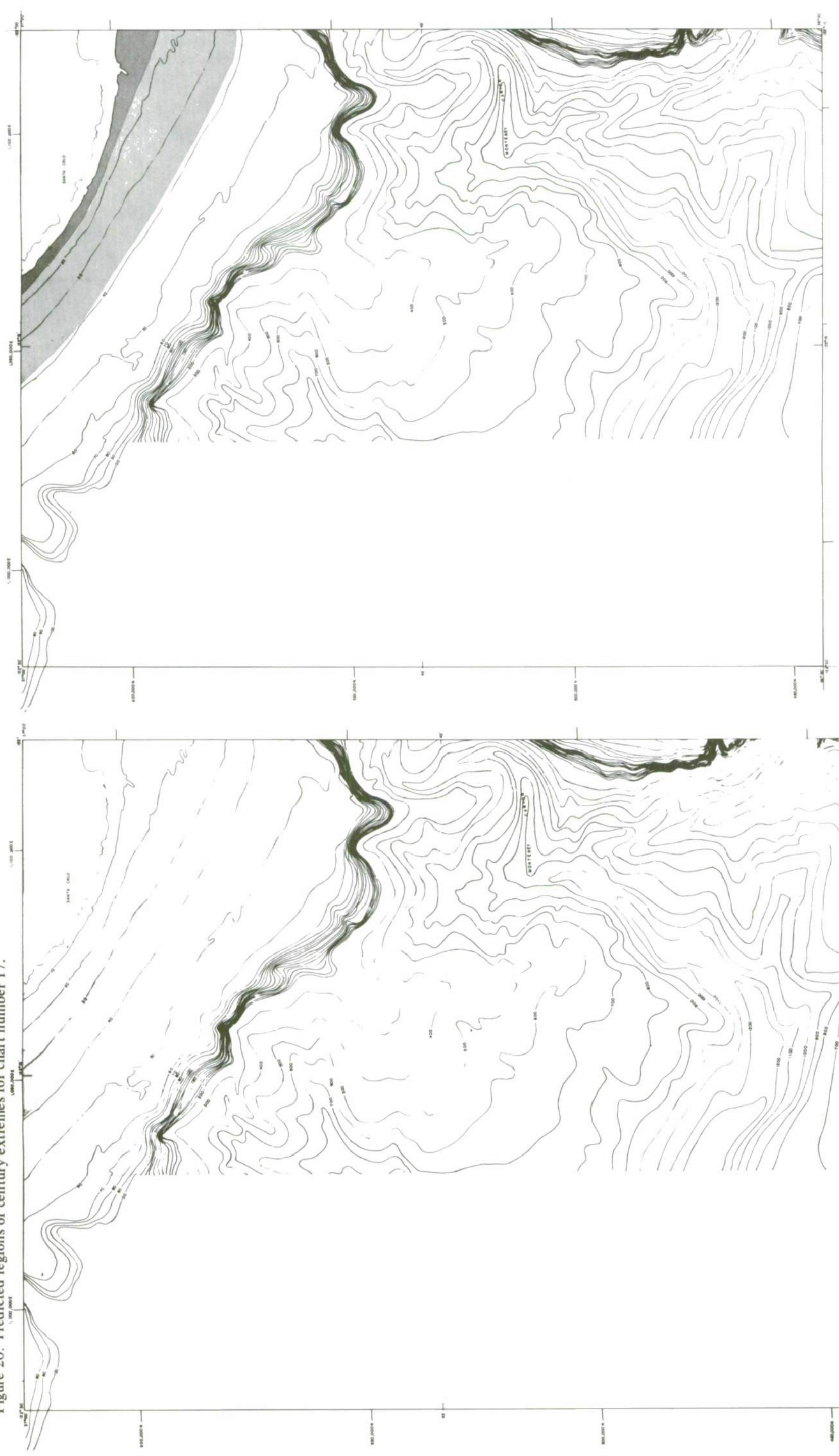


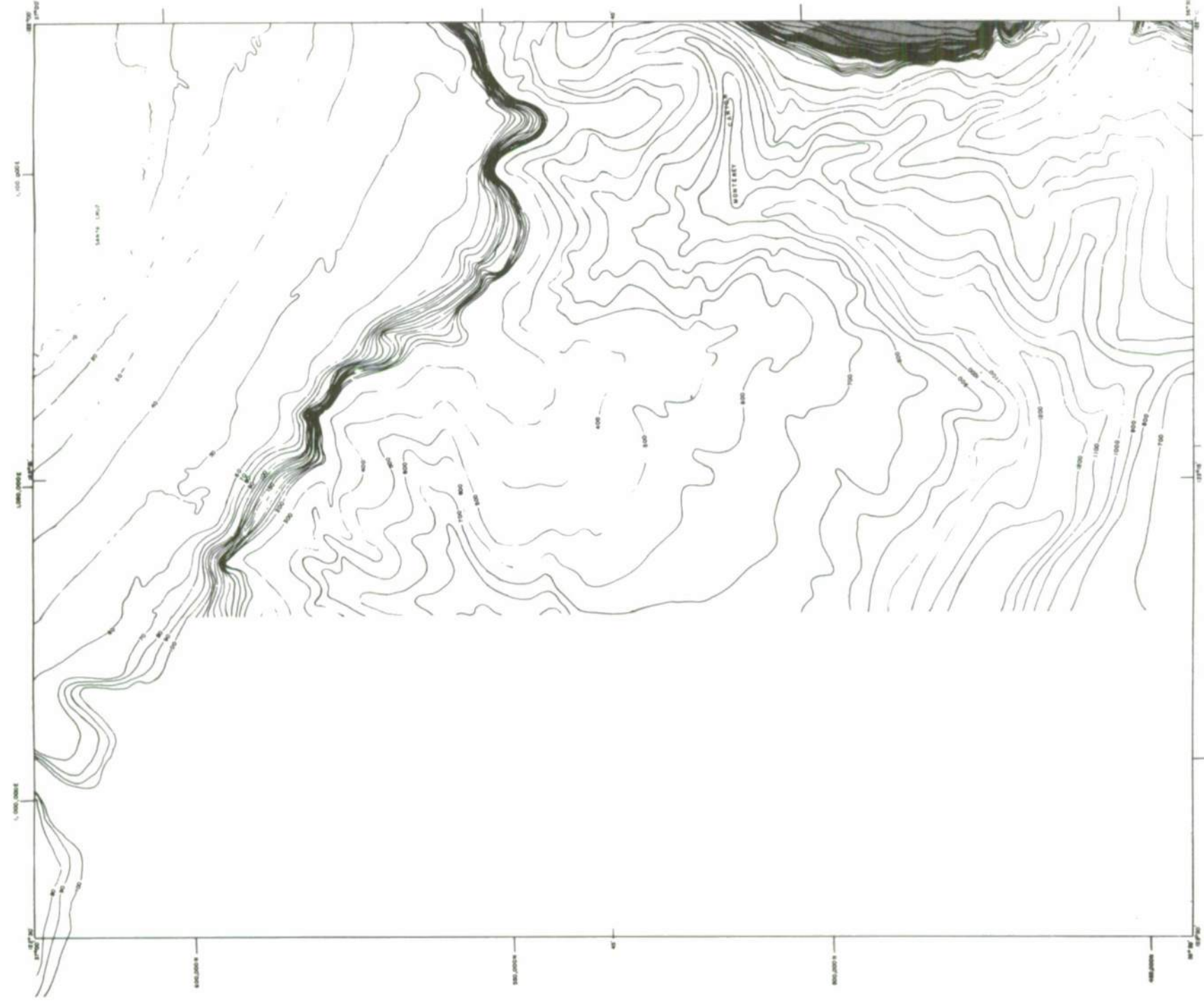
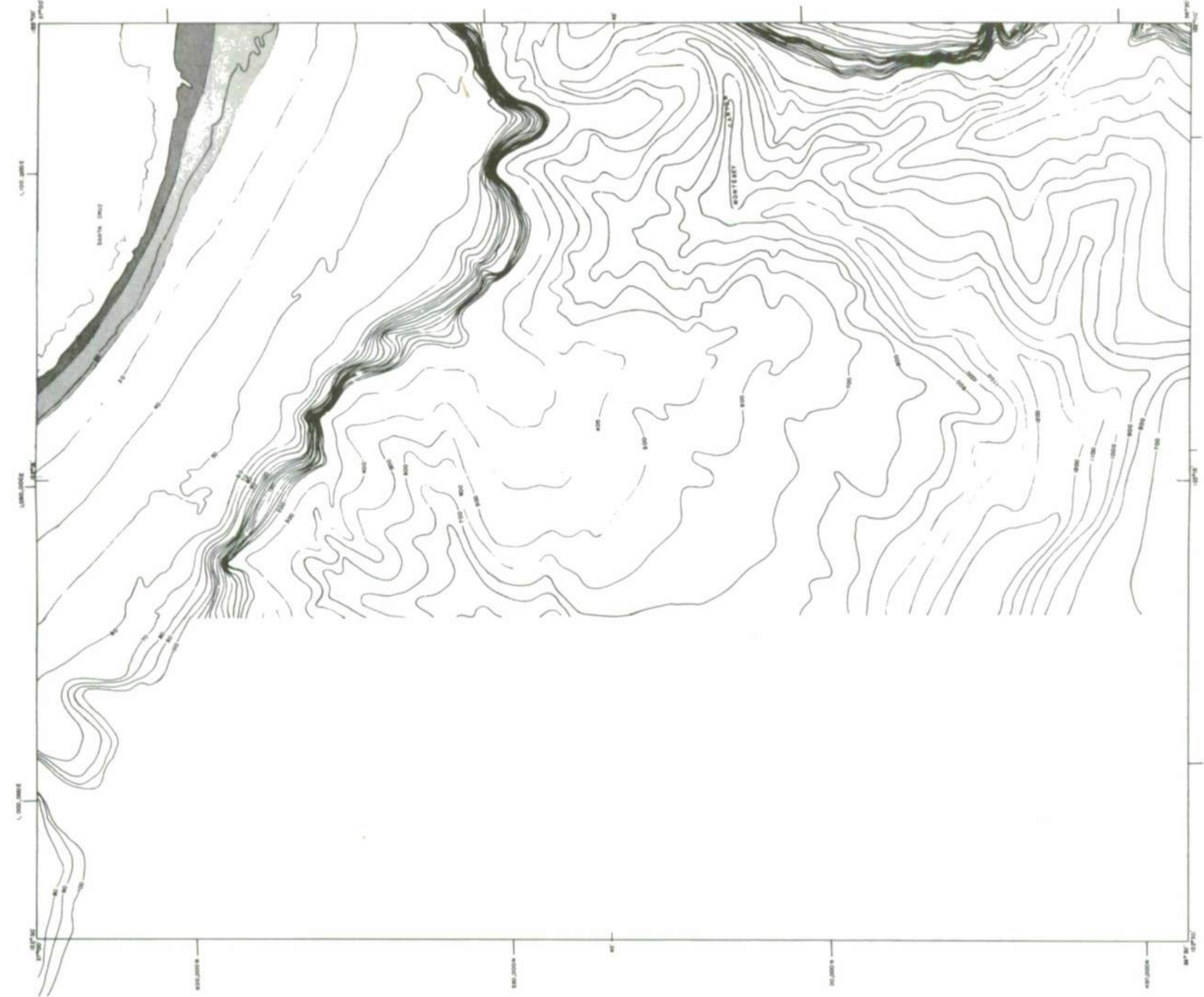
Part C. Bottom current velocity.



Part D. Tsunami surge.

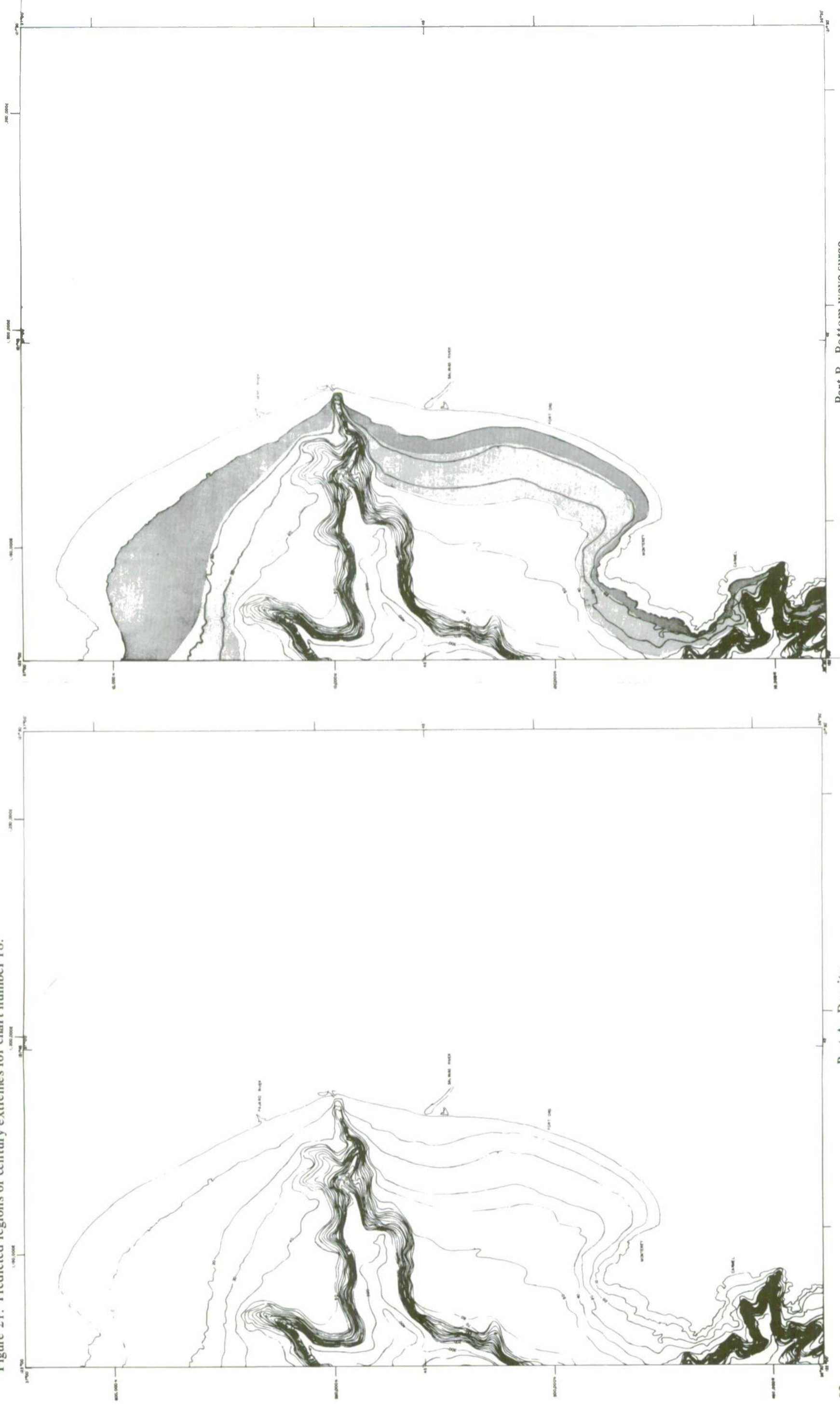
Figure 20. Predicted regions of century extremes for chart number 17.

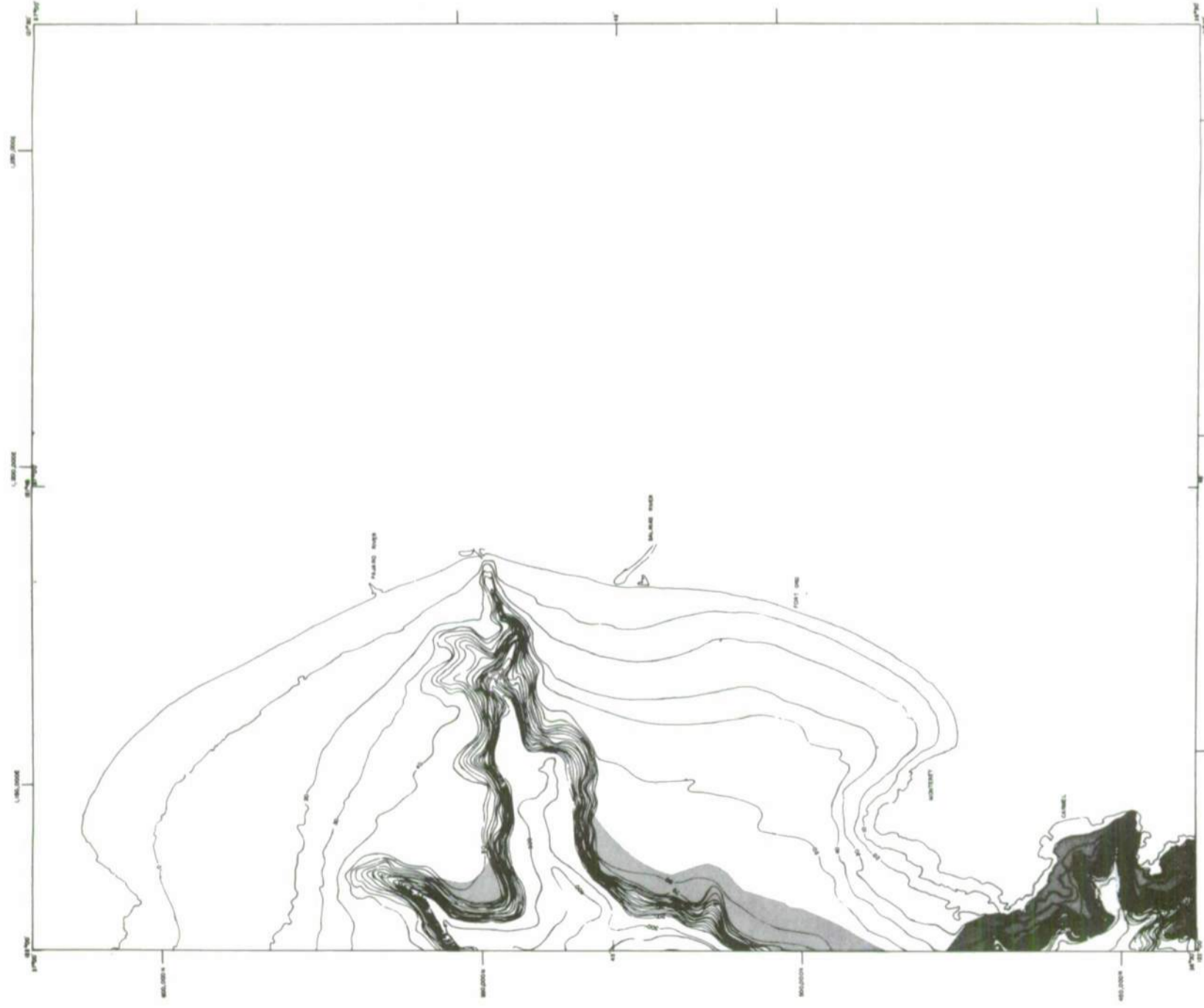




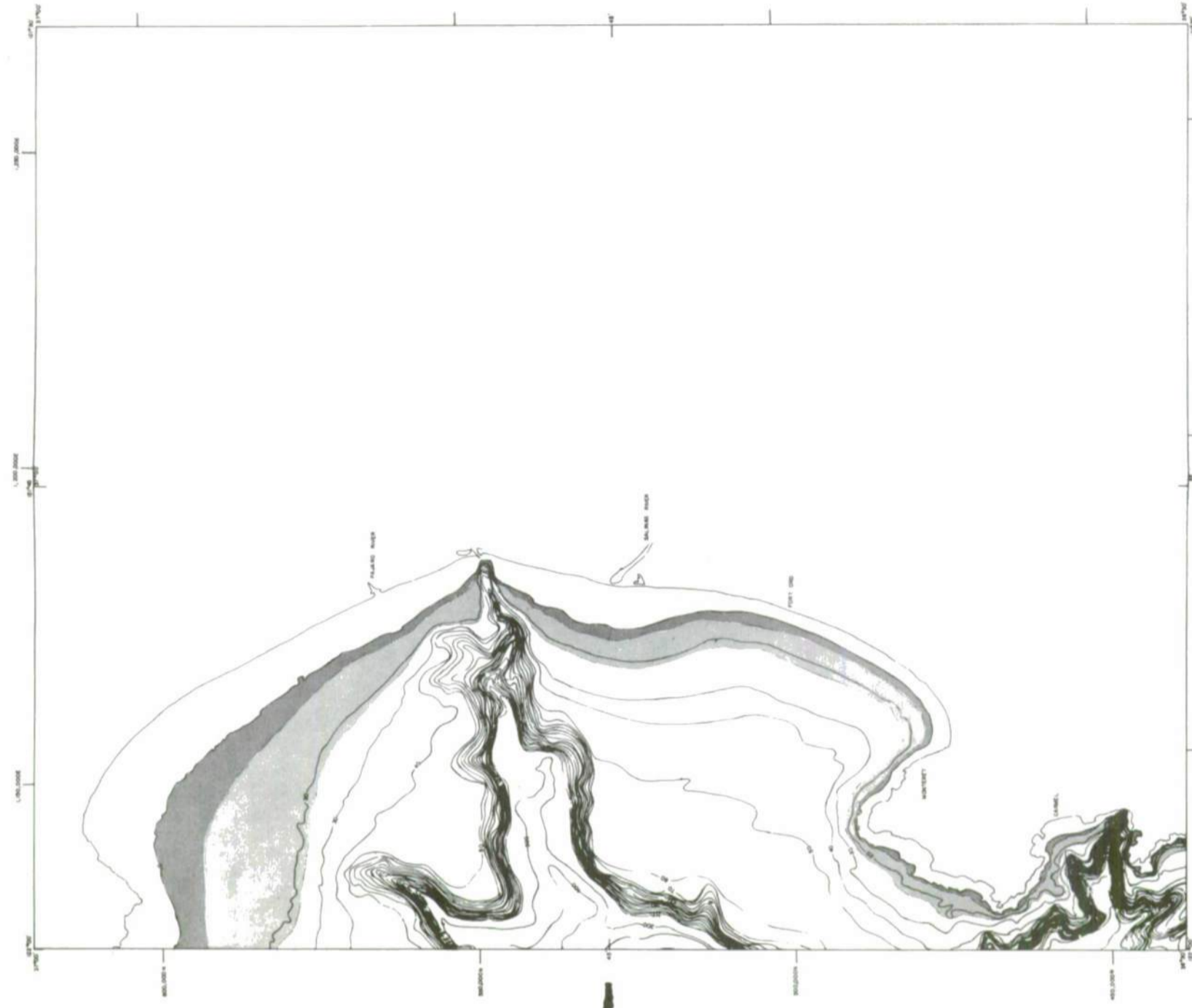
Part C. Bottom current velocity.

Figure 21. Predicted regions of century extremes for chart number 18.



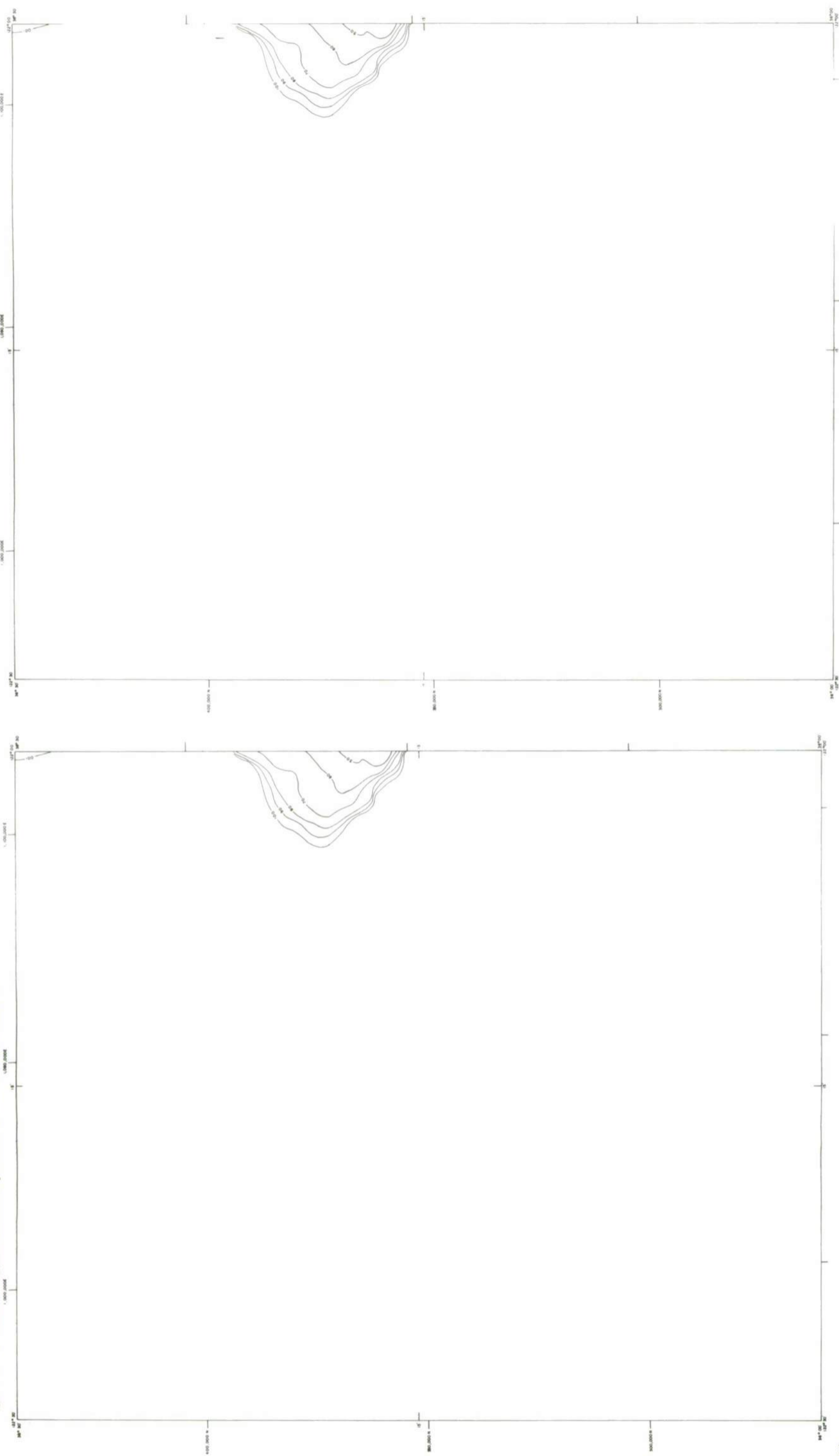


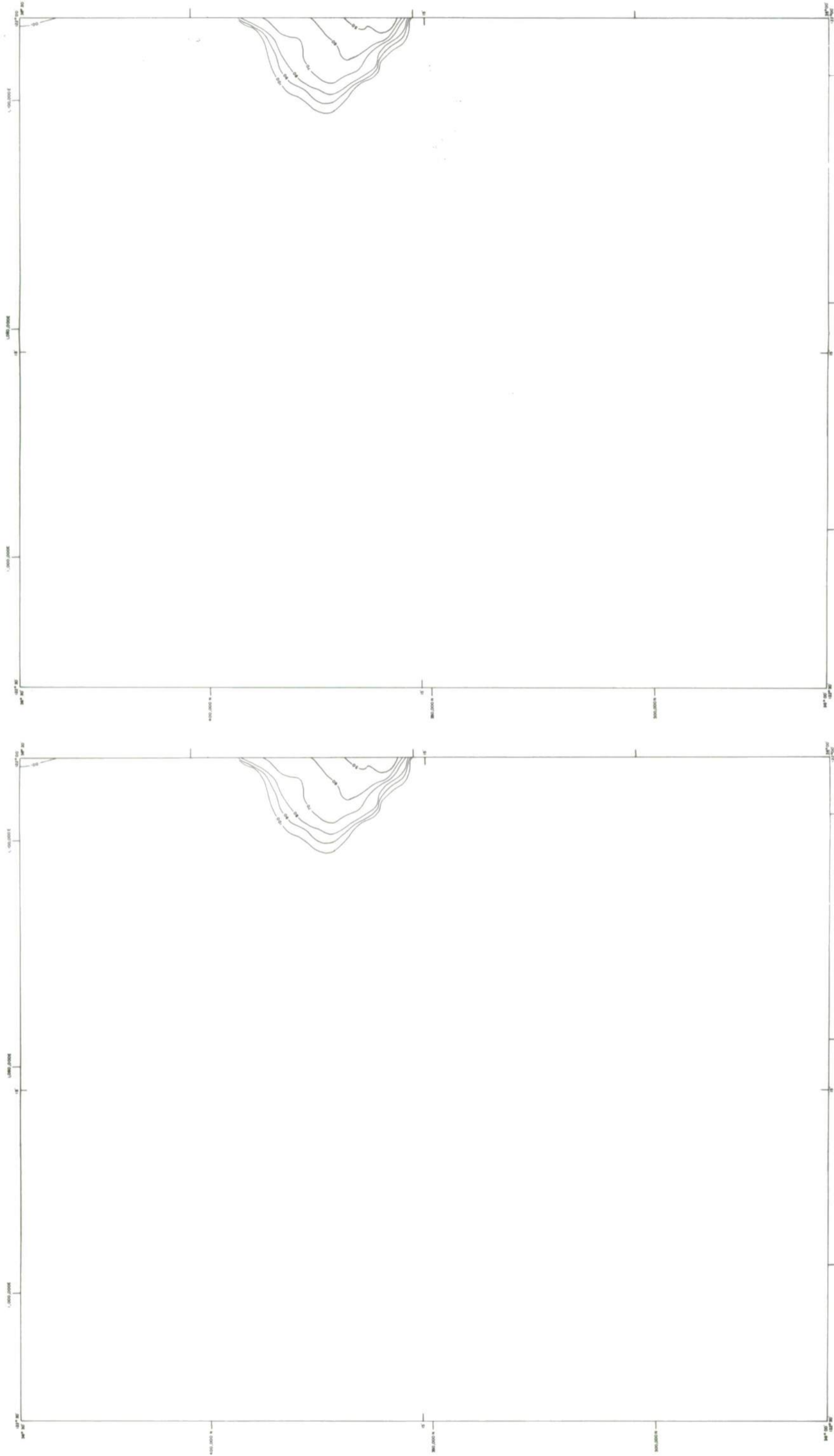
Part C. Bottom current velocity.



Part D. Tsunami surge.

Figure 22. Predicted regions of century extremes for chart number 19.

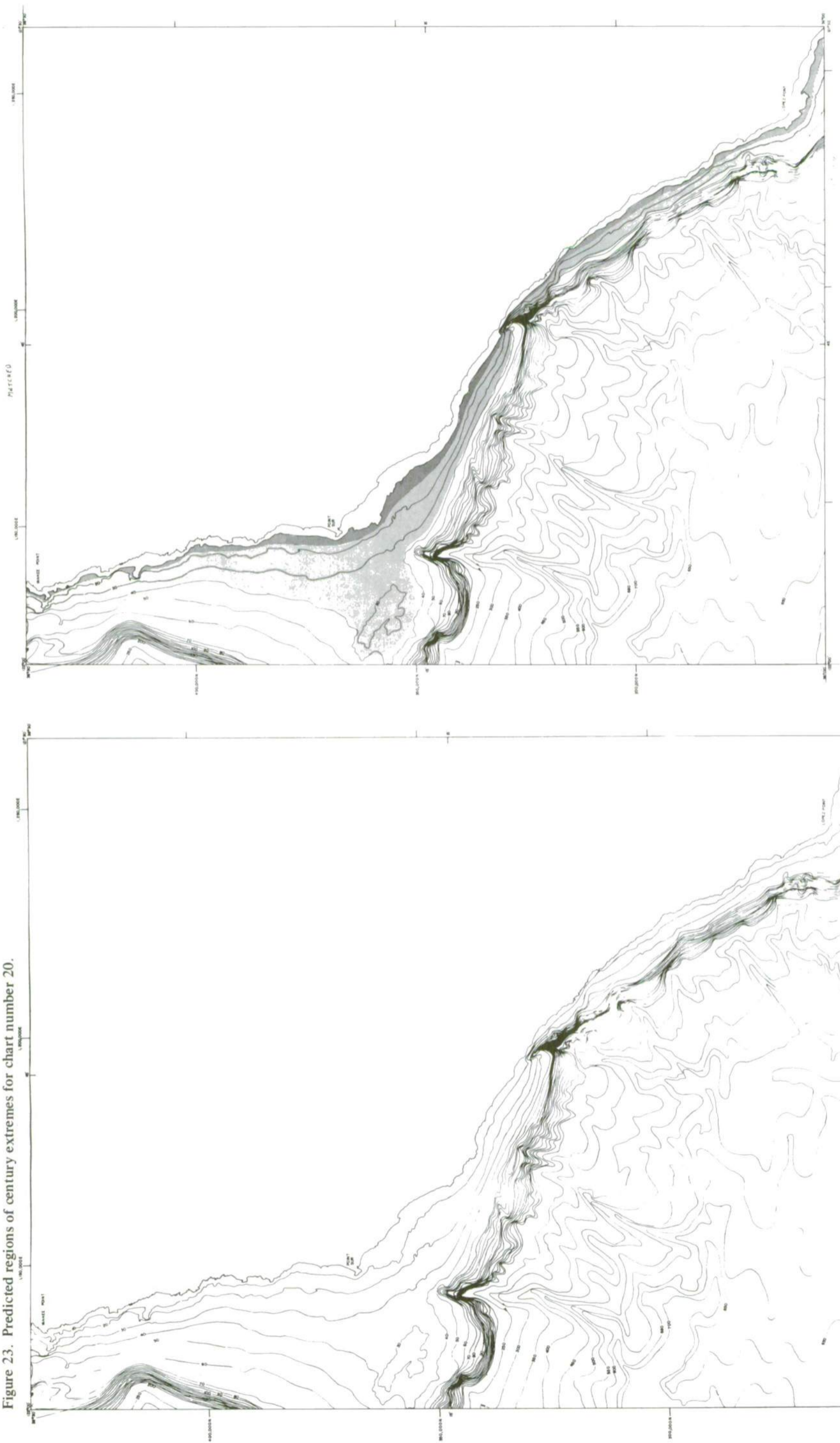




Part C. Bottom current velocity.

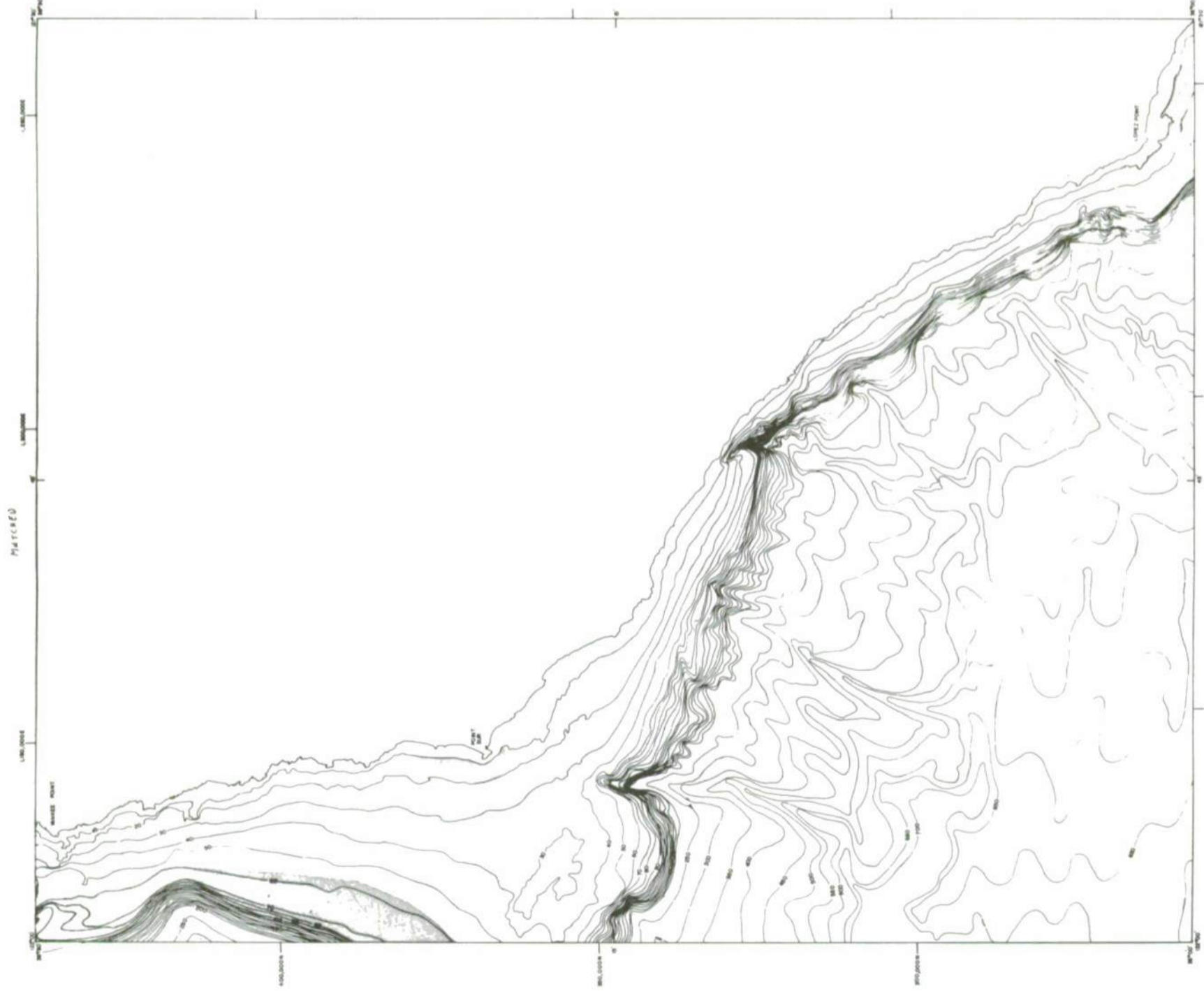
Part D. Tsunami surge.

Figure 23. Predicted regions of century extremes for chart number 20.

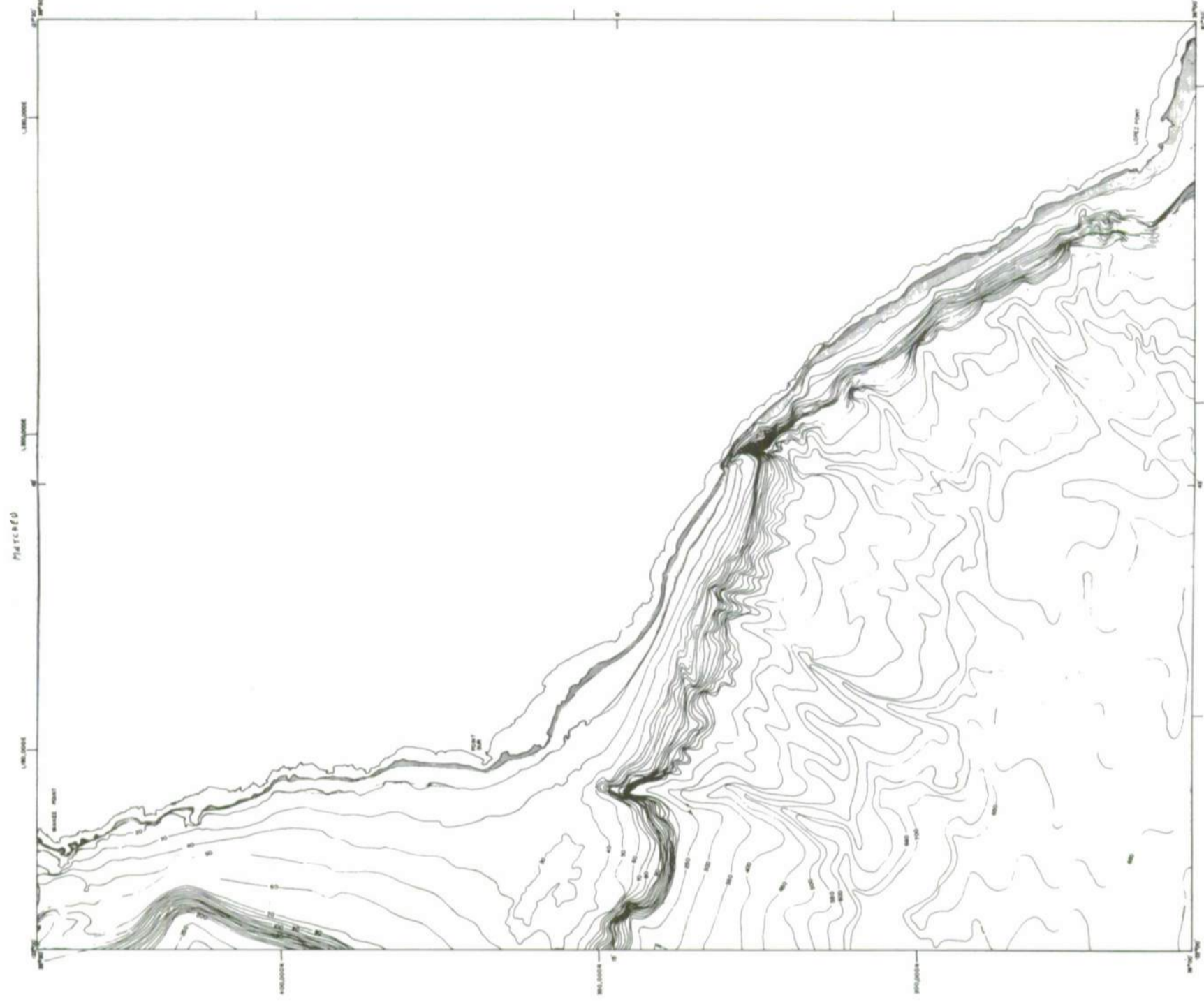


Part B. Bottom wave surge.

Part A. Density.

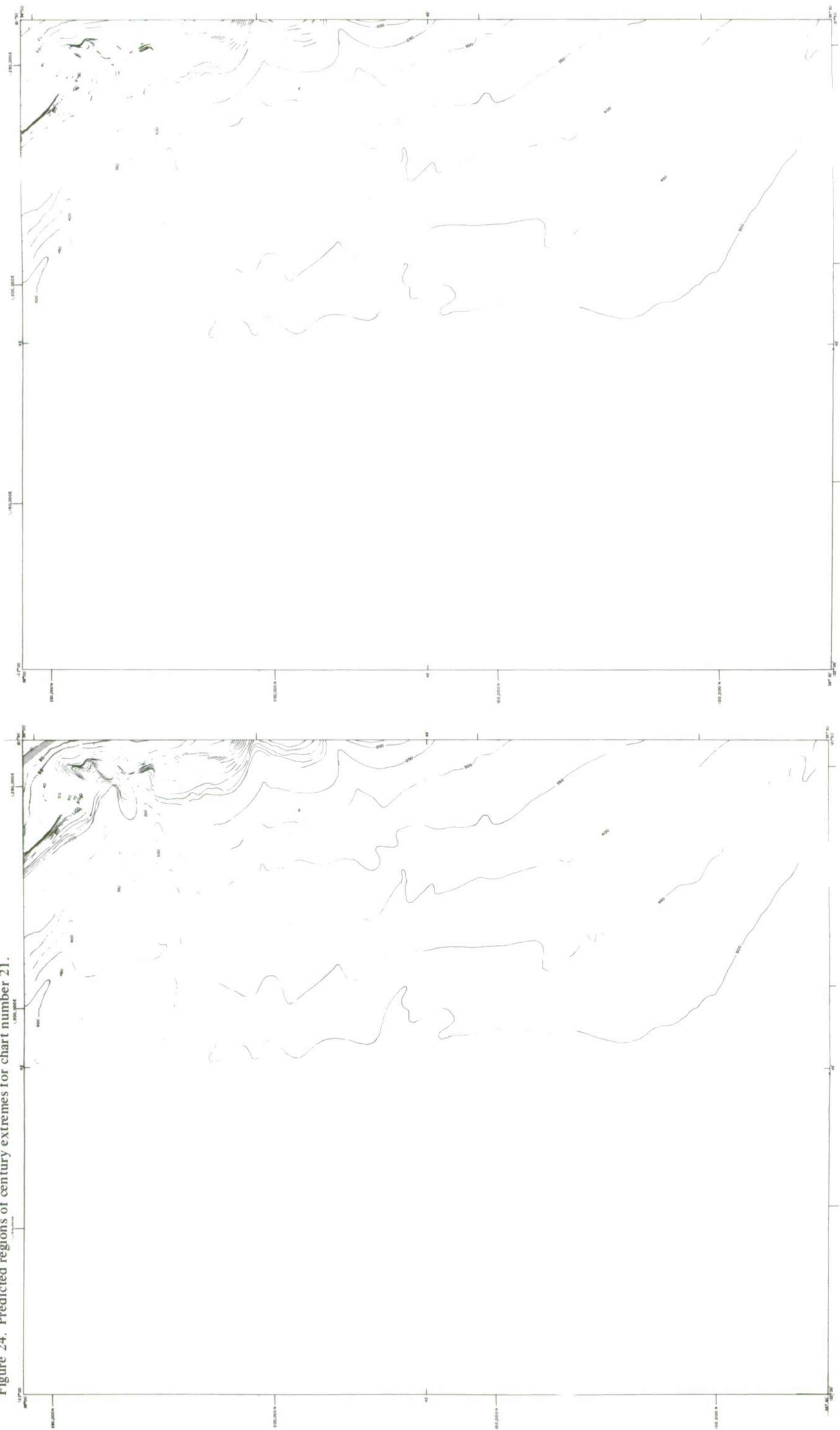


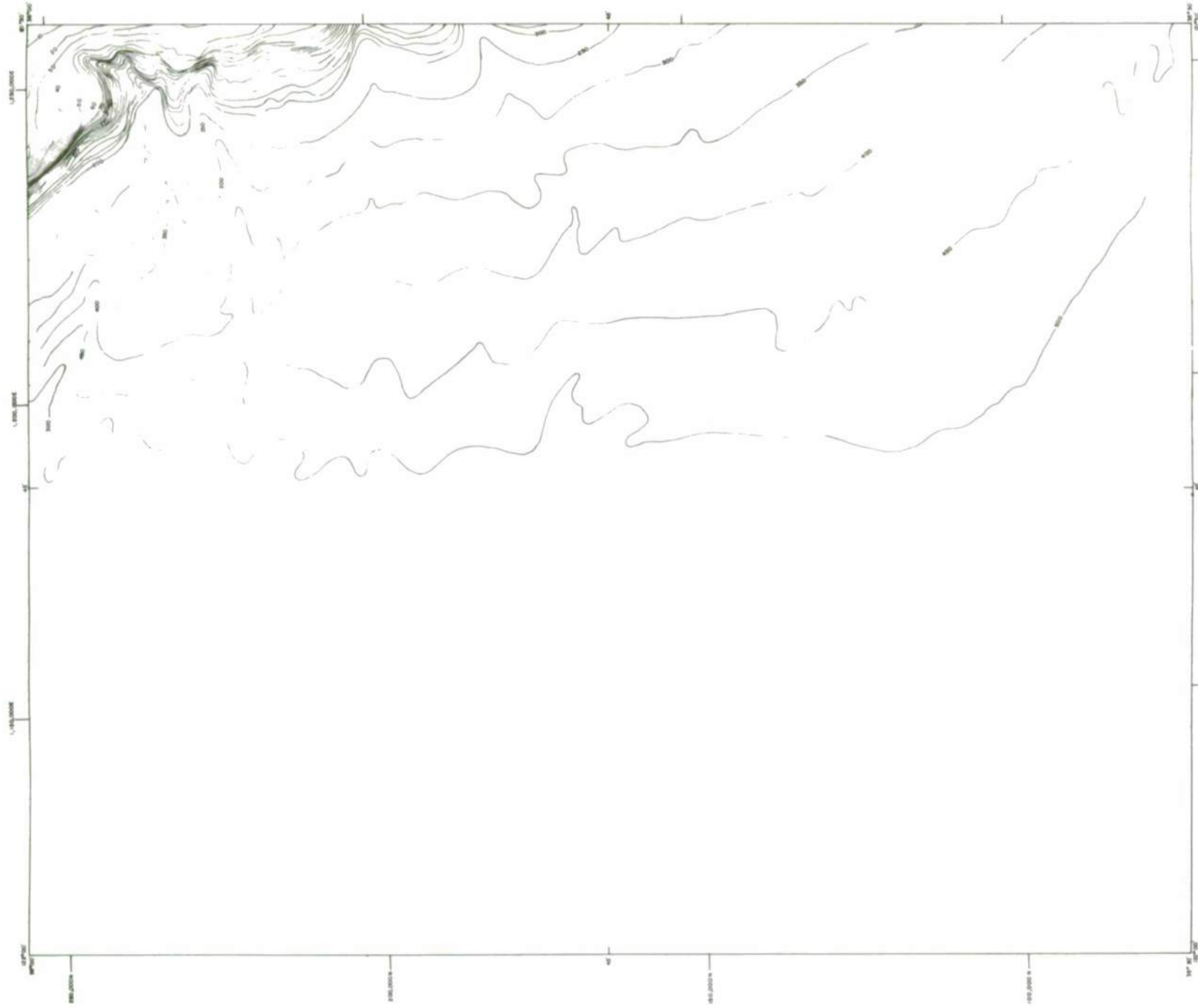
Part C. Bottom current velocity.



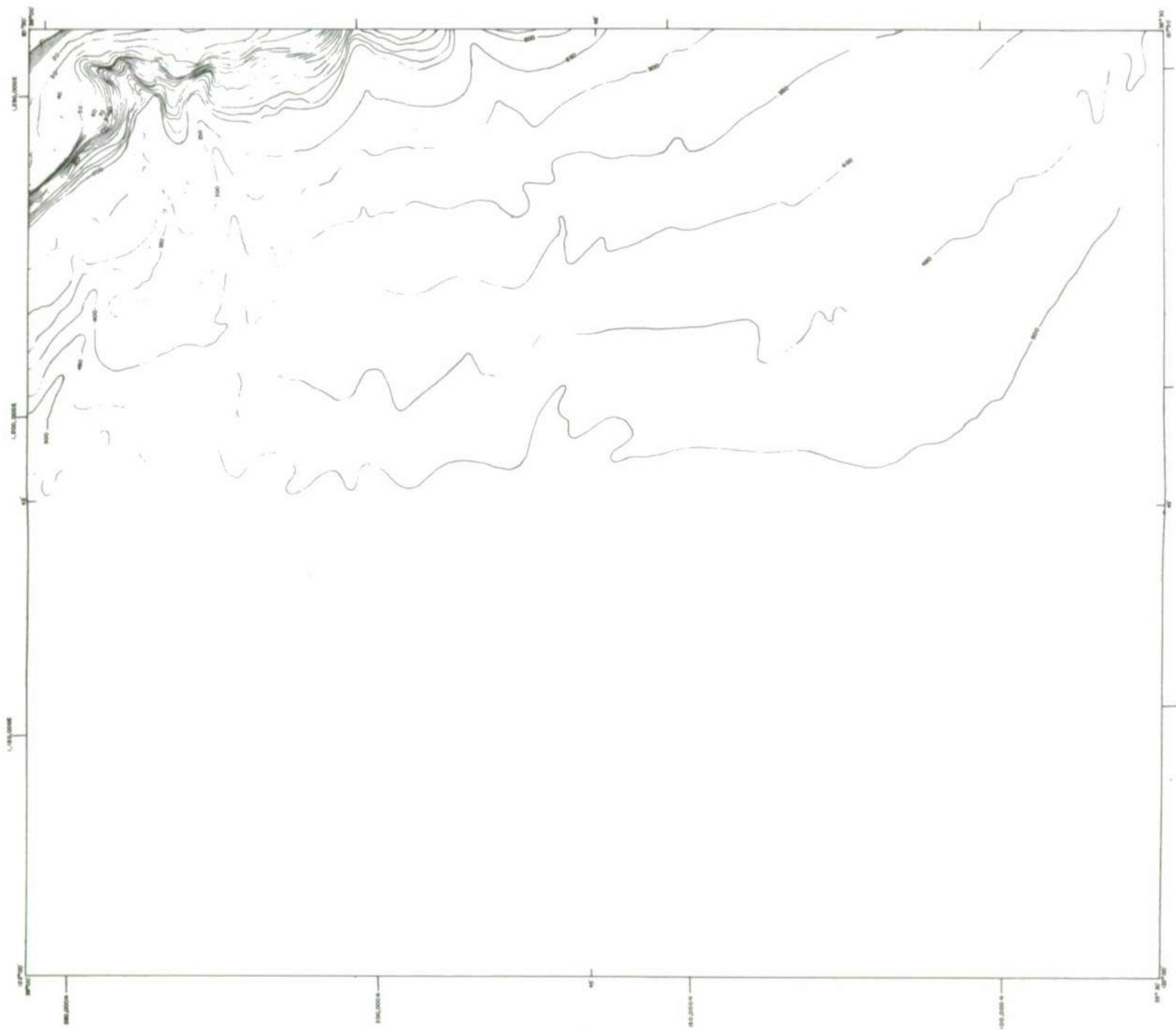
Part D. Tsunami surge.

Figure 24. Predicted regions of century extremes for chart number 21.



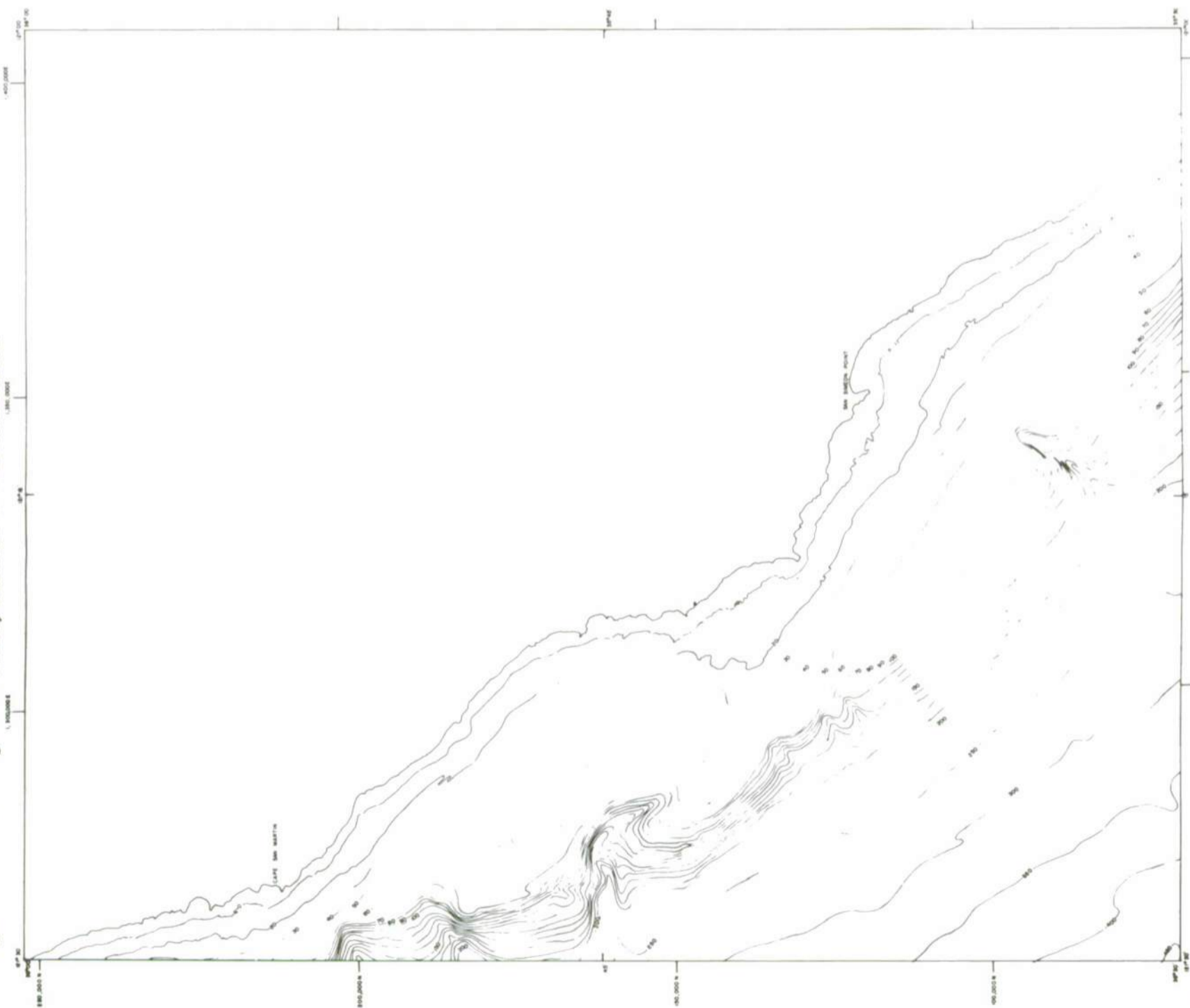


Part C. Bottom current velocity.

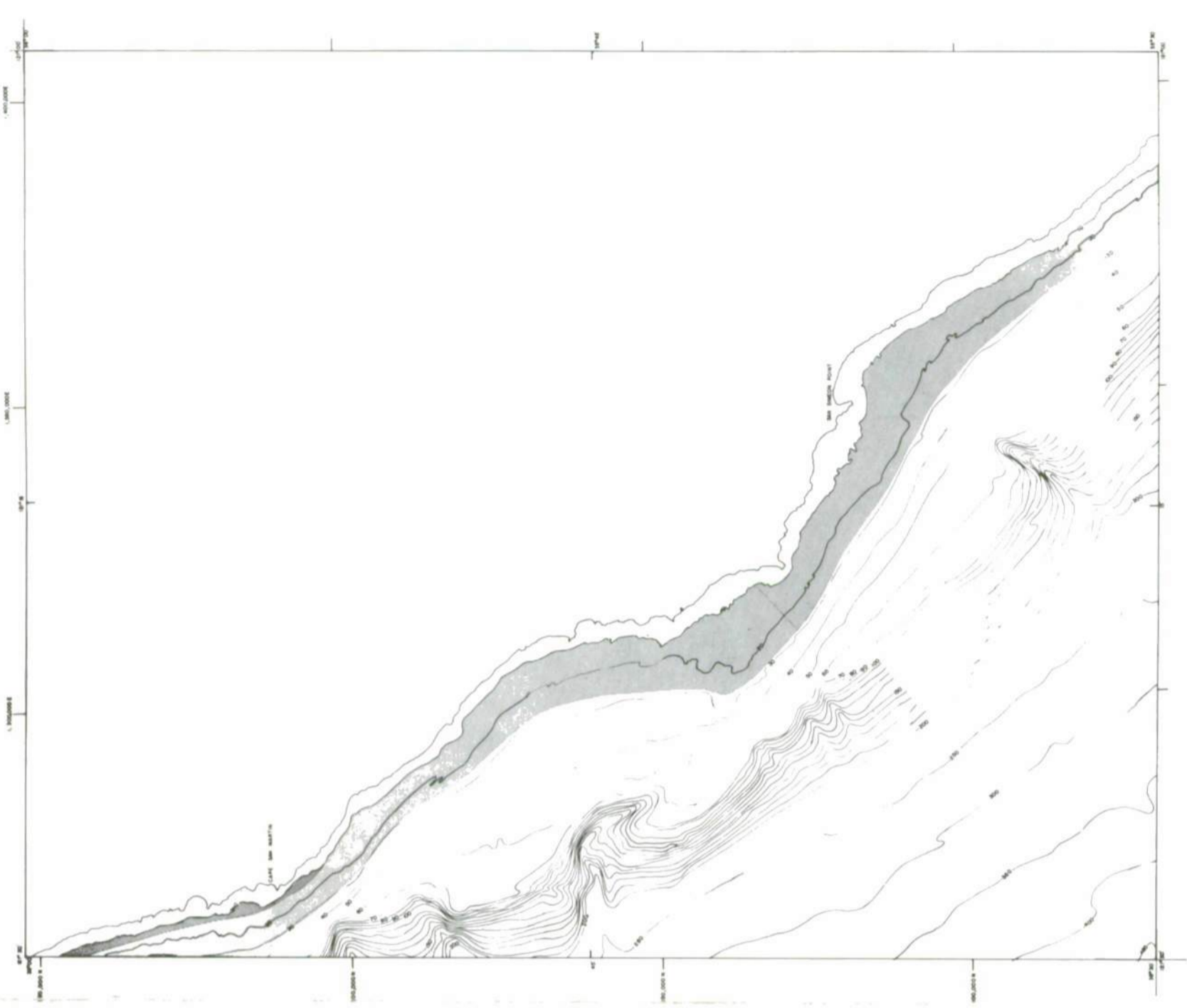


Part D. Tsunami surge.

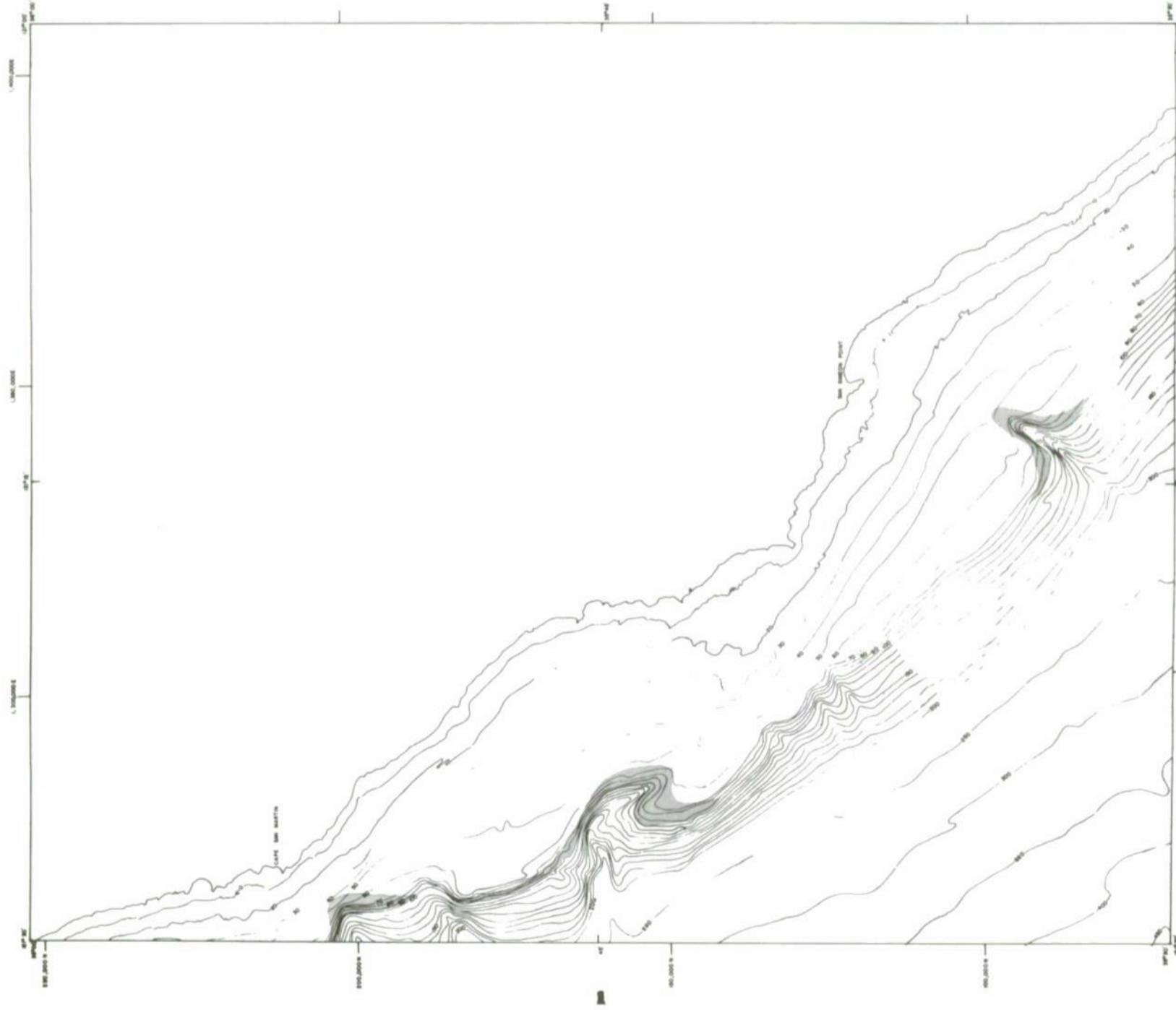
Figure 25. Predicted regions of century extremes for chart number 22.



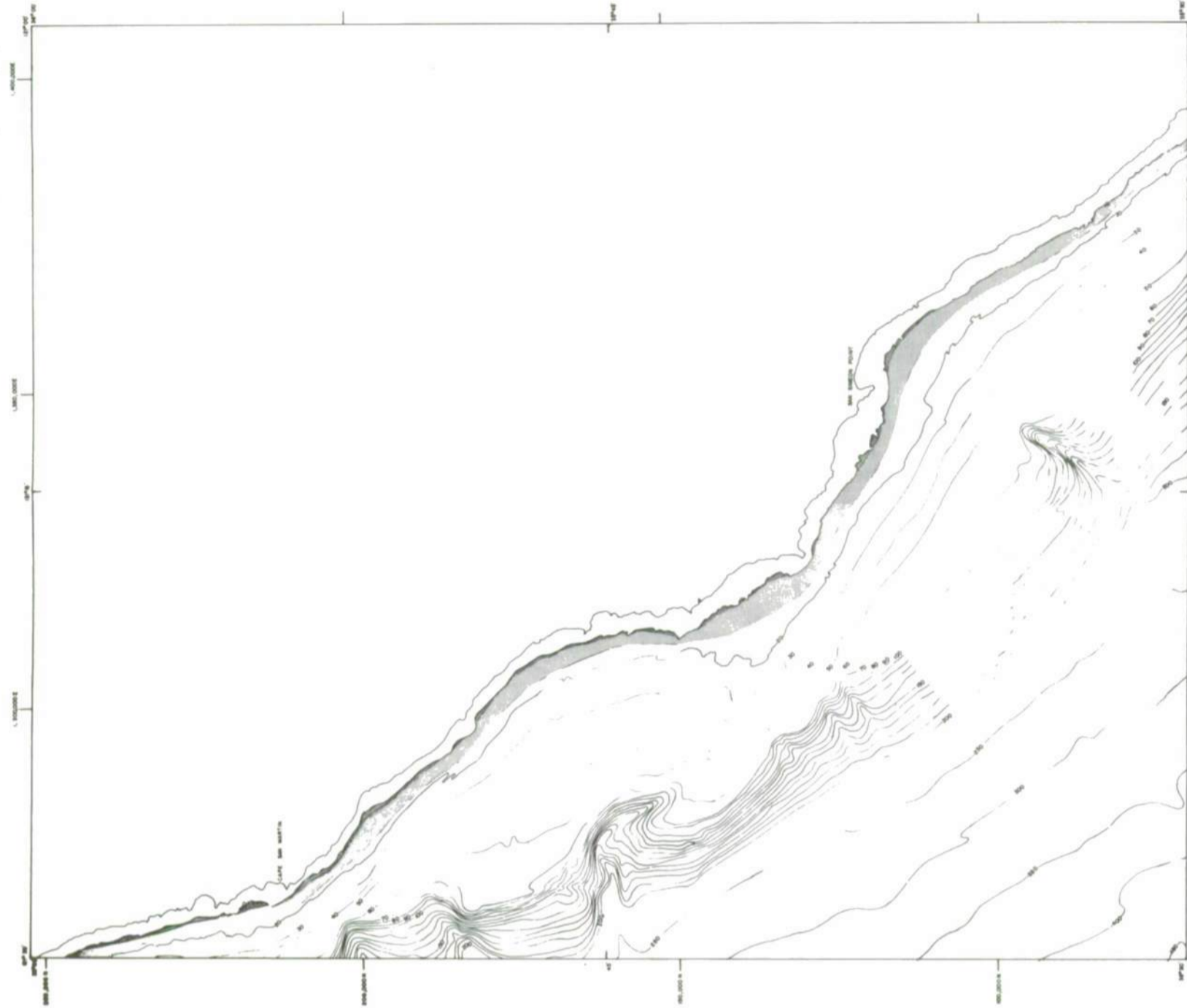
Part A. Density.



Part B. Bottom wave surge.

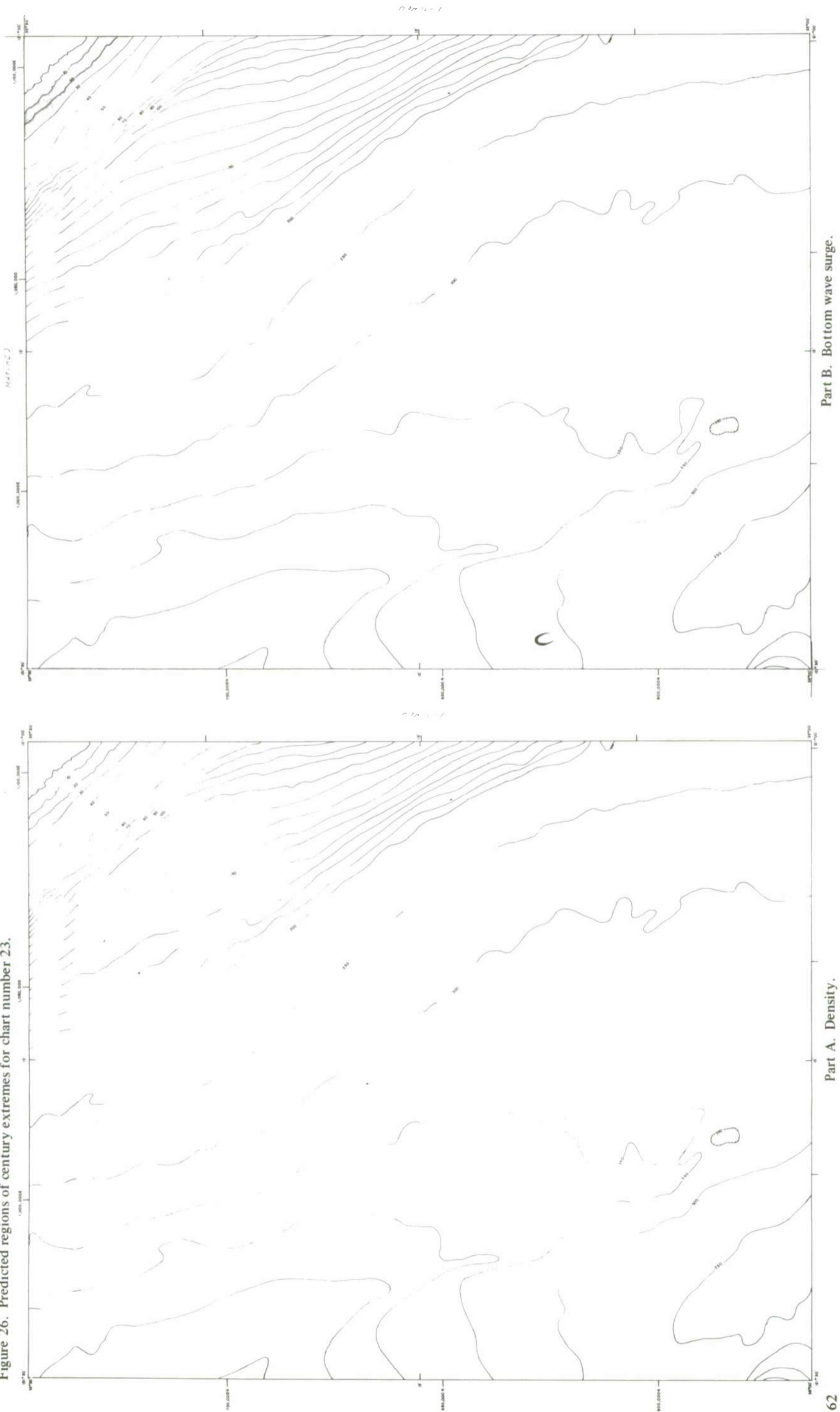


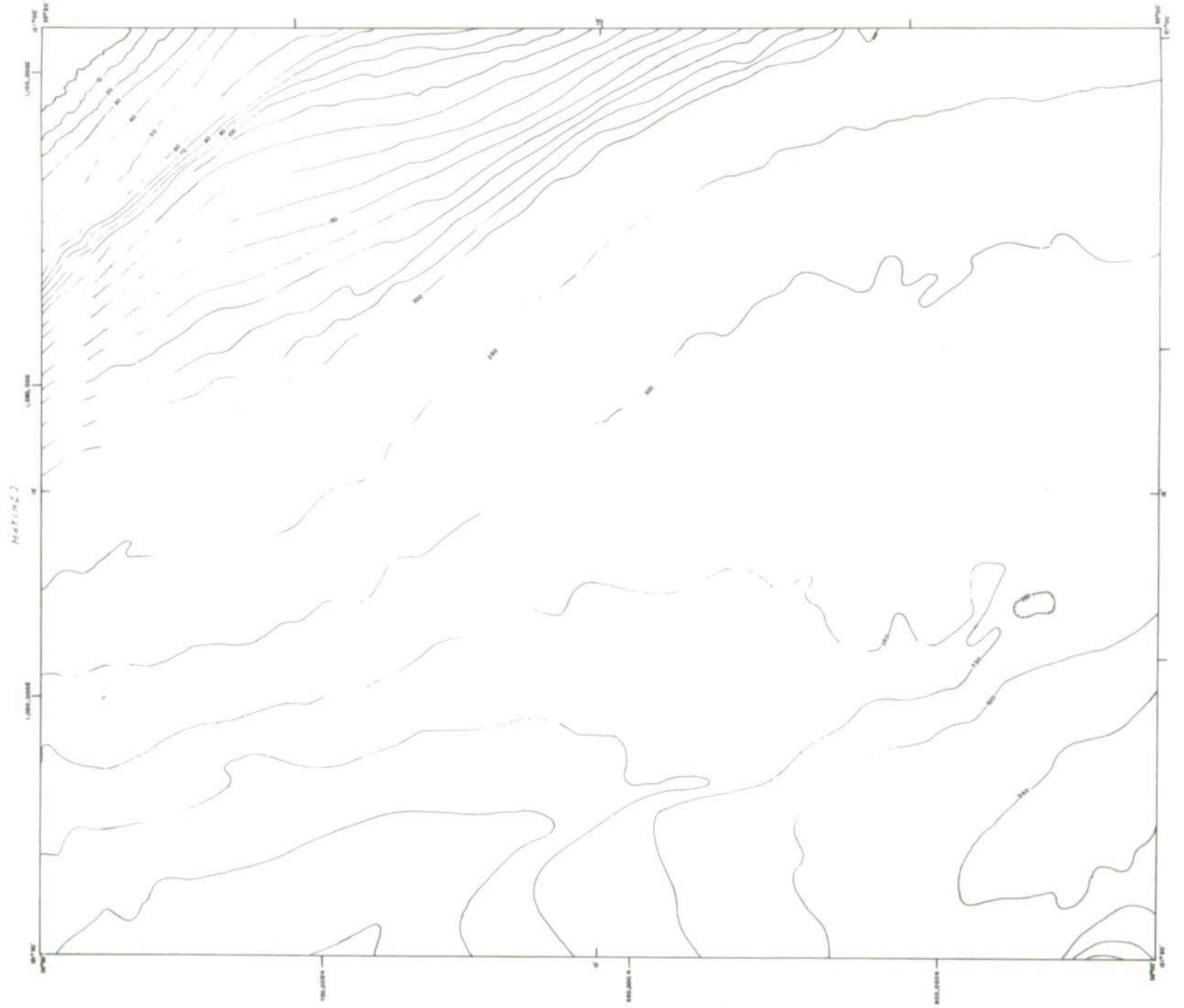
Part C. Bottom current velocity.



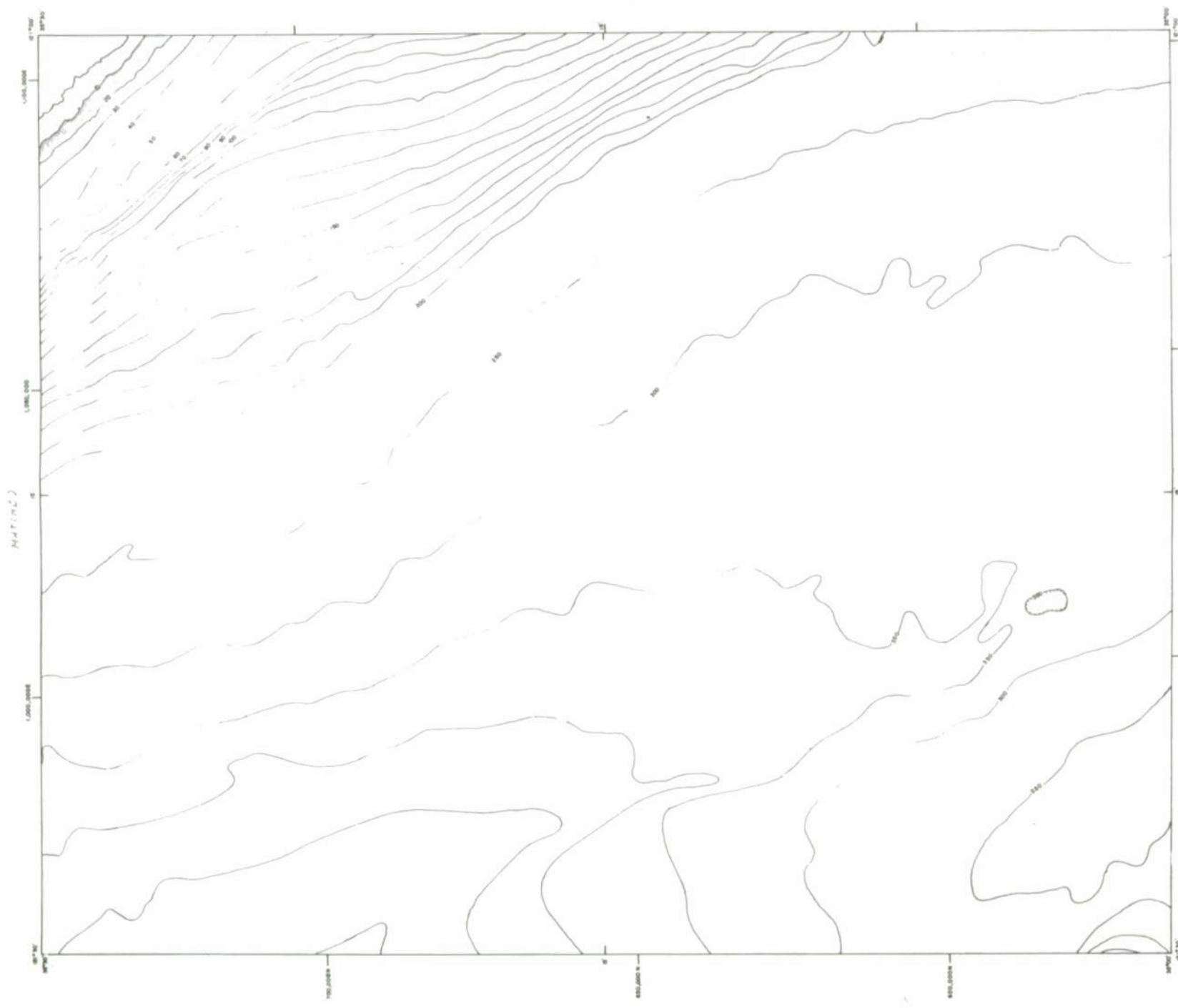
Part D. Tsunami surge.

Figure 26. Predicted regions of century extremes for chart number 23.



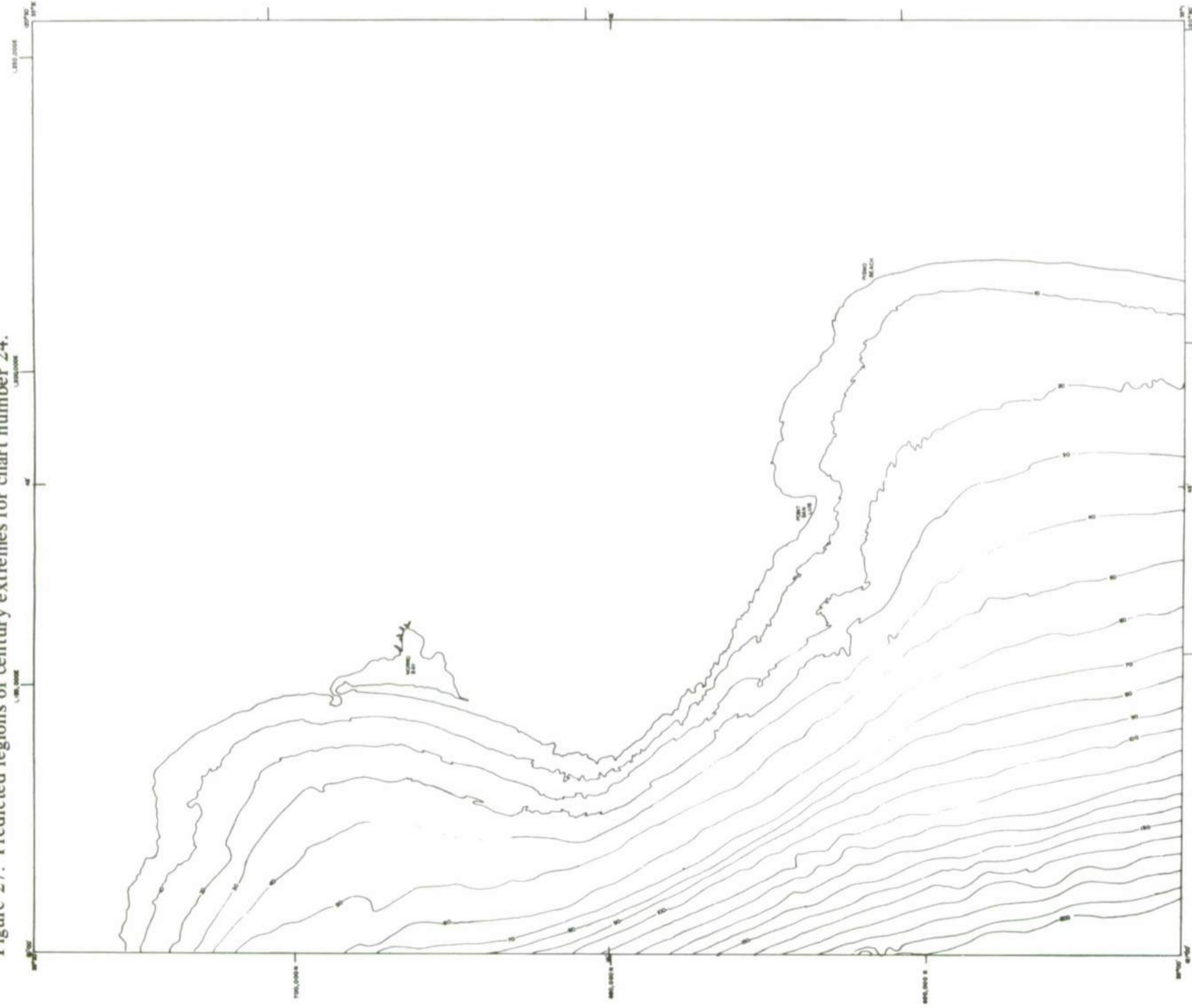


Part C. Bottom current velocity.

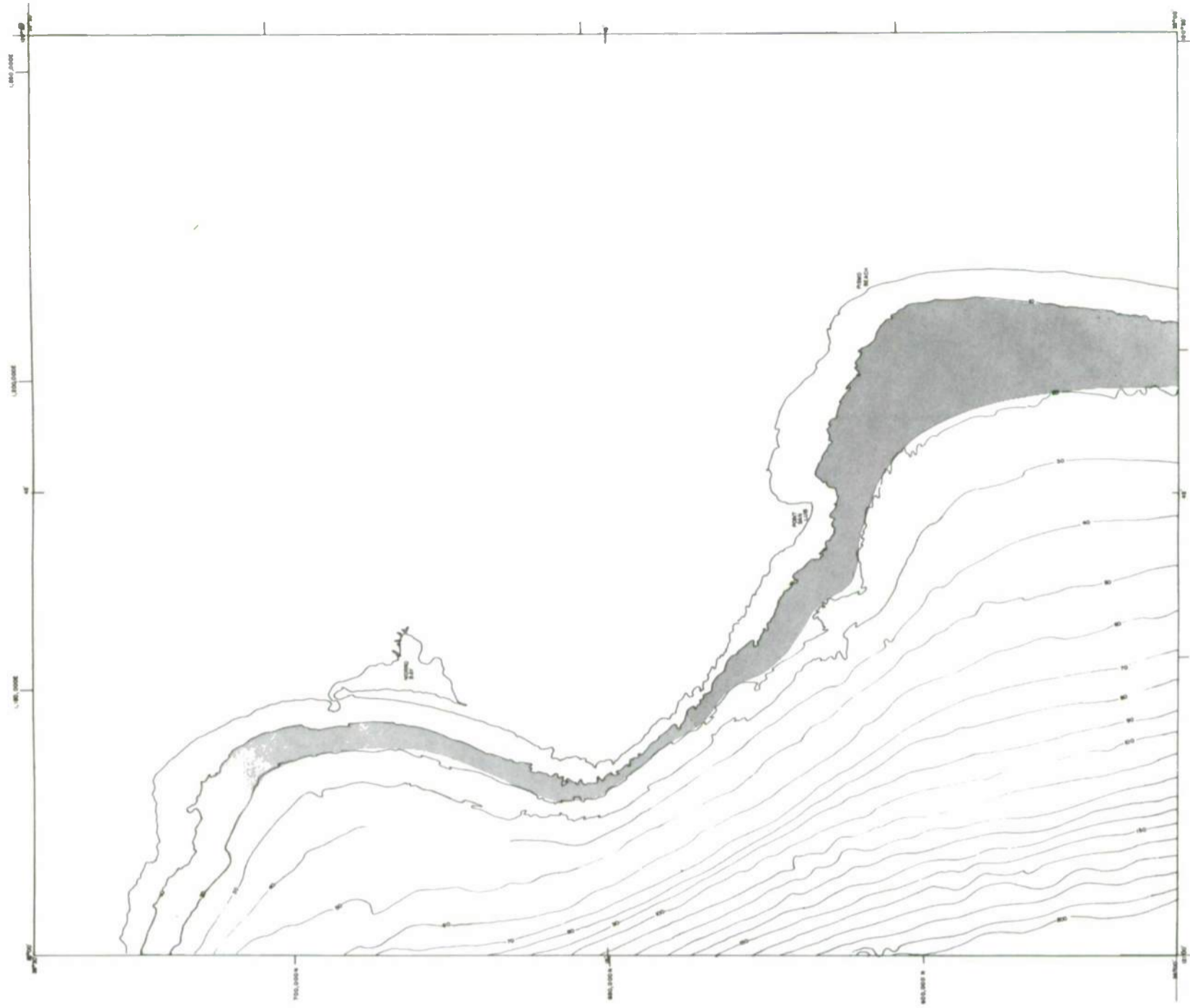


Part D. Tsunami surge.

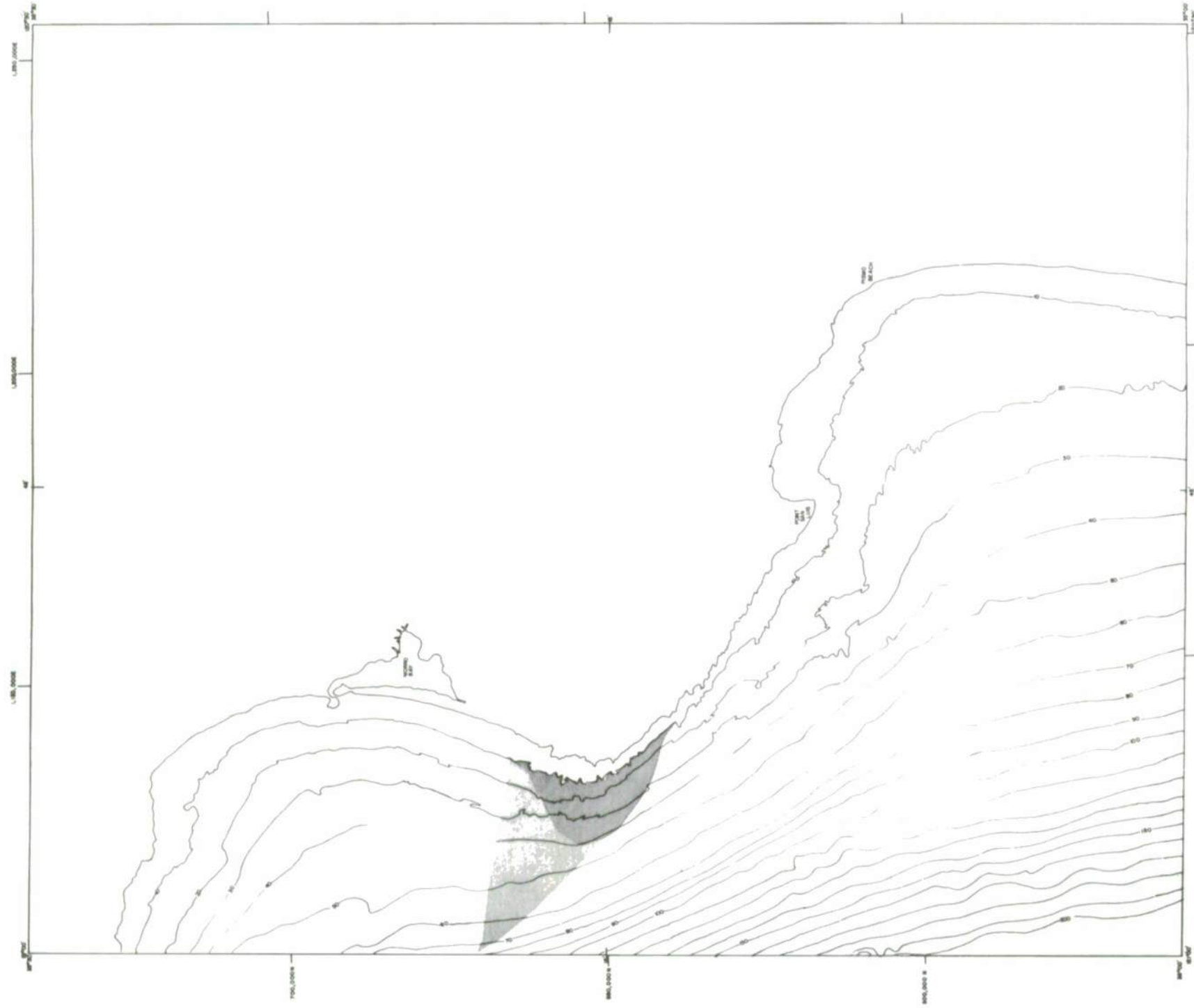
Figure 27. Predicted regions of century extremes for chart number 24.



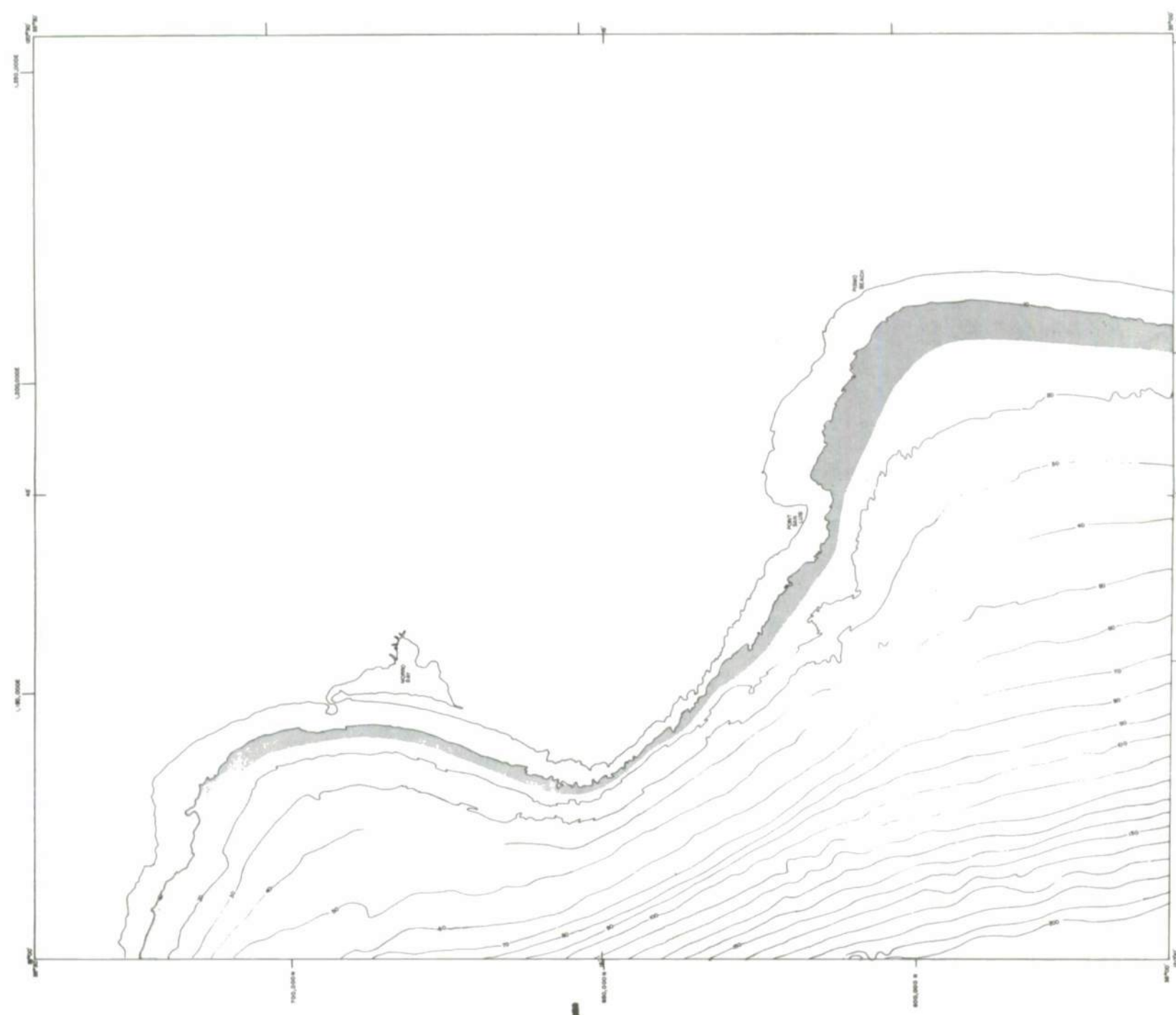
Part A. Density.



Part B. Bottom wave surge.

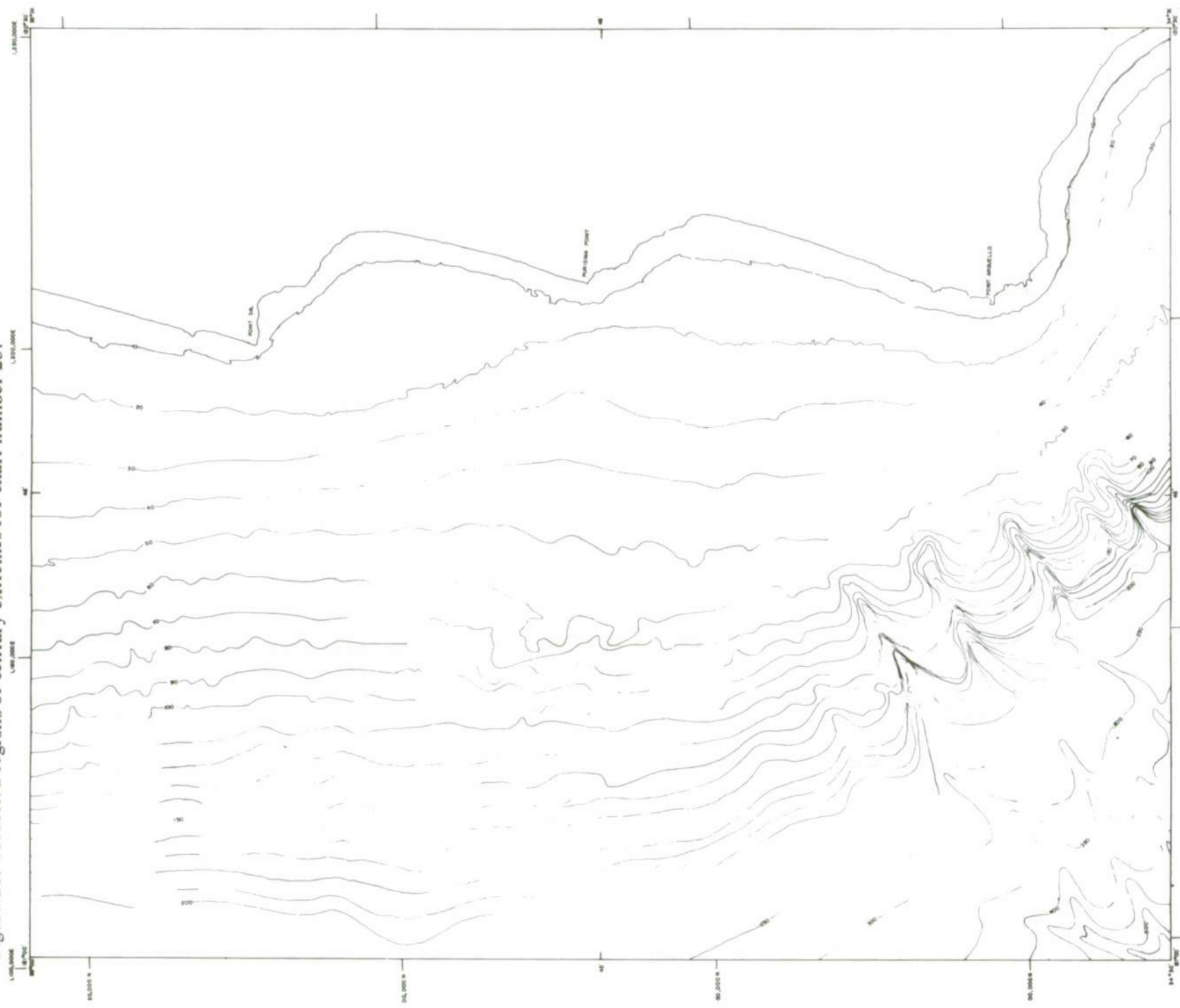


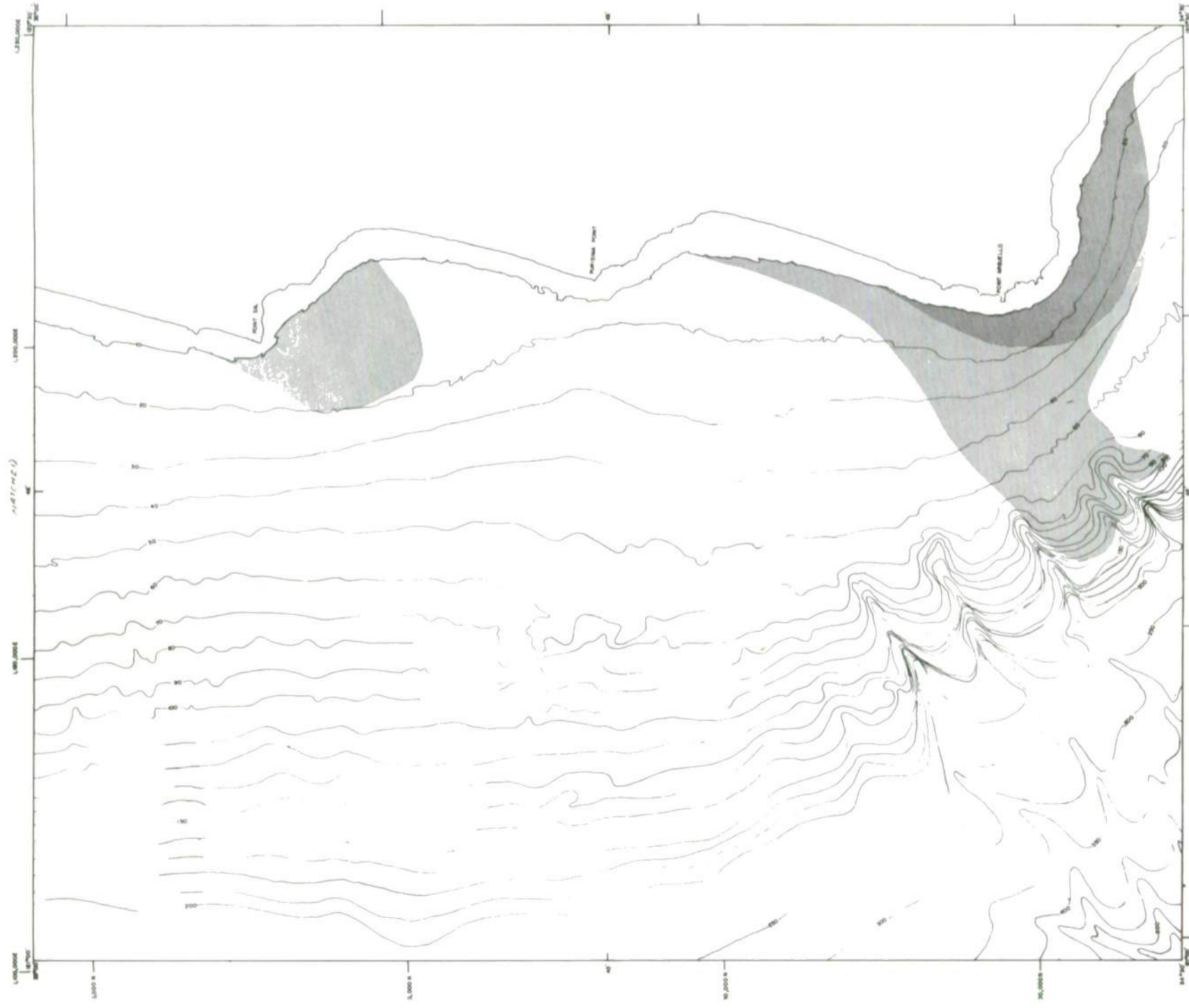
Part C. Bottom current velocity.



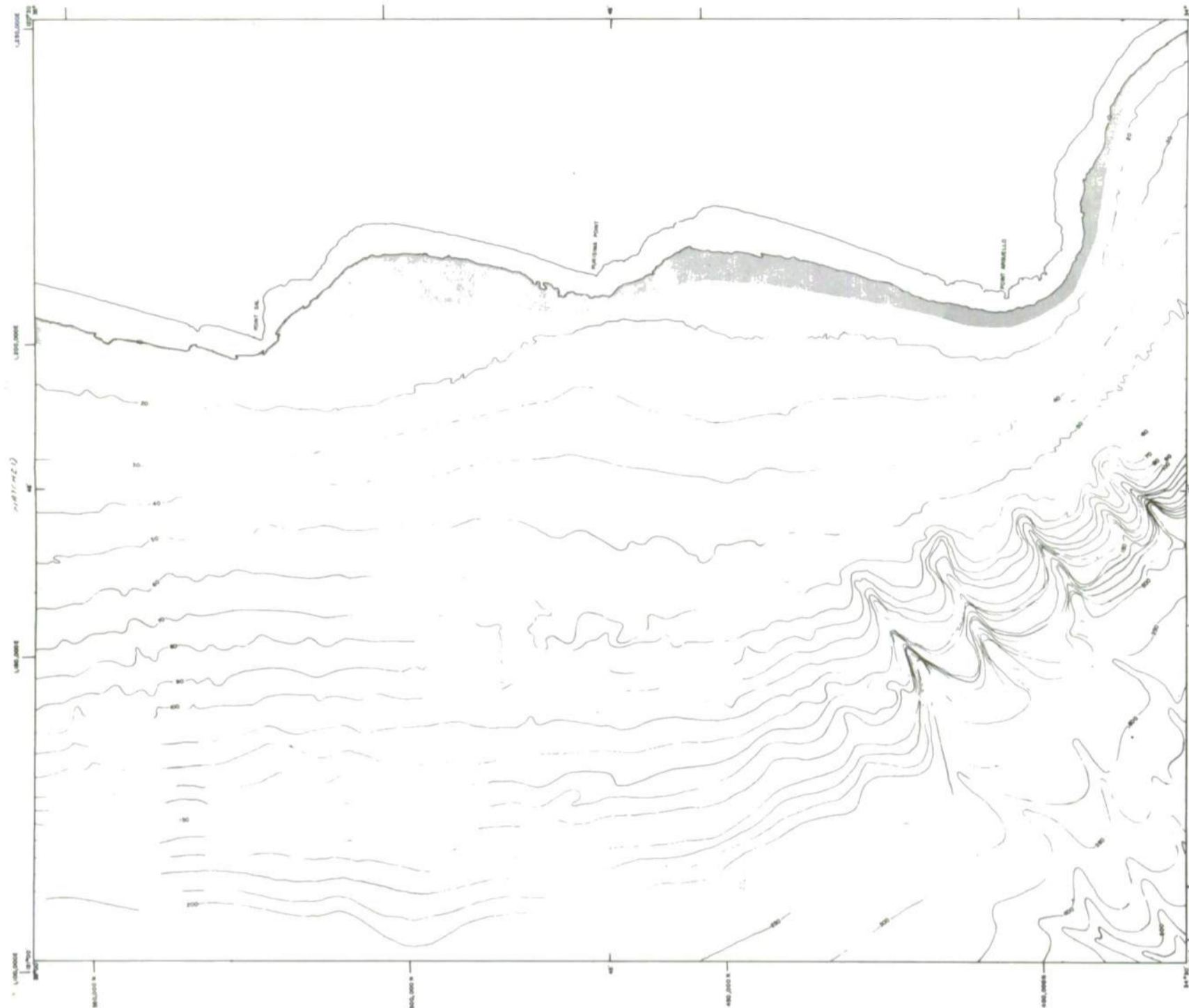
Part D. Tsunami surge.

Figure 28. Predicted regions of century extremes for chart number 25.

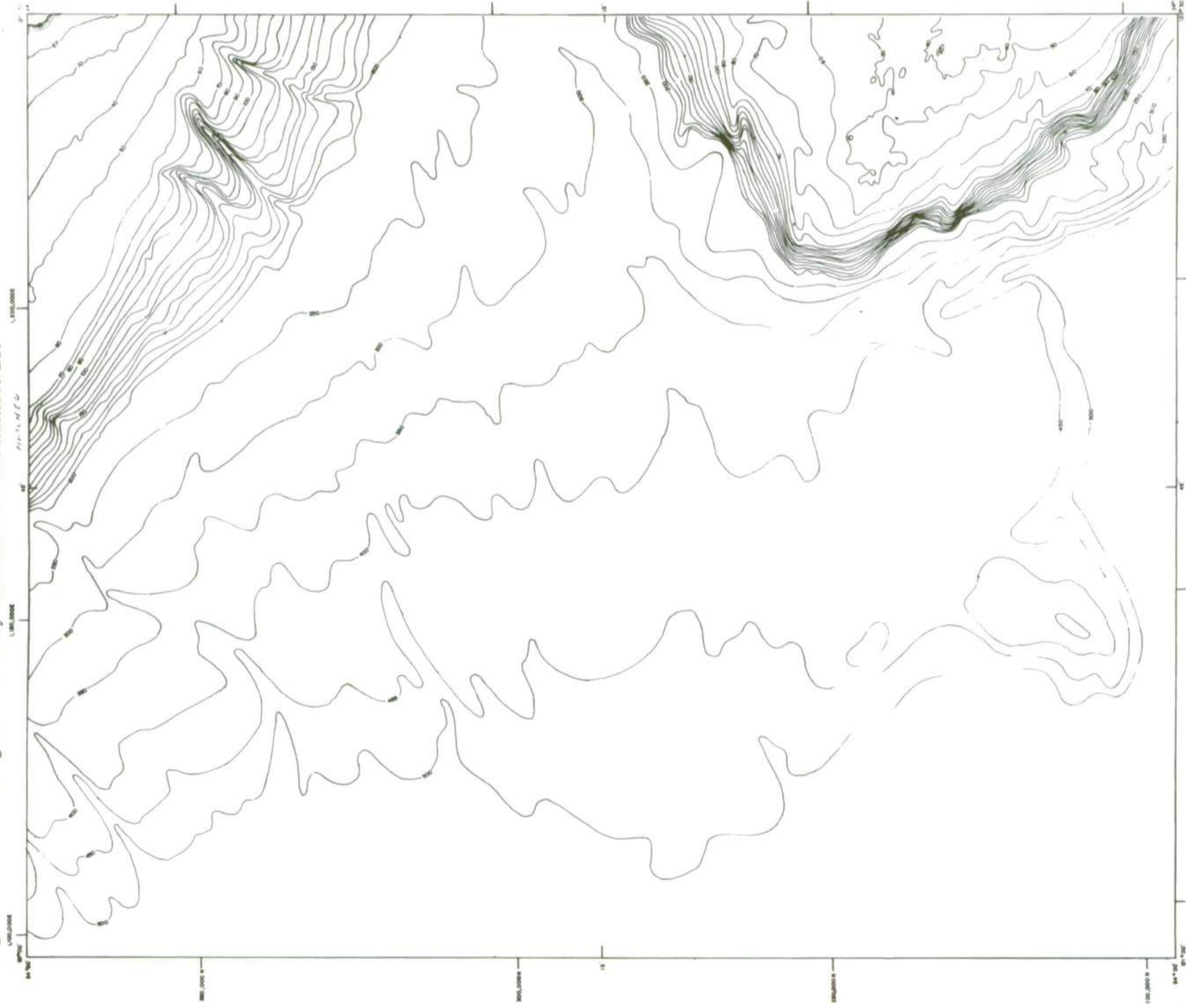




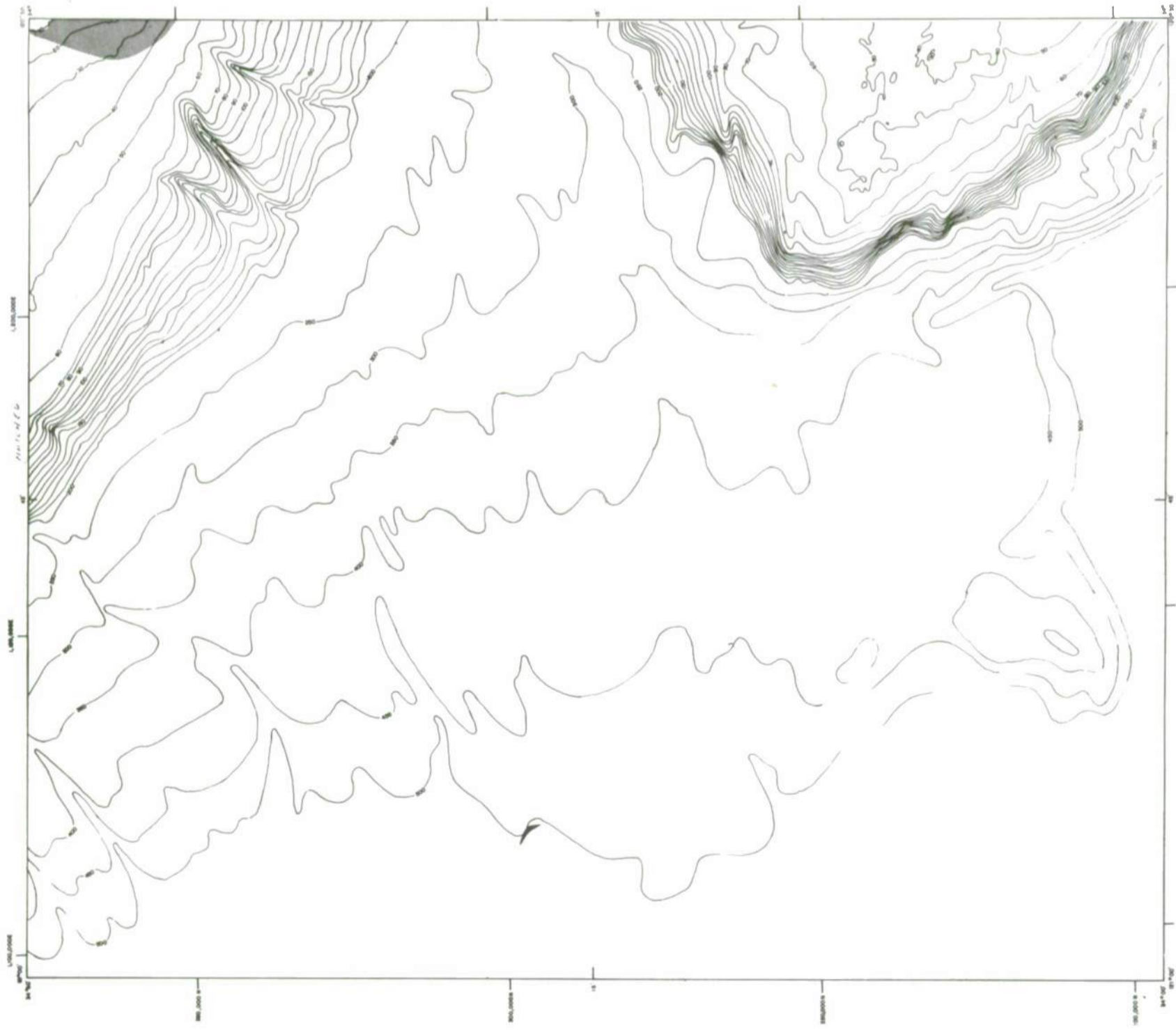
Part C. Bottom velocity current.



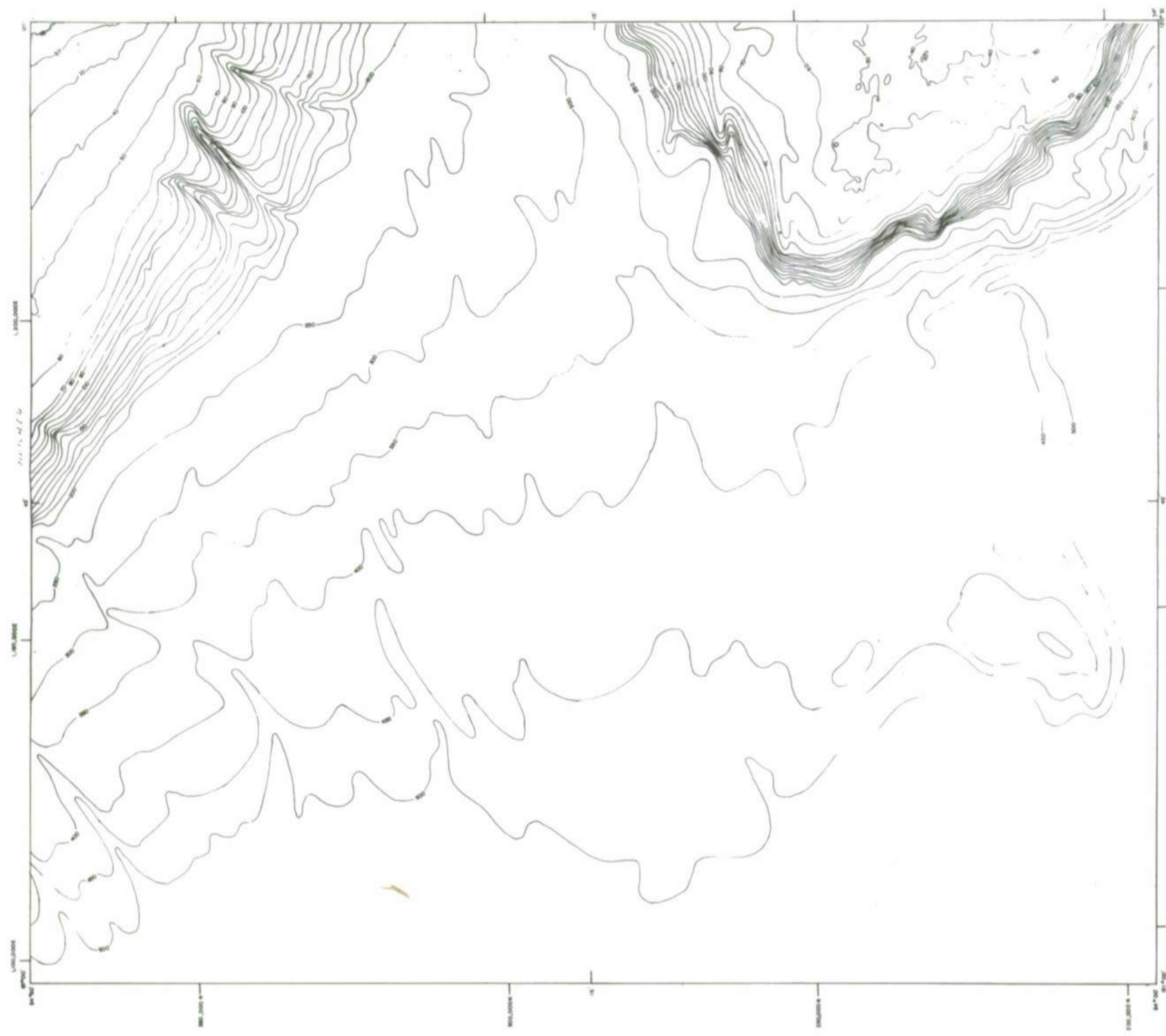
Part D. Tsunami surge.



Part B. Bottom wave surge.

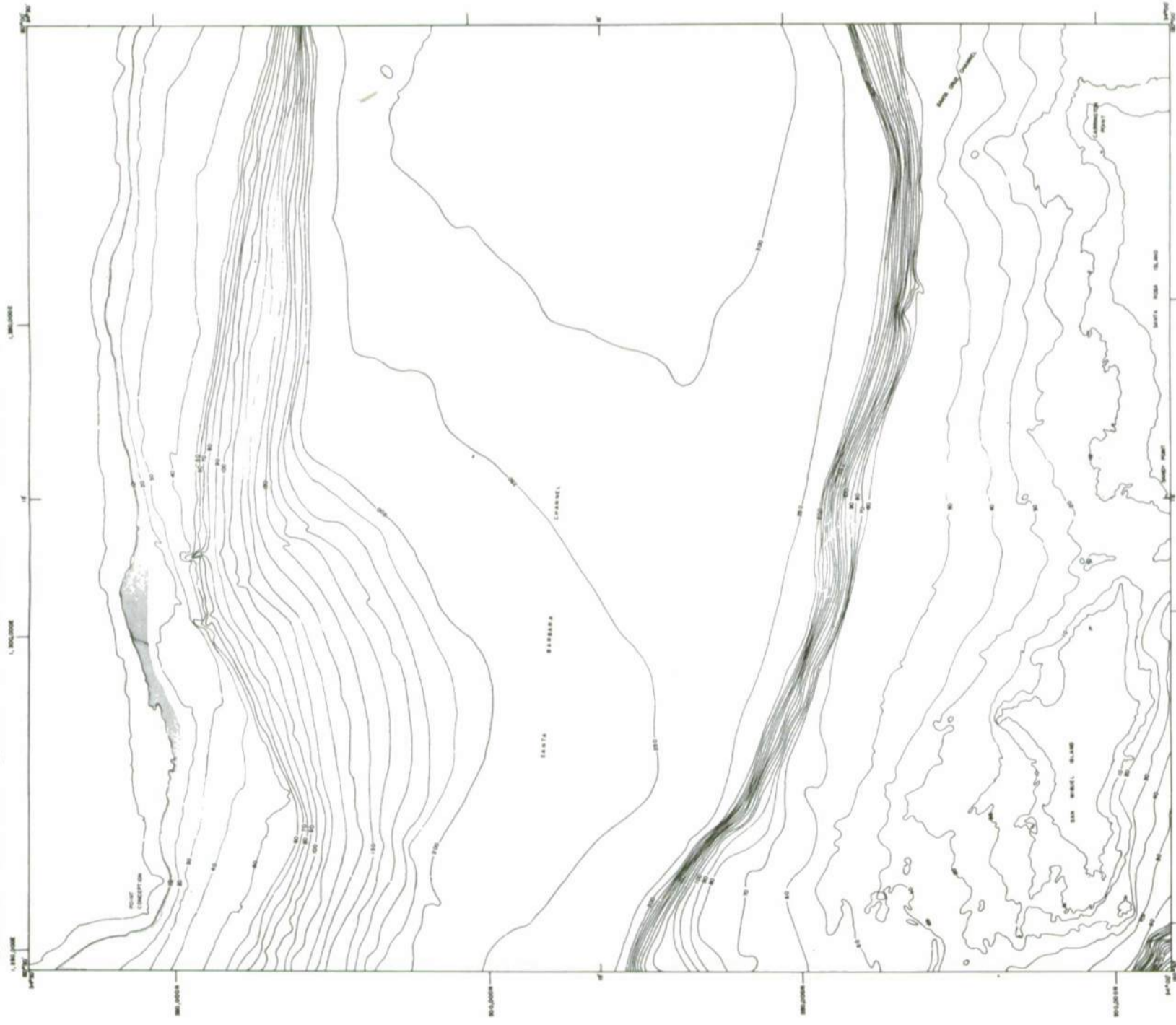


Part C. Bottom current velocity.

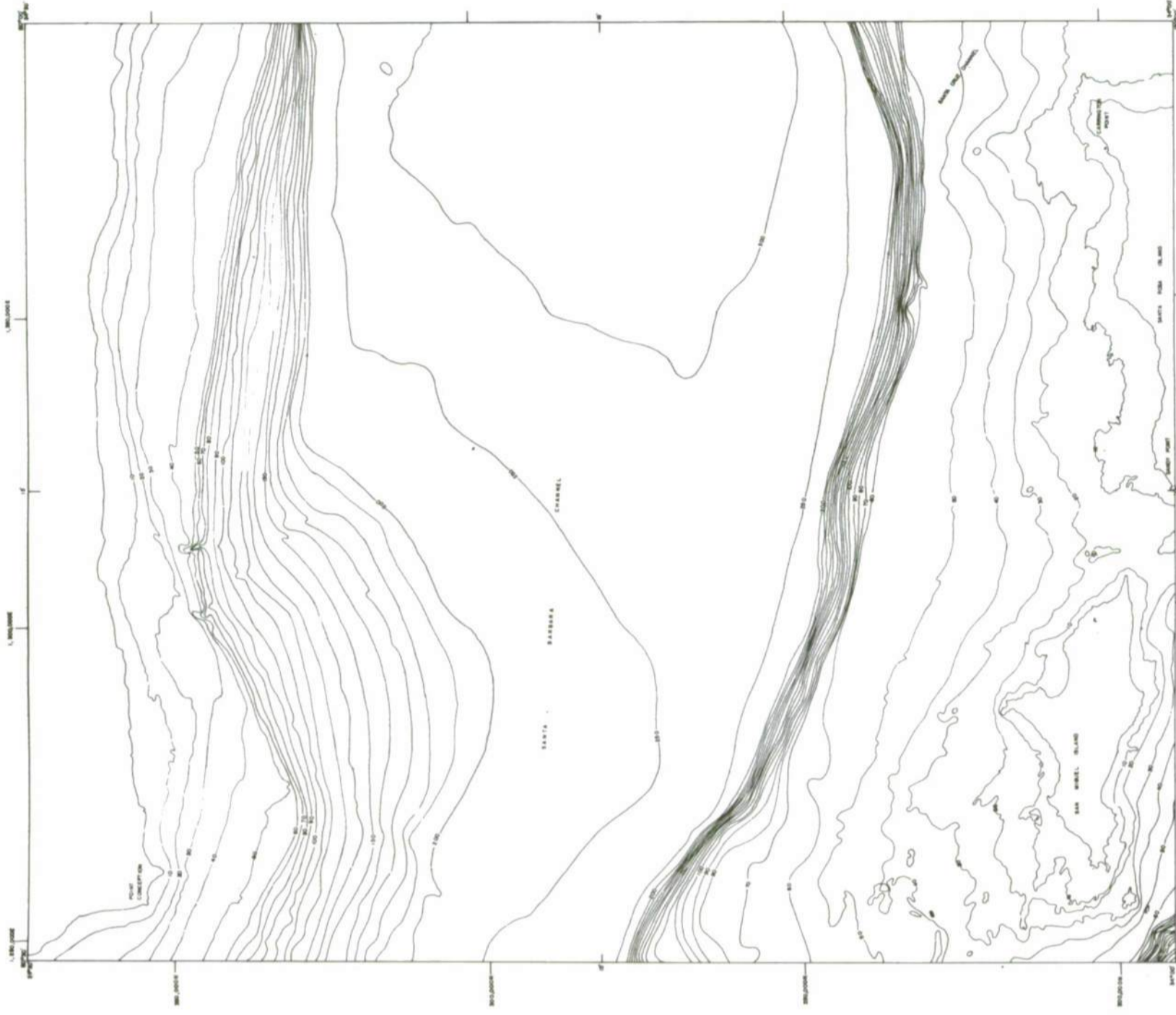


Part D. Tsunami surge.

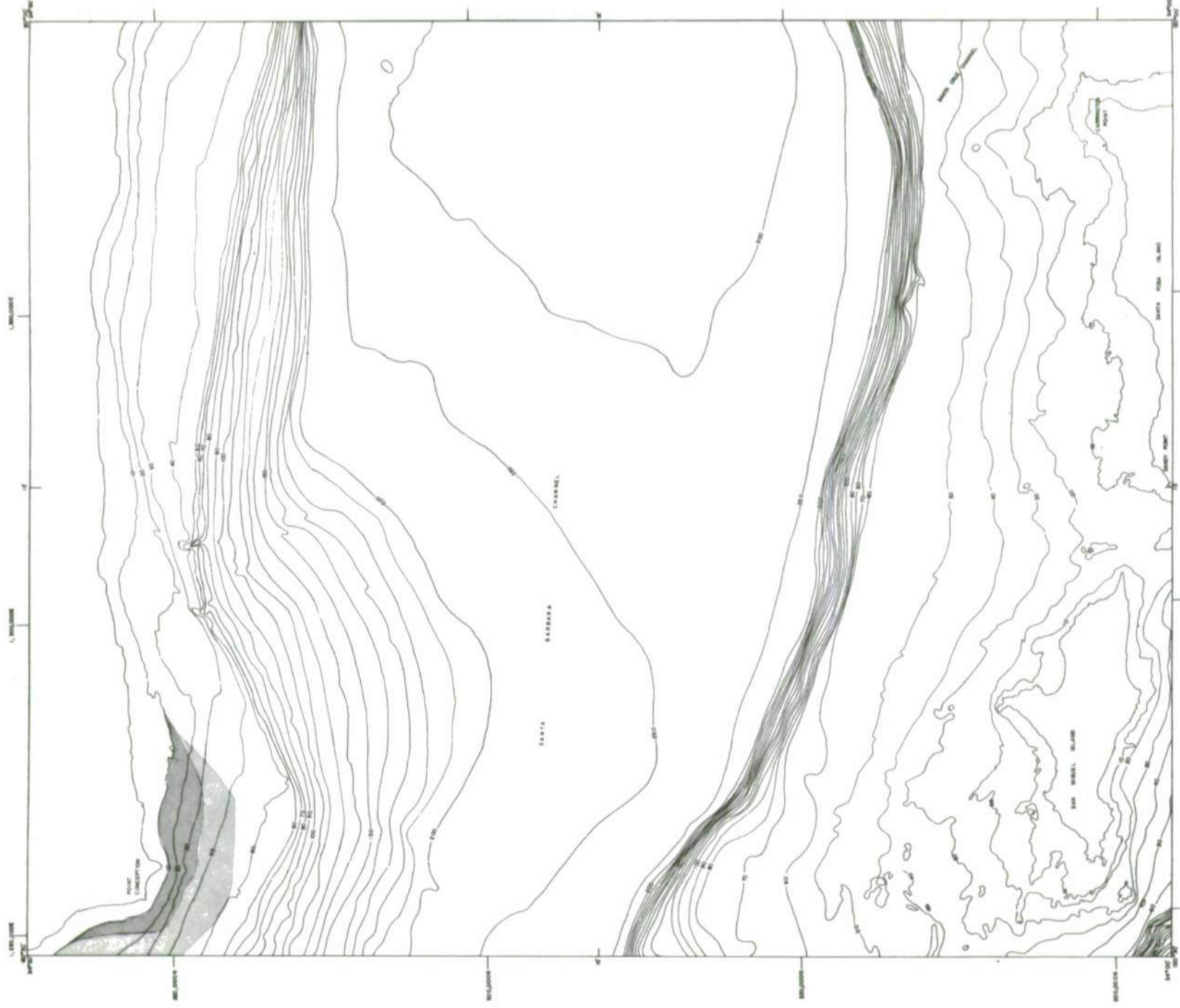
Figure 30. Predicted regions of century extremes for chart number 27.



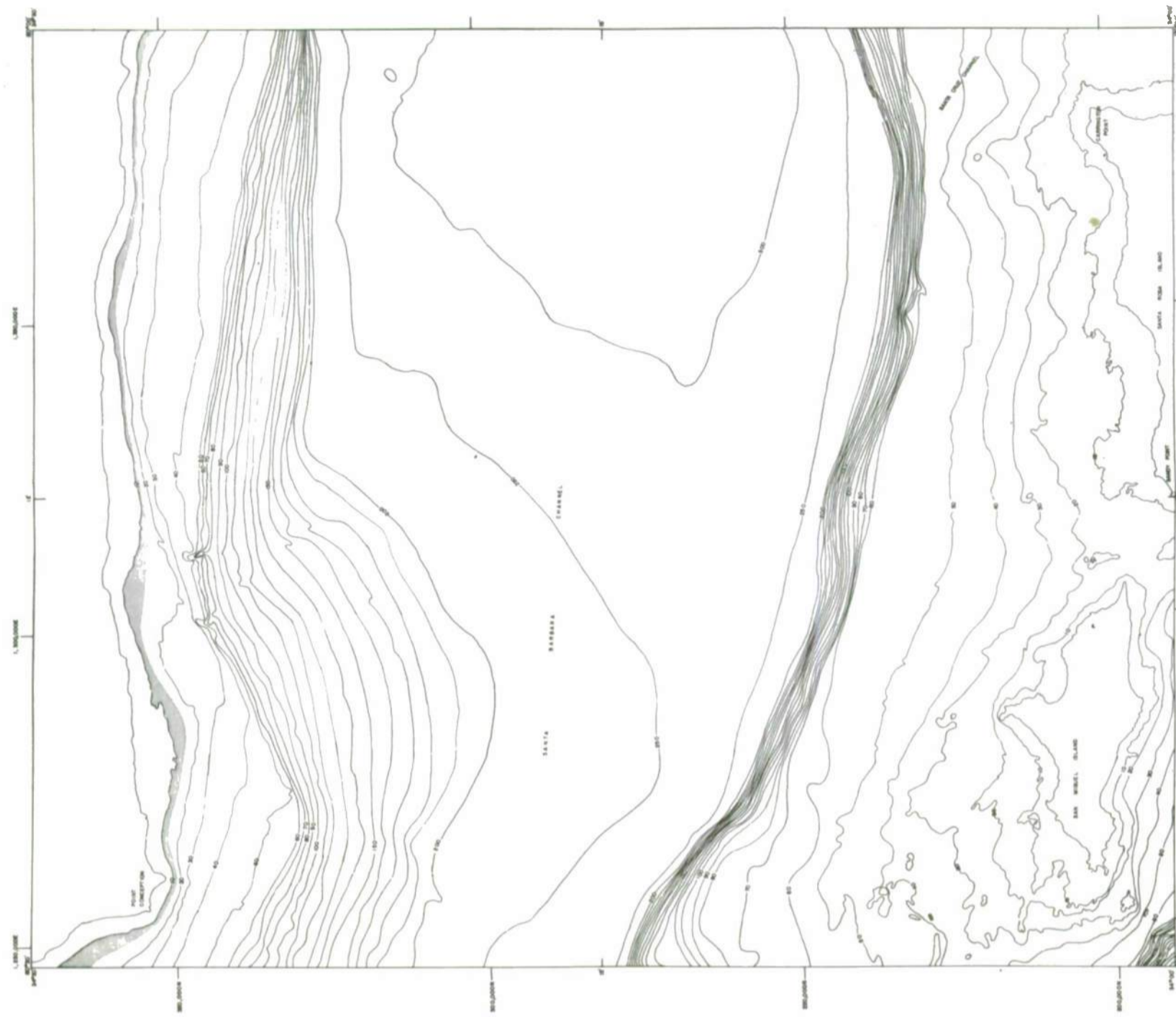
Part A. Density.



Part B. Bottom wave surge.

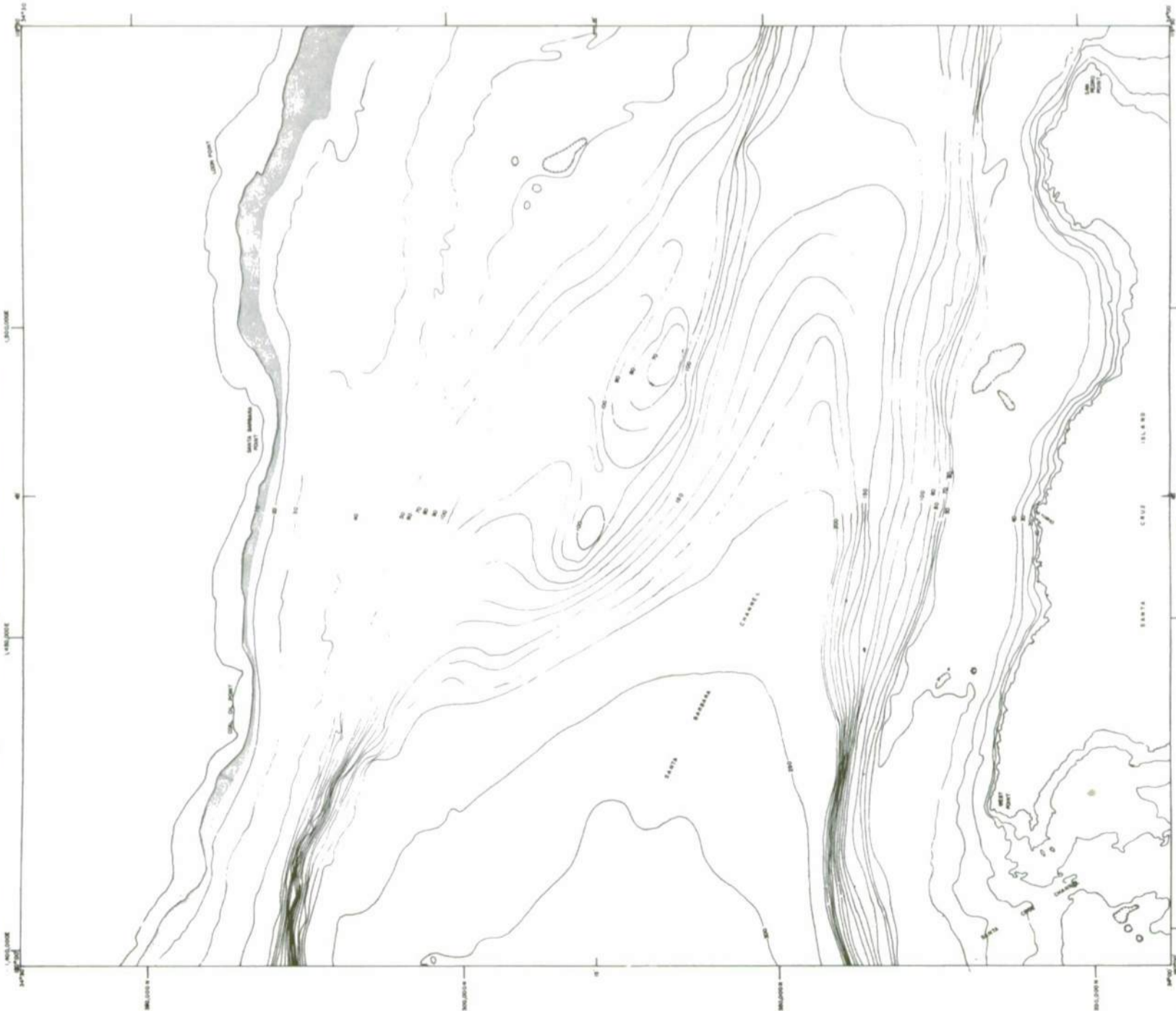


Part C. Bottom current velocity.

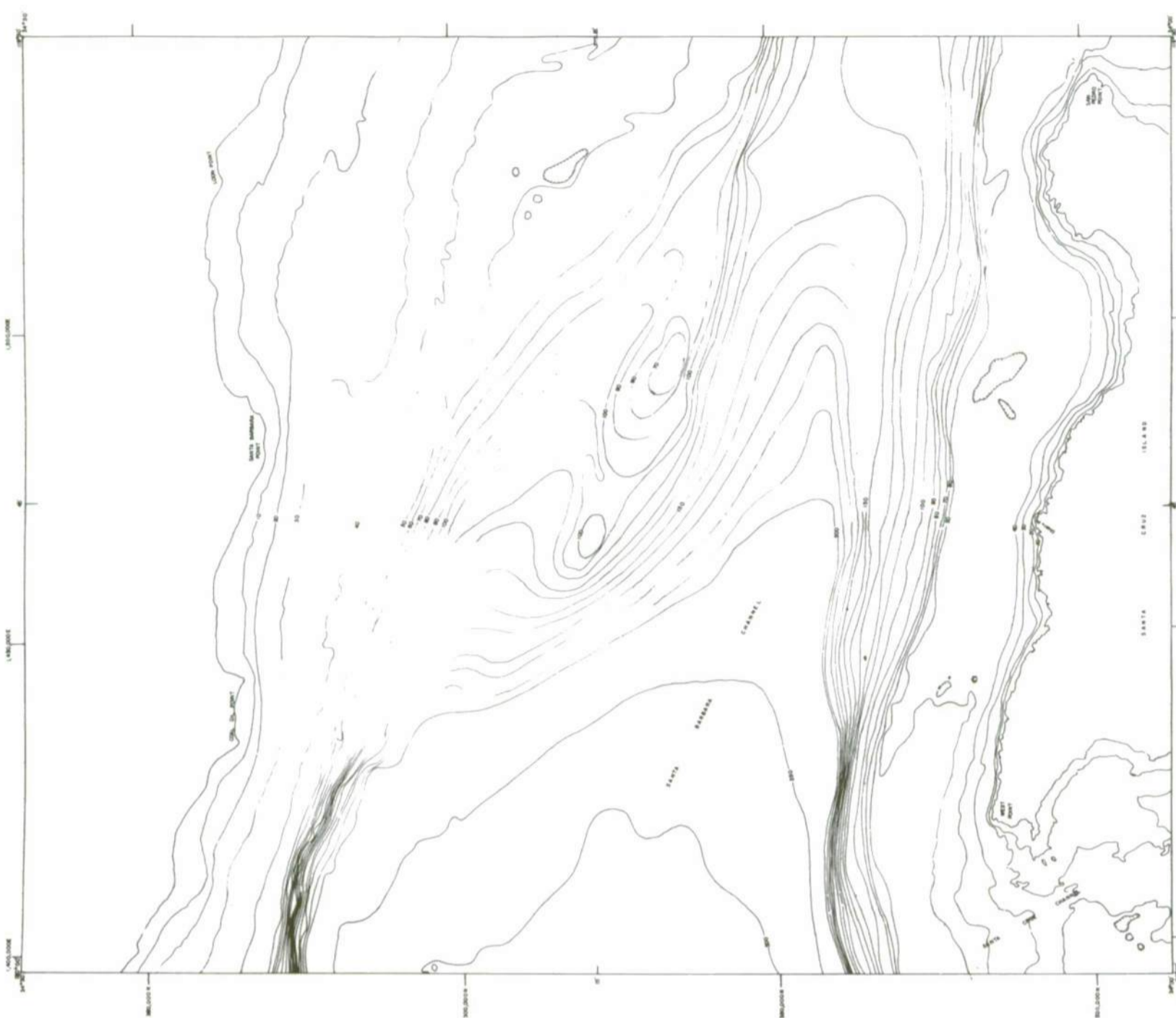


Part D. Tsunami surge.

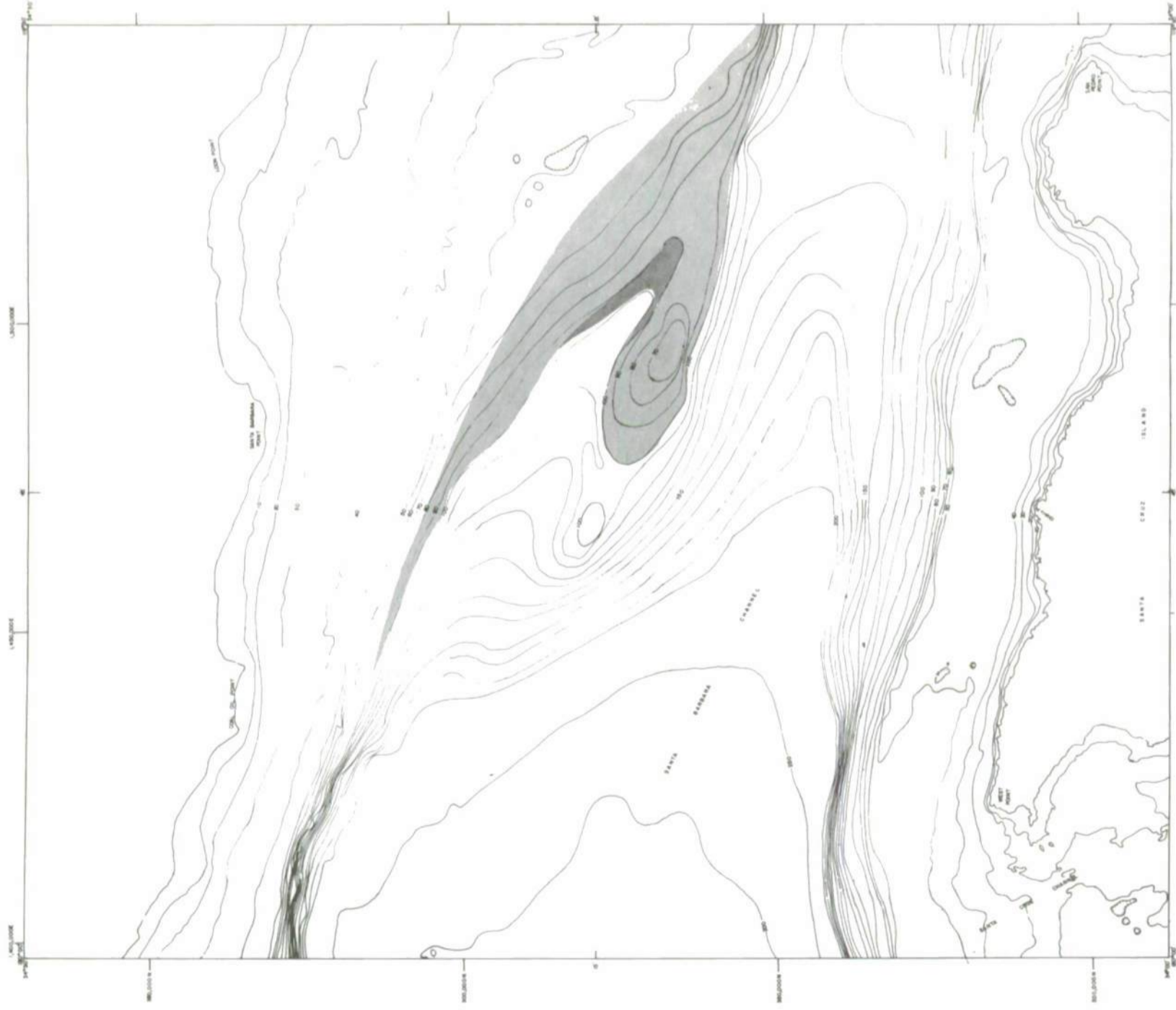
Figure 31. Predicted regions of century extremes for chart number 28.



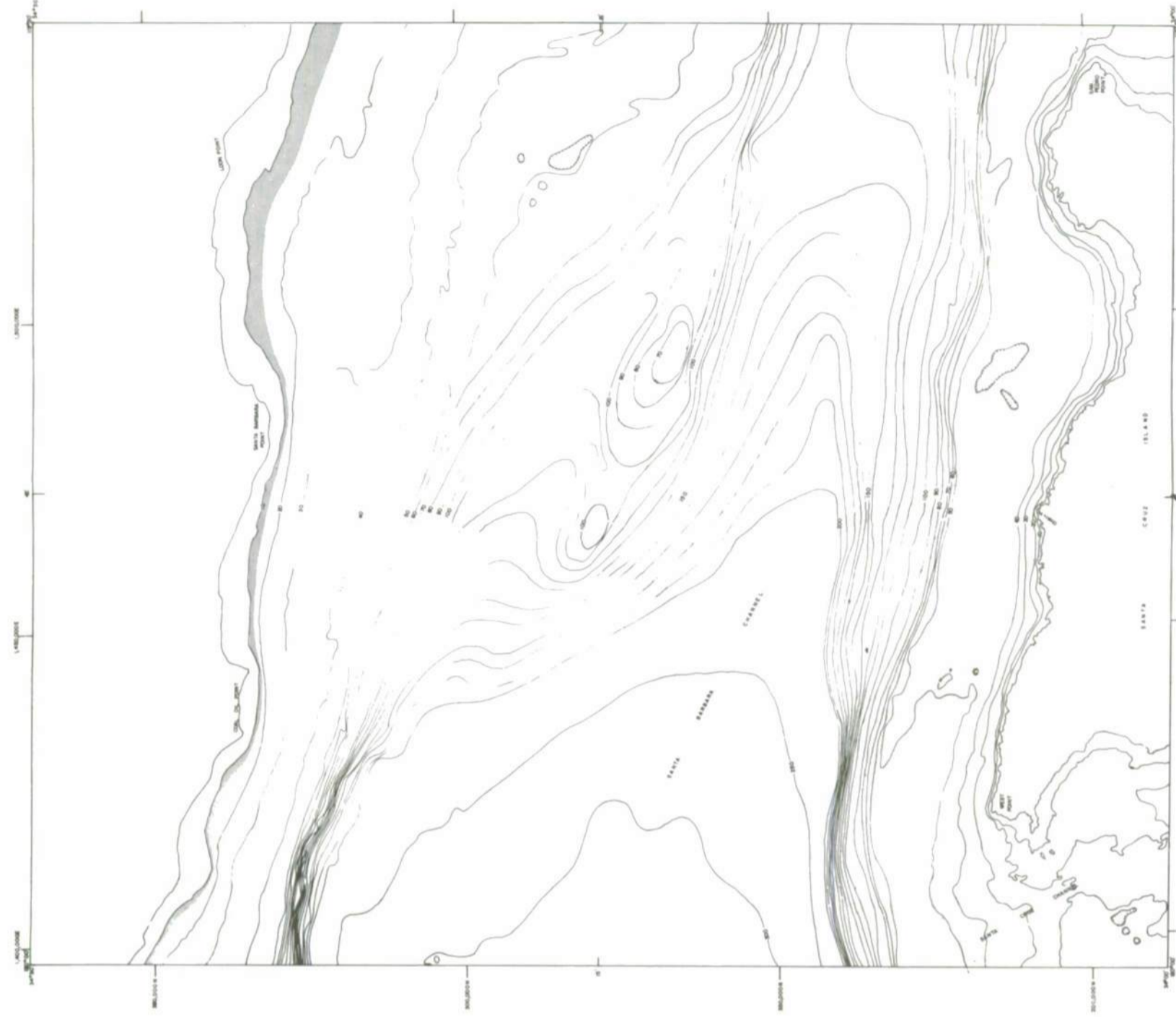
Part A. Density.



Part B. Bottom wave surge.

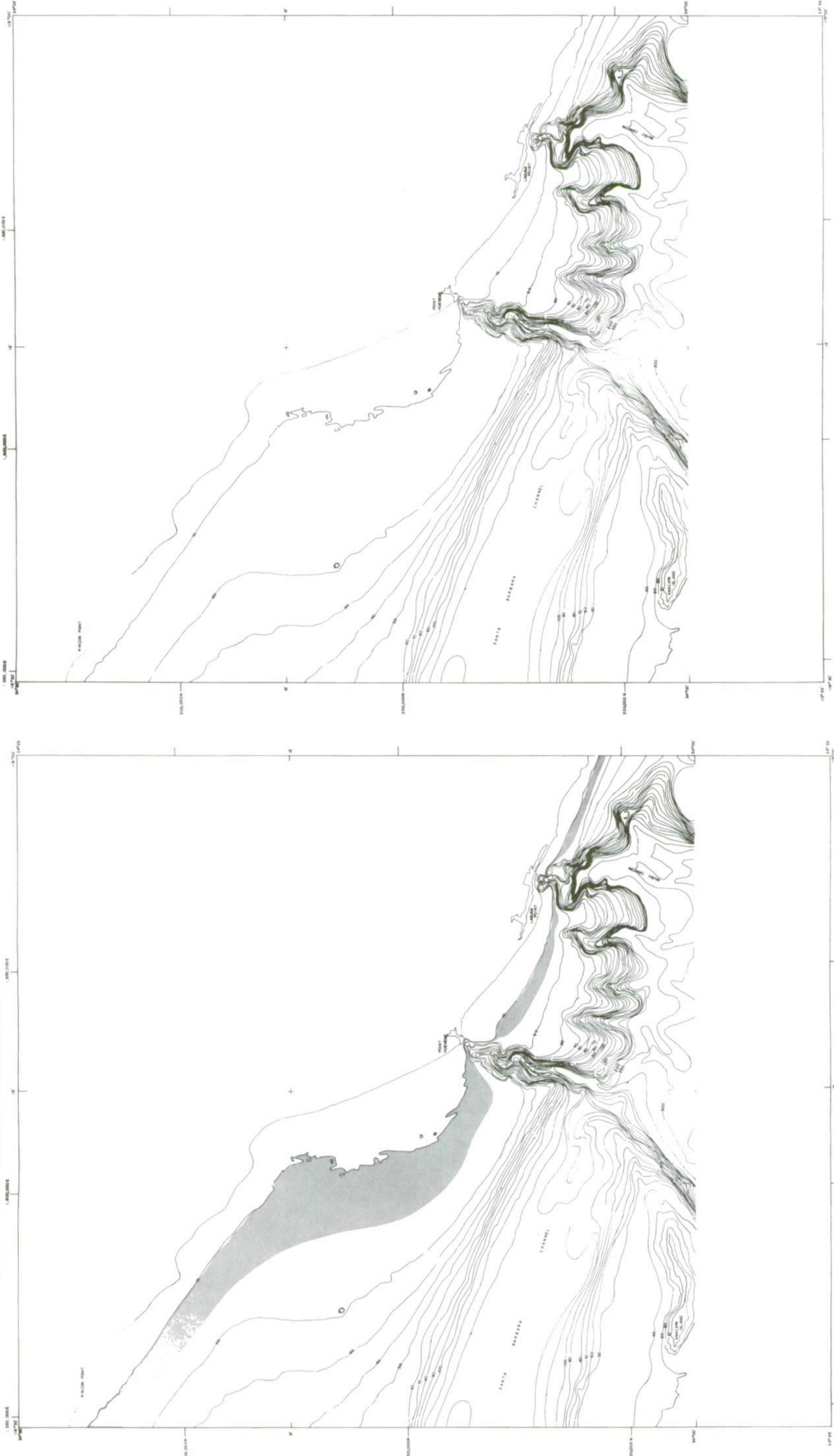


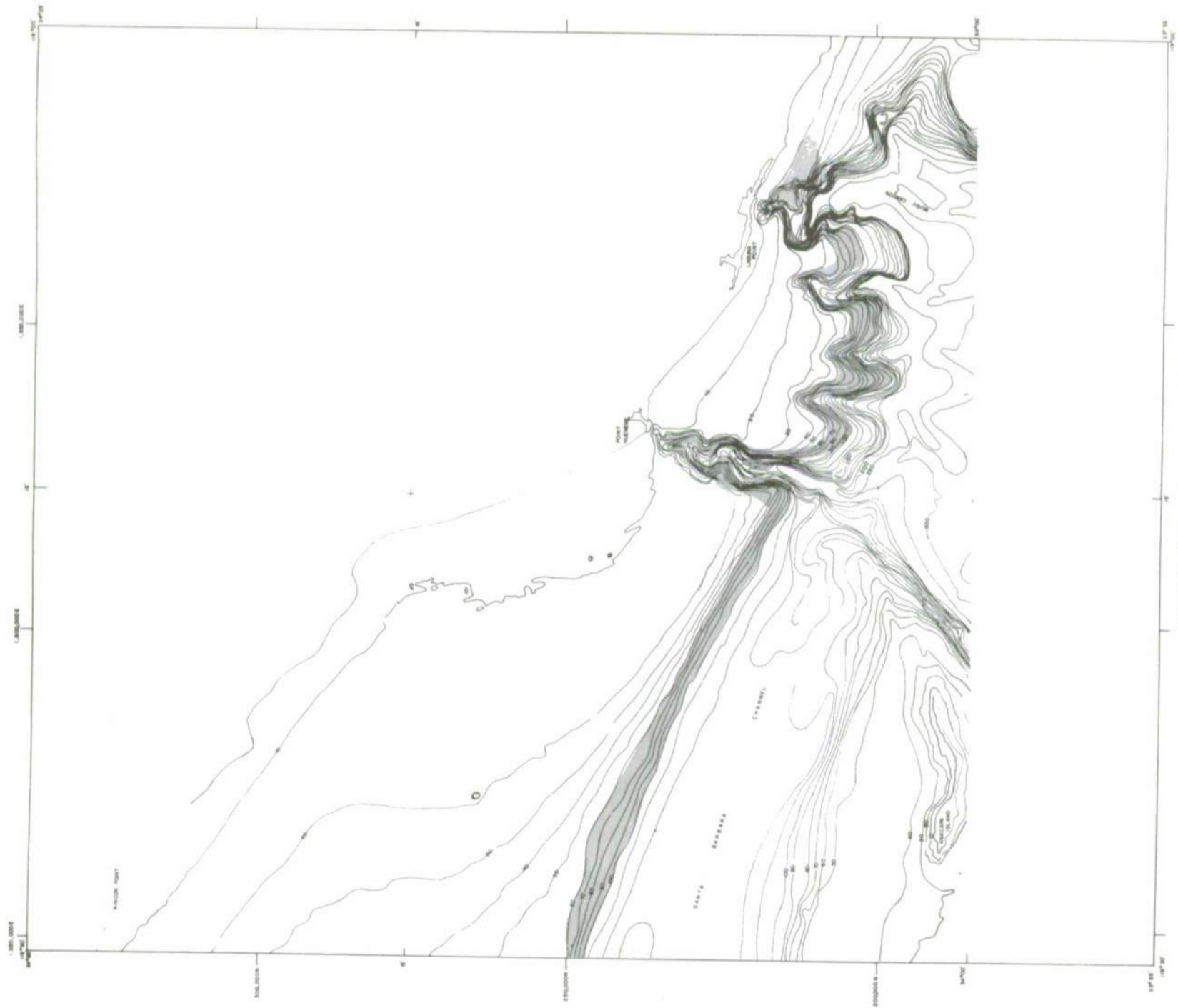
Part C. Bottom current velocity.



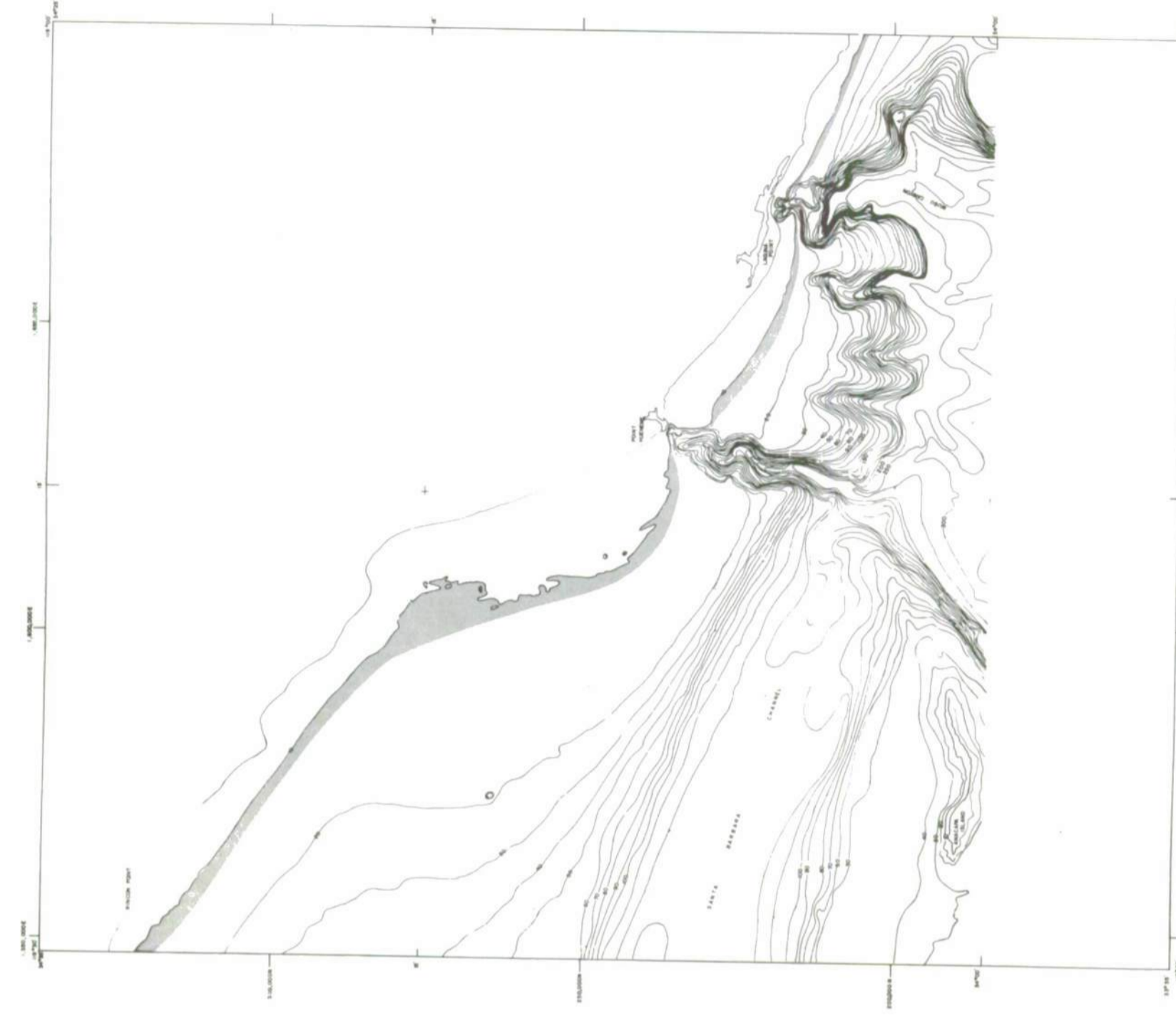
Part D. Tsunami surge.

Figure 32. Predicted regions of century extremes for chart number 29.



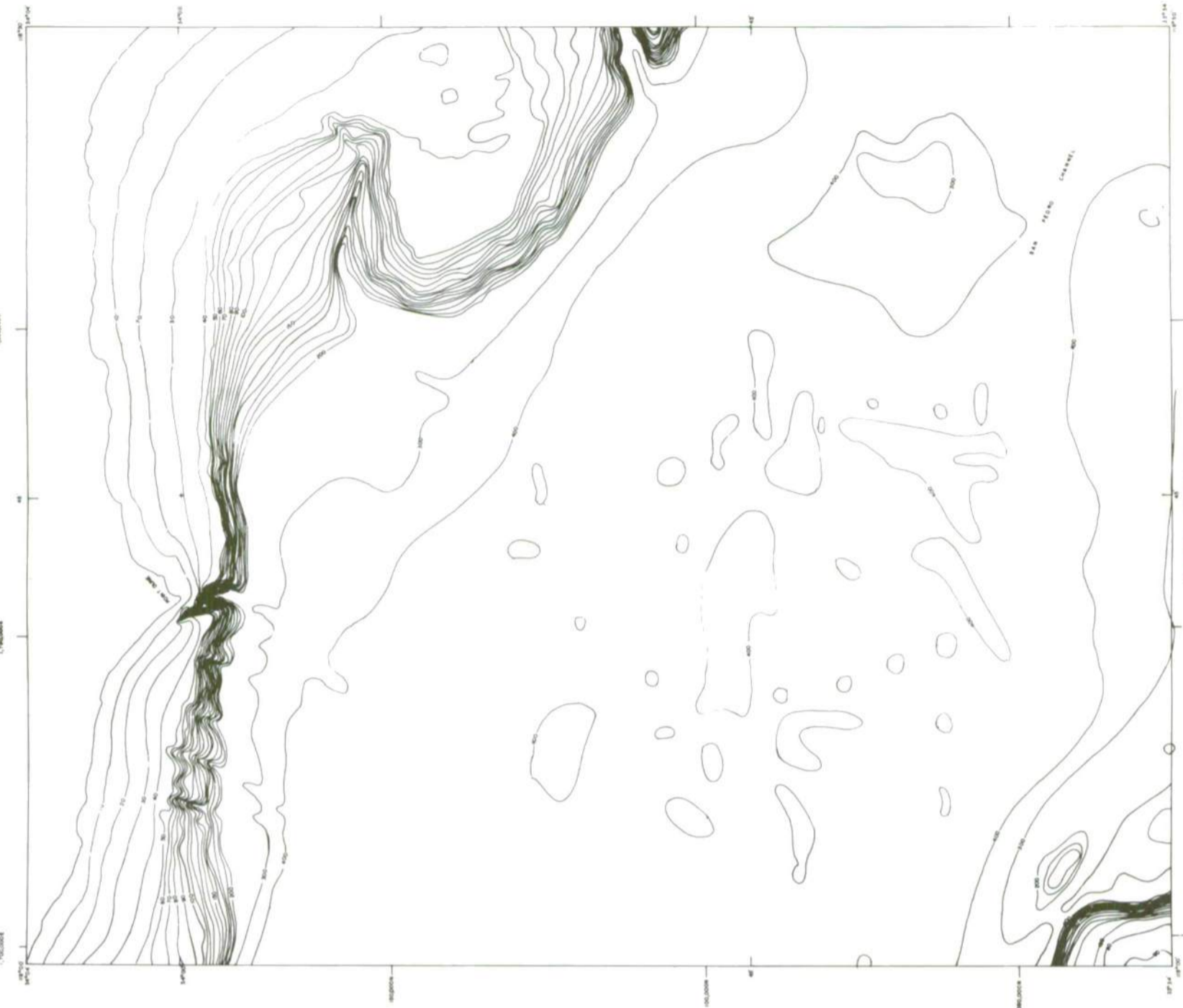
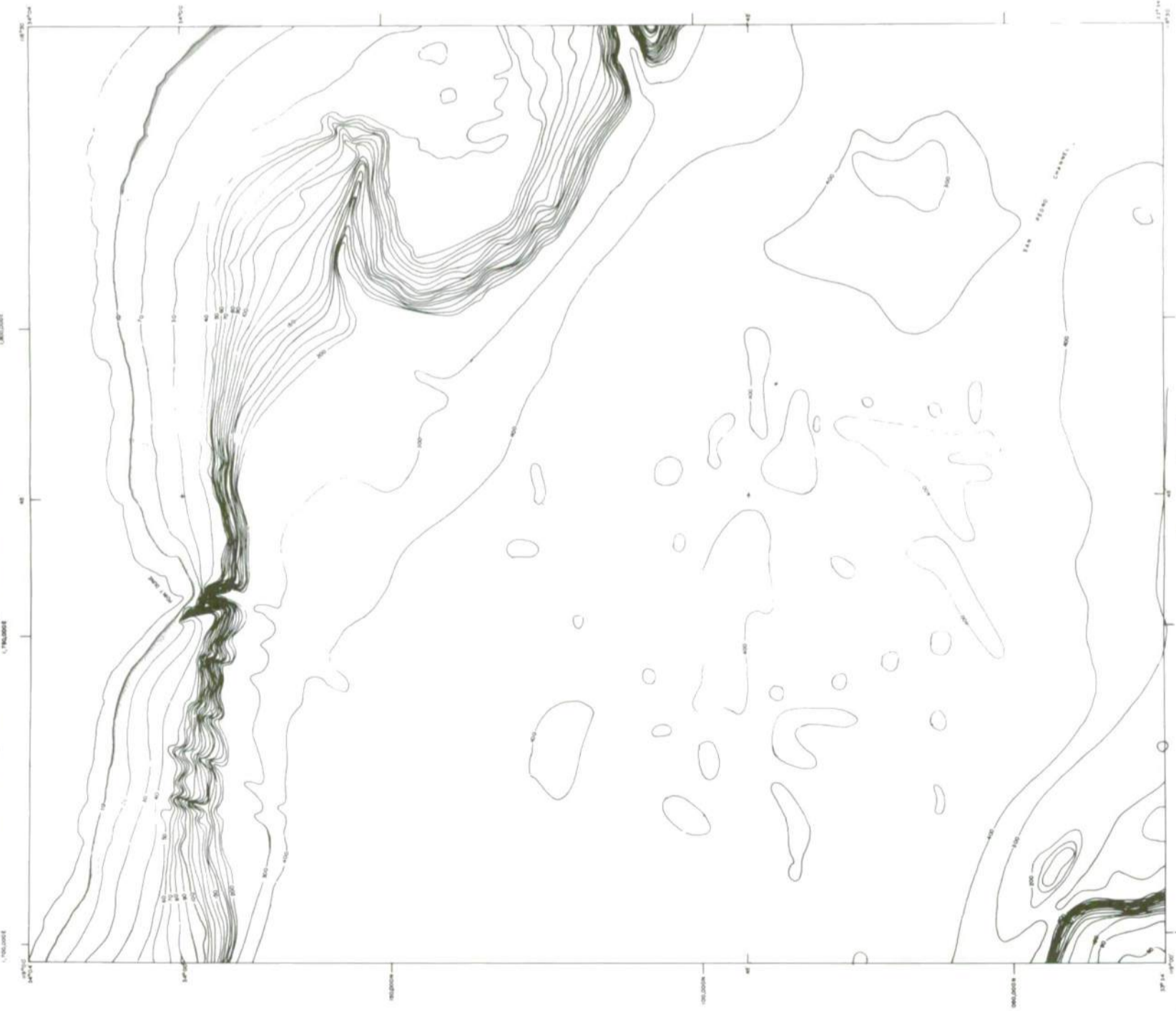


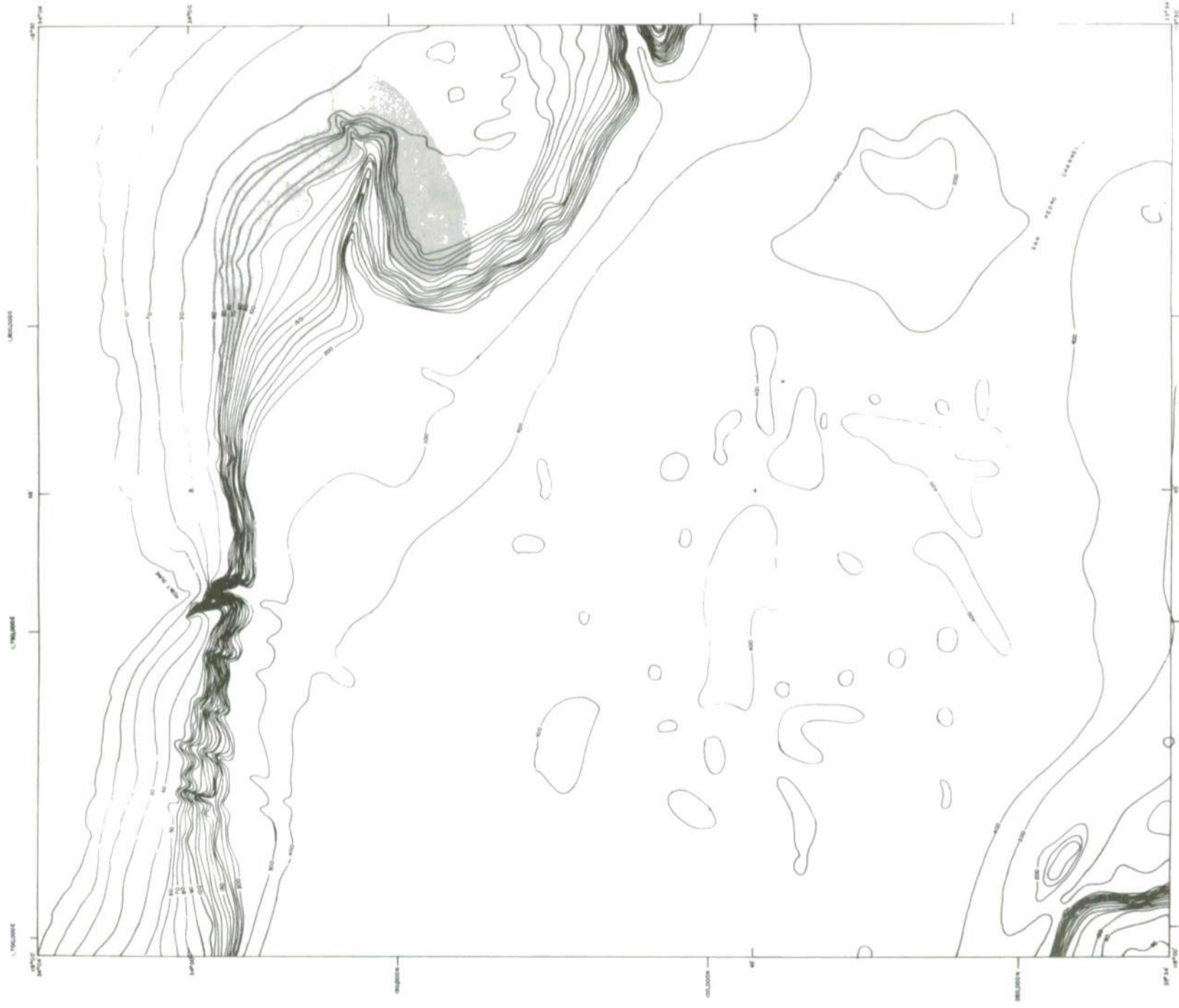
Part C. Bottom current velocity.



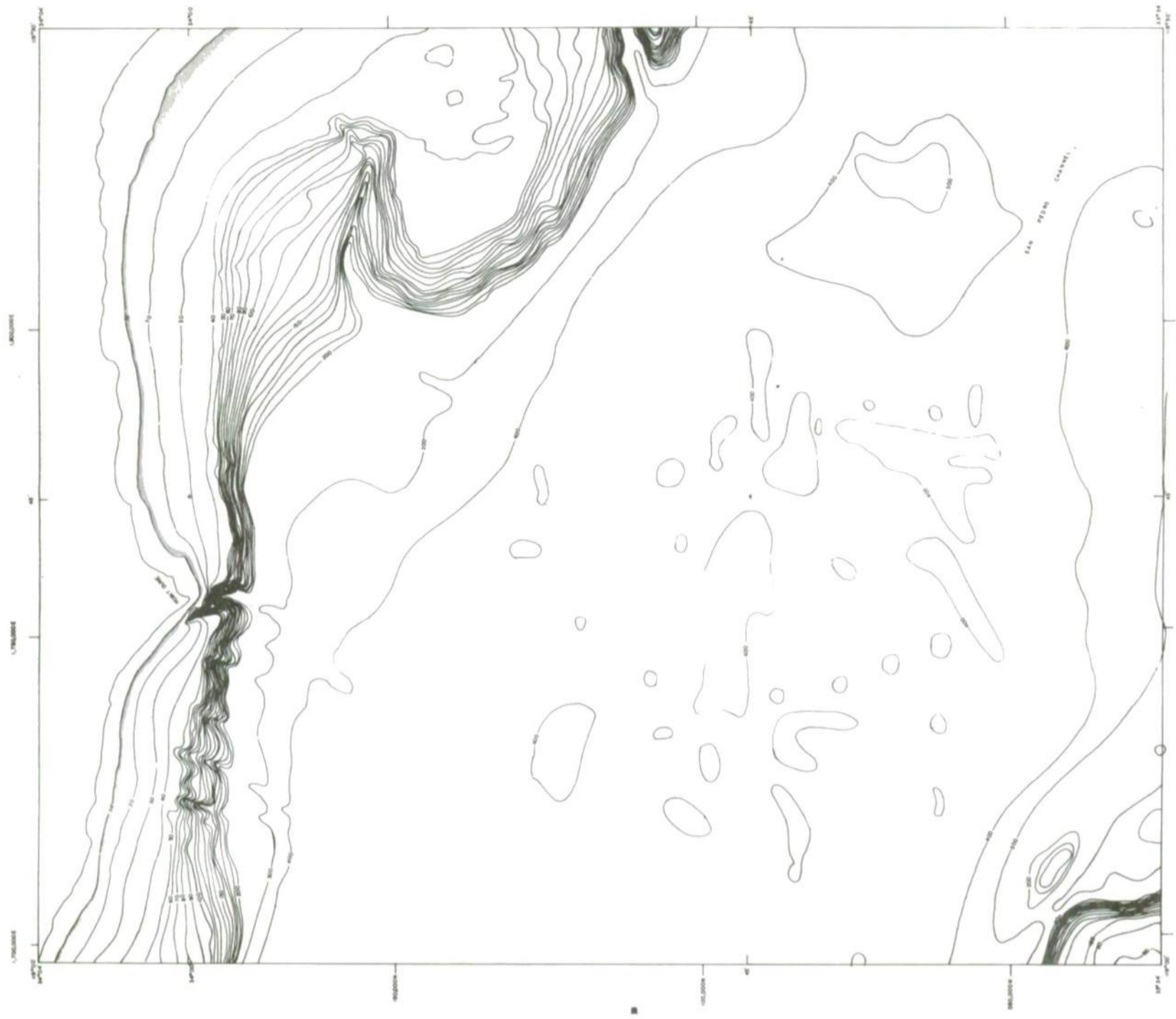
Part D. Tsunami surge.

Figure 33. Predicted regions of century extremes for chart number 30.



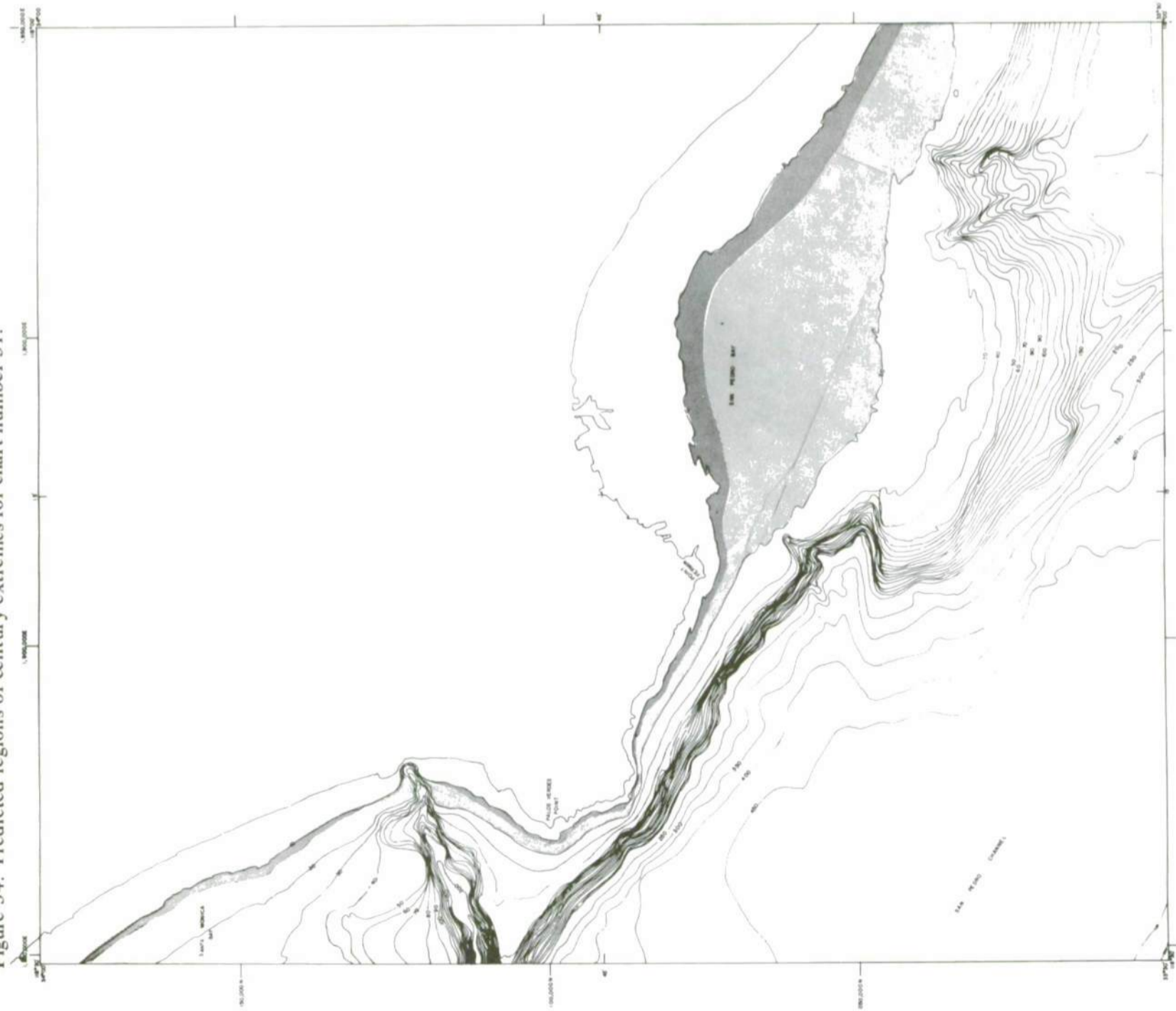


Part C. Bottom current velocity.

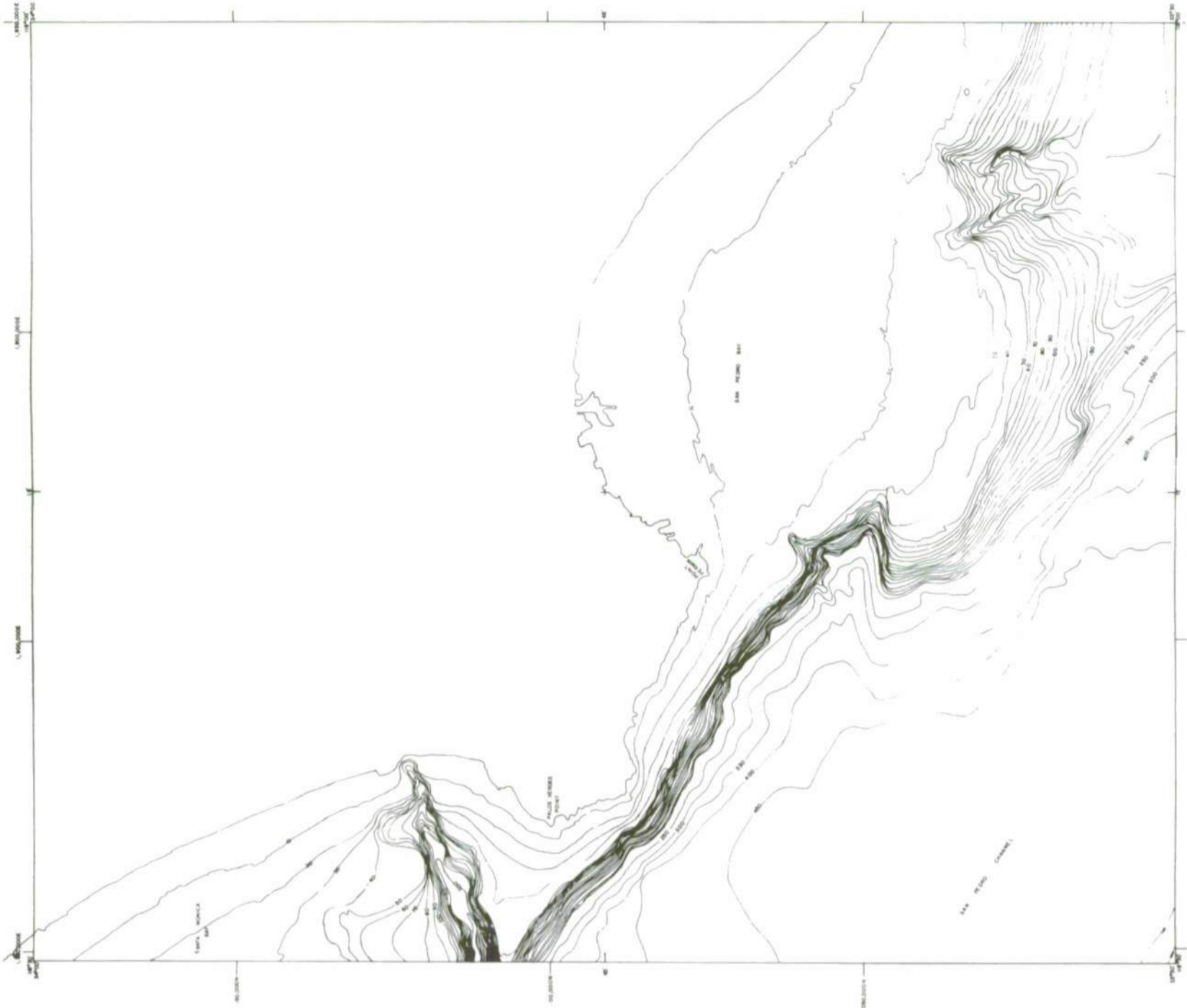


Part D. Tsunami surge.

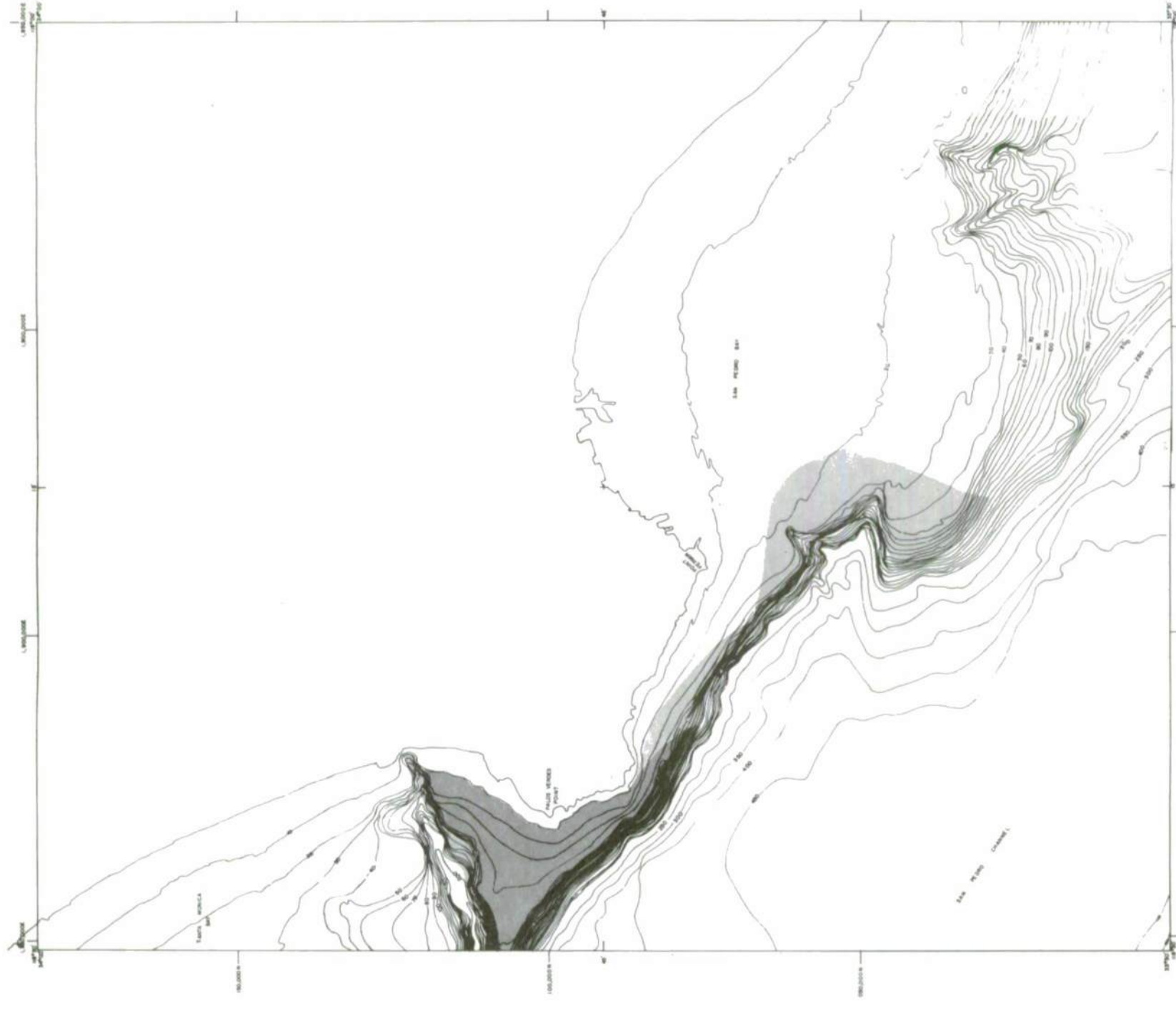
Figure 34. Predicted regions of century extremes for chart number 31.



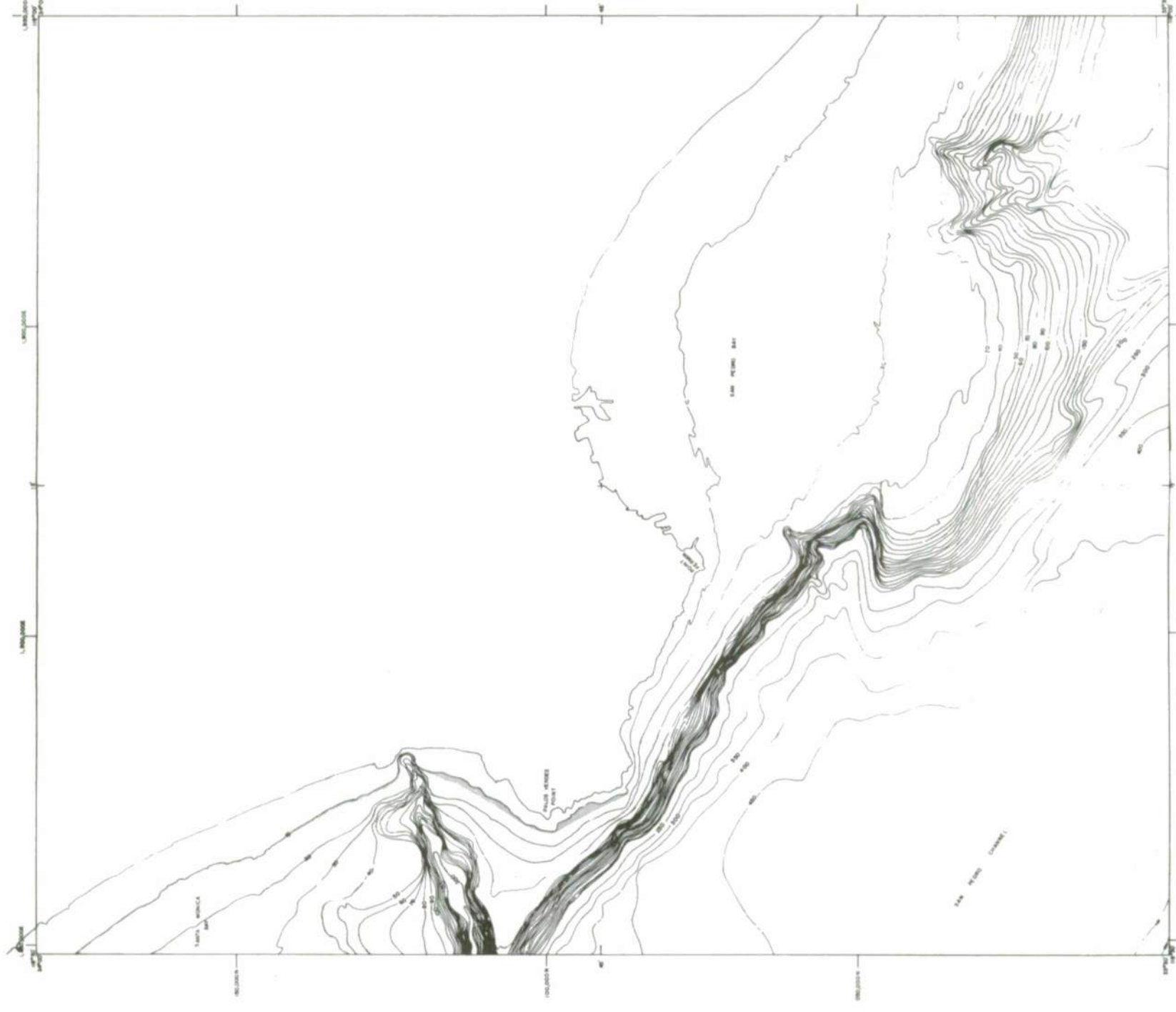
Part A. Density.



Part B. Bottom wave surge.

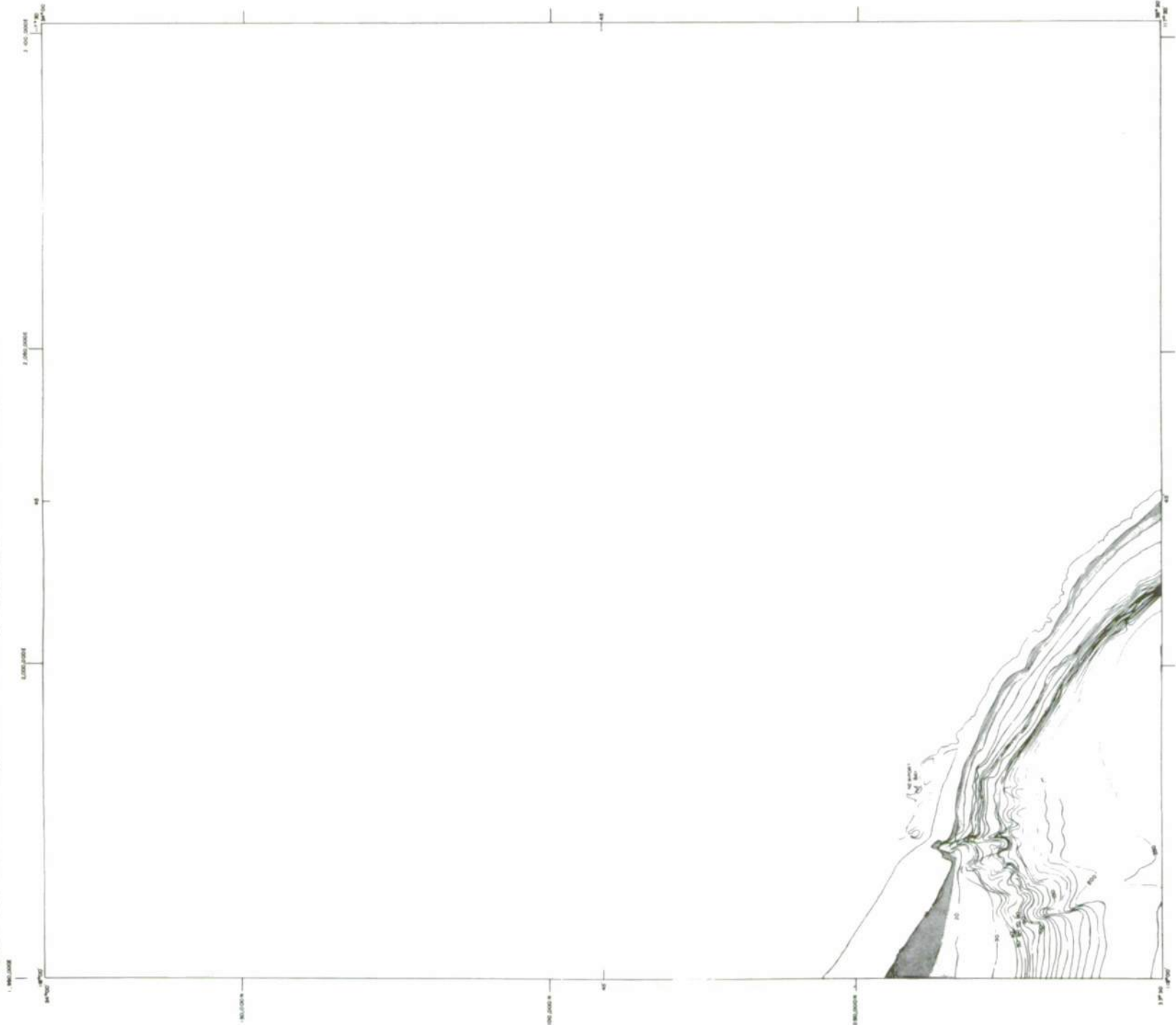


Part C. Bottom current velocity.

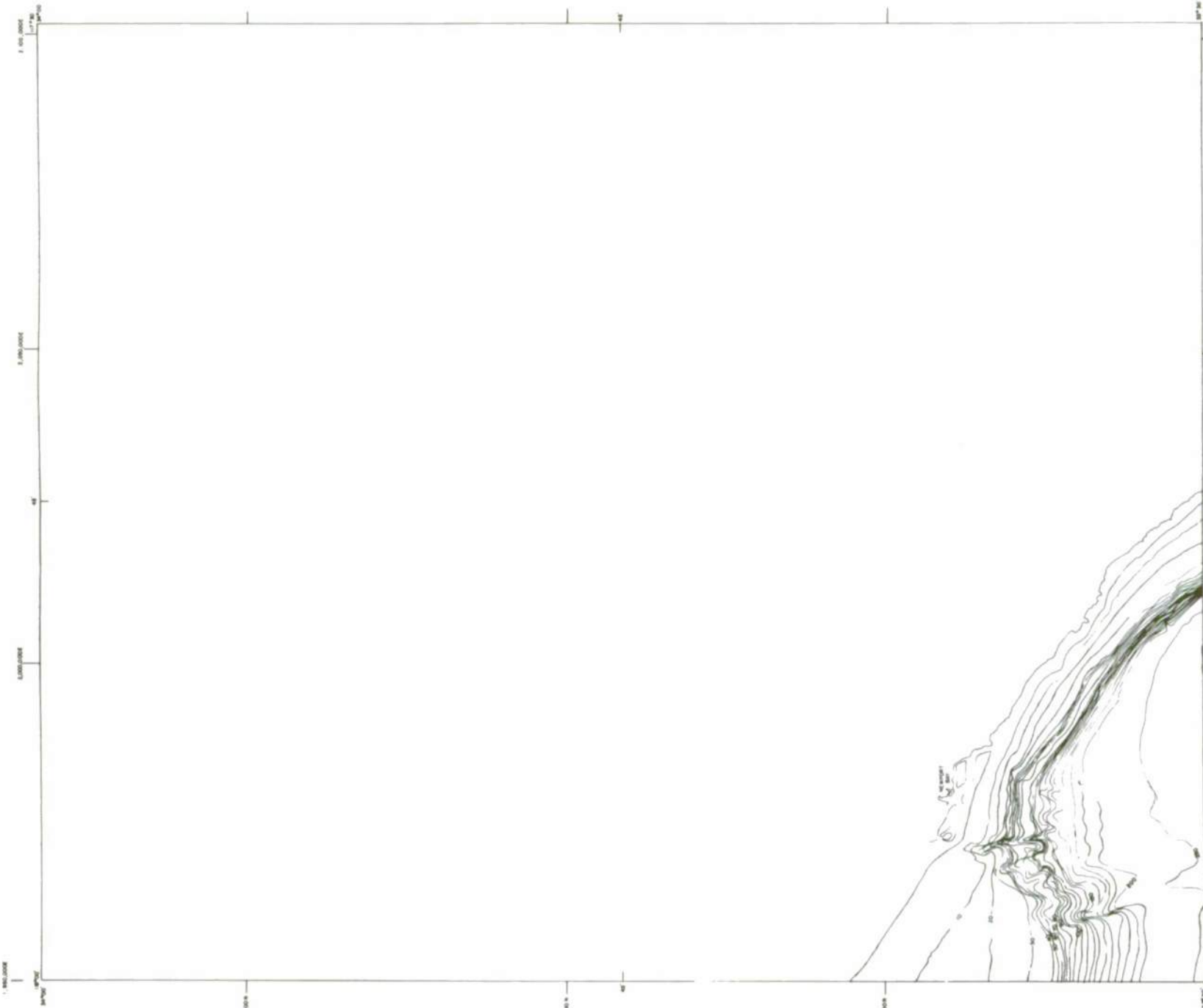


Part D. Tsunami surge.

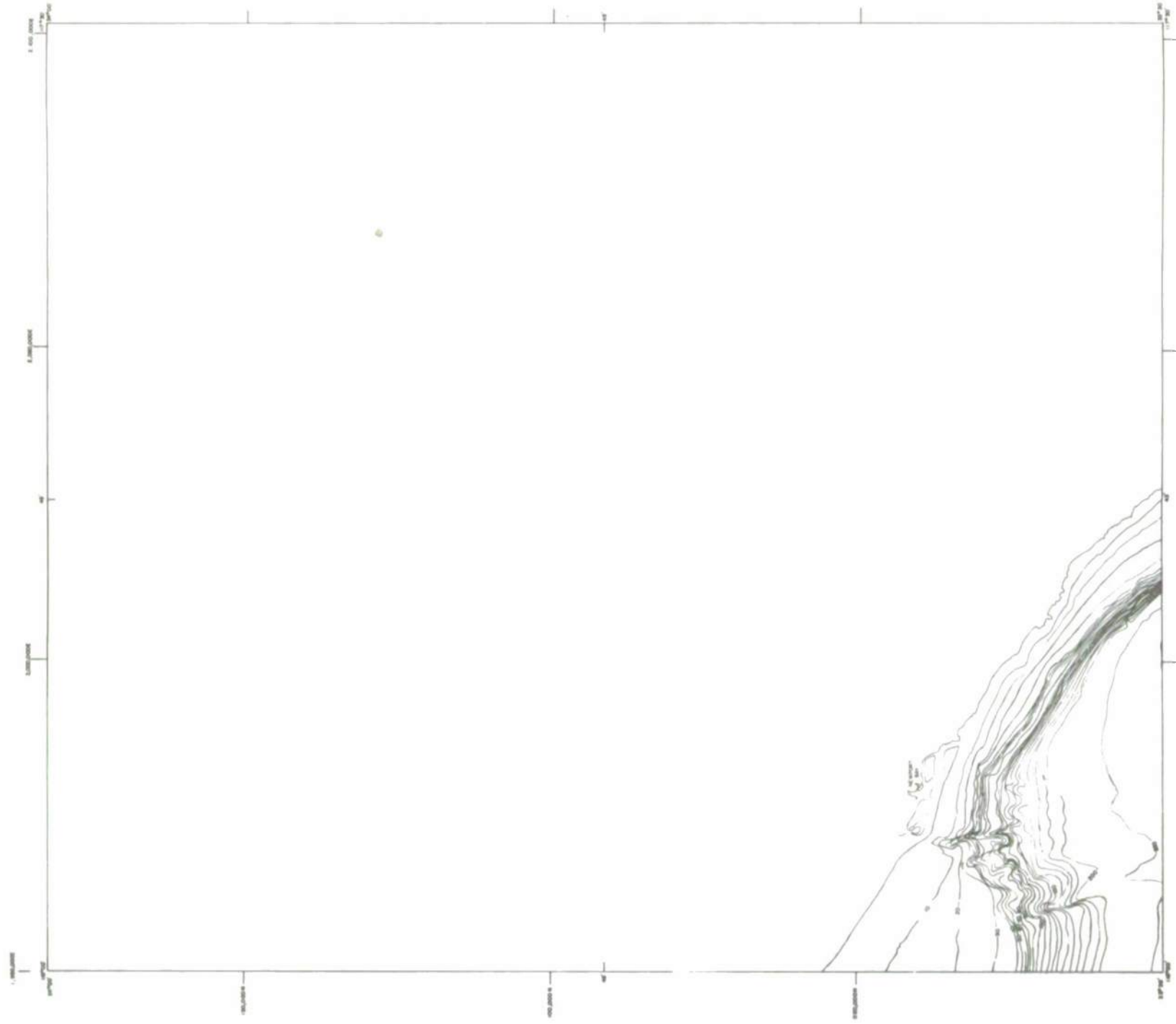
Figure 35. Predicted regions of century extremes for chart number 32.



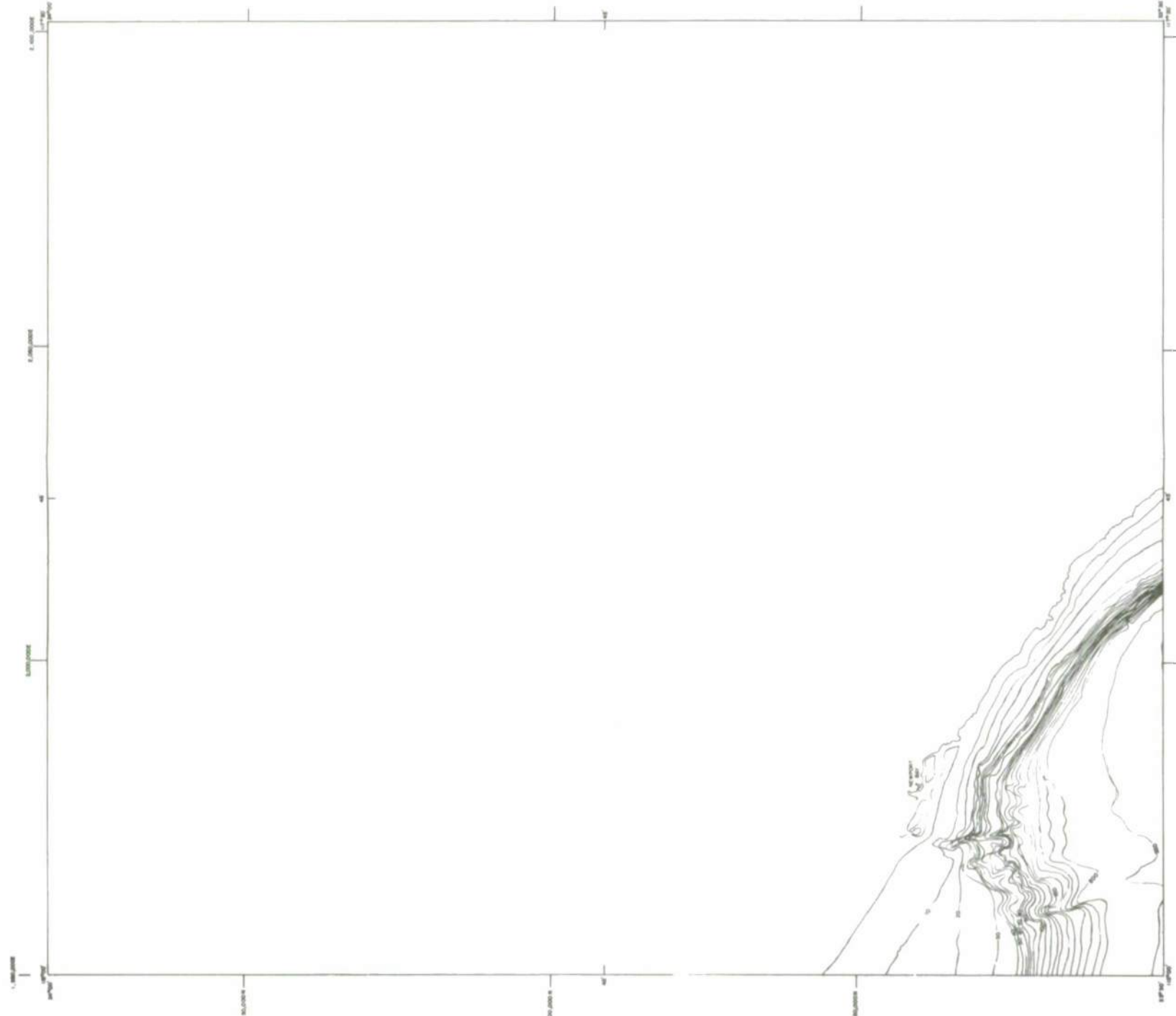
Part A. Density.



Part B. Bottom wave surge.

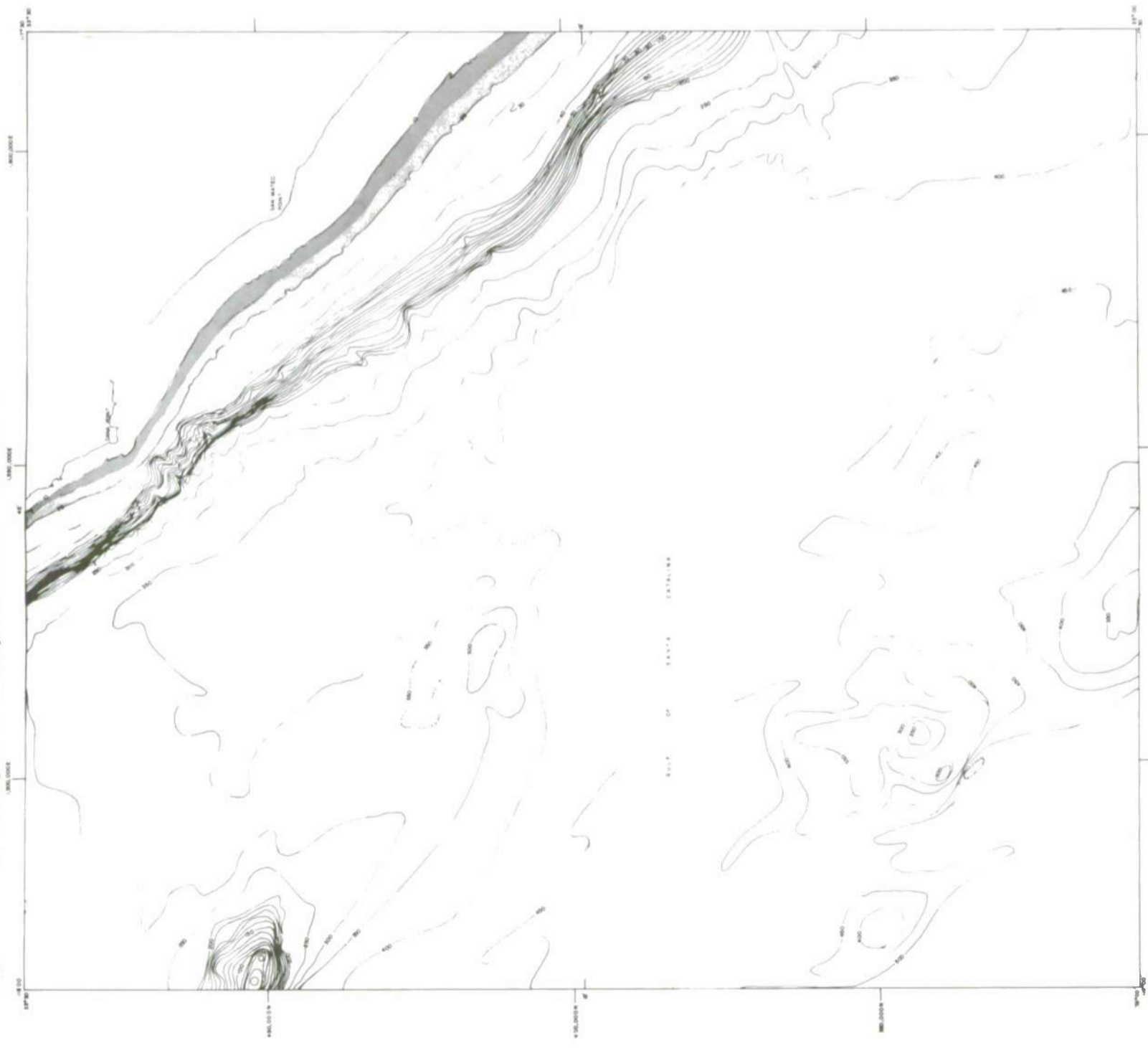


Part C. Bottom current velocity.

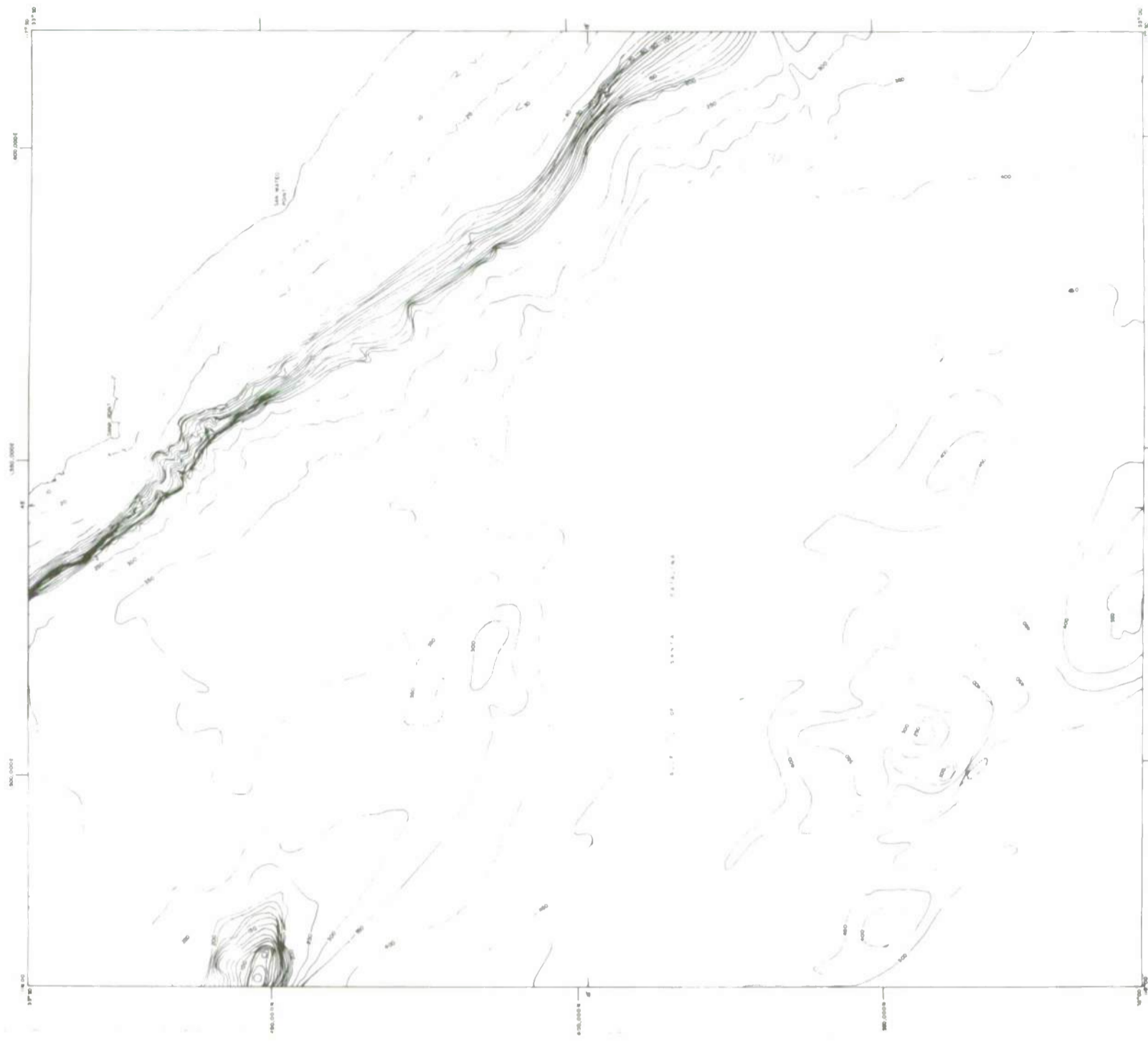


Part D. Tsunami surge.

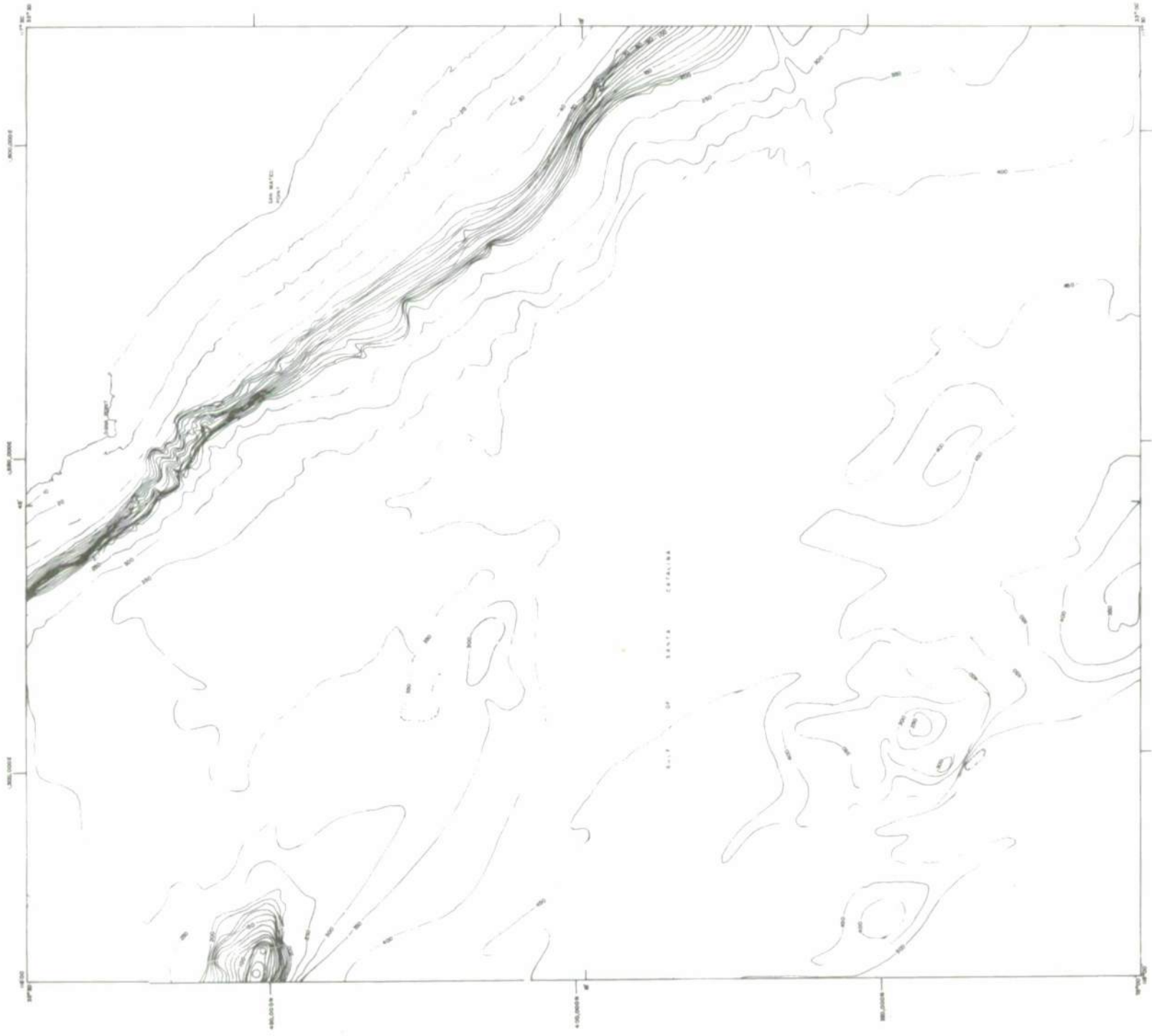
Figure 36. Predicted regions of century extremes for chart number 33.



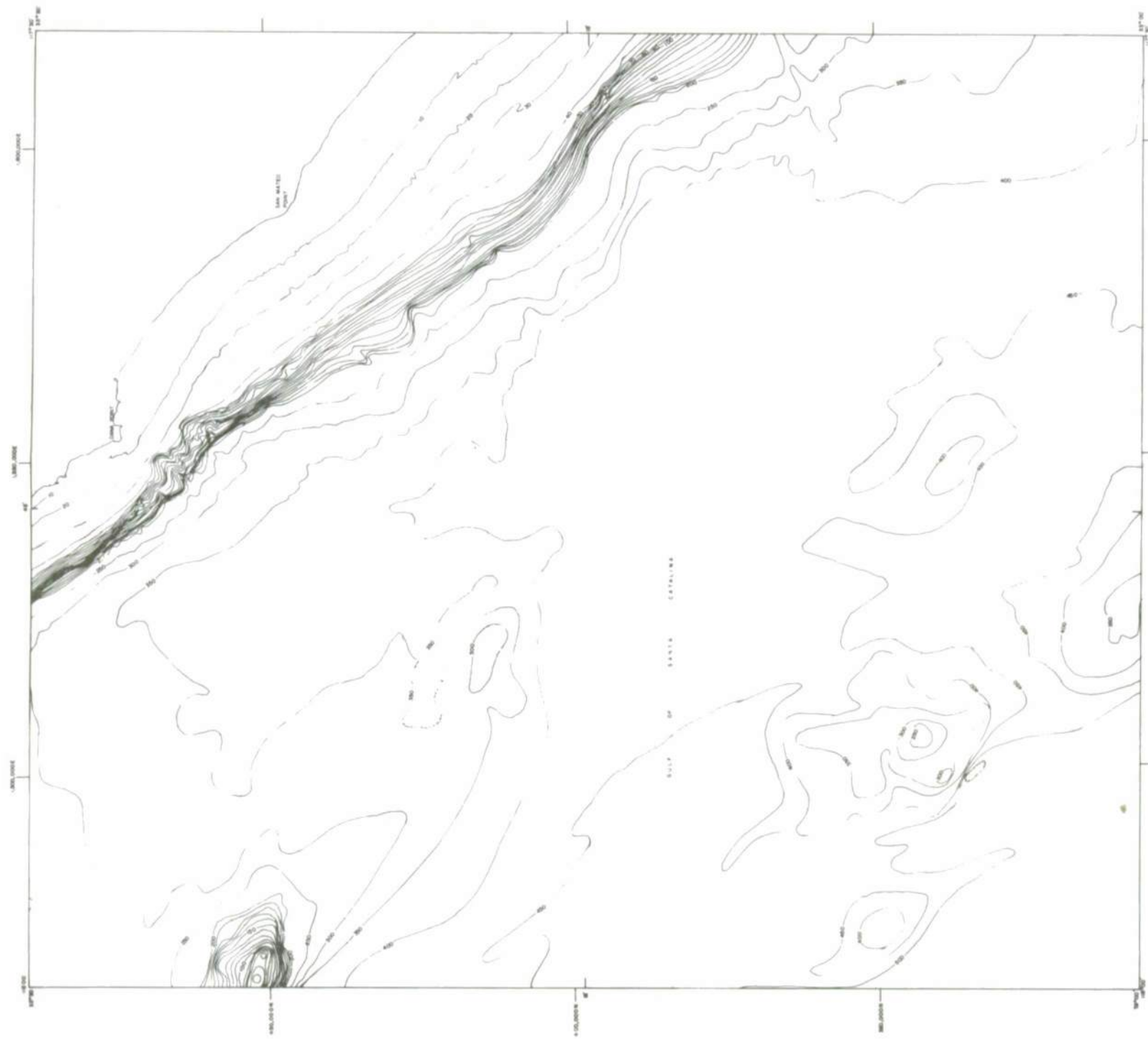
Part A. Density.



Part B. Bottom wave surge.

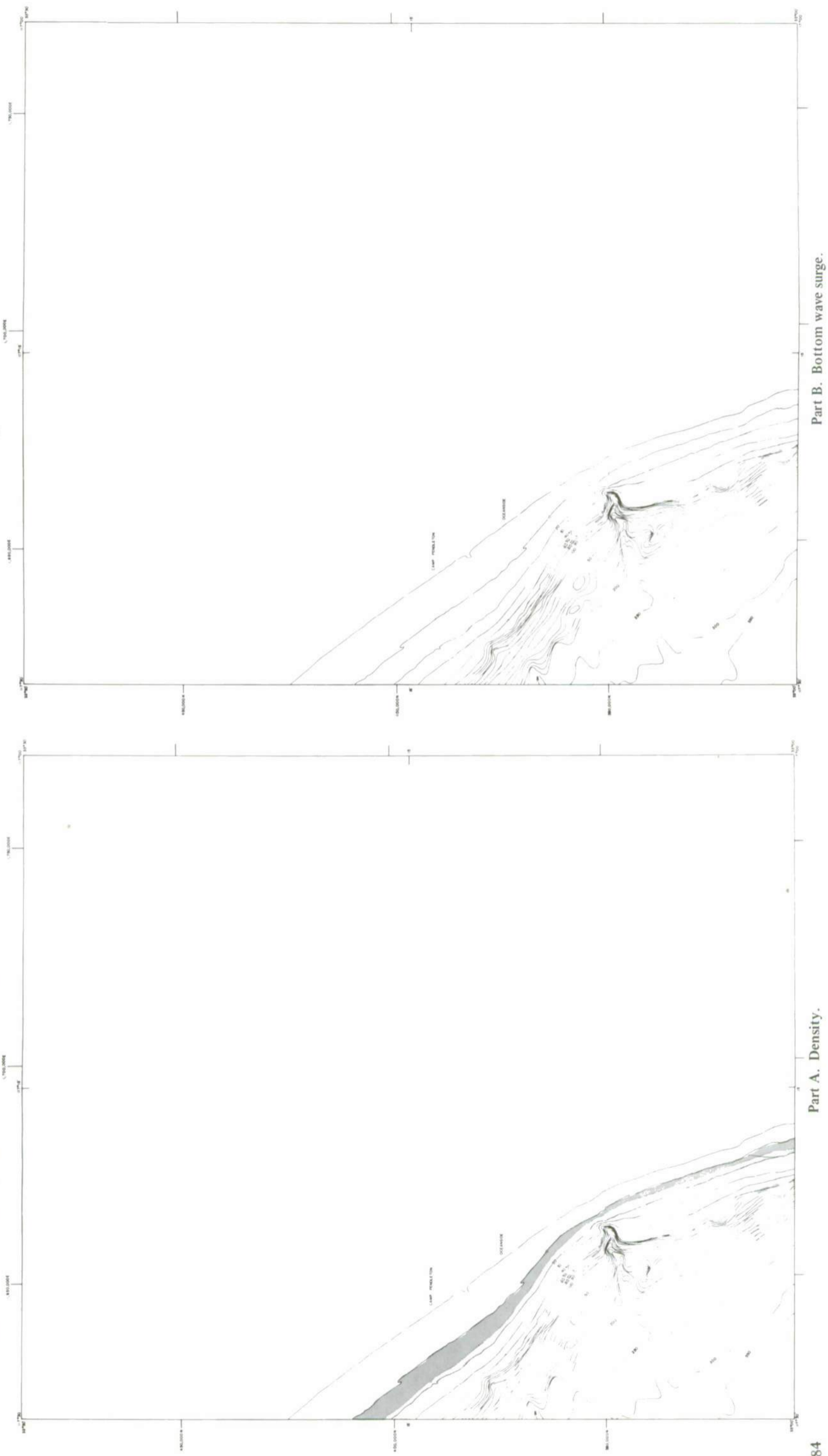


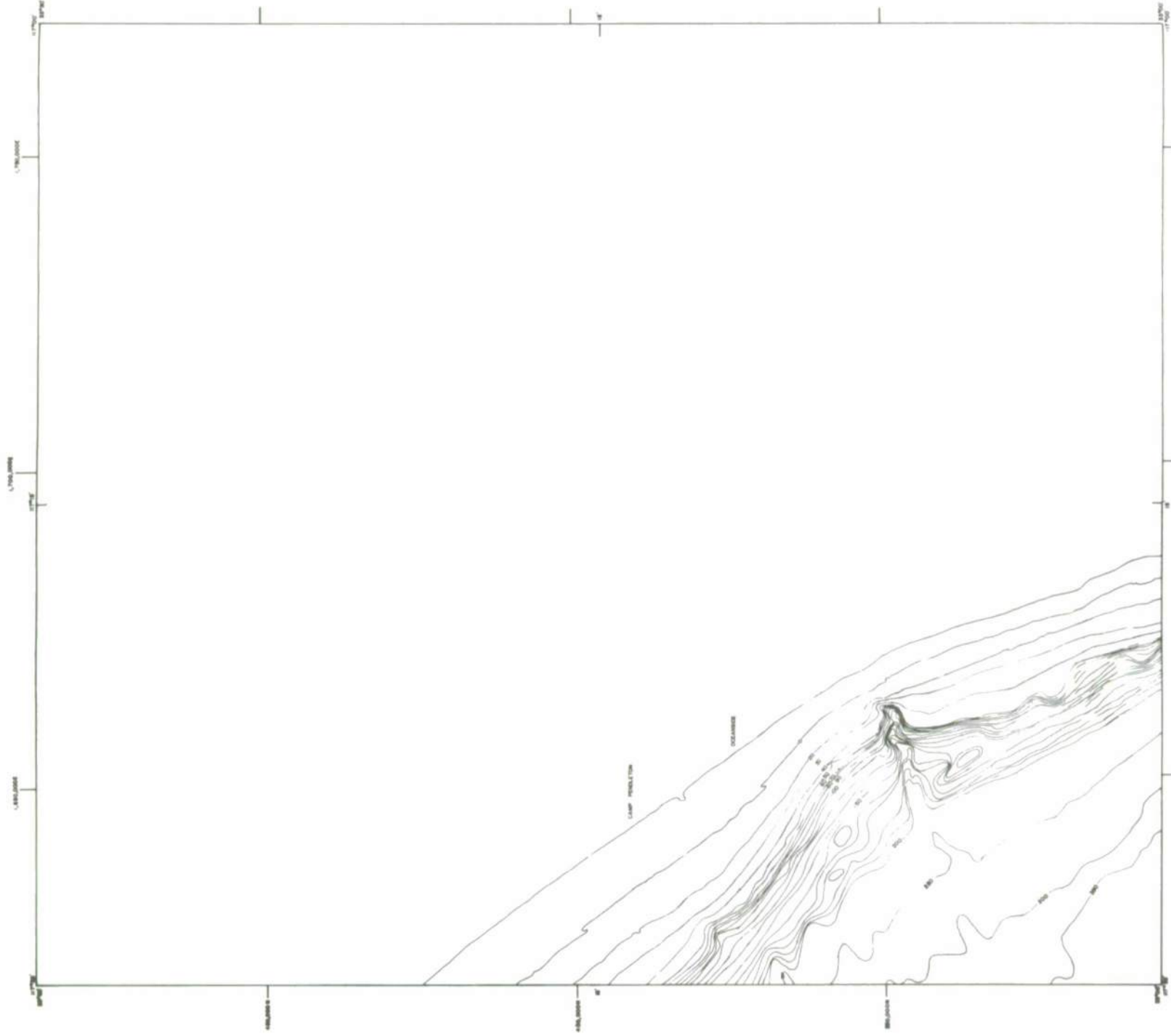
Part C. Bottom current velocity.



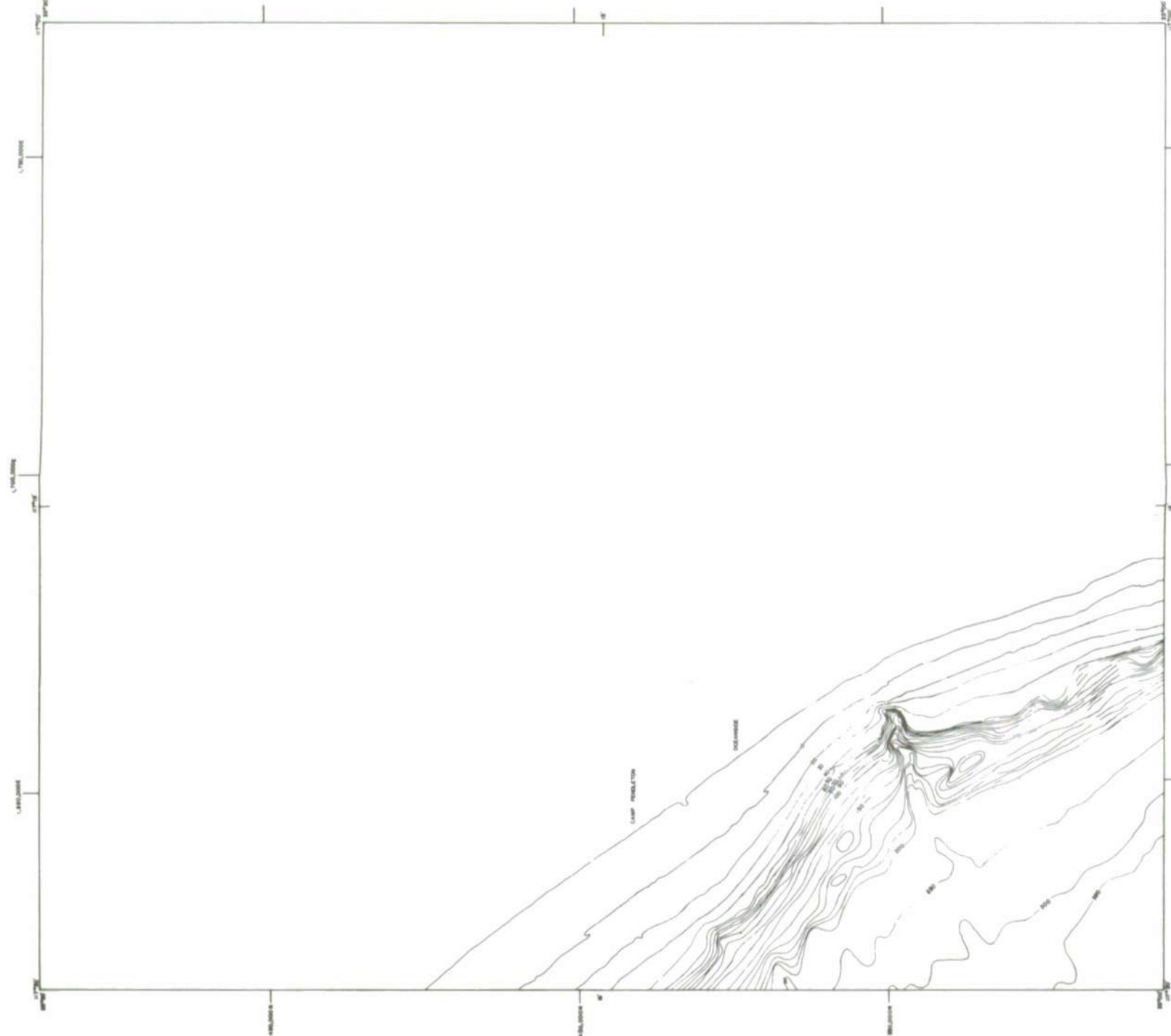
Part D. Tsunami surge.

Figure 37. Predicted regions of century extremes for chart number 34.



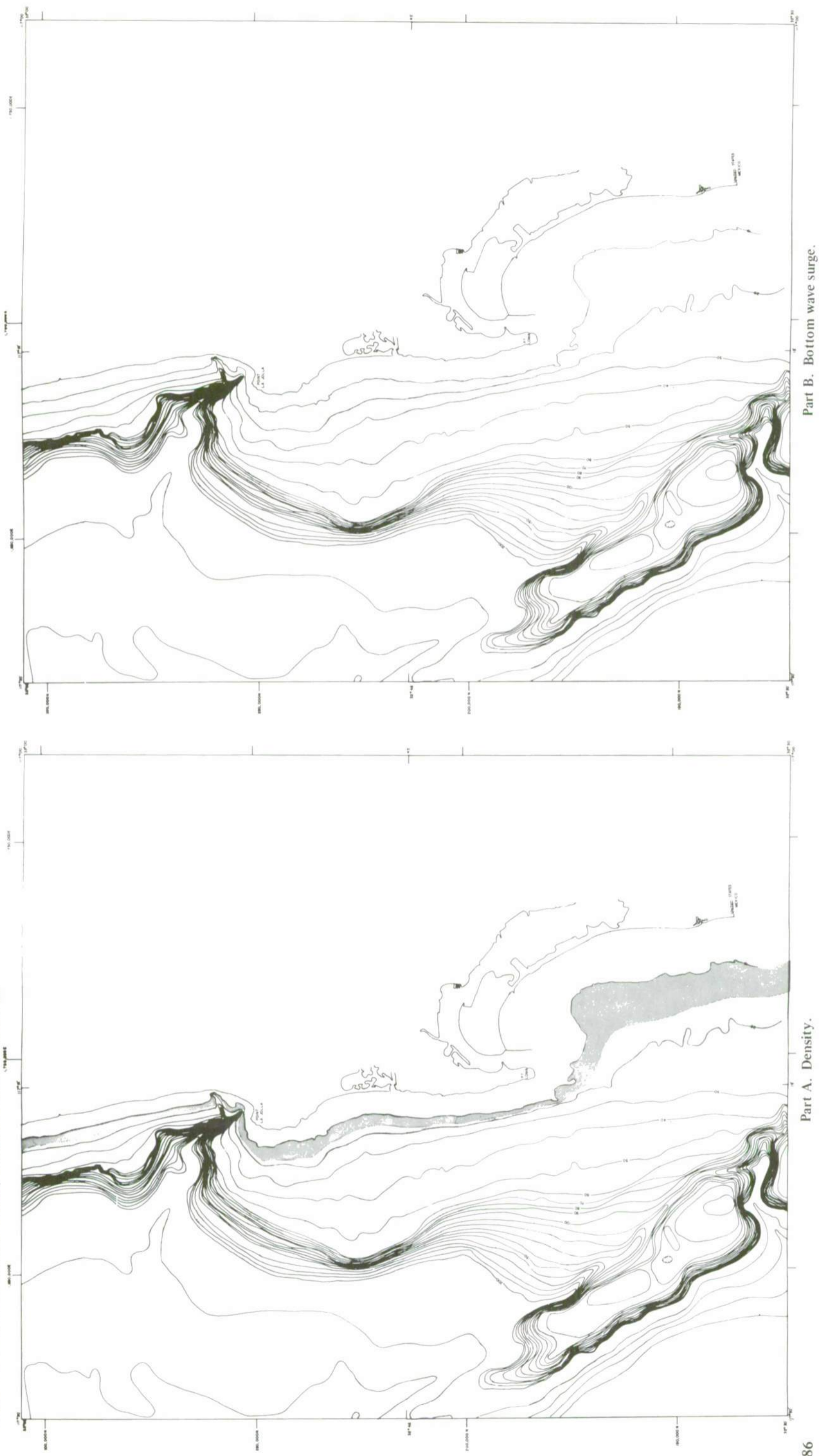


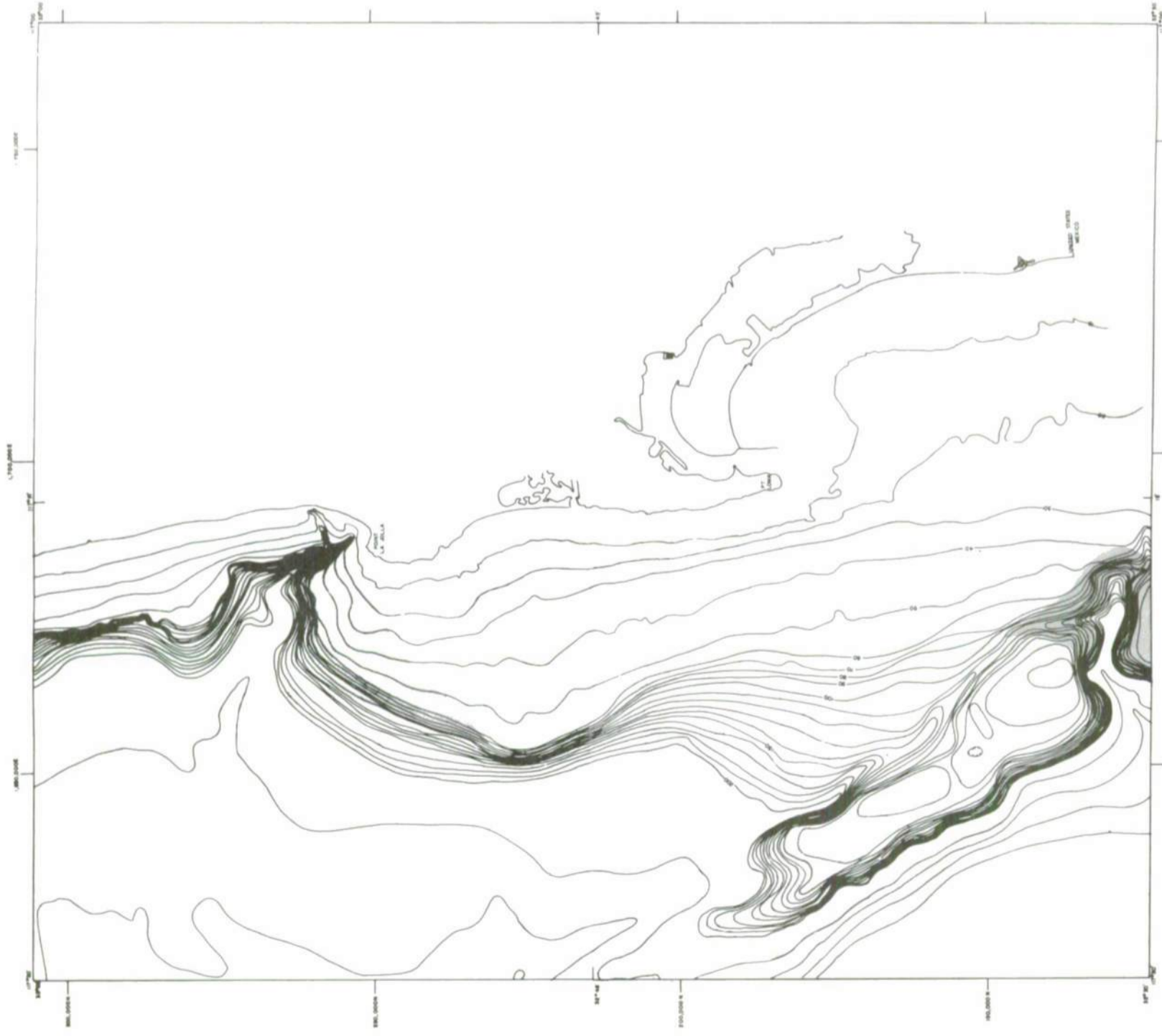
Part C. Bottom current velocity.



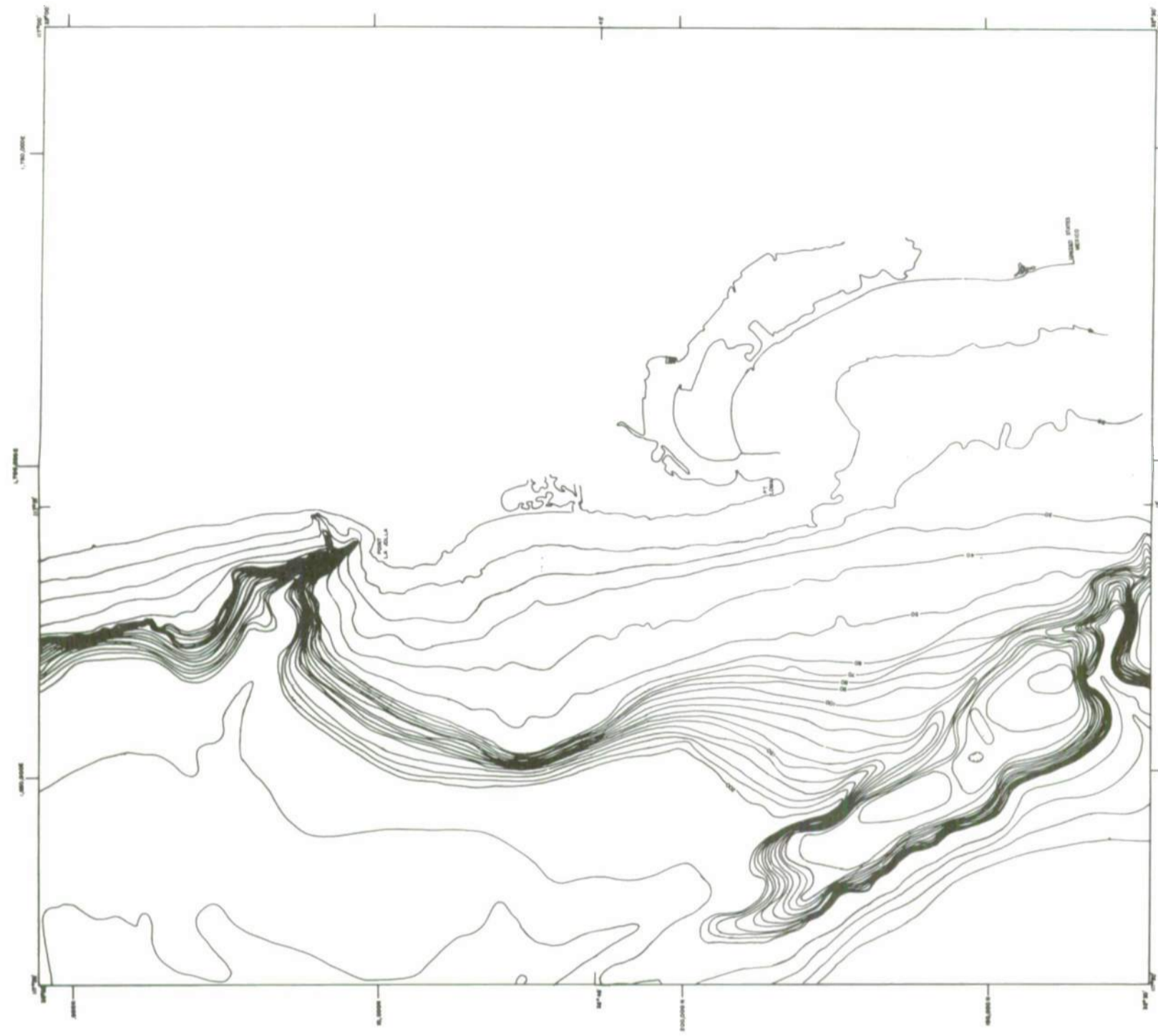
Part D. Tsunami surge.

Figure 38. Predicted regions of century extremes for chart number 35.





Part C. Bottom current velocity.



Part D. Tsunami surge.

RESULTS AND DISCUSSION OF CENTURY RISKS

The 35 coastal regions to be discussed in this section can be located on the index stored in the pocket inside the back cover.

DENSITY ON THE BOTTOM

Confidence bounds of several levels for extremely high and low density are given in table 3. As an example, the first entry in table 3, part A, can be read: "We may be 80 percent confident that the lowest density which will occur in the next 100 years at 50 m of depth at latitude $40^{\circ}14'N$, longitude $124^{\circ}20'W$, will not be less than 24.99."

Reduction of the shaded mylar charts of the σ_t extremes for 35 coastal regions are given as figures 4 through 38, part A.

Temperature and salinity, from which σ_t is calculated, vary considerably near the surface. The variability reduces at least exponentially with depth so that extremes are expected to occur near the surface for either high or low density (Riffenburgh [1970]); this variability is verified in table 3. The pattern which can be observed in figures 4 through 38, part A, indicates a northern strip of extremely high density water at 50-m depths and a southern strip of extremely low density water at 20-m depths (and probably into the surfline). Also, parallel bands of the highest (50 m) and lowest (20 m) densities expected in a century exist in the San Francisco vicinity almost adjacent to each other.

Seawater density increases as temperature decreases, but increases as salinity increases. In the north, there is considerable precipitation and land runoff of fresh water, which reduces the salinity and in turn the density. In the south, there is little cloud cover and a high sun angle, creating more solar warming which reduces the density. Thus, there exists a net surface effect of lower density along the coastline from the northern to the southern border. This effect and its results are shown in figure 39. In part A, time average and extreme bounds (dashed lines) of density for a hypothetical location are drawn as a function of depth as they would appear without the density-lowering surface effect. In the other parts, the density-lowering surface effect is drawn, reducing both average and extreme bounds of density near the top. In part B, the entire water column is colder so that the entire curve is pushed to the right; thus, the bulge of high density in the 50-m vicinity is pushed by cold water past the upper 10 percent limit and shading appears at this depth. In part C, the high density bulge of 50 m is still present, but extreme dilution plus very shallow water (to expose a larger volume of water to what solar radiation is present) combine to enhance the surface effect, and the near-surface density is pushed into the lower 10 percent region of shading. In part D, the entire water column is warmer, so that the 50-m bulge does not extend into the shaded region. However, increased solar warming has enhanced the density-lowering surface effect so that the near-surface density is pushed well into the lower 10 percent region of shading.

In table 3, the greatest difference between extremely low and extremely high densities appears near San Francisco. The 99 percent confidence low extreme P_t (defined on page 11) is 1.02477, and the high is 1.02813. In the San Francisco region, using the average P_t of 1.02525 as P_0 , the calculated buoyancies for the lowest and highest density waters are

$$b_{\text{low}} = 0.004586 \qquad b_{\text{high}} = -0.027528.$$

Table 3. Lowest and highest extreme values of σ_t likely to be observed over a century.

Part A.								
Latitude 40° 14' Longitude 124° 25';								
Approximate location: Cape Mendocino								
Confidence Bound (Probability)	Depth, m							
	Low Density				High Density			
	200	100	50	20	200	100	50	20
0.80			24.99	24.00			26.80	27.20
0.85			24.97	23.96			26.83	27.26
0.90			24.95	23.92			26.88	27.34
0.95			24.93	23.87			26.95	27.48
0.96			24.92	23.86			26.98	27.52
0.97			24.91	23.84			27.01	27.57
0.98			24.90	23.82			27.05	27.65
0.99			24.88	23.79			27.12	27.78
0.995			24.87	23.76			27.20	27.91
0.999			24.84	23.71			27.36	28.21
Part B.								
Latitude 39° 46' Longitude 124° 00';								
Approximate location: Noya Canyon								
Confidence Bound (Probability)	Depth, m							
	Low Density				High Density			
	200	100	50	20	200	100	50	20
0.80			24.85				26.98	
0.85			24.83				27.02	
0.90			24.81				27.08	
0.95			24.78				27.18	
0.96			24.77				27.21	
0.97			24.76				27.24	
0.98			24.74				27.30	
0.99			24.72				27.39	
0.995			24.70				27.48	
0.999			24.67				27.70	

Table 3. Continued.

Part C.

Latitude 38° 30' Longitude 123° 22';

Approximate location: Bodega Bay

Confidence Bound (Probability)	Depth, m							
	Low Density				High Density			
	200	100	50	20	200	100	50	20
0.80			25.14	25.09			26.98	26.64
0.85			25.12	25.07			27.01	26.67
0.90			25.10	25.06			27.06	26.71
0.95			25.07	25.03			27.14	26.78
0.96			25.06	25.02			27.17	26.80
0.97			25.05	25.02			27.19	26.83
0.98			25.04	25.00			27.24	26.87
0.99			25.02	24.99			27.32	26.93
0.995			25.01	24.98			27.40	27.00
0.999			24.98	24.95			27.58	27.15

Part D.

Latitude 37° 53' Longitude 123° 01';

Approximate location: San Francisco

Confidence Bound (Probability)	Depth, m							
	Low Density				High Density			
	200	100	50	20	200	100	50	20
0.80			24.91	24.58			26.98	27.10
0.85			24.89	24.56			27.02	27.20
0.90			24.86	24.53			27.07	27.35
0.95			24.83	24.50			27.16	27.59
0.96			24.82	24.49			27.19	27.66
0.97			24.81	24.47			27.23	27.76
0.98			24.79	24.46			27.28	27.90
0.99			24.77	24.44			27.37	28.13
0.995			24.76	24.42			27.46	28.36
0.999			24.72	24.38			27.66	28.90

Table 3. Continued.

Part E.

Latitude 37° 19' Longitude 122° 36';

Approximate location: Ascension Canyon

Confidence Bound (Probability)	Depth, m							
	Low Density				High Density			
	200	100	50	20	200	100	50	20
0.80			24.90	24.24			26.94	26.79
0.85			24.87	24.21			26.98	26.84
0.90			24.85	24.18			27.03	26.91
0.95			24.81	24.14			27.13	27.01
0.96			24.81	24.13			27.16	27.05
0.97			24.79	24.12			27.19	27.09
0.98			24.78	24.10			27.25	27.16
0.99			24.76	24.08			27.34	27.26
0.995			24.74	24.06			27.42	27.37
0.999			24.71	24.02			27.63	27.62

Part F.

Latitude 35° 37' Longitude 121° 16'

Approximate location: Pt. Piedras Blancas

Confidence Bound (Probability)	Depth, m							
	Low Density				High Density			
	200	100	50	20	200	100	50	20
0.80			24.93	24.74			26.81	26.61
0.85			24.91	24.72			26.84	26.64
0.90			24.89	24.70			26.88	26.69
0.95			24.86	24.67			26.96	26.77
0.96			24.85	24.66			26.98	26.79
0.97			24.84	24.65			27.01	26.82
0.98			24.83	24.64			27.05	26.87
0.99			24.81	24.62			27.12	26.94
0.995			24.80	24.61			27.19	27.02
0.999			24.77	24.58			27.35	27.19

Table 3. Continued.

Part G.								
Latitude 35°04'			Longitude 120°52'					
Approximate location: San Luis Obispo Bay								
Confidence Bound (Probability)	Depth, m							
	Low Density				High Density			
	200	100	50	20	200	100	50	20
0.80		25.40	25.45			26.78	26.51	
0.85		25.39	25.43			26.81	26.53	
0.90		25.37	25.42			26.84	26.55	
0.95		25.35	25.41			26.91	26.59	
0.96		25.34	25.40			26.93	26.61	
0.97		25.33	25.40			26.96	26.63	
0.98		25.32	25.39			26.99	26.65	
0.99		25.30	25.38			27.05	26.69	
0.995		25.30	25.37			27.11	26.73	
0.999		25.27	25.36			27.25	26.83	

Part H.
Latitude 34°27' Longitude 120°32'
Approximate location: Pt. Arguello

Confidence Bound (Probability)	Depth, m							
	Low Density				High Density			
	200	100	50	20	200	100	50	20
0.80			24.70	24.37			26.73	26.50
0.85			24.68	24.34			26.77	26.54
0.90			24.65	24.32			26.82	26.59
0.95			24.62	24.28			26.91	26.68
0.96			24.61	24.27			26.94	26.71
0.97			24.60	24.26			26.97	26.75
0.98			24.58	24.25			27.02	26.80
0.99			24.57	24.22			27.10	26.89
0.995			24.56	24.20			27.19	26.98
0.999			24.55	24.17			27.38	27.19

Table 3. Continued.

Part I.

Latitude 34° 14' Longitude 119° 22'

Approximate location: Santa Barbara

Confidence Bound (Probability)	Depth, m							
	Low Density				High Density			
	200	100	50	20	200	100	50	20
0.80				24.43				26.30
0.85				24.41				26.34
0.90				24.39				26.39
0.95				24.36				26.46
0.96				24.35				26.49
0.97				24.34				26.52
0.98				24.33				26.57
0.99				24.31				26.64
0.995				24.30				26.72
0.999				24.27				26.90

Part J.

Latitude 33° 52' Longitude 120° 00'

Approximate location: Santa Rosa Island

Confidence Bound (Probability)	Depth, m							
	Low Density				High Density			
	200	100	50	20	200	100	50	20
0.80		25.72	24.79	24.19		26.64	26.78	26.47
0.85		25.71	24.77	24.16		26.66	26.81	26.51
0.90		25.70	24.75	24.13		26.68	26.86	26.57
0.95		25.69	24.72	24.10		26.72	26.95	26.67
0.96		25.68	24.71	24.09		26.74	26.97	26.70
0.97		25.68	24.71	24.07		26.76	27.00	26.24
0.98		25.67	24.70	24.06		26.78	27.05	26.80
0.99		25.66	24.68	24.04		26.82	27.13	26.89
0.995		25.65	24.66	24.02		26.86	27.21	26.99
0.999		25.64	26.63	23.98		26.96	27.40	27.21

Table 3. Continued.

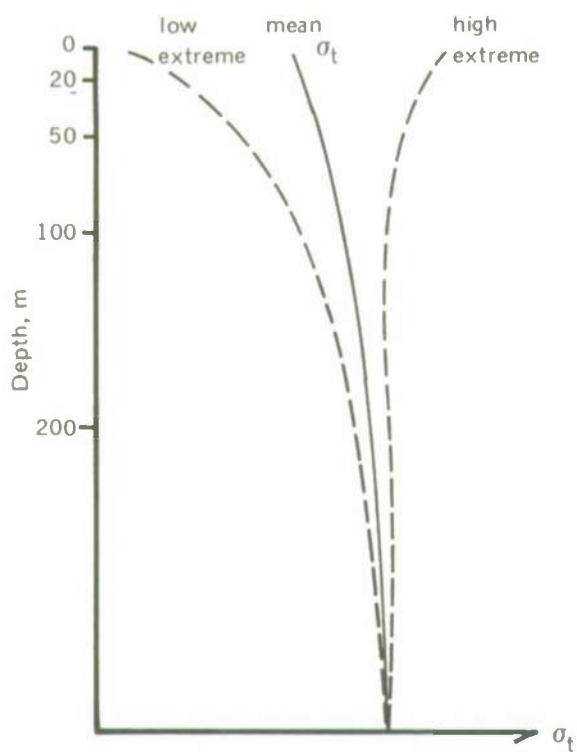
Part K.

Latitude 33°28' Longitude 117°46'

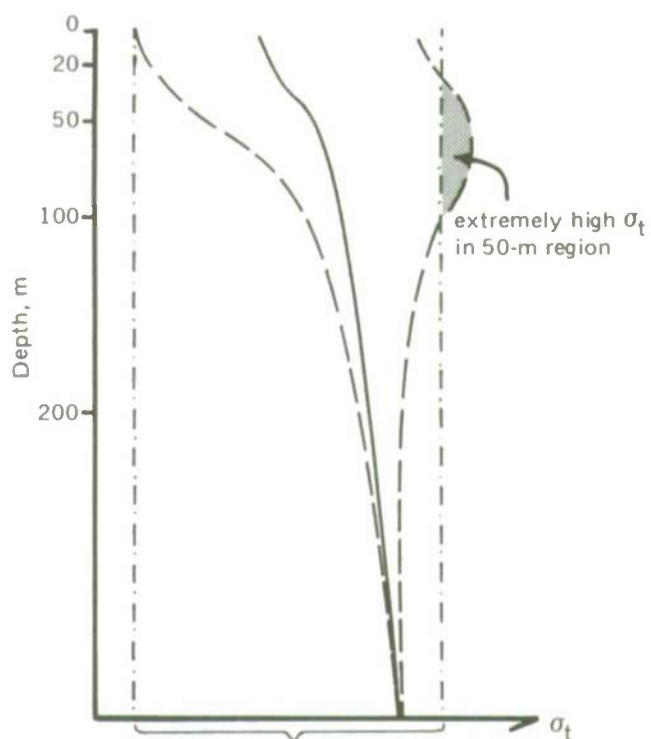
Approximate location: San Pedro

Confidence Bound (Probability)	Depth, m							
	Low Density				High Density			
	200	100	50	20	200	100	50	20
0.80	26.13	25.30	24.65	24.11	26.73	26.76	26.54	25.95
0.85	26.13	25.29	24.63	24.09	26.74	26.79	26.57	25.99
0.90	26.12	25.27	24.61	24.07	26.76	26.83	26.63	26.03
0.95	26.11	25.25	24.58	24.04	26.79	26.89	26.71	26.11
0.96	26.11	25.24	24.57	24.04	26.80	26.91	26.74	26.14
0.97	26.10	25.23	24.56	24.03	26.81	26.93	26.77	26.17
0.98	26.10	25.23	24.55	24.01	26.82	26.96	26.82	26.21
0.99	26.09	25.21	24.53	24.01	26.85	27.02	26.89	26.29
0.995	26.09	25.20	24.52	23.98	26.88	27.08	26.97	26.36
0.999	26.08	25.18	24.49	23.95	26.94	27.21	27.16	26.53

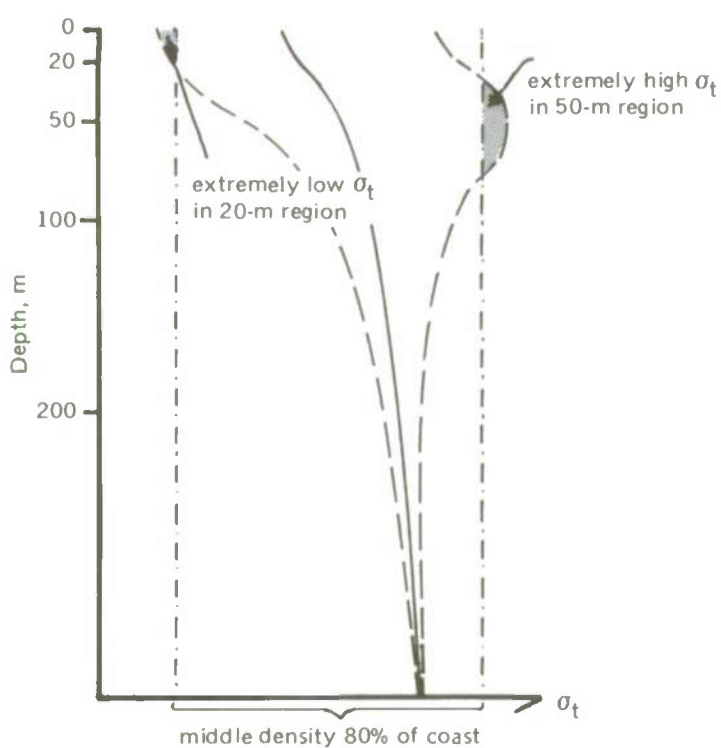
Figure 39. Average and extreme σ_t as a function of depth.



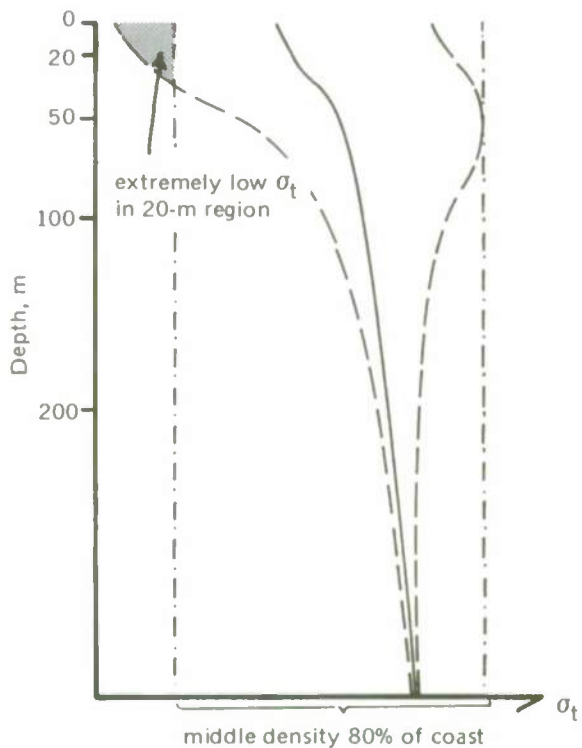
Part A. Without σ -lowering surface effect.



Part B. Modified by σ -lowering surface effect in Pt. Arena vicinity.



Part C. Modified by σ -lowering surface effect in San Francisco vicinity.



Part D. Modified by σ -lowering surface effect in Los Angeles vicinity.

BOTTOM SURGE

Several levels of confidence bounds for extremely high bottom surge velocity are given in table 4. As an example, the last entry in table 4, part A, can be read: "We may be 99.9 percent confident that the greatest bottom surge velocity which will occur in the next 100 years in the Crescent City vicinity at 20 m will not be greater than 294.9 cm/sec."

Reductions of the bottom surge extremes are shown as part B in figures 4 through 38. It is clear that the bottom effect from storm waves is most serious in shallow water and in the north. The shading disappears south of Pt. Conception, and all dark shading lies to the north of the Big Sur region. Also, the shading never extends out to waters deeper than about 75 m, and the dark shading is never deeper than about 40 m.

The predictions of extreme wave parameters, from which the extreme bottom surge values were calculated, may be useful. Several levels of confidence bounds for extremely large wave periods, lengths, and heights are given in table 5. As an example, the first four entries in the last line of table 5, part A, may be read: "We may be 99.9 percent confident that the greatest wave period which will occur in the next 100 years will not be greater than 22.4 seconds, the greatest wave height in the deep sea will not exceed 14.0 m, the greatest wave length over 200 m of depth will not exceed 736 m, and the greatest wave height over 200 m of depth will not exceed 14.0 m."

BOTTOM CURRENTS

Reductions of the shaded mylar charts of bottom current extremes are shown in figures 4 through 38, part C. It is apparent that current extremes occur quixotically with depth; thus, no fixed depth choice for the aqueduct will be free of bottom current extremes. In fact, the aqueduct itself, representing a rise and/or promontory effect to passing water, may cause a moderate current to become extreme. It is also apparent that the inadequacy of generalization at this time requires that the figures be used only for the grossest reconnaissance and not for specific planning.

Extreme bottom current particle velocity at CUARO standard depths for the California coast for several levels of confidence is in table 6.

TSUNAMI SURGE ON THE BOTTOM

Table 7 gives a sample of the horizontal water particle velocity caused by tsunamis. Reductions of the shaded mylar charts of tsunami-generated bottom velocities are given as figures 4 through 38, part D.

From both the table and figures, it is apparent that tsunami bottom effects are most serious in shallow water and in the north. The velocities at San Diego are about one-third the velocities at Crescent City for all depths. Also, the velocities at a 200-m depth are about one-fifth to one-sixth the velocities at 20 m for all latitudes. However, it should be noted that because of the long wave length the tsunami does not recognize the nuances of local features, treating the coastline more as an average phenomenon. An aqueduct following a 200-m contour, for example, might still be susceptible to tsunami damage if a local quirk brought the 200-m contour close to the shoreline for only a short distance.

Table 4. Greatest extreme bottom surge velocity (cm/sec)
likely to be observed over a century.

Part A.

Latitude 42°00' Longitude 125°00'

Approximate location: Crescent City

Confidence Bound (Probability)	Depth, m			
	200	100	50	20
0.80	15.0	49.1	94.3	253.9
0.85	16.2	50.9	96.6	256.5
0.90	17.8	53.4	99.8	260.0
0.95	20.4	57.6	105.1	265.7
0.96	21.3	58.9	106.8	267.6
0.97	22.5	60.6	108.9	269.8
0.98	24.1	62.9	111.9	273.1
0.99	27.0	66.8	117.0	278.5
0.995	29.8	70.7	122.0	283.5
0.999	36.6	79.7	133.5	294.9

Part B.

Latitude 39°36' Longitude 124°30'

Approximate location: Noya Canyon

Confidence Bound (Probability)	Depth, m			
	200	100	50	20
0.80	10.2	44.4	94.8	181.7
0.85	11.0	46.3	97.4	185.7
0.90	12.2	48.9	101.0	260.6
0.95	14.3	53.2	106.9	266.3
0.96	15.0	54.6	108.8	268.1
0.97	15.9	56.4	111.3	270.4
0.98	17.3	58.9	114.7	273.6
0.99	19.7	63.1	120.5	278.9
0.995	22.2	67.4	126.2	284.1
0.999	28.4	77.3	139.6	295.9

Table 4. Continued.

Part C.

Latitude 37° 36' Longitude 123° 30'

Approximate location: San Francisco

Confidence Bound (Probability)	Depth, m			
	200	100	50	20
0.80	9.6	46.0	101.4	261.1
0.85	10.5	48.2	104.7	264.1
0.90	11.7	51.2	109.3	268.3
0.95	13.9	56.4	116.9	275.1
0.96	14.7	58.1	119.3	277.3
0.97	15.7	60.2	122.4	280.0
0.98	17.9	63.2	126.8	283.8
0.99	19.7	68.5	134.2	290.2
0.995	22.5	73.7	141.7	296.4
0.999	29.5	86.1	159.1	310.6

Part D.

Latitude 34° 22' Longitude 120° 30'

Approximate location: Pt. Conception

Confidence Bound (Probability)	Depth, m			
	200	100	50	20
0.80	13.4	38.1	73.0	152.4
0.85	14.1	39.1	74.4	154.8
0.90	15.1	40.4	76.2	158.3
0.95	16.8	42.5	79.2	241.3
0.96	17.4	43.2	80.2	242.3
0.97	18.0	44.0	81.4	243.4
0.98	19.0	45.2	83.1	245.0
0.99	20.6	47.2	86.1	247.7
0.995	22.2	49.2	89.0	250.3
0.999	25.7	53.7	95.9	256.5

Table 4. Continued.

Part E.

Latitude 34° 22' Longitude 120° 05'

Approximate location: East of Pt. Conception

Confidence Bound (Probability)	Depth, m			
	200	100	50	20
0.80	14.7	34.4	63.1	129.9
0.85	15.5	35.4	64.6	132.7
0.90	16.6	36.8	66.6	136.5
0.95	18.4	39.1	70.0	224.6
0.96	19.0	39.8	71.1	225.7
0.97	19.7	40.7	72.5	227.1
0.98	20.7	42.0	74.4	229.0
0.99	22.3	44.1	77.7	232.3
0.995	23.9	46.2	81.1	235.5
0.999	27.4	51.1	88.8	242.7

Part F.

Latitude 34° 17' Longitude 119° 45'

Approximate location: Santa Barbara

Confidence Bound (Probability)	Depth, m			
	200	100	50	20
0.80	8.1	26.7	52.9	111.3
0.85	8.6	27.3	53.8	112.8
0.90	9.3	28.2	54.9	114.9
0.95	10.5	29.7	56.8	118.5
0.96	10.9	30.2	57.5	119.6
0.97	11.4	30.7	58.2	121.1
0.98	12.0	31.5	59.3	123.1
0.99	13.2	32.9	61.2	126.6
0.995	14.3	34.2	63.0	129.9
0.999	16.7	37.2	67.3	138.0

Table 4. Continued.

Part G.

Latitude 34° 10' Longitude 120° 20'

Approximate location: San Miguel Island

Confidence Bound (Probability)	Depth, m			
	200	100	50	20
0.80	9.0	30.0	59.8	125.8
0.85	9.6	30.9	60.9	128.0
0.90	10.5	32.1	62.5	130.9
0.95	12.0	34.0	65.2	135.9
0.96	12.4	34.6	66.0	137.5
0.97	13.0	35.4	67.1	139.6
0.98	13.8	36.4	68.6	142.5
0.99	15.3	38.2	71.2	147.4
0.995	16.6	40.0	73.8	152.2
0.999	19.8	44.1	79.9	239.0

Part H.

Latitude 34° 05' Longitude 119° 40'

Approximate location: Santa Cruz Island

Confidence Bound (Probability)	Depth, m			
	200	100	50	20
0.80	10.9	38.3	77.2	163.2
0.85	11.6	39.3	78.7	165.9
0.90	12.5	40.7	80.6	169.6
0.95	14.1	43.1	83.9	175.7
0.96	14.6	43.8	84.9	250.7
0.97	15.3	44.7	86.3	252.2
0.98	16.2	46.0	88.2	254.2
0.99	17.8	48.3	91.4	257.6
0.995	19.5	50.5	94.6	260.8
0.999	23.3	55.5	102.2	267.8

Table 5. Greatest extreme wave periods, lengths, and heights likely to be observed over a century.

Part A. Latitude 40°00' Longitude 125°00' Approximate location: Crescent City											
Confidence Bound (Probability)	Period, sec	Deep Sea Height, m	200-m Depth		100-m Depth		50-m Depth		20-m Depth		
			Length, m	Height, m	Length, m	Height, m	Length, m	Height, m	Length, m	Height, m	
0.80	17.9	10.8	495	10.8	445	10.8	355	10.8	242	10.8	
0.85	18.2	11.0	508	11.0	455	11.0	361	11.0	248	11.0	
0.90	18.5	11.2	528	11.2	468	11.2	370	11.2	257	11.2	
0.95	19.1	11.7	559	11.7	490	11.7	385	11.7	272	11.7	
0.96	19.3	11.8	569	11.8	497	11.8	389	11.8	277	11.8	
0.97	19.6	12.0	582	12.0	506	12.0	395	12.0	283	12.0	
0.98	19.9	12.2	601	12.2	519	12.2	404	12.2	292	12.2	
0.99	20.5	12.6	632	12.6	540	12.6	418	12.6	308	12.6	
0.995	21.9	13.0	663	13.0	561	13.0	432	13.0	323	13.0	
0.999	22.4	14.0	736	14.0	609	14.0	464	14.0	361	14.0	

Table 5. Continued.

Part B.		Longitude 124° 30'								
Latitude 39° 36'		Approximate location: Noya Canyon								
Confidence Bound (Probability)	Period, sec	Deep Sea Height, m	200-m Depth		100-m Depth		50-m Depth		20-m Depth	
			Length, m	Height, m	Length, m	Height, m	Length, m	Height, m	Length, m	Height, m
0.80	16.1	11.5	405	11.5	378	11.5	311	11.5	214	11.5
0.85	16.3	11.8	415	11.8	386	11.8	316	11.8	217	11.8
0.90	16.6	12.1	428	12.1	396	12.1	323	12.1	223	12.1
0.95	17.0	12.6	450	12.6	412	12.6	334	12.6	234	12.6
0.96	17.2	12.8	457	12.8	418	12.8	337	12.8	238	12.8
0.97	17.4	13.0	466	13.0	424	13.0	342	13.0	243	13.0
0.98	17.6	13.3	479	13.3	434	13.3	348	13.3	249	13.3
0.99	18.0	13.8	502	13.8	450	13.8	358	13.8	261	13.8
0.995	18.5	14.2	524	14.2	466	14.2	369	14.2	273	14.2
0.999	19.5	15.4	577	15.4	502	15.4	393	15.4	300	15.4

Table 5. Continued.

Part C. Latitude 37° 36' Longitude 123° 30' Approximate location: San Francisco										
Confidence Bound (Probability)	Period, sec	Deep Sea Height, m	200-m Depth		100-m Depth		50-m Depth		20-m Depth	
			Length, m	Height, m	Length, m	Height, m	Length, m	Height, m	Length, m	Height, m
0.80	15.7	12.6	384	12.6	362	12.6	300	12.6	208	12.6
0.85	15.9	12.9	393	12.9	369	12.9	305	12.9	213	12.9
0.90	16.1	13.4	405	13.4	378	13.4	311	13.4	220	13.4
0.95	16.6	14.0	425	14.0	394	14.0	321	14.0	232	14.0
0.96	16.7	14.2	432	14.2	399	14.2	325	14.2	235	14.2
0.97	16.8	14.5	440	14.5	405	14.5	329	14.5	240	14.5
0.98	17.1	14.9	452	14.9	414	14.9	335	14.9	247	14.9
0.99	17.5	15.6	473	15.6	429	15.6	345	15.6	258	15.6
0.995	17.9	16.2	494	16.2	444	16.2	354	16.2	270	16.2
0.999	18.8	17.8	542	17.8	479	17.8	377	17.8	298	17.8

Table 5. Continued.

Part D. Latitude 34° 22' Longitude 120° 30' Approximate location: Pt. Conception										
Confidence Bound (Probability)	Period, sec	Deep Sea Height, m	200-m Depth		100-m Depth		50-m Depth		20-m Depth	
			Length, m	Height, m	Length, m	Height, m	Length, m	Height, m	Length, m	Height, m
0.80	18.5	8.8	527	8.5	468	8.0	370	8.2	249	9.4
0.85	18.8	8.8	540	8.6	477	8.1	376	8.3	253	9.6
0.90	19.1	8.9	560	8.6	491	8.2	385	8.4	258	9.8
0.95	19.8	9.1	592	8.7	513	8.3	400	8.7	268	14.9
0.96	19.9	9.2	602	8.8	520	8.4	404	8.7	273	15.0
0.97	20.2	9.2	615	8.8	528	8.4	410	8.8	278	15.2
0.98	20.5	9.3	634	8.9	541	8.5	418	9.0	286	15.5
0.99	21.1	9.5	664	9.0	562	8.7	432	9.2	299	15.9
0.995	21.7	9.6	696	9.1	582	8.8	446	9.4	313	16.3
0.999	23.0	10.0	768	9.3	630	9.2	478	9.9	346	17.3

Table 5. Continued.

Part E. Latitude 34° 22' Longitude 120° 05' Approximate location: East of Pt. Conception										
Confidence Bound (Probability)	Period, sec	Deep Sea Height, m	200-m Depth		100-m Depth		50-m Depth		20-m Depth	
			Length, m	Height, m	Length, m	Height, m	Length, m	Height, m	Length, m	Height, m
0.80	20.7	7.0	644	6.7	548	6.4	423	6.8	281	7.9
0.85	21.2	7.1	667	6.7	563	6.5	433	6.9	287	8.1
0.90	21.7	7.2	698	6.8	584	6.6	447	7.0	296	8.3
0.95	22.7	7.4	751	6.9	619	6.8	470	7.3	313	13.7
0.96	23.0	7.4	767	6.9	630	6.8	478	7.4	319	13.8
0.97	23.4	7.5	789	6.9	644	6.9	487	7.5	328	14.0
0.98	24.0	7.6	818	7.0	663	7.0	500	7.6	341	14.3
0.99	24.9	7.7	868	7.1	696	7.2	522	7.9	362	14.8
0.995	25.9	7.9	918	7.2	729	7.4	544	8.2	383	15.3
0.999	28.1	8.3	1031	7.6	804	7.9	595	8.8	435	16.4

Table 5. Continued.

Part F. Latitude 34° 17' Longitude 119° 45' Approximate location: Santa Barbara											
Confidence Bound (Probability)	Period, sec	Deep Sea Height, m	200-m Depth		100-m Depth		50-m Depth		20-m Depth		
			Length, m	Height, m	Length, m	Height, m	Length, m	Height, m	Length, m	Height, m	
0.80	17.4	6.6	470	6.5	427	6.1	343	6.2	233	6.2	7.0
0.85	17.7	6.7	483	6.5	437	6.1	350	6.2	237	6.2	7.1
0.90	18.0	6.7	501	6.6	449	6.2	358	6.3	242	6.3	7.2
0.95	18.6	6.8	530	6.6	470	6.2	371	6.4	250	6.4	7.3
0.96	18.8	6.8	539	6.6	477	6.3	376	6.4	253	6.4	7.4
0.97	19.0	6.9	551	6.6	485	6.3	381	6.5	256	6.5	7.5
0.98	19.3	6.9	568	6.7	497	6.3	389	6.6	261	6.6	7.6
0.99	19.9	7.0	598	6.7	517	6.4	402	6.7	269	6.7	7.8
0.995	20.4	7.1	627	6.8	536	6.5	415	6.8	276	6.8	8.0
0.999	21.7	7.3	694	6.9	581	6.7	445	7.1	295	7.1	8.2

Table 5. Continued.

Part G. Latitude 34° 10' Longitude 120° 20' Approximate location: San Miguel Island											
Confidence Bound (Probability)	Period, sec	Deep Sea Height, m	200-m Depth		100-m Depth		50-m Depth		20-m Depth		Height, m
			Length, m	Height, m	Length, m	Height, m	Length, m	Height, m	Length, m	Height, m	
0.80	17.4	7.5	466	7.4	425	6.9	342	7.0	232	7.9	7.9
0.85	17.6	7.6	479	7.4	434	7.0	348	7.0	236	8.0	8.0
0.90	18.0	7.7	497	7.5	447	7.0	356	7.2	241	8.2	8.2
0.95	18.5	7.8	527	7.6	468	7.2	370	7.3	249	8.4	8.4
0.96	18.7	7.9	536	7.6	474	7.2	374	7.4	252	8.5	8.5
0.97	18.9	7.9	548	7.7	483	7.3	380	7.5	255	8.6	8.6
0.98	19.3	8.0	565	7.7	495	7.3	388	7.6	260	8.8	8.8
0.99	19.8	8.2	595	7.8	515	7.5	401	7.8	268	9.0	9.0
0.995	20.4	8.3	624	7.9	534	7.6	414	8.0	276	9.3	9.3
0.999	21.6	8.7	692	8.2	580	8.0	444	8.4	303	15.0	15.0

Table 5. Continued.

Part H. Latitude 34°05' Longitude 119°40' Approximate location: Santa Cruz Island											
Confidence Bound (Probability)	Period, sec	Deep Sea Height, m	200-m Depth		100-m Depth		50-m Depth		20-m Depth		
			Length, m	Height, m	Length, m	Height, m	Length, m	Height, m	Length, m	Height, m	
0.80	17.0	9.8	449	9.7	412	9.1	333	9.1	227	10.3	
0.85	17.2	9.9	460	9.8	419	9.2	338	9.2	230	10.4	
0.90	17.5	10.1	473	9.9	430	9.3	345	9.4	234	10.6	
0.95	18.0	10.3	497	10.0	447	9.4	356	9.6	241	11.0	
0.96	18.1	10.4	505	10.1	452	9.5	360	9.7	243	15.6	
0.97	18.3	10.4	515	10.2	459	9.6	364	9.8	247	15.8	
0.98	18.6	10.6	529	10.3	469	9.7	371	9.9	253	16.1	
0.99	19.0	10.8	552	10.4	485	9.9	382	10.2	264	16.5	
0.995	19.5	11.0	576	10.6	502	10.0	392	10.4	275	17.0	
0.999	20.5	11.5	631	10.9	539	10.5	417	11.0	300	18.0	

Table 6. Greatest extreme bottom current particle velocity (cm/sec) likely to be observed over a century along the California coast.

Confidence Bound (Probability)	Depth, m			
	200	100	50	20
0.80	336.6	328.9	249.2	279.9
0.85	341.4	333.5	254.0	284.8
0.90	347.9	339.8	260.5	291.5
0.95	358.7	350.3	271.3	302.7
0.96	362.2	353.7	274.8	306.3
0.97	366.6	357.9	279.1	310.8
0.98	372.8	363.9	285.3	317.2
0.99	383.3	374.1	295.8	328.0
0.995	393.8	384.3	306.3	338.8
0.999	418.1	407.8	330.5	363.9

Table 7. A sample of horizontal water particle velocity (cm/sec) caused by an extreme tsunami as predicted by solitary wave theory for six depths at ten latitudes.

Latitude, deg	Depth, m					
	200	150	100	75	50	20
42	32.78	40.64	55.13	86.36	92.71	184.31
41	30.43	37.75	51.17	63.50	86.06	171.11
40	28.09	34.85	47.24	58.61	79.44	157.95
39	25.75	31.95	43.30	53.73	72.82	144.78
38	23.41	29.04	39.36	48.84	66.20	131.62
37	21.07	26.14	35.43	43.96	59.58	118.46
36	18.72	23.23	31.49	39.07	52.96	105.50
35	16.38	20.33	29.31	34.19	46.34	92.13
34	14.04	17.43	23.62	29.31	39.72	78.97
33	11.70	14.52	19.68	24.42	33.10	65.81

CONSTRUCTION VARIABLES

GENERAL APPROACH TO CONSTRUCTION VARIABLES

The question to be answered for the purpose of construction and maintenance of the aqueduct is

“What are the average conditions to which we must adjust for day-to-day construction and maintenance operations and with what tolerance in both time and conditions?”

(For example, what is average, how often may we expect great deviations from the average, and how should we plan for great deviations in day-to-day operations?) To answer these questions, we amalgamated all reliable data for each location, adjusted the data to be compatible for different sampling conditions and gear, and computed summarizing statistics. Since conditions usually vary from one time of year to another, data were separated by season, the “seasons” being chosen as winter (November through April) and summer (May through October). Although the boundary dates are slightly late for surface events, there exists a lag in the physical phenomena reaching the bottom so that the boundary dates are appropriate or slightly early for 200-m depths. In addition, the boundary dates vary yearly with no information concerning the actual dates, and we must combine these data from different years.

The amalgamation by location was also arbitrary. Station locations used by different investigators for different years varied slightly. Data were combined in a way which was a compromise between grouping stations to provide an adequate statistical sample and keeping the geographical area small enough to retain some homogeneity of physical parameters.

The variables investigated were density at the surface, 50 m, and 200 m, surface waves, bottom surge, surface and bottom currents, and light transmittance, each for summer and winter seasons (except bottom currents). The mean and standard deviations were calculated for various depths as indicated for each case. The mean is a measure of average conditions. In a symmetric or nearly symmetric probability distribution, e.g., density, the mean is similar to the bulk of observations and any other measure of average would give approximately the same value. In a skewed distribution, e.g., wave height, the mean is “pulled upward” by the occasional large values, e.g., during storms, and will be slightly larger than the bulk or mode of observations. The standard deviation is a measure of how frequently and how far a measure on a variate deviates from its mean. If events are measured at sufficiently long intervals, e.g., several days to avoid time-dependent correlations as in storms, they approach the assumption that one value is as likely to occur in a sampling as any other. Under such an assumption, an interval given by endpoints [mean – one standard deviation, mean + one standard deviation] is often considered to contain about 68 percent of the possible observations. This consideration is true only for the normal distribution; however, most distributions in physical oceanography are not so deviant from the normal that they are excessively in error. As a “rule of thumb” one may say, “About two-thirds of the time, the variable under consideration will fall in the interval given by $\text{mean} \pm \text{standard deviation}$.” In all cases for construction variables (figure 40), the diagram for a location shows the mean as a cross bar on a scale with a strip of black extending out one standard deviation in either direction. The observations used in the computations are indicated by dots at the location

where taken, the number of dots in an enclosure connected to the graph (representing the sample size), or by a dotted circle (the size of the circle representing the sample size where the dots are too concentrated to show).

DENSITY

The statistics of σ_t were calculated for three depths: surface, 50 m, and 200 m. Data taken within 5 m of depth of the standard depth were included. Because almost no data were available at the bottom itself, *i.e.*, a 50-m σ_t in 50 m of water, it was assumed that the z -m σ_t , where the depth was greater than z , was the same as the bottom σ_t at a z -m depth. Some violation of this assumption is known to exist from upwelling waters, but most consultants felt that the bulk of the upwelling was farther to sea than the CUA contour strip so that the assumption was not violated. Further investigation should be made.

Figure 40, parts A and B, show surface σ_t for winter and summer, respectively. Winter surface σ_t is higher between San Francisco and Monterey than for the rest of the coast. The greatest coastal within-season variation is in the vicinity of San Francisco. Summer surface σ_t is always greater than winter σ_t . It is largest from Mendocino to San Francisco with a high patch off Big Sur, but its variability is greatest off Pt. Arguello and in the Santa Barbara Channel. The seasonal density difference is probably caused by the seasonal difference in the Davidson countercurrent.

Parts C and D show σ_t for 50-m depths for winter and summer, respectively. Densities of 50 m are greater than surface densities for both seasons over the entire coast and exhibit less variability. The north-to-south differences are much less than for surface densities. Summer densities are again greater than winter densities and show a smaller variability.

Part E and F show σ_t for 200-m depths for winter and summer, respectively. The scarcity of data is obvious. Densities of 200 m average larger than for all shallower depths, but the variability is quite small, indicating a stable environment.

WAVES AND BOTTOM SURGE

Averages and standard deviations of surface wave periods, lengths, and amplitudes were computed for winter and summer for CUARO standard depths (table 8).

Parts G and H of figure 40 show surface wave amplitudes by season. Winter waves are highest near Mendocino, Monterey, and rounding Pt. Conception; the greatest variability is in the same areas and San Francisco. Summer surface waves, smaller and less variable than winter waves, are most variable in the Santa Barbara Channel. For both seasons, wave amplitude and variability do not vary greatly with distance from shore. It is apparent that summer is a much more stable season for construction than is winter.

Parts I and J show the mean, standard deviation, and sample size for bottom surge particle velocity in cm/sec for winter and summer, respectively. Bottom surge is clearly negligible at 200 m for all latitudes and both seasons. For other depths, surge uniformly increases as depth decreases, is greater in winter than summer, is more variable in winter than summer, and shows a larger gradient with depth in winter than summer.

Table 8. Averages and standard deviations of periods, lengths, and amplitudes for surface waves off the California coast.*

Season	Location		Depth, m	Period, sec	Length, m	Amplitude, m
	Latitude, deg	Longitude, deg				
Winter	42.00	125.00	20	12.41 (6.37)	157.8 (91.2)	1.96 (1.69)
			50	12.41 (6.37)	214.1 (147.9)	1.91 (1.64)
			100	12.41 (6.37)	243.0 (208.8)	2.00 (1.72)
			200	12.41 (6.37)	253.8 (285.3)	2.04 (1.76)
Summer	42.00	125.00	20	11.99 (2.80)	151.6 (42.8)	1.10 (0.91)
			50	11.99 (2.80)	203.9 (72.8)	1.07 (0.86)
			100	11.99 (2.80)	228.8 (98.3)	1.11 (0.89)
			200	11.99 (2.80)	236.0 (110.1)	1.14 (0.92)
Winter	39.60	124.50	20	12.29 (2.82)	156.3 (42.9)	2.13 (1.72)
			50	12.29 (2.82)	211.7 (73.1)	2.08 (1.67)
			100	12.29 (2.82)	239.1 (99.8)	2.17 (1.75)
			200	12.29 (2.82)	247.4 (113.0)	2.21 (1.98)
Summer	39.60	124.50	20	12.31 (2.84)	156.6 (43.2)	1.07 (0.89)
			50	12.31 (2.84)	212.3 (73.6)	1.03 (0.83)
			100	12.31 (2.84)	240.0 (100.4)	1.07 (0.87)
			200	12.31 (2.84)	248.5 (113.9)	1.10 (0.90)
Winter	37.00	123.50	20	12.41 (2.98)	158.0 (45.3)	1.93 (1.59)
			50	12.41 (2.98)	214.7 (77.1)	1.88 (1.54)
			100	12.41 (2.98)	243.8 (105.2)	1.96 (1.61)
			200	12.41 (2.98)	253.2 (119.7)	2.00 (1.65)
	37.60	123.50	20	12.31 (2.92)	156.6 (44.5)	0.97 (0.73)
			50	12.31 (2.92)	212.4 (75.7)	0.94 (0.69)
			100	12.31 (2.92)	240.5 (103.0)	0.98 (0.71)
			200	12.31 (2.92)	249.3 (116.8)	1.00 (0.74)

Table 8. Continued.

Season	Location		Depth, m	Period, sec	Length, m	Amplitude, m
	Latitude, deg	Longitude, deg				
Winter	36.37	121.56	20	13.47 (2.04)	174.4 (31.0)	1.27 (0.84)
			50	13.47 (2.04)	242.8 (53.1)	1.27 (0.84)
			100	13.47 (2.04)	279.5 (73.2)	1.27 (0.84)
			200	13.47 (2.04)	289.0 (82.1)	1.27 (0.84)
Winter	36.37	121.52	20	13.50 (2.03)	174.9 (30.8)	2.01 (1.07)
			50	13.50 (2.03)	243.7 (52.7)	2.01 (1.07)
			100	13.50 (2.03)	280.7 (72.7)	2.01 (1.07)
			200	13.50 (2.03)	290.3 (81.5)	2.01 (1.07)
Winter	35.50	122.00	20	12.71 (3.15)	162.6 (47.8)	1.49 (1.20)
			50	12.71 (3.15)	222.7 (80.9)	1.43 (1.14)
			100	12.71 (3.15)	255.2 (110.8)	1.56 (1.31)
			200	12.71 (3.15)	266.6 (127.2)	1.62 (1.35)
Summer	35.50	122.00	20	12.49 (3.30)	159.1 (49.9)	0.88 (0.62)
			50	12.49 (3.30)	216.8 (84.3)	0.79 (0.60)
			100	12.49 (3.30)	247.8 (115.1)	0.94 (0.64)
			200	12.49 (3.30)	259.0 (132.3)	0.96 (0.67)
Winter	34.50	123.50	20	12.67 (3.07)	161.9 (46.7)	1.44 (0.97)
			50	12.67 (3.07)	221.3 (79.4)	1.39 (0.91)
			100	12.67 (3.07)	253.0 (109.4)	1.49 (0.95)
			200	12.67 (3.07)	264.0 (125.9)	1.48 (0.99)
Summer	34.50	123.50	20	12.40 (2.77)	158.1 (42.1)	1.33 (1.26)
			50	12.40 (2.77)	214.7 (21.9)	1.30 (1.25)
			100	12.40 (2.77)	242.9 (98.2)	1.35 (1.28)
			200	12.40 (2.77)	251.4 (111.3)	1.38 (1.30)

Table 8. Continued.

Season	Location		Depth, m	Period, sec	Length, m	Amplitude, m
	Latitude, deg	Longitude, deg				
Winter	34.22	120.30	20	9.46 (2.83)	111.9 (44.8)	1.18 (0.52)
			50	9.46 (2.83)	139.9 (71.4)	1.18 (0.52)
			100	9.46 (2.83)	149.9 (87.3)	1.18 (0.52)
			200	9.46 (2.83)	151.9 (92.4)	1.18 (0.52)
Summer	34.23	120.22	20	9.82 (0.40)	118.7 (6.5)	1.31 (0.63)
			50	9.82 (0.40)	146.8 (10.6)	1.31 (0.63)
			100	9.82 (0.40)	150.6 (12.0)	1.31 (0.63)
			200	9.82 (0.40)	150.6 (12.0)	1.31 (0.63)
Winter	34.21	120.18	20	9.77 (0.44)	118.0 (7.0)	2.42 (0.94)
			50	9.77 (0.44)	145.5 (11.4)	2.42 (0.94)
			100	9.77 (0.44)	149.1 (13.0)	2.42 (0.94)
			200	9.77 (0.44)	149.1 (13.0)	2.42 (0.94)
Summer	34.21	120.18	20	9.67 (0.48)	116.3 (17.8)	1.90 (0.76)
			50	9.67 (0.48)	142.9 (12.6)	1.90 (0.76)
			100	9.67 (0.48)	146.1 (14.3)	1.90 (0.76)
			200	9.67 (0.48)	146.1 (14.3)	1.90 (0.76)
Winter	34.21	120.17	20	10.21 (0.42)	124.9 (6.5)	2.27 (0.98)
			50	10.21 (0.42)	157.2 (11.2)	2.27 (0.98)
			100	10.21 (0.42)	162.8 (13.6)	2.27 (0.98)
			200	10.21 (0.42)	162.8 (13.6)	2.27 (0.98)
Winter	34.23	120.17	20	10.69 (0.84)	132.5 (13.1)	2.30 (1.15)
			50	10.69 (0.84)	170.2 (22.4)	2.30 (1.15)
			100	10.69 (0.84)	179.2 (27.9)	2.30 (1.15)
			200	10.69 (0.84)	179.4 (28.2)	2.30 (1.15)

Table 8. Continued.

Season	Location		Depth, m	Period, sec	Length, m	Amplitude, m
	Latitude, deg	Longitude, deg				
Summer	34.23	120.17	20	10.32 (0.79)	126.7 (12.3)	1.64 (0.67)
			50	10.32 (0.79)	160.3 (21.1)	1.64 (0.67)
			100	10.32 (0.79)	167.1 (26.4)	1.64 (0.67)
			200	10.32 (0.79)	167.3 (27.7)	1.64 (0.67)
Winter	34.22	120.05	20	9.32 (2.79)	109.9 (43.8)	0.94 (0.39)
			50	9.32 (2.79)	136.7 (69.5)	0.94 (0.39)
			100	9.32 (2.79)	145.8 (84.7)	0.94 (0.39)
			200	9.32 (2.79)	147.6 (89.2)	0.94 (0.39)
Winter	34.20	120.00	20	12.94 (3.05)	166.0 (46.2)	1.38 (0.95)
			50	12.94 (3.05)	228.3 (78.8)	1.38 (0.95)
			100	12.94 (3.05)	262.3 (109.2)	1.38 (0.95)
			200	12.94 (3.05)	274.4 (126.3)	1.38 (0.95)
Summer	34.20	120.00	20	12.29 (2.69)	156.4 (40.6)	0.99 (0.55)
			50	12.29 (2.69)	211.5 (69.5)	0.99 (0.55)
			100	12.29 (2.69)	238.0 (96.5)	0.99 (0.55)
			200	12.29 (2.69)	246.0 (110.8)	0.99 (0.55)
Winter	34.10	120.20	20	9.90 (2.68)	119.0 (42.6)	1.39 (0.58)
			50	9.90 (2.68)	151.6 (66.8)	1.39 (0.58)
			100	9.90 (2.68)	162.6 (79.7)	1.39 (0.58)
			200	9.90 (2.68)	163.9 (82.2)	1.39 (0.58)
Winter	34.17	119.45	20	10.26 (3.00)	124.7 (47.2)	1.06 (0.41)
			50	10.26 (3.00)	161.3 (74.5)	1.06 (0.41)
			100	10.26 (3.00)	175.4 (91.4)	1.06 (0.41)
			200	10.26 (3.00)	178.1 (97.3)	1.06 (0.41)

Table 8. Continued.

Season	Location		Depth, m	Period, sec	Length, m	Amplitude, m
	Latitude, deg	Longitude, deg				
Winter	34.05	119.40	20	10.12 (2.45)	122.7 (38.7)	1.36 (0.44)
			50	10.12 (2.45)	156.5 (61.6)	1.36 (0.44)
			100	10.12 (2.45)	167.4 (74.9)	1.36 (0.44)
			200	10.12 (2.45)	168.9 (78.1)	1.36 (0.44)
Winter	33.50	119.50	20	12.80 (3.18)	163.8 (48.1)	1.30 (0.77)
			50	12.80 (3.18)	224.7 (81.9)	1.30 (0.77)
			100	12.80 (3.18)	259.7 (113.1)	1.30 (0.77)
			200	12.80 (3.18)	270.0 (130.9)	1.30 (0.77)
Summer	33.50	119.50	20	12.34 (2.93)	157.0 (44.5)	0.92 (0.50)
			50	12.34 (2.93)	212.8 (75.8)	0.92 (0.50)
			100	12.34 (2.93)	240.8 (104.6)	0.92 (0.50)
			200	12.34 (2.93)	250.0 (120.2)	0.92 (0.50)

* Standard deviations are in parentheses.

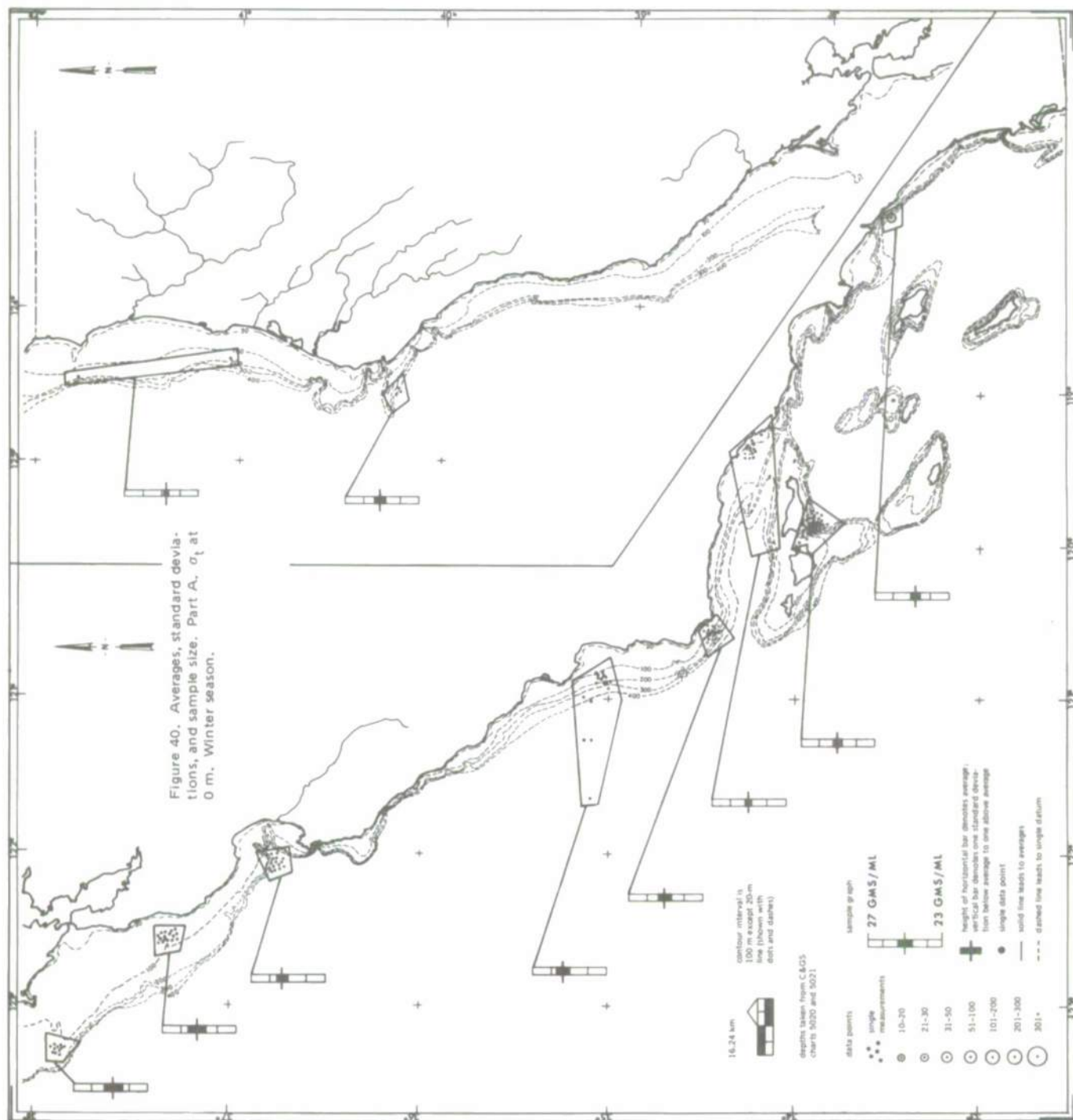
SURFACE CURRENTS

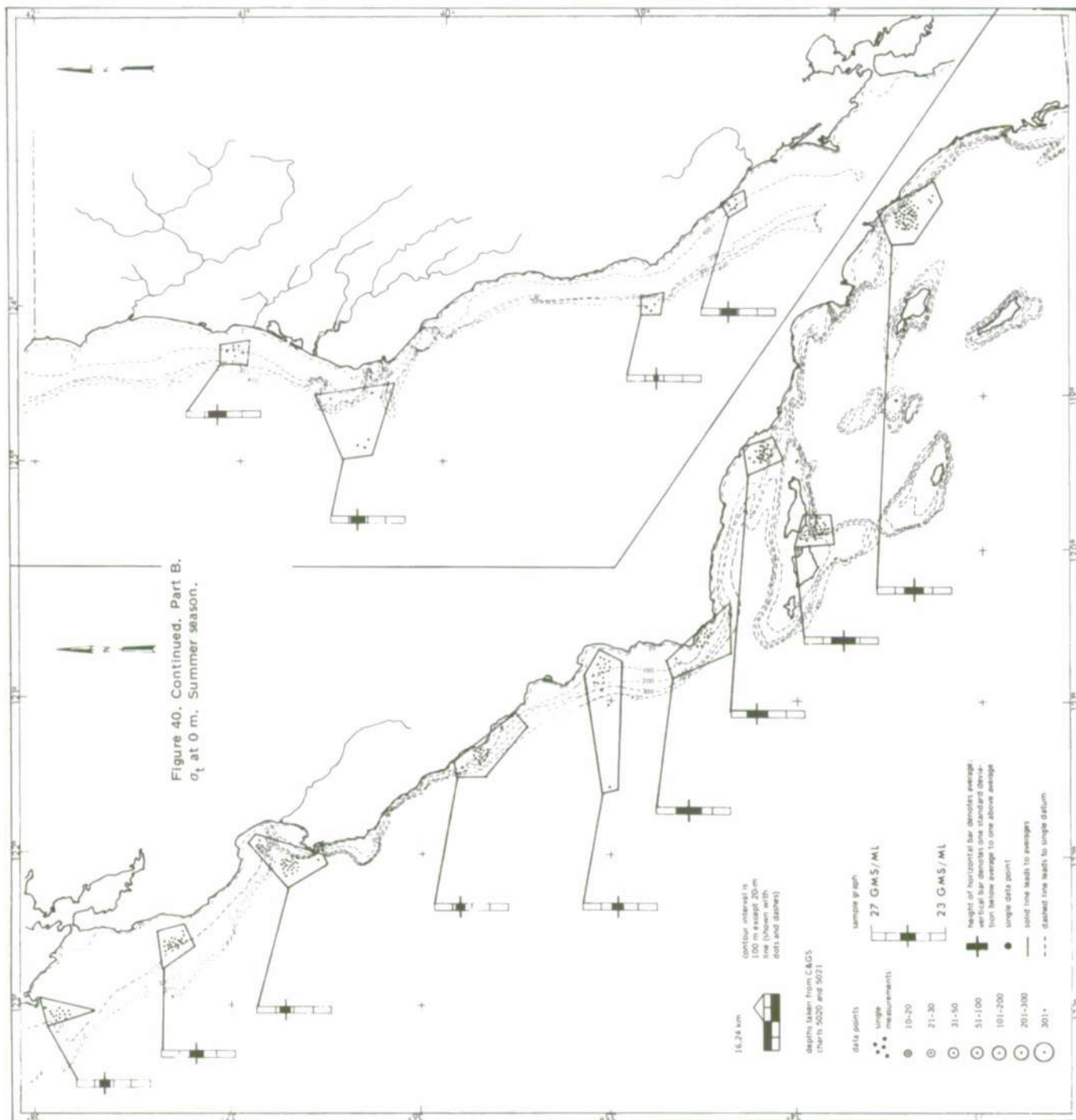
Surface currents were calculated in cm/sec from available data for 25 key locations scattered somewhat regularly by latitude for winter and summer. Means, standard deviations, and sample sizes are shown in figure 40, parts K and L. Surface currents are very strong near San Francisco for both seasons, probably because of the flow and turbulence from San Francisco Bay runoff. For the remainder of the coast, both means and variabilities varied greatly with local conditions. It is apparent that the California and Davidson currents should be considered only in terms of net flow over long periods and long distances. They should not be applied locally for a short time period for sea-surface operations, and they should probably not be considered as true permanent currents, but rather as "net migrations." When velocity direction vectors are examined, the picture of local and temporal instability is enhanced.

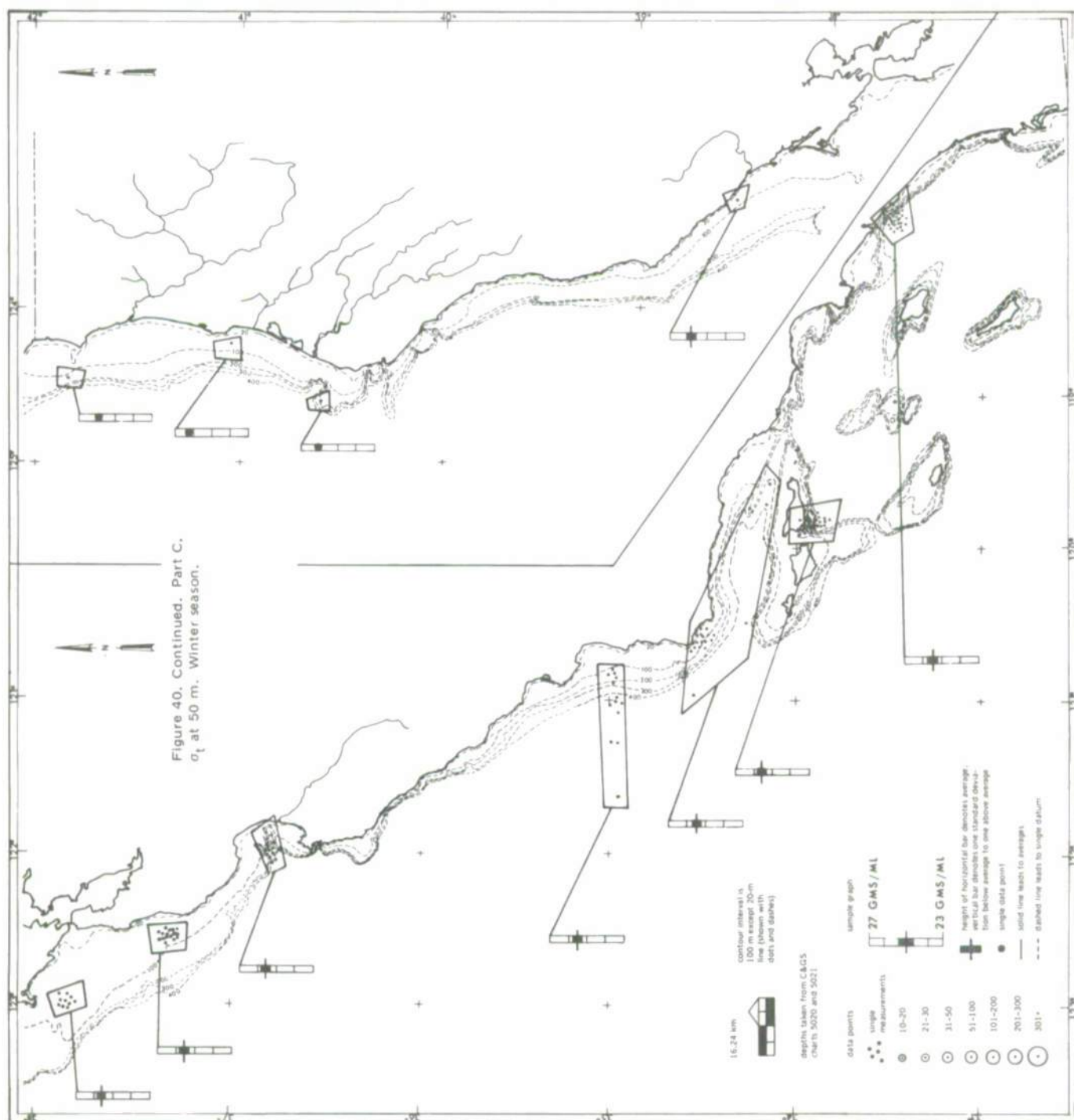
BOTTOM CURRENTS

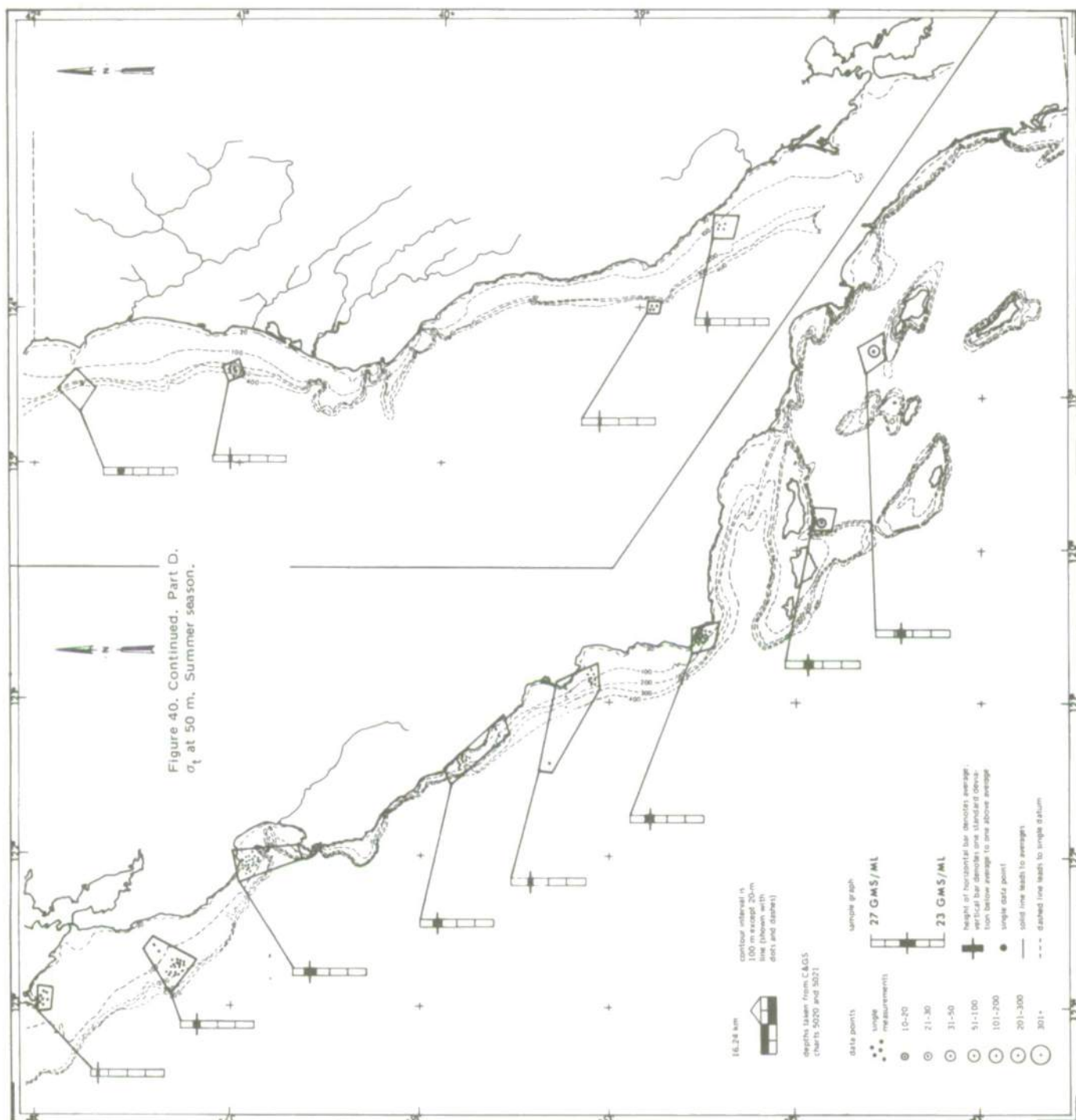
The computer simulation of bottom currents by Hansen's Hydrodynamical-Numerical Model by EPRF has been discussed. Computer outputs of bottom current were amalgamated for regions of grossly similar nature, e.g., a protected region or a promontory region, and for the means, standard deviations, and (computer output) sample sizes calculated and shown in figure 40, part M. The inputs for the model were permanent current, tides, and wind. EPRF ran the simulation with average tidal flows and a wind of 8 m/sec for all regions. Since there are no seasonal data, the results are shown in a single chart. Bottom currents for the 200-, 100-, and 50-m depths are not expected to vary noticeably with season for any climatological condition. In 20 m of water, bottom currents would vary seasonably, *i.e.*, more storms occur in winter, creating more high winds of sufficient fetch and duration which increase the seasonal average current. However, this is only an average; it does not affect construction operations at any nonstorm time. If storm periods are deleted, the 20-m bottom currents would not be greatly different from the simulated values, and construction efforts would be expected to cease during storm periods.

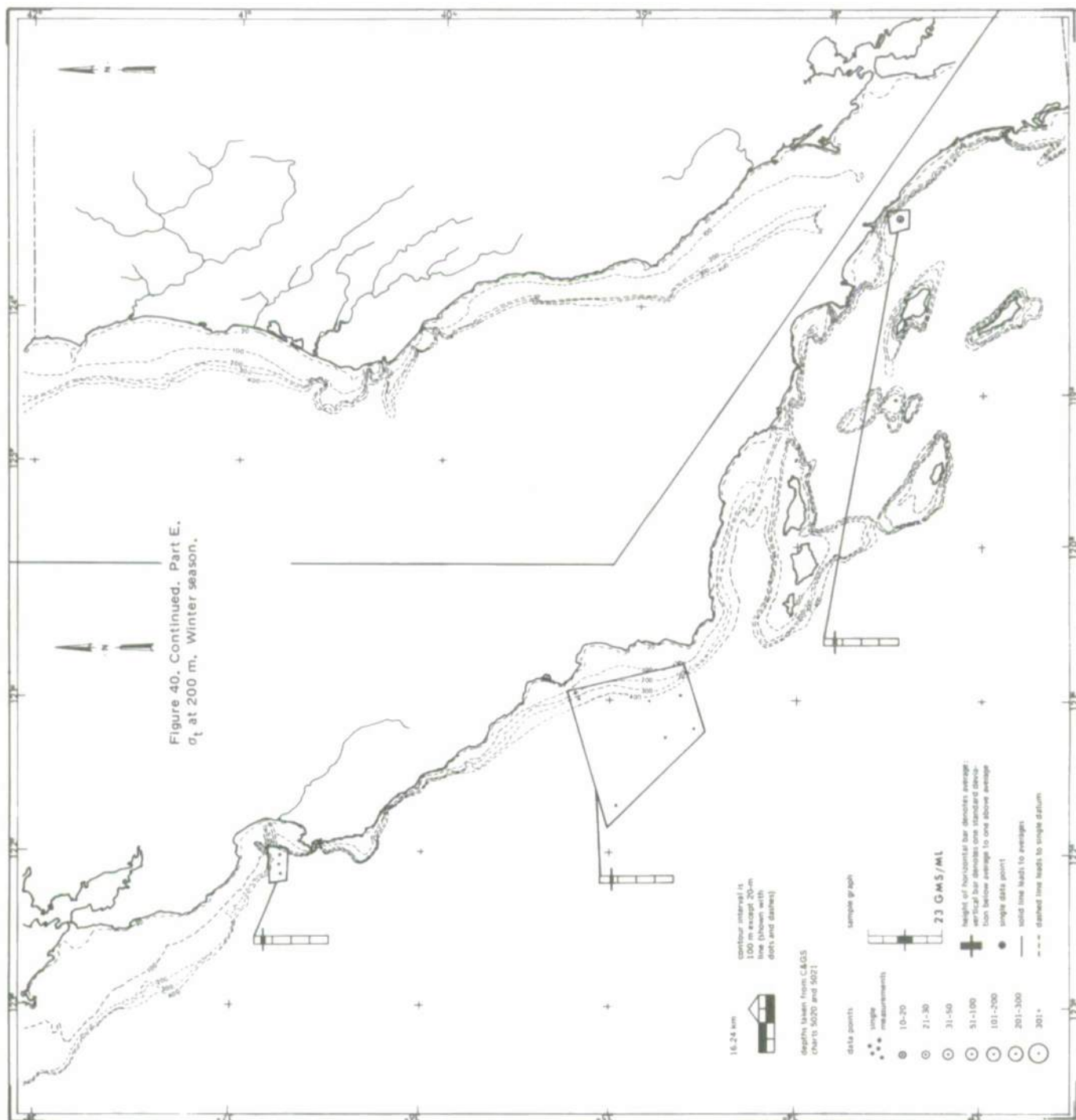
The same pattern of severe local and temporal instability observed for surface currents is also apparent in the simulated bottom currents. Bottom currents clearly pose the greatest threat to both construction and survival of the aqueduct, and it is about bottom currents that the least information is available.

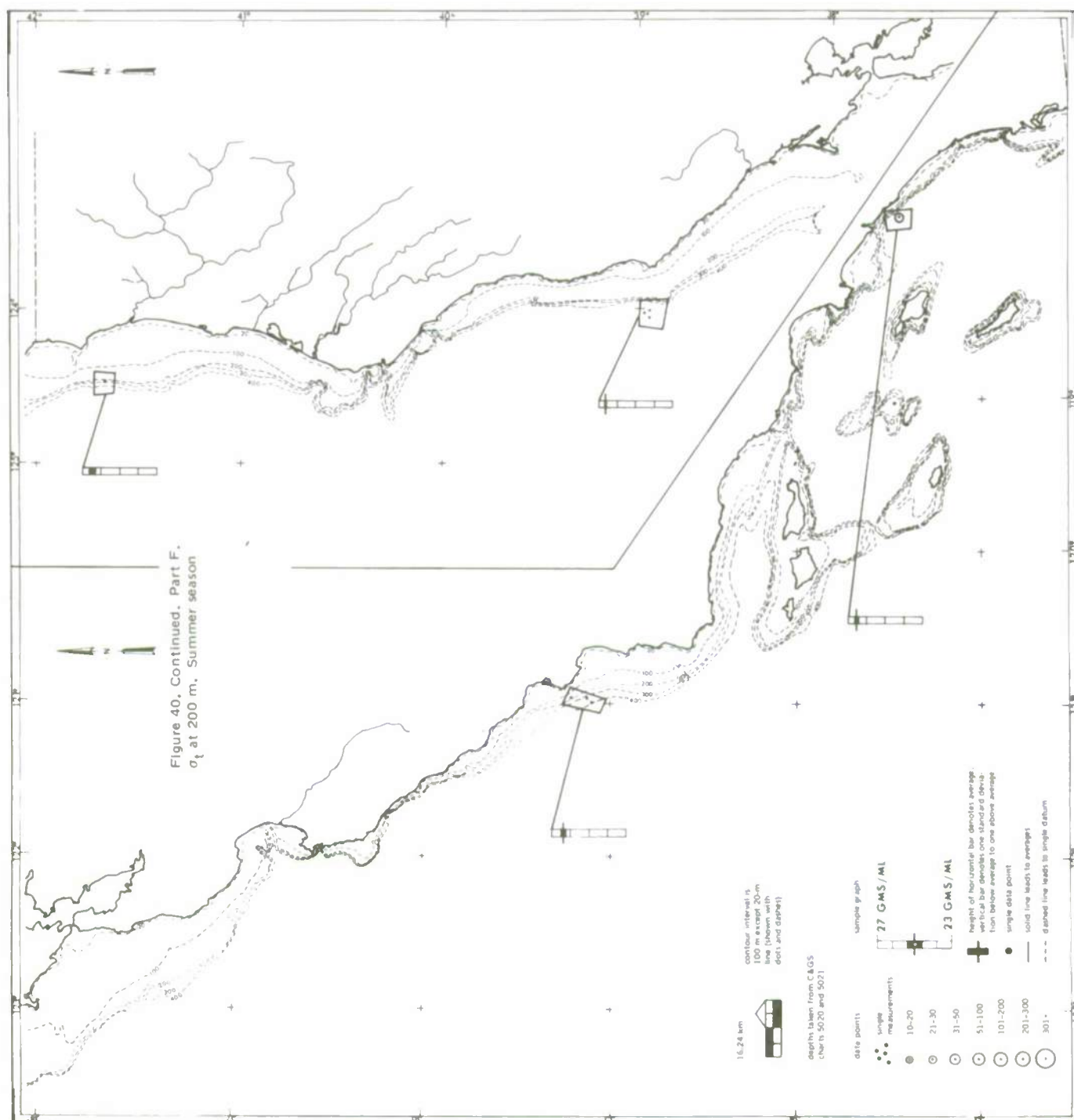


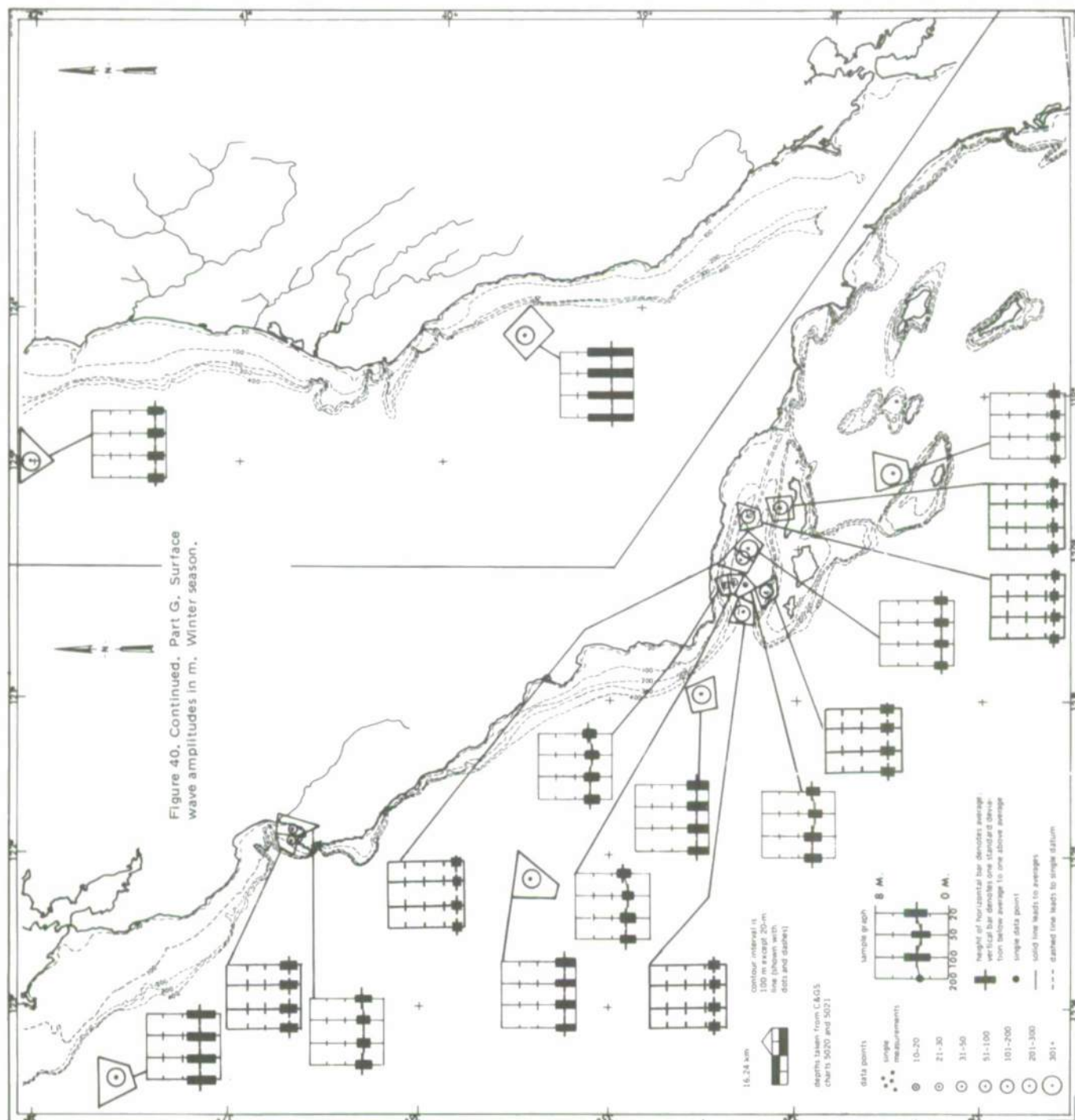


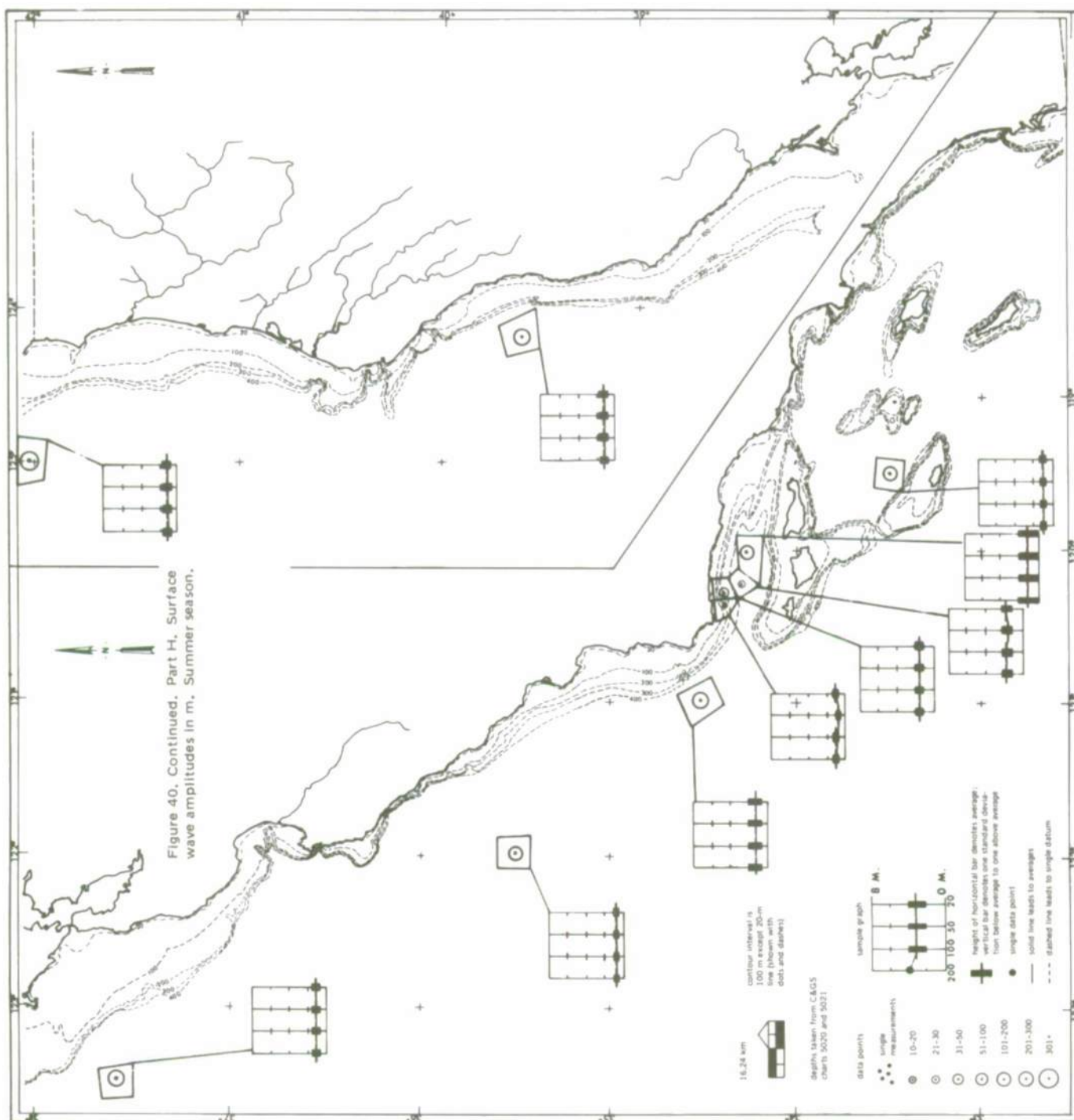


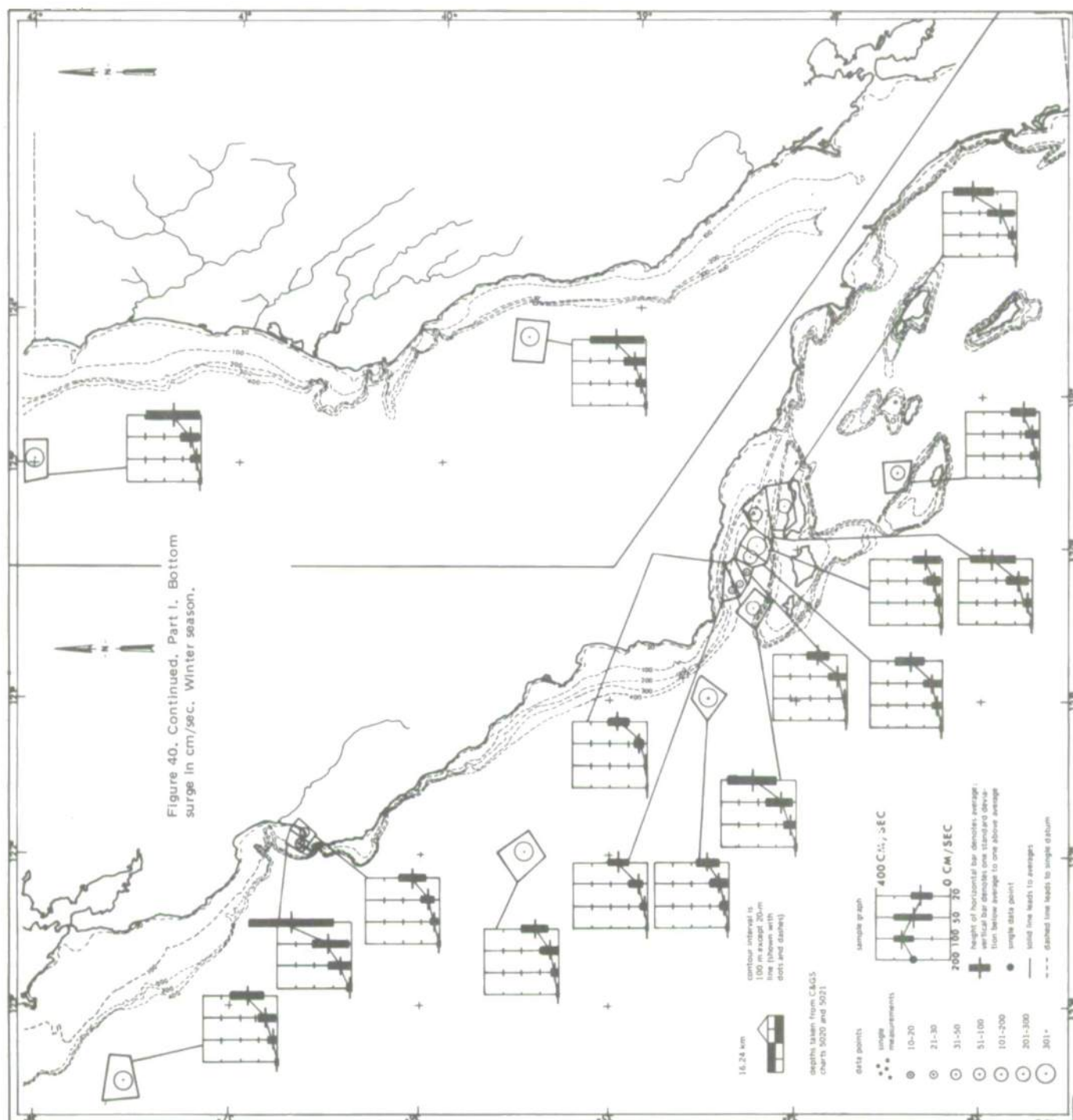


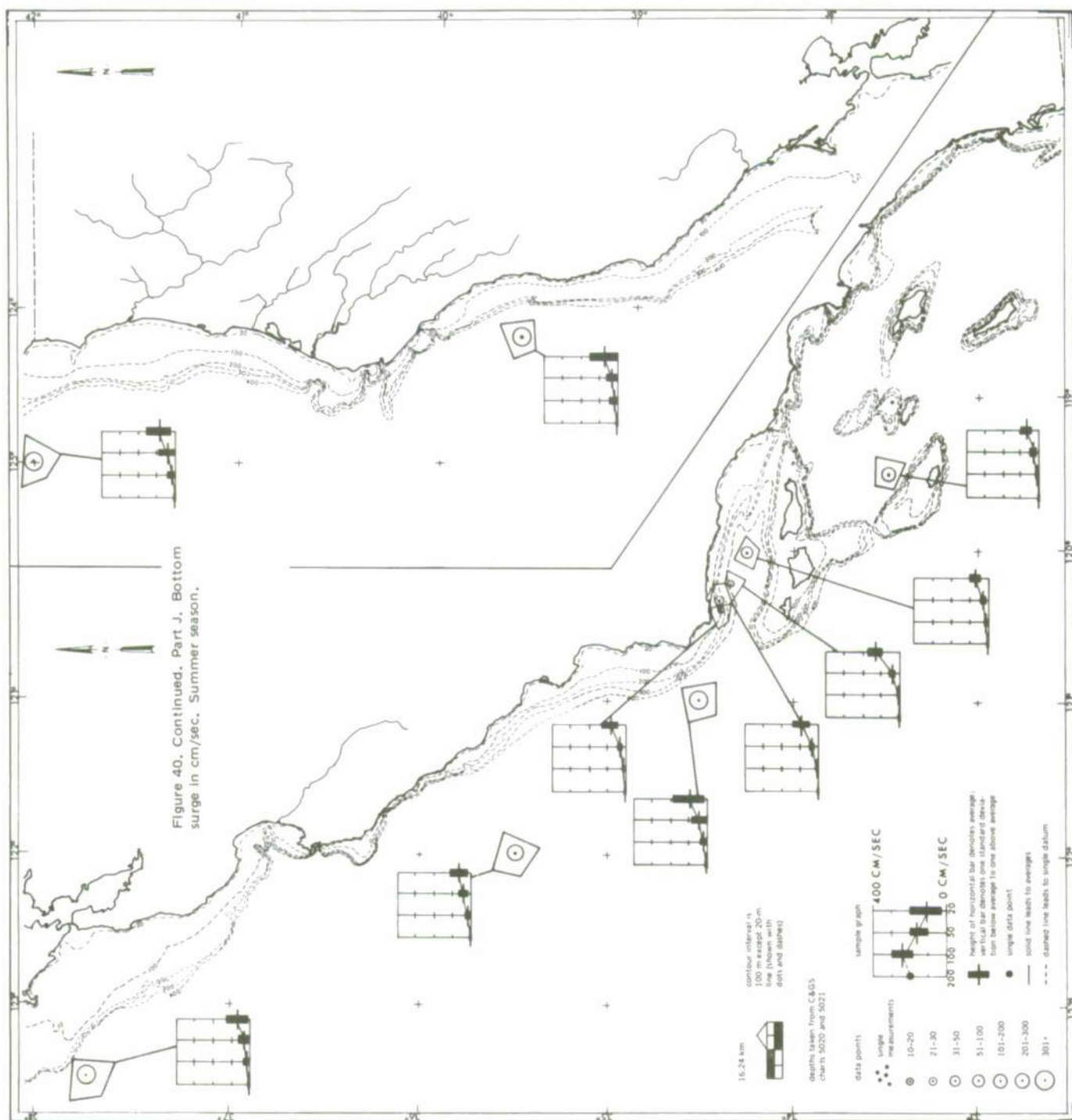


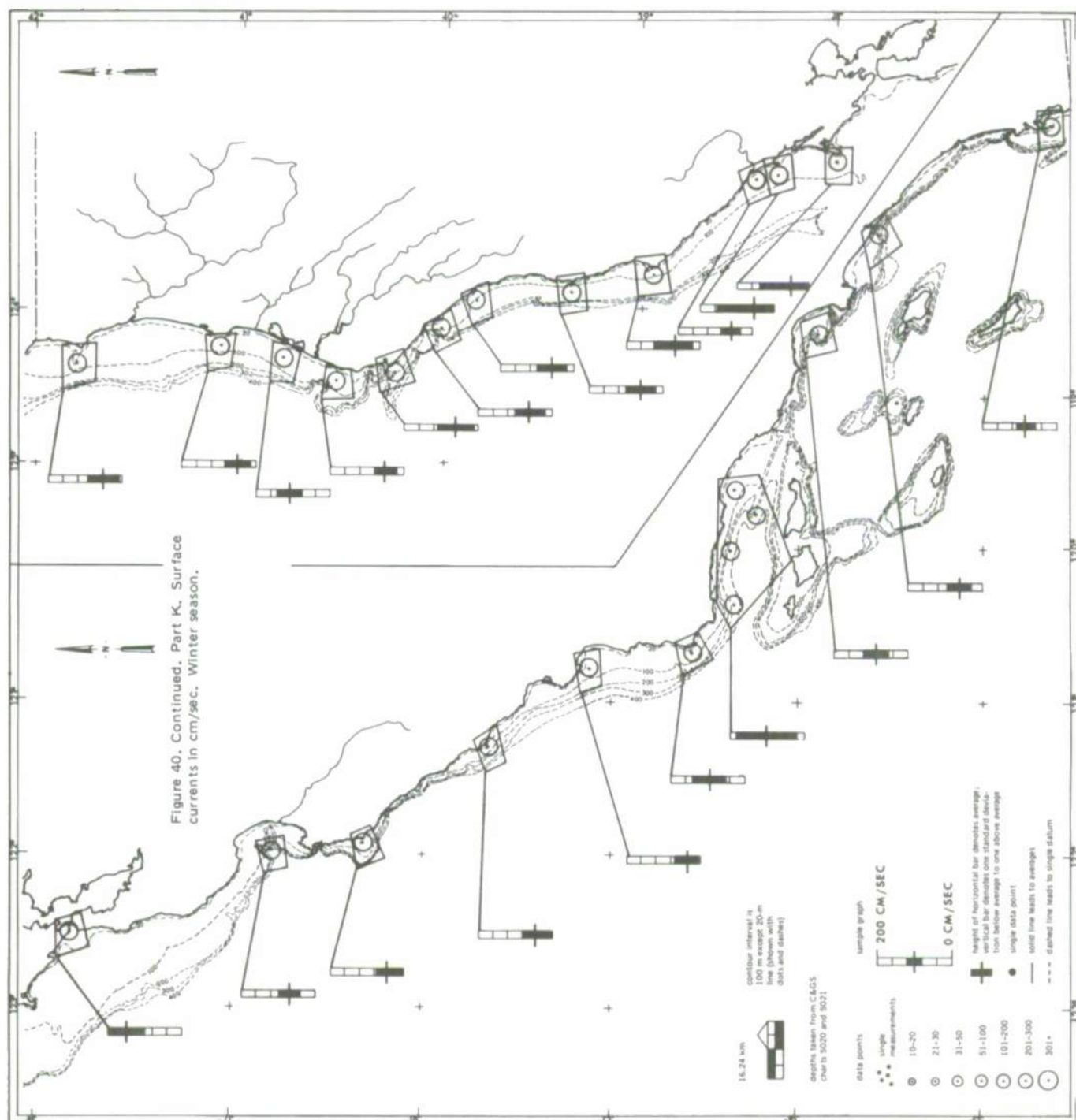


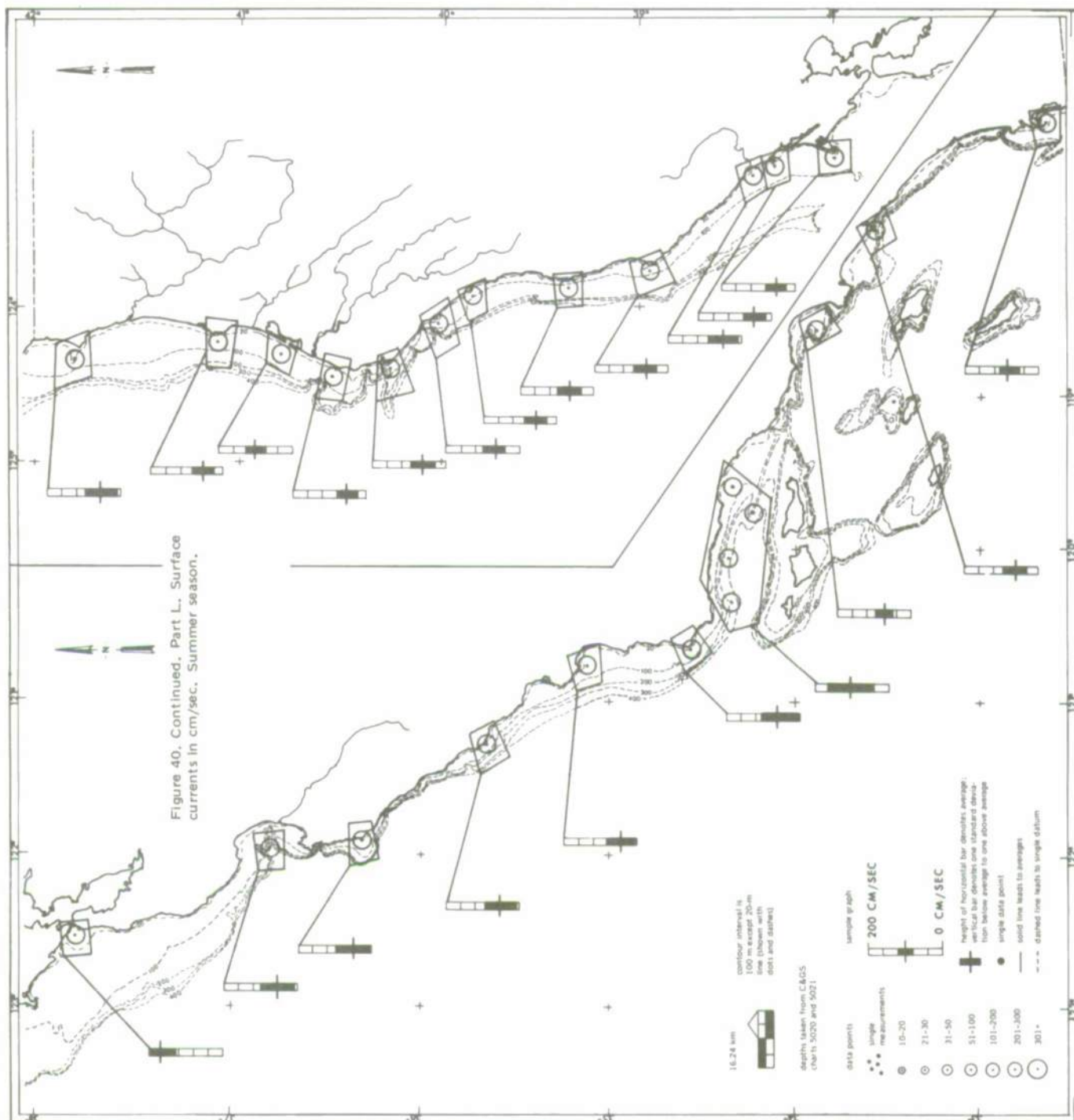


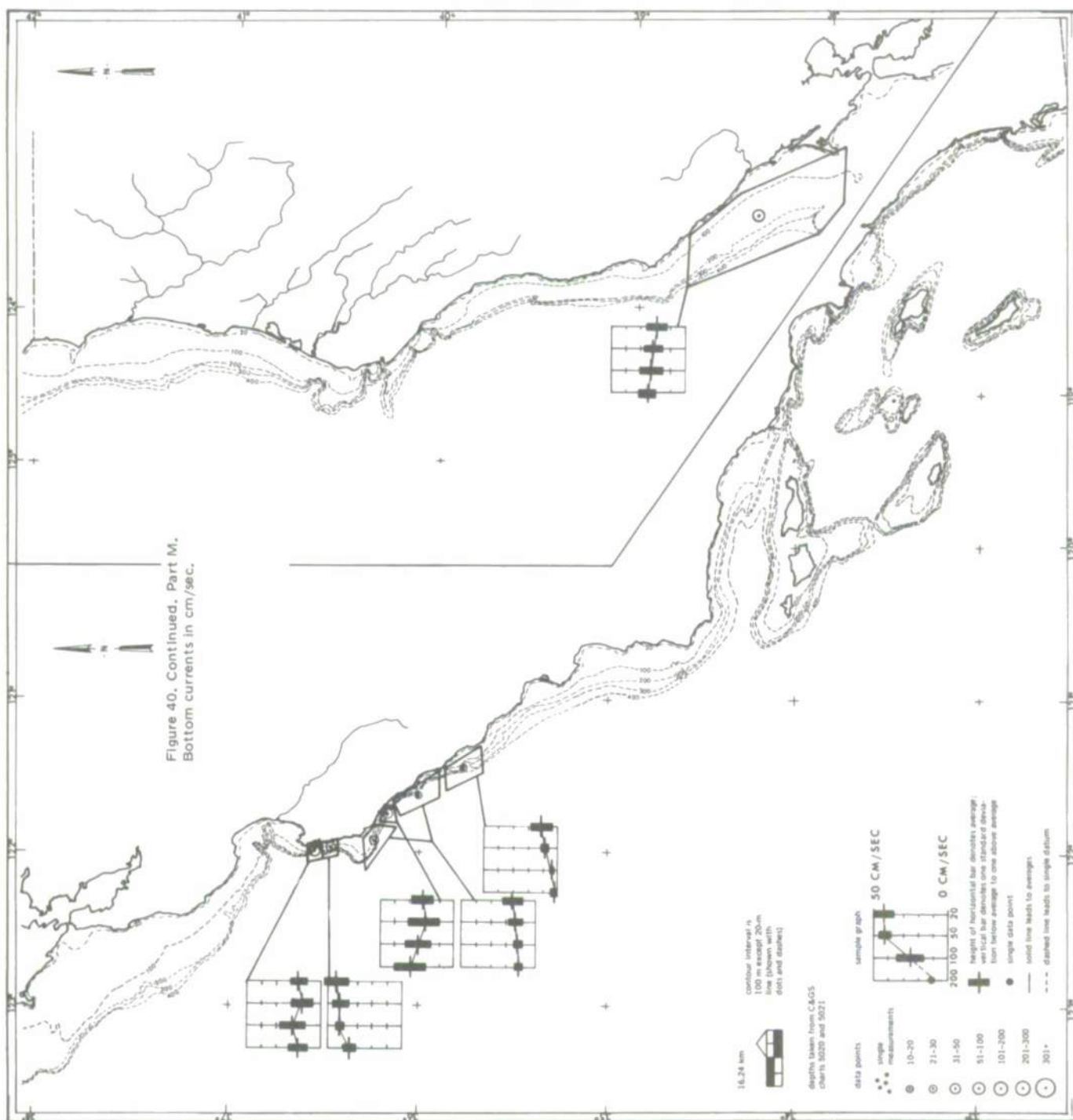


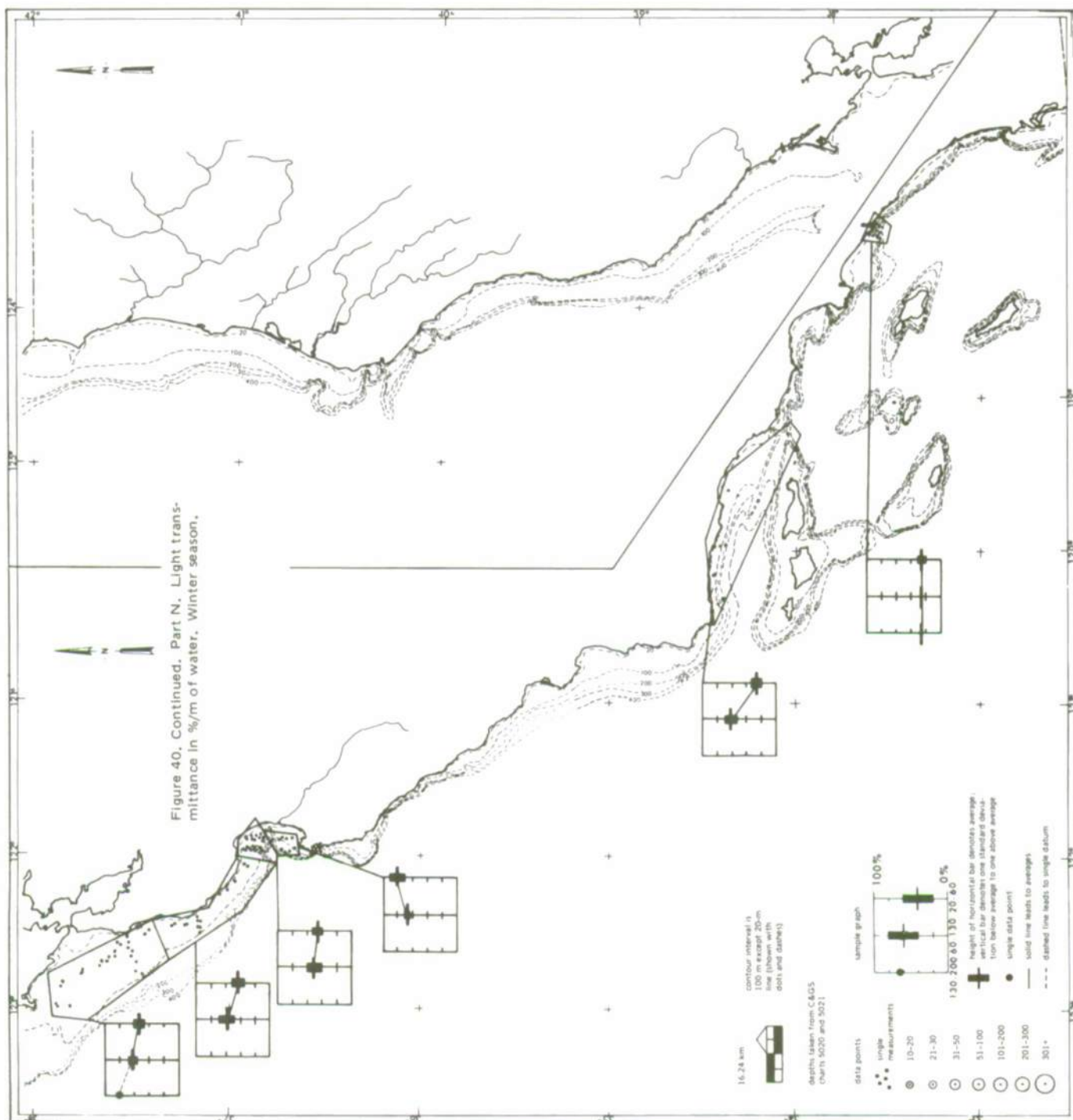


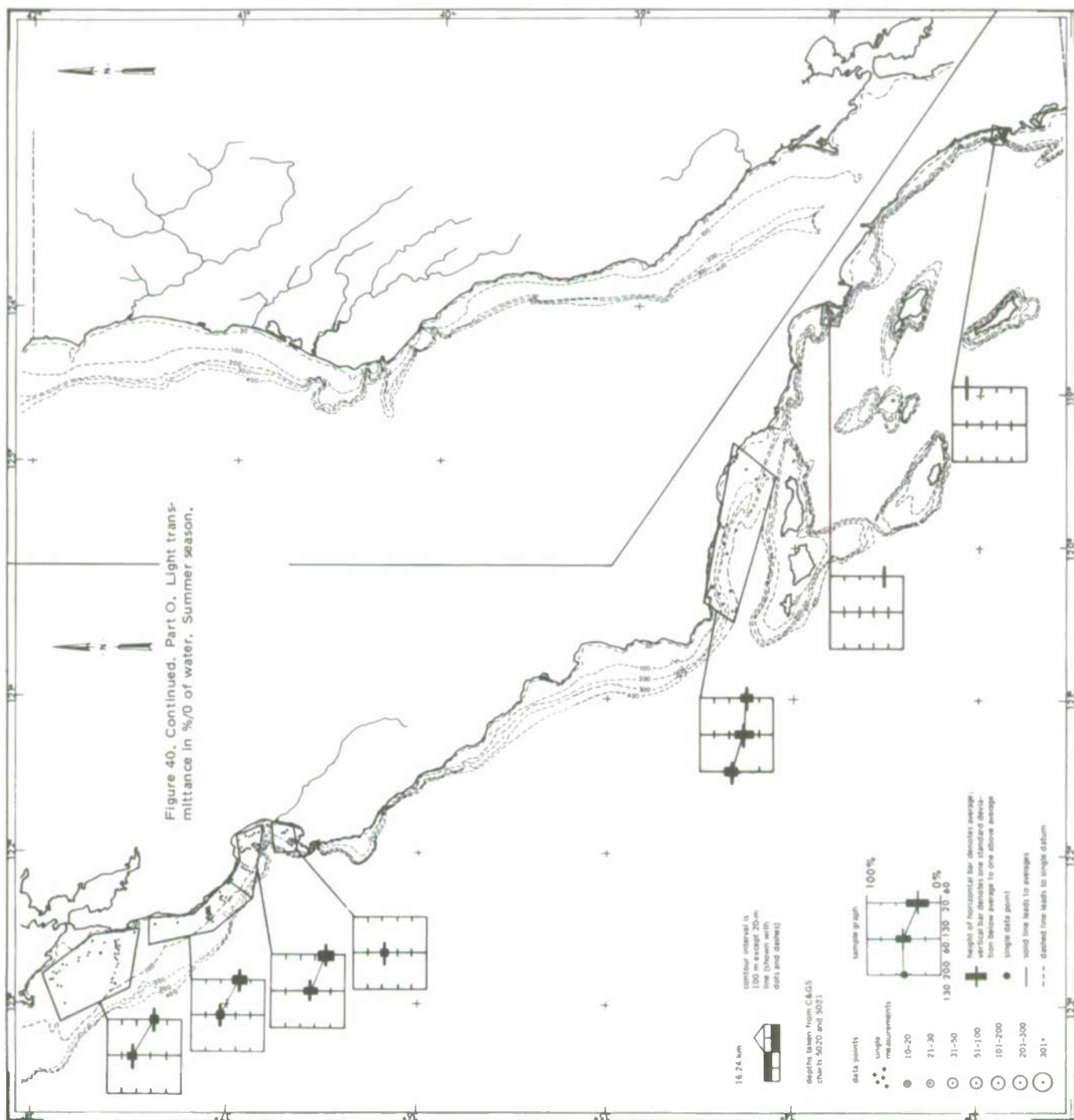












LIGHT TRANSMITTANCE

In the measurement of light transmittance near the bottom, the transmittance may be reduced by the stirring of sediment by gear or divers. Observations are very sparse, and no observations were found north of Pt. Reyes or between Monterey and Pt. Conception. For the entire coast, only about a dozen observations were found in water deeper than 100 m.

The most common measure of light transmittance is the percentage of emitted light energy received on a standard area a standard distance from the source. The measure used in this report is percent/cm²/m. Light transmittance measurements were amalgamated for 20- to 60-, 60- to 130-, and 130- to 200-m depths for regions where results and geography were close for winter and summer. Figure 40, parts N and O, show the percentage of transmittance for these seasons, respectively. The only samples of satisfactory size are at Monterey in summer and San Pedro in winter. It is clear that transmittance increases with depth in most regions, as it theoretically should.

A related topic of interest to construction and maintenance planning for the CUA is sunlight penetration into the sea. The theory as adapted from Clarke and Denton [1962] for applicability in coastal waters is shown in figure 41. The figure shows the theoretical intensity of sunlight and moonlight for clear water as a function of depth. Results reveal that man becomes completely blinded at about 200 m. It should be noted that construction does not occur in unstirred waters with activity in full view of surface illumination; some work must be accomplished on the underside of construction materials with surface illumination as a blinding backlight and in bottom-stirred waters. The experience of consultants and CUARO team divers is that practical construction work cannot be accomplished by daylight in California coastal waters in depths greater than 50 m. Even at such depths, the time to adapt visually to limited light has become long, and the time available on an air tank and without decompression has become short. It is clear that the construction should be planned on the basis of artificial lighting.

One serious problem related to light transmission is likely to be the stirring of bottom sediments during construction efforts, reducing or eliminating visual control. This problem will be most severe in usually calm waters, *i.e.*, waters with small ambient currents, because the sediment size will be finer.

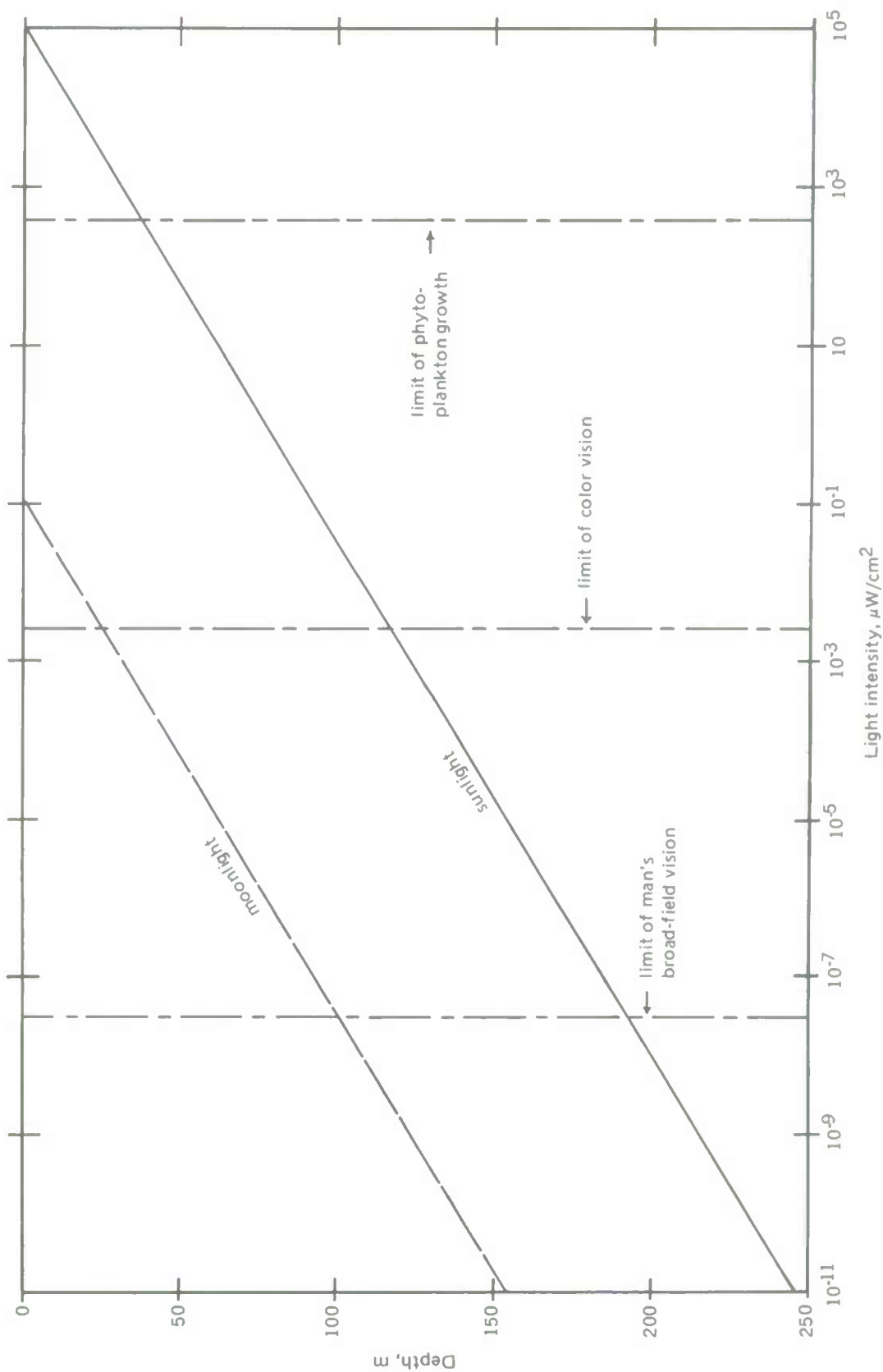


Figure 41. Penetration of light into clear coastal water as a function of depth. (Adapted from figure 1 of G. L. Clarke and E. J. Denton: "Light and Animal Life," *The Sea, Vol. 1: Physical Oceanography*, M. N. Hill, Ed., Interscience Publishers, New York, 1962.)

PROBABILITIES OF CONFLUENCES OF SURVIVAL THREATS TO THE CUA

Suppose we have two independent events, random in time, with variables t and w representing their beginning points. (The events may be tsunami bottom surge and wind wave bottom surge, or they may be any general events.) Let us use the following symbols.

<u>Symbol</u>	<u>Meaning</u>
ℓ_t	Length of occurrence of t event
ℓ_w	Length of occurrence of w event
$f_t(t)$	Probability density of t event
$f_w(w)$	Probability density of w event
Ω_t	Time interval(s) in which t may occur
Ω_w	Time interval(s) in which w may occur
$\Omega_{t_1}, \Omega_{t_2}, \dots, \Omega_{t_{k_t}}$	Possible starting points of t if Ω_t is composed of k_t separated intervals
$\Omega_{w_1}, \Omega_{w_2}, \dots, \Omega_{w_{k_w}}$	Possible starting points of w if Ω_w is composed of k_w separated intervals
CE	Confluence of events

The probability of a confluence of the two events is the probability that the two intervals $[t, t+\ell_t)$ and $[w, w+\ell_w)$ overlap, or

$$P\{CE(w, t)\} = \int_{\Omega_t \cap \Omega_w} f_w(w) \int_{w-\ell_t}^{w+\ell_w} f_t(t) dt dw. \quad (16)$$

In particular, if the events are as likely at any one moment as any other when they are possible to occur, which will be assumed in this report, the f 's are uniform distributions and

$$\left[\begin{array}{l} f_t(t) = \lambda_t^{-1}, \quad t \in \sum_{i=1}^{k_t} \Omega_{t_i}, \\ f_w(w) = \lambda_w^{-1}, \quad w \in \sum_{i=1}^{k_w} \Omega_{w_i}, \end{array} \right. \quad (17)$$

where the λ 's are constants. In this case, Eq. (16) becomes

$$P\{CE(w,t)\} = \int_{\Omega_t \cap \Omega_w} \int_{w-\ell_t}^{w+\ell_w} (\lambda_t \lambda_w)^{-1} dt dw = \frac{\ell_t + \ell_w}{\lambda_t \lambda_w} \int_{\Omega_t \cap \Omega_w} dw. \quad (18)$$

Let us consider the case of confluence of three independent events, adding a new variable c with definitions equivalent to those of t and w . $P\{CE(w,c,t)\}$ is given by the probability that all of $[w, w+\ell_w)$, $[c, c+\ell_c)$, and $[t, t+\ell_t)$ overlap, or

$$P\{CE(w,c,t)\} = \int_{\Omega_c \cap \Omega_w \cap \Omega_t} f_c(c) \int_{c-\ell_w}^{c+\ell_c} f_w(w) \int_{c-\ell_t}^{c+\ell_c} f_t(t) dt dw dc. \quad (19)$$

In particular, for uniform probability densities,

$$\begin{aligned} P\{CE(w,c,t)\} &= \int_{\Omega_c \cap \Omega_w \cap \Omega_t} \int_{c-\ell_w}^{c+\ell_c} \int_{c-\ell_t}^{c+\ell_c} (\lambda_t \lambda_w \lambda_c)^{-1} dt dw dc \\ &= \frac{(\ell_c + \ell_w)(\ell_c + \ell_t)}{\lambda_t \lambda_w \lambda_c} \int_{\Omega_c \cap \Omega_w \cap \Omega_t} dc. \end{aligned} \quad (20)$$

Let t , w , and c denote the start times of the century's greatest tsunami, wind wave bottom surge, and bottom current, respectively. Let us make the following assumptions, where the scale of all variables is measured in hours.

A tsunami wave train's largest portion will last 3 hours; $\ell_t = 3$. The largest portion of the wave train of the century's worst storm will last 3 days; $\ell_w = 72$. A century's worst current will last during either the ebb or flood (depending on direction) of the semidiurnal tide; $\ell_c = 6$. The great tsunami may occur at any time of any year; 100 years contains $24 \times 365.25 \times 100 = 876,600$ hours; $f_t(t) = \lambda_t^{-1} = (876600)^{-1}$, $t \in [0, 876600)$. The great wind wave bottom surge may occur only in winter; one-half of each year for 100 years contains 438,300 hours; $f_w(w) = \lambda_w^{-1} = (438300)^{-1}$, $w \in [0, 4383), [8766, 13149), \dots, [429429534, 433917)$. The bottom current modelled by EPRF has as its tidal component the typical year's greatest spring tide. In 50 to 200 m of water, deeper than the wind effect (calculated by Eq. (10)) and over a century of time, the greatest current may be considered as occurring equally in time. Then $f_c(c) = \lambda_c^{-1} \geq 50 = (876600)^{-1}$, $c \in [0, 876600)$, when $z \geq 50$ m. In 20 m of water, storm winds add a component to the current; the great storm may occur only in winter; the great tide would be expected to occur in winter in only half the years. Thus, the 20-m great current may occur only in winter in half the years. $f_c(c) = \lambda_c^{-1} < 50 = (219150)^{-1}$, $c \in [0, 2191.5), [8766.0, 10957.5), \dots, [210384.0, 212575.5)$, when $z < 50$ m. When the great current does occur, it must occur simultaneously with the great wind wave bottom surge since both require the great storm. This situation provides the only departure from independent events in this section, but it is simple enough to be discussed without using more sophisticated formulation.

Since the 20-m great current has half as many opportunities to occur as the great wind surge and since the greatest wind surge in the century has a probability of one of occurring, the probability of confluence of the 20-m great current and great wind surge is one-half. By similar reasoning, the probability of confluence of the 20-m great current, great wind surge, and great tsunami is half the probability of confluence of the great wind surge and great tsunami alone.

Let us calculate the other confluence probabilities. Substituting appropriate values in Eq. (18), we obtain

$$\begin{aligned} P\{CE(w,t)\} &= \frac{75}{3.8421378 \times 10^{11}} \left(\int_0^{4383} dw + \dots + \int_{429534}^{433917} dw \right) \\ &= 1.952038264 \times 10^{-10} \times 100 \int_0^{4383} dw = 8.555783711 \times 10^{-5} \\ &\doteq 0.000\ 086. \end{aligned}$$

$$P\{CE(w,c(\geq 50m))\} = \frac{78}{3.8421378 \times 10^{11}} \times 100 \int_0^{4383} dw \doteq 0.000\ 089.$$

$$\begin{aligned} P\{CE(c(\geq 50m),t)\} &= \frac{9}{7.6842756 \times 10^{11}} \int_0^{876600} dt = 1.026694045 \times 10^{-5} \\ &\doteq 0.000\ 010. \end{aligned}$$

$$\begin{aligned} P\{CE(c(< 50m),t)\} &= \frac{9}{1.9210689 \times 10^{11}} \left(\int_0^{2191.5} dc + \dots + \int_{210384.0}^{212575.5} dc \right) \\ &= 4.684891833 \times 10^{-9} \times 100 \int_0^{2191.5} dc = 1.026694045 \times 10^{-5} \\ &\doteq 0.000\ 010. \end{aligned}$$

(Note that while $P\{CE(c(\geq 50m),t)\} = P\{CE(c(< 50m),t)\}$ the c events involved are quite different. In the latter probability, the chance of the great current occurring on any day for which it is possible is four times as likely as in the former, but the chance of confluence with the great tsunami is one-fourth as great.)

To calculate a triple confluence, we substitute the appropriate values in Eq. (20).

$$\begin{aligned}
P\{CE(w, c(\geq 50m), t)\} &= \frac{702}{8.420044989 \times 10^{16}} \left(\int_0^{2191.5} dc + \dots + \int_{210384.0}^{212575.5} dc \right) \\
&= 8.337247615 \times 10^{-15} \times 100 \int_0^{2191.5} dc = 1.827107815 \times 10^{-9} \\
&\doteq 0.000\ 000\ 001\ 8.
\end{aligned}$$

The confluence-of-events probabilities for all confluences at CUARO standard depths, with associated particle velocities, for northern, central, and southern California coastal regions are given in table 9.

Table 9. Confluence-of-events probabilities for all confluences at CUARO standard depths with associated particle velocities for northern, central, and southern coastal California.

Type of Confluence	Depth, m	Probability of Confluence	Probable Extreme Velocity, cm/sec, Given Confluence Occurs		
			Crescent City	San Francisco	Santa Barbara
w, c	20	0.500 000	606.5	618.2	454.6
	50	0.000 089	412.8	430.0	357.0
	100	0.000 089	440.9	442.6	407.0
	200	0.000 089	410.3	403.0	396.5
w, t	20	0.000 086	462.8	421.8	205.6
	50	0.000 086	209.7	200.4	100.9
	100	0.000 086	121.9	107.9	56.5
	200	0.000 086	59.8	43.1	27.2
c, t	20	0.000 010	512.3	459.6	407.0
	50	0.000 010	388.5	362.0	335.5
	100	0.000 010	429.2	413.5	397.7
	200	0.000 010	416.1	406.7	396.5
w, c, t	20	0.000 043	790.8	749.8	533.6
	50	0.000 000 001 8	505.5	496.2	396.7
	100	0.000 000 001 8	496.0	482.0	430.6
	200	0.000 000 001 8	443.1	426.4	410.5

The probabilistically loaded values for confluences are given in table 10. These values are not meaningful in any dimensionality, but will serve as relative indices of the seriousness of threats to the CUA.

Table 10. Probabilistically loaded values for all confluences at CUARO standard depths for northern, central, and southern California coastal regions. (Quantities are not in meaningful dimensions and are of relative value only.)

Type of Confluence	Depth, m	Locality		
		Crescent City	San Francisco	Santa Barbara
w, c	20	303.250	309.200	227.300
	50	0.037	0.038	0.032
	100	0.039	0.039	0.036
	200	0.037	0.036	0.035
w, t	20	0.039	0.036	0.018
	50	0.018	0.017	0.008
	100	0.010	0.009	0.005
	200	0.005	0.004	0.002
c, t	20	0.005	0.005	0.004
	50	0.004	0.004	0.003
	100	0.004	0.004	0.004
	200	0.004	0.004	0.004
w, c, t	20	0.034	0.032	0.023
	50	0.000 000 9	0.000 000 9	0.000 000 7
	100	0.000 000 9	0.000 000 9	0.000 000 8
	200	0.000 000 8	0.000 000 8	0.000 000 7

The probabilities in table 9 may be interpreted as in the following example. The probability that the great current and great tsunami occur at the same time is about 1 in 100,000; if we had 100,000 planets like earth and built a CUA on each, within a century we would expect one of the aqueducts to have simultaneously experienced the great current and the great tsunami. If this experience did occur, the particle velocity in the Crescent City area would be about 500 cm/sec at the bottom in 20 m of water and about 400 cm/sec at the bottom in deeper waters.

From the probabilistic loadings in table 10, we can see that 20-m depths are by several orders of magnitude the greatest threat to CUA survival. The deeper the CUA, the safer it is from forces other than currents; also, the loadings appear to be about the same for 50- to 200-m depths.

CONCLUSIONS AND RECOMMENDATIONS

Large bottom surge, great tsunami risk, and unstable density are found close to the shore. Waters about 200-m deep avoid these problems, but with at least one reservation. Because of its long wave length, the tsunami does not recognize the nuance of local features, treating the coastline as an average phenomenon. An aqueduct following a contour near 200 m might yet be susceptible to tsunami damage if a local quirk brought the 200-m contour close to the shoreline, even if only for a short distance. On this basis, the recommendation should clearly be in favor of an aqueduct near the 200-m contour, bridging or deepening if necessary to avoid sudden and short influxes to near shore.

Currents are unstable off the California coast, and evidence indicates that hazards are so ubiquitous that they are difficult to avoid with any depth policy. A 200-m-contour aqueduct will be no better nor worse than a 20-m-contour aqueduct, as far as current problems are concerned. Currents appear to be almost incredibly local in comparison with other oceanographic phenomena. For limited-risk planning, the current must be studied virtually kilometer by kilometer along the projected aqueduct path (or strip containing potential paths). In addition, the influence of upwelling waters near shore and the internal wave forces near the ascending bottom act as complicating agents. With data almost totally absent, a primary approach is to gain oceanographic data of a basic nature on bottom currents, upwelling, and internal waves along the CUA contour strip.

In entering the water from shore and exiting to shore, the designers should consider burying the aqueduct in order to escape near-shore surge, tsunami, and density problems.

Because of turbidity currents and the evidence of strong currents in and over the rims of canyons, the reconnaissance results indicate that canyons should be avoided. Canyons might be bridged by initiating the project from flatland bottom areas away from the rims (a prodigious engineering feat), or the aqueduct might be brought ashore to skirt the canyons, burying it in shallower waters (a process that would involve buying the shoreline and numerous engineering challenges). Regardless of the approach, canyon processes should be further studied.

The designers should plan on using artificial lighting. Light transmittance is greater in deeper waters, strengthening the recommendation for a 200-m-contour aqueduct and agreeing with the economics of 24-hour seaborne operations. However, the stirring of bottom sediments during construction may pose a serious problem, especially where the current is weak enough to leave fine particles; thus, this problem should be further examined.

Summer is the best season for construction operations. As a summary recommendation, waves, surge, tsunamis, density, and light do not appear on the basis of reconnaissance data to pose insurmountable problems. Surface, water column, and bottom currents, including upwelling and internal wave phenomena, may or may not be prohibitive; data are inadequate, and additional information must be obtained from *in situ* observations. Canyons are not an insurmountable threat, but will pose innovative engineering challenges and will probably be quite expensive. Further *in situ* studies will also be required on canyon processes.

REFERENCES

- Baker, R. E. [1970]. "The comparison of oceanic parameters with light attenuation in the waters between San Francisco Bay and Monterey Bay, California," M. S. Thesis in Oceanography, NPGS.
- Barlow, Richard E. and Singpurwalla, Nozer D. [1972]. "Averaging Time and Maxima for Dependent Observations," Proceedings of the Symposium on Statistical Aspects of Air Quality Data. Triangle Universities Consortium on Air Pollution and Division of Meteorology. Environmental Protection Agency, Chapel Hill, November 1972. In press.
- Bixby, H. L. [1962]. "Storms causing harbor and shoreline damage through wind and waves near Monterey," M. S. Thesis in Oceanography, NPGS.
- Borgman, L. E. [1961]. "The exact frequency distribution by near extremes," presented Pacific Southwest Regional Meeting, American Geophysical Union, 26 Jan 61, Berkeley, California.
- California Cooperative Oceanic Fisheries Investigations (CalCOFI) [1966]. "Geostrophic flow of the California current: CalCOFI Atlas No. 4," prepared by John G. Wyllie, MLRG, SIO, UCSD, La Jolla.
- Clarke, G. L., and Denton, E. J. [1962]. "Light and animal life," in *The Sea, Vol 1: Physical Oceanography*, M. N. Hill, Ed., NY: Interscience Publishers.
- Drake, D. E. [1970]. "Distribution and transport of suspended matter, Santa Barbara Channel, California," Ph.D. Thesis, University of Southern California. Supplement: transmissivity cross sections in Southern California, unpublished from Dr. Drake's personal files.
- Gumbel, E. J. [1958]. *Statistics of Extremes*, NY: Columbia Univ. Press.
- Hamilton, G. D., and Laevastu, T. [1972]. "Field measurements required for verification of pollution dispersion computations with hydrodynamical-numerical models," EPRF Report.
- Hubert, W. E., and Laevastu, T. [1965]. "Synoptic analysis and forecasting of surface currents," *Fleet Numerical Weather Facility Technical Note No. 9*, June, 50 pp.
- Humble Oil [1970, 1971]. "Daily marine report—Santa Barbara Channel."

- Hunkins, K. [1966]. "Ekman drift currents in the Arctic Ocean," *Deep-Sea Research*, 13, 607-620.
- Komar, P. [1972]. Notes from a paper presented, *13th Conference on Coastal Engineering, Proceedings*, in press.
- Labyak, P. S. [1969]. "An oceanographic survey of the coastal waters between San Francisco Bay and Monterey Bay, California," M. S. Thesis in Oceanography, NPGS.
- Laevastu, T. [1972]. "Reproduction of currents and water exchange in the Strait of Gibraltar with hydrodynamical numerical (HN) model of Walter Hansen," pp. 219-232 in Gordon, Arnold L., Ed., *Studies in Physical Oceanography*, Vol. 2, NY: Gordon & Breach.
- Laevastu, T., and Hamilton, G. D. [1972a]. "Reproduction of currents in the Strait of Florida with a hydrodynamical-numerical (HN) model," *Proceedings 1972 Summer Simulation Conference, San Diego*.
- Laevastu, T., and Hamilton, G. D. [1972b]. "Computation of flushing and dispersion of pollutants in Pearl Harbor and in San Diego Bay with hydrodynamical-numerical models," *Proceedings of Symposium on the Physical Processes Responsible for the Dispersal of Pollutants in the Sea with Special Reference to the Nearshore Zone, Conseil International pour l'Exploration de la Mer, Arhus*.
- Laevastu, T., and Rabe, K. [1972]. "A description of the EPRF hydrodynamical-numerical model," EPRF Report.
- Le Méhauté, B., Divoky, D., and Lin, A. [1968]. "Shallow water waves: a compilation of theories and experiments," *11th Conference on Coastal Engineering, Proceedings*, September, London.
- Marine Advisors, Inc. [1961]. "A statistical survey of ocean wave characteristics in Southern California waters," prepared for the U. S. Army Corps of Engineers (USACE).
- National Marine Consultants, Inc. [1960]. "Wave statistics for ten most severe storms of Northern California," prepared for USACE.
- National Marine Consultants, Inc. [1960]. "Wave statistics for seven deep water stations along the California coast," prepared for USACE.
- National Oceanographic and Atmospheric Administration (NOAA) [1971]. "U. S. Coast Pilot 7, Pacific Coast," 8th Edit., NOAA, Washington, D. C. National Oceanographic and Atmospheric Administration [1972]. "Tidal current tables, 1972: Pacific Coast of North America and Asia," Washington, D. C.
- Naval Weather Service Environmental Detachment (Asheville) [1971]. "Climatological study of Southern California operating area," prepared for Fleet Weather Facility, San Diego.

- Oceanographic Services, Inc. [1969]. "Storm wave study—Santa Barbara Channel," prepared for Esso Oil Corporation.
- Paquette, R. G. [1972]. "Some statistical properties of ocean currents," *Ocean Engineering*, 2, pp. 95-114.
- Phillips, O. M. [1966]. *The dynamics of the upper ocean*, Cambridge: The University Press.
- Pierson, W. J., Neumann, G., and James, R. W. [1955]. "Practical methods for observing and forecasting ocean waves by means of wave spectra and statistics," U. S. Navy Hydrographic Office Publication No. 503.
- Riffenburgh, R. H. [1970]. "Probable depths of interfaces between temperature layers, with a generalization," *Deep-Sea Research*, 17, 303-316.
- Shepard, A. B. [1970]. "A comparison of oceanic parameters during upwelling off the central coast of California," M. S. Thesis in Oceanography, NPGS.
- Soluri, E. A. [1971]. "A comparison of oceanic parameters during the oceanic period off the central coast of California," M. S. Thesis in Oceanography, NPGS.
- Sverdrup, H. U., Johnson, M. W., and Fleming, R. H. [1942]. *The Oceans*, Englewood Cliffs, N. J.: Prentice-Hall, Inc.
- Thompson, William A. [1969]. *Applied Probability*, NY: Holt, Reinhart, and Winston.
- U. S. Coast & Geodetic Survey (USCGS) [1972]. "USCGS Coastal Charts, Series 51," USCGS, Washington, D. C.
- Wiegel, R. L. [1964]. *Oceanographical Engineering*, Prentice-Hall, Inc., Englewood Cliffs, New Jersey.
- Yeske, L. A., and Waer, R. D. [1968]. "The correlation of oceanic parameters with light attenuation in Monterey Bay, California," M. S. Thesis in Oceanography, NPGS.

Appendix A

INSTITUTIONAL SOURCES OF ARCHIVED DATA

American Geophysical Union
Army Corps of Engineers
 Beach Erosion Board
 Navigation and Shoreline Planning Branch
Association of Monterey Bay Area Governments
Bodega Marine Laboratory
California Academy of Science, Steinhart Aquarium
California Institute of Technology
California Research Corporation
California State University, San Diego
Crescent City
Coastal Engineers Research Center
Coast and Geodetic Survey
Department of Fish and Game, State of California
Engineering Foundation
Engineering Science, Inc.
Environmental Protection Agency
Environmental Prediction Research Facility, U. S. Navy
Environmental Science Service Foundation, Department of Commerce
Esso Oil Corporation
Fleet Numerical Weather Central, Monterey, U. S. Navy
Hopkins Marine Station, Stanford University
Humble Oil Corporation
Humboldt State College
Intersea Research Corporation
Marine Resources Laboratory, Marine Technology Center, State of California
 Menlo Park Laboratory
 Monterey Laboratory
Moss Landing Marine Laboratory
National Academy of Science
National Bureau of Standards
National Marine Fisheries Service
 La Jolla
 Monterey
 Tiburon
National Marine Consultants

National Marine Minerals Technology Center
 National Oceanographic Data Center, NOAA
 National Ocean Survey, NOAA
 National Research Council
 Naval Civil Engineering Laboratory
 Naval Postgraduate School
 Naval Supply Center
 Naval Undersea Center
 Office of Naval Research, General Oceanography Support
 Oregon State University
 Pacific Gas and Electric Co., Inc.
 Pacific Marine Station, Dillon Beach
 Plessey Environmental Systems
 San Diego Marine Consultants
 San Francisco Bar Pilots Association
 Southern California Coastal Water Resources Project
 Stanford University, Department of Geology
 State Department of Navigation and Ocean Development (California)
 State Division of Mines and Geology, Department of Conservation (California)
 State Water Quality Control Board (California)
 Los Angeles
 Sacramento
 San Diego
 Tetra-Tech, Inc.
 University of California, Berkeley
 College of Engineering
 Hydraulics Engineering Laboratory
 Water Resources Center Archives
 University of California, Los Angeles
 University of California, Santa Cruz
 University of California, San Diego
 Institute for Geophysics and Planetary Physics
 Scripps Institution of Oceanography
 University of Southern California, Hancock Foundation
 United States Coast Guard, San Diego
 United States Geological Survey
 National Center for Earthquake Research
 Office of Marine Geology and Hydrology
 Westinghouse Ocean Research Laboratory

Appendix B

INDIVIDUALS AS SOURCES OF DATA

Anderson, Dr. Victor, MPL, SIO, UCSD, Ca.
Arnel, Dr. Robert, Director, Moss Landing Marine Laboratory, Moss Landing, Ca.
Austin Roz, Visibility Laboratory, MPL, SIO, UCSD, Ca.
Bakun, Andrew, NMFS, Monterey, Ca.
Baldridge, Allan, Hopkins Marine Station, Stanford University, Pacific Grove, Ca.
Barakos, Dr. Peter, Marine Environment Division, NUC, San Diego, Ca.
Beeman, Dr. Robert, Department of Marine Biology, San Francisco State College, San Francisco, Ca.
Bell, Robert, Department of Fish and Game, State of California, Long Beach, Ca.
Bissell, Harold, Department of Water Resources, State of California, Sacramento, Ca.
Boden, Dr. Bette, Marine Biology Research Division, SIO, UCSD, Ca.
Broenkow, Dr. Walter, Moss Landing Marine Laboratory, Moss Landing, Ca.
Brown, Daniel, MLRG, SIO, UCSD, Ca.
Brown, Robert, Plessey Environmental Systems, San Diego, Ca.
Cairns, James, IGPP, UCSD, on leave from Marine Environment Division, NUC, San Diego, Ca.
Carlson, P. R., USGS, Menlo Park, Ca.
Carsola, Dr. Al, SCCWRP, Los Angeles, Ca.
Chase, Thomas, GRD, SIO, UCSD, Ca.
Church, Dr. Ron, Environmental Protection Agency, Washington, D. C.
Clark, William, Westinghouse Ocean Research Laboratory, Annapolis, Md.
Conomos, John, USGS, Menlo Park, Ca.
Corliss, Roy E., Coastal Pollution Program, Naval Supply Center, Oakland, Ca.
Costello, James, MLRG, SIO, UCSD, Ca.
Cotton, William, USGS, Menlo Park, Ca.
Cox, Dr. Charles, Department SIO, UCSD, Ca.
Crandall, Dr., Department of Oceanography, Humboldt State College, Arcata, Ca.
Davoll, Peter, Hopkins Marine Station, Stanford University, Pacific Grove, Ca.
Dill, Dr. Robert F., NOAA, Washington, D. C.
Doyle, James, Engineering Research Division, Pacific Gas and Electric Co., Emeryville, Ca.
Drake, Dr. David, Hancock Foundation, USC, Los Angeles, Ca.
Eaton, Dr. Jerry, Director, National Center for Earthquake Research, Menlo Park, Ca.
Fager, Dr. William, Department SIO, CSUSD, Ca.
Ferris, David, Department of Biology, CSUSD, Ca.
Flittner, Dr. Glenn, Director, Office of Marine Research, CSUSD, Ca.
Forsberg, Eric, NMFS, La Jolla, Ca.
Fox, Dean, Simonson Logging Co. (diver), Crescent City, Ca.

Gast, Dr. James, Department of Oceanography, Humboldt State College, Arcata, Ca.
 Gorsline, Dr. Donald, Hancock Foundation, USC, Los Angeles, Ca.
 Gotshall, David, Marine Resources Agency, MTC, State of California, Monterey, Ca.
 Griggs, Dr. Gary, Department of Geology, University of California, Santa Cruz, Ca.
 Hamilton, CDR Glen (Ph. D.), EPRF, Monterey, Ca.
 Hand, Dr. Cadet, Director, Bodega Marine Laboratory, Bodega Bay, Ca.
 Harrison, CDR Avery, United States Coast Guard, San Diego, Ca.
 Hedgpeth, Dr. Joel, Pacific Marine Station, Dillon Beach, Ca.
 Ingle, Dr. James, Department of Geology, Stanford University, Stanford, Ca.
 Inman, Dr. Douglas, ORD, SIO, UCSD, Ca.
 Isaacs, Prof. John, MLRG, SIO, UCSD, Ca.
 Johnson, James H., NMFS, Monterey, Ca.
 Johnson, Dr. J. W., Hydraulics Laboratory, UCB, Ca.
 Kolpack, Dr. Ronald, Hancock Foundation, USC, Los Angeles, Ca.
 Kor, Benjamin, State Water Quality Control Board, Sacramento, Ca.
 Laevastu, Dr. Taivo, EPRF, Monterey, Ca.
 LaFond, Dr. Eugene, Consultant for Oceanography, NUC, San Diego, Ca.
 Laurs, Dr. Michael, NMFS, La Jolla, Ca.
 Lazanoff, Shelley, Naval Oceanographic Office, Monterey, Ca.
 Lee, Dr., Hopkins Marine Station, Stanford University, Pacific Grove, Ca.
 Lee, Sara, CalCOFI, La Jolla, Ca.
 Leiper, Dr. Dale, Chairman, Department of Oceanography, NPGS, Monterey, Ca.
 Le Méhauté, Dr., Tetra-Tech, Inc., Pasadena, Ca.
 Lewitt, LCDR Howard, Fleet Numerical Weather Facility, Monterey, Ca.
 Lynn, Ronald, NMFS, La Jolla, Ca.
 Mallett, Linford, diver, Crescent City, Ca.
 Marshall, Neil, ORD, SIO, UCSD, Ca.
 McAlister, Ed, MPL, SIO, UCSD, Ca.
 McLain, Dr. Douglas, NMFS, Monterey, Ca.
 Mudie, Dr. John, MPL, SIO, UCSD, Ca.
 Munk, Dr. Walter, Director, IGPP, UCSD, Ca.
 Nelson, Arthur P., Director, Marine Minerals Technology Center, NOAA, Tiberon, Ca.
 Noda, Ed, Tetra-Tech, Inc., Pasadena, Ca.
 Nordstrom, Charles, ORD, SIO, UCSD, Ca.
 North, Dr. Wheeler J., Environmental Studies Program, California Institute of Technology,
 Pasadena, Ca.
 O'Leary, Dennis, State Water Quality Control Board, San Diego, Ca.
 Olson, Jack, Marine Environment Division, NUC, San Diego, Ca.
 Orcutt, Dr. Harold, Marine Research Laboratory, MTC, Menlo Park, Ca.
 Paquette, Dr. Robert, NPGS, Monterey, Ca.
 Pequegnat, Dr., Department of Oceanography, Humboldt State College, Arcata, Ca.
 Pestrong, Raymond, Chairman, Department of Geology, San Francisco State College, San
 Francisco, Ca.
 Petrie, William L., National Academy of Sciences, Washington, D. C.
 Rabe, Kevin, EPRF, Monterey, Ca.
 Reid, Joseph, Department SIO, UCSD, Ca.

Richcreek, Darold G., Harbor Master, Creseent City, Ca.
 Robinson, Margaret, ORD, SIO, UCSD, Ca.
 Schafran, Walter C., Fisheries Program, Humboldt State College, Areata, Ca.
 Schwartzlose, Dr. Richard P., MLRG, SIO, UCSD, Ca.
 Seekel, Gunther R., NMFS, Monterey, Ca.
 Shepard, Dr. Franeis P., Professor Emeritus, GRD, SIO, UCSD, Ca.
 Silver, Ely, USGS, Menlo Park, Ca.
 Simons, Richard, IGPP, UCSD, Ca.
 Sloan, Robert L., U. S. Army Corps of Engineers, San Francisco, Ca.
 Smith, Berry Gardner, Map Librarian, SIO, UCSD, Ca.
 Smith, Dr. E. H., Direetor, Pacific Marine Laboratory, Dillon Beach, Ca.
 Smith, Greg, Tetra-Tech, Inc., Pasadena, Ca.
 Snodgrass, Dr. James, SIO, UCSD, Ca.
 Thompson, Dr. Warren, Department of Oceanography, NPGS, Monterey, Ca.
 Thornton, Dr. E., Department of Oceanography, NPGS, Monterey, Ca.
 Tibby, Dr. Richard, Hancock Foundation, USC, Los Angeles, Ca.
 Tubbs, Tony, MLRG, SIO, UCSD, Ca.
 Tucker, Dr. Stephen, Department of Oceanography, NPGS, Monterey, Ca.
 Tunstall, Ed, ORD, SIO, UCSD, on leave from Marine Environment Division, NUC, San Diego, Ca.
 Van Dorn, Dr. William G., Department SIO, UCSD, Ca.
 Von Schwind, Dr., Department of Oceanography, NPGS, Monterey, Ca.
 Wiegel, Prof. Robert, Hydraulics Laboratory, UCB, Ca.
 Wilkes, Frances, ORD, SIO, UCSD, Ca.
 Williams, Alvin, diver, Crescent City, Ca.
 Wilson, Donald, City Manager, Crescent City, Ca.
 Wooster, Dr. Warren, Department SIO, UCSD, Ca.
 Wylde, Dr. Pat, Hydraulics Laboratory, UCB, Ca.
 Wyllie, John, MLRG, SIO, UCSD, Ca.
 Young, Dr. Joseph H., Chairman, Department of Biology, San Jose State College, San Jose, Ca.
 Young, Manly, CalCOFI, La Jolla, Ca.

